218 SPRINGER TRACTS IN MODERN PHYSICS

Georg Heinz Hoffstaetter

High-Energy Polarized Proton Beams

A Modern View

Springer

Springer Tracts in Modern Physics
Volume 218

Springer Tracts in Modern Physics

Springer Tracts in Modern Physics provides comprehensive and critical reviews of topics of current interest in physics. The following fields are emphasized: elementary particle physics, solid-state physics, complex systems, and fundamental astrophysics.
Suitable reviews of other fields can also be accepted. The editors encourage prospective authors to correspond with them in advance of submitting an article. For reviews of topics belonging to the above mentioned fields, they should address the responsible editor, otherwise the managing editor.
See also springeronline.com

Georg Heinz Hoffstaetter

High-Energy Polarized Proton Beams

A Modern View

Springer

Georg Heinz Hoffstaetter
Department of Physics
Laboratory of Elementary Particle Physics
Cornell University
Ithaca, NY 14853-2501
E-mail: Georg.Hoffstaetter@cornell.edu

Cover concept: eStudio Calamar Steinen

Physics and Astronomy Classification Scheme (PACS): 73.22.-29.27.Hj, 29.27.-a, 29.20.-c, 41.75.Lx,02.60.Lj, 02.60.Cb, 02.70.-c

Library of Congress Control Number: 2006926923

ISBN-10: 0-387 -34679-1 e-ISBN 0-387-34754-2
ISBN-13: 978-0387-34679-3

Printed on acid-free paper.

Printed in Singapore. (KYO)

9 8 7 6 5 4 3 2 1

springer.com

To Anke, Samuel, Lydia, Tabea, Prisca, Silas, and Debora

Preface

This book deals with the acceleration and storage of polarized proton beams in cyclic accelerators. Polarized proton beams with hundreds of GeV are, for example, essential for resolving the “spin crisis,” i.e., for understanding the angular momentum distribution inside nucleons.

Experience with the Relativistic Heavy Ion Collider at the Brookhaven National Laboratory (RHIC at BNL) has shown that polarization at 205 GeV can be obtained, and tests at the pre-accelerating Alternating Gradient Synchrotron (AGS) have shown that at least up to 24 GeV, the beam polarization can be quite undisturbed when the accelerator is well adjusted, except at special energies where resonances occur. In particular, it has not been necessary to study closely the variation of the protons’ spin directions across the phase space of the beam. However, at very high energies such as in RHIC, TEVATRON, HERA-p, LHC, or a future VLHC, new phenomena can occur that can lead to a significantly diminished beam polarization.

For these high energies, it is necessary to look in more detail at the spin motion at each point in phase space, and for this the *invariant spin field* proves to be a useful tool. This field gives rise to an adiabatic invariant of spin-orbit motion, and it defines the maximum time-average polarization that is usable in a particle physics experiment. Furthermore, the invariant spin field allows the *amplitude dependent spin tune* to be defined and computed and thereby opens the way to a clear evaluation of the effects of higher-order spin orbit resonances. In particular, the strengths and the depolarizing effects of these resonances can only be determined once the amplitude-dependent spin tune has been computed.

These concepts provide a *modern view of high-energy polarized proton beams* and furnish powerful criteria for optimizing high-energy rings for acceleration and storage of a polarized proton beam. For example, it will be shown how schemes with 4 and 8 Siberian Snakes can be so chosen that the influence of higher-order spin-orbit resonances, the spread of the spin tune over the particle amplitudes in the beam, and the variation of the invariant spin field over orbital phase space are reduced. This has the consequence that the polarization can then be maintained for a significantly increased region of the beam while accelerating to high energy, and more polarization can then be delivered for particle physics experiments.

The utility of the invariant spin field will be mainly illustrated by simulations of spin motion up to 920 GeV in HERA-p, and various methods for computing the invariant spin field, the adiabatic spin invariant, and the amplitude-dependent spin tune will be presented. Moreover, several high-energy spin-orbit dynamical effects will be discussed that go beyond conventional models of spin dynamics and were observed with these novel methods. The reader will gain a much clearer view of spin dynamics at high energy than has hitherto been available.

Parts of this monograph were originally written as a partial requirement for Habilitation at the Darmstadt University of Technology in the year 2000 under the title "Aspects of the Invariant Spin Field for High Energy Polarized Proton Beams." Because I was strongly engaged in upgrading the HERA accelerator at the DESY Laboratory in Hamburg and in investigating its future applications, most of the examples come from HERA. For this tract, these parts have been updated, and examples from other high-energy accelerators such as the Relativistic Heavy Ion Collider at the Brookhaven National Laboratory, the Large Hadron Collider at CERN, and the TEVATRON at the Fermi National Accelerator Laboratory are presented, too.

Many ideas in this book have been developed together with Drs. D. Barber, J. Ellison, K. Heinemann, M. Vogt, and K. Yokoya, and I am much in debt to these colleagues. Furthermore, I gratefully acknowledge that D. Barber has not only given valuable scientific advice but has also proven an untiring reader and corrector of the manuscript.

Ithaca, New York,
May 2006

Contents

1 Introduction

The story of polarized proton acceleration in high-energy circular accelerators began in the 1970s at the Zero Gradient Synchrotron (ZGS) at Argonne [1] where energies of up to 12 GeV were reached. Since that time, there has been a steady development of polarized sources, of polarimetry, and of techniques to maintain polarization during acceleration. The next step in energy came in the 1980s with work at the AGS at Brookhaven National Laboratory (BNL) near New York City where energies of up to 24 GeV were reached [2]. The concept of Siberian Snakes [3], already invented in the 1970s, opened the possibility to achieve even higher energies. A test of principle of Siberian Snakes with a low-energy polarized proton beam was performed at the Indiana University Cyclotron Facility (IUCF) in 1989 [4]. Then in 1999, the efficacy of partial Siberian Snakes and radio-frequency dipoles for maintaining polarization during acceleration in the AGS was demonstrated [5]. The next big advance came with the acceleration of polarized protons to 100 GeV [6, 7] and in 2005 to 205 GeV with 30% polarization [8, 9].

This tract describes spin-dynamical phenomena that occur when accelerating polarized proton beams to energies of several hundred GeV. At these energies a modern view of spin dynamical concepts and of techniques to optimize polarized beams is required. This view will be introduced and illustrated by numerical calculations for various high-energy rings. In particular, I will treat spin motion in the Relativistic Heavy Ion Collider (RHIC) [10], the Large Hadrom Collider (LHC) [11], and the TEVATRON [12]. I also mention the VLHC [13]. RHIC is at BNL. It is designed to accelerate unpolarized ion beams and polarized proton beams and to provide proton-proton collisions of longitudinally polarized beams at a center of mass energy of 500 GeV. The TEVATRON is at the Fermi National Accelerator Laboratory, Fermilab, near Chicago. This circular accelerator collides protons with anti-protons at a center of mass energy of 1800 GeV. The LHC is currently being constructed at CERN in Geneva and will provide proton-proton collisions at 14 TeV center of mass energy. Finally, the VLHC is a very large hadron collider for which designs have been worked out during the past few years. However, because of the obvious advantage, for presenting and comparing results, of concentrating on just one accelerator, the emphasis will be on calculations for the feasibility of using polarized proton beams in HERA, the "Hadron-Electron-

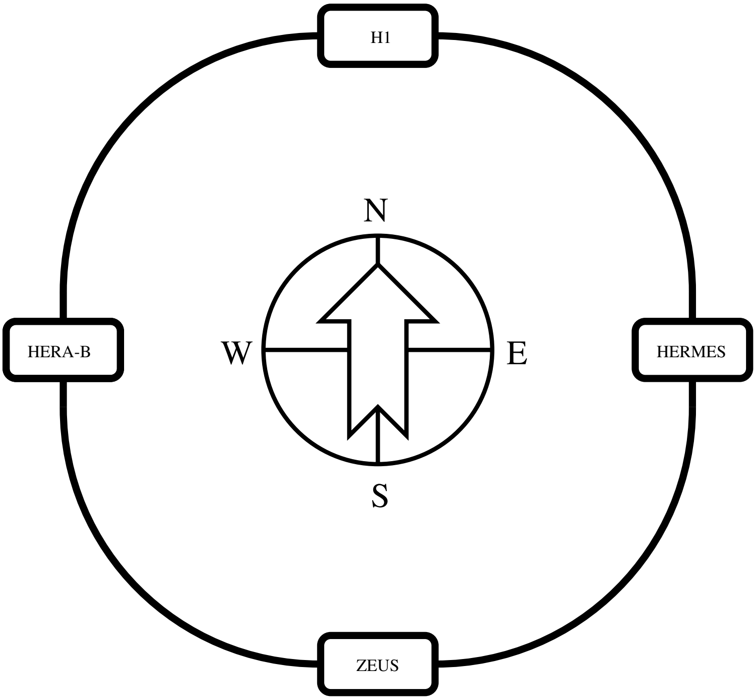

Fig. 1.1. Schematic view of the HERA ring.

Ring-Accelerator" in Hamburg, Germany. Then, once the basic concepts have been illustrated, I return to the other rings.

HERA has a ring (HERA-e) for electrons and positrons ($e^{\pm}$) and a proton ring (HERA-p) and they are contained in the same 6335-m-long tunnel. HERA-p stores protons at 920 GeV and HERA-e stores $e^{\pm}$ at 27.5 GeV for typically about 10 hours. Both rings have 4 straight sections and 4 arcs that bend the beams by $\pi/2$. Proton and electron beams are brought to collision in two experimental detectors, H1 in the north and ZEUS in the south. The east straight section contains HERMES, a fixed target experiment for the electron beam, and the west straight section contains HERA-B, a fixed target experiment for the proton beam. This layout is sketched in Fig. 1.1.

The electron or positron beam in HERA-e becomes polarized by spin-flip synchrotron radiation [14, 15]. When the disturbing effects of misalignments are compensated, a polarization of 60% can be routinely obtained. Around the HERMES experiment, spin rotators consisting of interleaved vertical and horizontal bends have been installed, which disturb the orbit only marginally but orient the polarization parallel to the beam direction in the HERMES experiment while it remains vertical in the arcs. Installing such spin rotators in a high-energy storage ring while keeping a high degree of the polarization was only possible after spin matching of spin-orbit motion [16, 17, 18, 19, 20]. This has not been achieved in any other laboratory, and the attainment of longitudinally polarized high-energy electron or positron beams in HERA-e was, and still is, a unique achievement.

The HERMES experiment studies interactions of the polarized electron or positron beam with polarized nuclei in an internal gas target. The center of mass energy of these collisions is approximately 7 GeV. A 920 GeV polarized proton beam in HERA-p would allow measurements to be made at center of mass energies of up to 318 GeV for collisions between polarized protons and polarized electrons in the detectors H1 and ZEUS. In a future experiment, collisions of the polarized protons with a polarized gas target at 42 GeV center of mass energy could also be investigated. A very active group of many high-energy physicists has already been studying which experiments could be performed with polarized protons and electrons at HERA energies [21, 22, 23, 24].

The spin-flip synchrotron radiation leads to a typical polarization buildup time of roughly $\tau = \tau_{ST}\frac{L}{2\pi\rho}$ [25, 26, 27] where L is the length of the ring, ρ is the bending radius in the dipole magnets, and

$$\frac{1}{\tau_{ST}} = C\frac{1}{\rho^3}\frac{E^5}{(mc^2)^7} \tag{1.1}$$

with the constant $C = 0.92214 \times 10^{-7}(\mathrm{eV})^2\mathrm{m}^3\mathrm{s}^{-1}$, the energy E, and the rest energy mc^2. The fraction $2\pi\rho/L$ takes the absence of synchrotron radiation between the dipoles into account. With $L = 6335$ m and $\rho = 608$ m for the main dipoles of the electron ring HERA-e, the characteristic buildup time is 38 minutes for $E = 27.5$ GeV. The energies in modern proton accelerators are still too low to produce a sufficient amount of synchrotron radiation for polarization buildup. For protons in HERA-p with $\rho = 583$ m, the corresponding buildup time would be 7×10^{10} years. For this reason, the energy of polarized proton beams has not increased along with the achievement of higher and higher energies for unpolarized proton beams. Thus the record remained at 24 GeV for many years [28, 29, 30, 31] until polarized beams with momentum of 100 GeV were produced in December 2001 [6, 7, 32, 33, 34] and 205 GeV in 2005 [8, 9]. During this time, theoretical and numerical studies of very-high-energy polarized proton acceleration have been undertaken for RHIC (250 GeV/c) [10], TEVATRON (900 GeV/c) [12, 13], and HERA-p (920 GeV/c) [35, 36, 37, 38, 39, 40, 41, 42]. These studies also made clear how a new accelerator, like the LHC [11] or a possible VLHC [13], would have to be optimized for polarized beams.

Because the protons in HERA-p do not become polarized by spin-flip synchrotron radiation, methods for obtaining polarized proton beams will be completely different from the well established methods of obtaining polarized electron beams. Various ideas for creating a polarized high-energy proton beam have been discussed:

- Resonance excitation by the Stern-Gerlach effect. This method has not been tested and requires very difficult phase space manipulations [43, 44, 45, 46, 47].
- Spin flipping by scattering the proton beam on a polarized electron beam. The polarization buildup would be too slow [48, 49] and protons would get lost due to the scattering process.
- Spin filtering with a polarized internal target. This method has been tested and is understood for low energies [50, 51]. For high energies, the polarization buildup would be too slow.
- Acceleration of polarized protons after creation in a polarized source. This method has been tested at several accelerators [52, 28].

Here I concentrate on the last possibility because all of these ideas except the last are currently either too difficult or not very promising. In this scenario, polarized protons would be produced in a polarized H^- source. At DESY, a H^- beam is accelerated by an RFQ to 750 keV and then by the LINAC III to 50 MeV. The H^- ions are stripped at a foil in the DESY III synchrotron and the protons are then accelerated to a momentum of 7.5 GeV/c. They are then accelerated to 40 GeV/c in the PETRA ring and by HERA-p to 920 GeV/c. This accelerator chain is shown in Fig. 1.2. The 4 main challenges for the DESY polarized proton project are therefore

- Production of a polarized H^- beam with sufficient current.
- Polarimetry at various stages in the acceleration chain.
- Acceleration through the complete accelerator chain with little loss of polarization.
- Storage of a polarized beam at the top energy over many hours with little loss of polarization.

Today, polarized H^- beams can be produced either by a polarized atomic beam source (ABS) or in an optically pumped polarized ion source (OPPIS). Pulsed beams with polarization of up to 87% for 1 mA H^- beam current [53, 54] and up to 60% for 5 mA [55], respectively, have been achieved with these sources. Compared with the 60 mA of DESY's current source, this sounds rather limited. However, experts claim that currents of up to 20 mA could be possible in OPPIS sources [56, 55]. The maximum current that can be accelerated to 7.5 GeV/c in DESY III is 205 mA, and this current can already be obtained with a 20 mA source current. If DESY III were to become capable of handling more current, then to supply it, the transfer efficiency of DESY's low-energy beam transport (LEBT) and of the radio-frequency quadrupole (RFQ), which is around 50%, would have to be improved.

For polarization monitoring and optimization, polarimeters will have to be installed at several crucial places in the accelerator chain. The source would contain a Lyman-α polarimeter. This does not disturb the beam [57]. Another polarimeter could be installed after the RFQ at 750 keV [58]. This could not be operated continuously because it disturbs the beam. The transfer

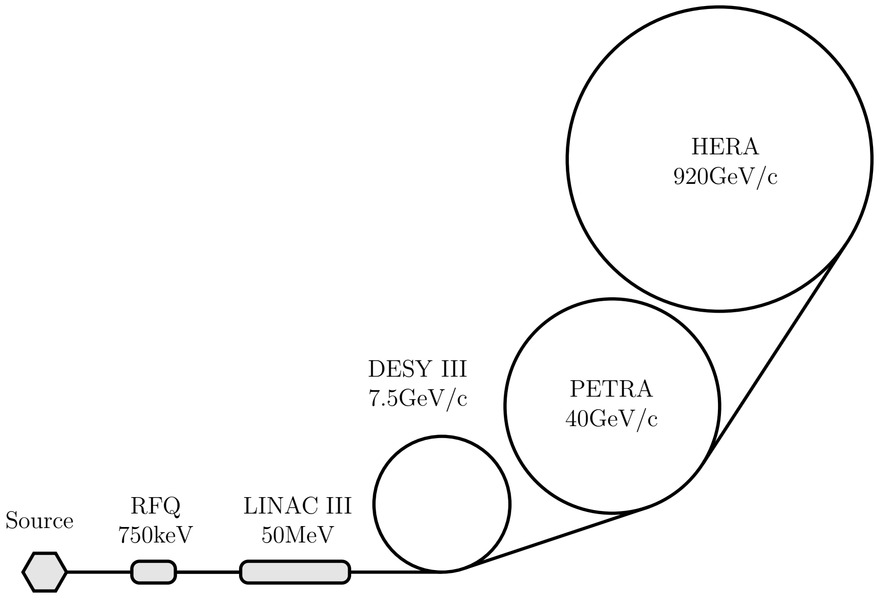

Fig. 1.2. The accelerator chain for HERA-p.

of polarized particles through LINAC III has to be optimized with the aid of yet another polarimeter, which could be similar to that of the AGS LINAC [52]. Each of the other accelerator rings will need its own polarimeter. The polarimeter for DESY III could be similar to the AGS internal polarimeter.

Because polarization at the DESY III momentum of up to 7.5 GeV/c has been achieved at several laboratories, the technology of all the polarimeters mentioned so far is well understood. It is different with the polarimeters required for PETRA and HERA-p energies; for these high energies, there is no established polarimeter. Here one has to wait and see how the novel techniques developed for RHIC [59, 60, 61] will work. It has been shown that the CNI polarimeter at RHIC gives a good and reproducible signal at least up to 100 GeV [6, 62, 63, 32, 34], and an absolute calibration of the polarimeter at this energy is possible.

The problems arising in DESY III and in PETRA when accelerating polarized proton beams will be briefly discussed, but because polarized beams at these energies have already been produced by other accelerators, the main emphasis of the work presented here will be on polarization dynamics in the high-energy region, which would be unique to HERA-p. After a polarized proton beam has been accelerated to the high energy of 920 GeV, the polarization has to be stable for several hours in order to be useful for the experiments H1 and ZEUS. Furthermore, the polarization in all parts of the beam has to be nearly parallel during this storage time, so that the spread of the polarization direction across the beam is small.

After a review in Sect. 2.1 of the various ways of formulating spin motion to be used in this tract, it will be shown in Sect. 2.2 that the concept of an invariant spin field is essential to our understanding of both acceleration and storage of polarized protons. The beam average of this field describes the maximum time-average polarization available for particle physics experiments. It will be shown that this maximum time-average polarization depends on the particle energy and that it can be strongly reduced at critical energies. Furthermore, this field allows an amplitude-dependent spin tune to be defined and it allows us to demonstrate that the critical energies correspond to resonance between the amplitude-dependent spin tune and the orbital tunes, so that high-order resonances can be analyzed. Crossing these resonances while accelerating the beam can lead to a reduction of polarization. I will show how the invariant spin field and the amplitude-dependent spin tune can be used to compute high-order resonance strengths and how to describe this reduction of polarization.

An analysis of the ranges of applicability of linearized spin-orbit motion in Sect. 3.1 will show that higher-order effects have to be taken into account at HERA-p energies of up to 920 GeV. Nevertheless, this approximation is successfully used to find optimal schemes of Siberian Snakes for HERA-p.

Non-perturbative methods for computing the invariant spin field and the amplitude-dependent spin tune are introduced in Chapt. 4. They are used to show that the optimization of snake schemes is important for HERA-p but that one cannot eliminate all destructive higher-order resonance effects. Furthermore, these methods are used to compute a limit for the proton emittance with which a polarized beam can be accelerated in HERA-p according to current knowledge and technology. For this purpose, phase space amplitudes of particles are found for which the polarization is not satisfactory even with the most optimized scheme of 8 Siberian Snakes.

The novel methods for using the invariant spin field to analyze spin dynamics at high proton energies that will be emphasized in this tract are also the basis of a very detailed analysis of the acceleration process in HERA-p [64] and have proven useful for the planned 250 GeV polarized proton beam in RHIC [65] and for simulations of polarized beam in the AGS.

References

1. T. Khoe et al.: Polarized proton acceleration in the ZGS *Particle Accelerators*, 6, 213 (1975)
2. T. Roser: Polarized protons at the AGS and high $P(T)^2$ spin effects. *Proceedings, Intersections between particle and nuclear physics, Lake Louise*, 1148-1152 (1986)

3. Ya. S. Derbenev and A. M. Kondratenko: Acceleration of polarized particles. *Sov. Phys. Doklady*, 20:562, 1976. also in Russian: *Dokl. Akad. Nauk Ser. Fiz.* 223:830-833 (1975)
4. A. D. Krisch, S. R. Mane, R. S. Raymond, T. Roser, *et al*: First test of the Siberian Snake magnet arrangement to overcome depolarizing resonances in a circular accelerator. *Phys. Rev. Lett.* 63(11):1137–1140 (1989)
5. M. Bai eta l.: Overcoming intrinsic spin resonances with an rf dipole. *Phys. Rev. Lett.* 80, 4673 (1998)
6. G. Bunce and T. Roser: The first RHIC Spin Run. In S. Davis, A. Deshpande, S. Ozaki and R. Venugopalan, editors, *Proceedings of the Electron Ion Collider workshop*, BNL Report-52663-Vol.II (2002)
7. T. Roser et al.: Accelerating and colliding polarized protons in RHIC with Siberian Snakes. In *Proceedings EPAC02*, Paris (2002)
8. W. Fischer: Presentation at the BNL Machine Advisory Committee Meeting (January 2006)
9. T. Roser: RHIC operational status. In *Proceedings PAC05*, Knoxville/TN (2005)
10. K. Brown, G. Bunce, E. Courant, R. Fernew, R. Gupta, S. Y. Lee, *et al*: Conceptual design for the acceleration of polarized protons in RHIC. AGS/RHIC/SN 001, Brookhaven (1995)
11. The LHC Study Group: The Large Hadron Collider Conceptual Design. Report CERN/AC/95-05, October (2003)
12. SPIN Collaboration: Acceleration of polarized protons to 120 GeV and 1TeV at Fermilab. UM–HE 95–09, University of Michigan (1995)
13. M. Blaskiewicz, A. Drees, W. Fischer, R. Gupta, S. Peggs,(ed.), F. Pilat *et al.*: VLHC accelerator physics. Report FERMILAB-TM-2158, (2001)
14. A. A. Sokolov and I. M. Ternov: On polarization and spin effects in the theory of synchrotron radiation. *Sov. Phys. Doklady*, 8:1203 (1964)
15. A. A. Sokolov and I. M. Ternov: *Radiation from Relativistic Electrons.* American Institute of Physics, New York (1986)
16. A. W. Chao and K. Yokoya: An alternative longitudinal polarization scheme for TRISTAN. KEK–81–7, Tsukuba (1981)
17. K. Yokoya: Improvement of radiative polarization in plane storage rings. In *Polarized Electron Acceleration and Storage.* DESY–M–82–09 and KEK–81–19, Tsukuba (1982)
18. D. P. Barber, J. Kewisch, G. Ripken, R. Rossmanith, and R. Schmidt: A solenoid spin rotator for large electron storage rings. *Particle Accelerators*, 17:243–262 (1985)
19. D. P. Barber, M. Böge, H.-D. Bremer, R. Brinkmann, W. Brückner, *et al*: The first achievement of longitudinal spin polarization in a high energy electron storage ring. *Phys. Lett.* B(343):436–443 (1995)
20. D. P. Barber and G. Ripken: Radiative polarization in electron storage rings. In A. W. Chao and M. Tigner, editors. *Handbook of accelerator physics and engineering* World Scientific (1999)
21. J. Blümlein and W.-D. Nowak, editors: *Workshop on the Prospects of Spin Physics at HERA.* DESY–95–200 (1995)
22. J. Blümlein, A. De Roeck, T. Gehrmann, and W.-D. Nowak, editors: *Deep inelastic scattering off polarized targets: Theory meets experiment.* DESY–95–200 (1997)

23. A. De Roeck and T. Gehrmann, editors: *Physics with polarized protons at HERA*. DESY–Proceedings–1998–01 (1998)
24. D. P. Barber and A. De Roeck, editors: *Proceedings of Polarized Protons at High Energies*, DESY–Proceedings–1999–03 (1999)
25. A. W. Chao: Polarization of a stored electron beam. In *Conference proceedings 87*. US Particle Accelerator School, Batavia, USA, American Institute of Physics (1981)
26. A. W. Chao: Evaluation of radiative spin polarization in an electron storage ring. *Nucl. Instr. Meth.* 180:29 (1981)
27. Bryan W. Montague: Polarized beams in high-energy storage rings. *Physics Reports*, 113(1):1–96 (1984)
28. T. Roser: Polarized proton beam in the AGS. In *Proceedings of SPIN98*, Protvino (1998)
29. T. Roser: Acceleration of polarized proton beams. In *Proceedings of SPIN98*, Protvino (1998)
30. M. Bai, L. Ahrens, J. Alessi, K. Brown, G. Bunce, P. Cameron, *et al*: Overcoming intrinsic spin resonances with an rf dipole. *Phys. Rev. Lett.* 80(21):4673–4676 (1998)
31. T. Roser: RHIC spin program: machine aspects and recent progress. In [24].
32. H. Huang, L. Ahrens, J. G. Alessi, I. Alekseev, M. Bai, J. Beebe-Wang, *et al*: Polarized proton acceleration at the Brookhaven AGS and RHIC. In Proceedings of PAC03, Portland/OR (2003)
33. W. W. MacKay, L. Ahrens, M. Bai, K. Brown, E. D. Courant, J. W. Glenn, *et al*: Spin Dynamics in AGS and RHIC. In Proceedings of PAC03, Portland/OR (2003)
34. W. W. MacKay, L. Ahrens, M. Bai, E. D. Courant, W. Fischer, H. Huang, *et al*: Commissioning spin rotators in RHIC. In Proceedings of PAC03, Portland/OR (2003)
35. D. P. Barber: Possibilities for polarized protons at HERA. In *Prospects of spin physics at HERA*, DESY–95–200 (1995)
36. G. H. Hoffstaetter: Polarized protons in HERA. In DESY–96–05 (1996)
37. SPIN Collaboration and the DESY Polarization Team: Acceleration of polarized protons to 820 GeV at HERA. UM–HE–96–20, University of Michigan (1996)
38. D. P. Barber, G. H. Hoffstaetter, and M. Vogt: Polarized protons in HERA. In *Future Physics at HERA*, volume 2, p. 1205–1216. DESY (1996)
39. G. H. Hoffstaetter: Polarized protons in HERA. In *Proceedings SPIN96*, Amsterdam (1996)
40. D. P. Barber, M. Vogt, and G. H. Hoffstaetter: Polarized protons in HERA – the status. In DESY–97–200 (241–246) and DESY–Proceedings–1998–01 p. 460–465 (1997)
41. SPIN Collaboration and the DESY Polarization Team: Acceleration of polarized protons to 920 GeV at HERA. UM–HE–99–05, University of Michigan (1999)
42. G. H. Hoffstaetter: Polarized protons at HERA: the accelerator issues. In [24].
43. Ya. S. Derbenev: The Stern-Gerlach method in charge particle storage rings (1) The double-resonance Stern-Gerlach effect. UM-HE-90-30, University of Michigan (1990)

44. Ya. S. Derbenev: The Stern-Gerlach method in charged particle storage rings (2) The neo-classical Stern-Gerlach effect. UM-HE-90-32, University of Michigan (1990)
45. Ya. S. Derbenev: Concepts for Stern-Gerlach polarization in storage rings. DESY Accelerator Physics Seminar (1995)
46. M. Conte, A. Penzo, and M. Pusterla: Spin splitting due to longitudinal Stern-Gerlach kicks. *Nuovo Cimento*, 108 A(1):127–136 (1995)
47. M. Conte, B. E. Norum, A. Penzo, M. Pusterla, and R. Rossmanith: A proposed test of the spin splitter effect in HERA-p. DESY–HERA-96-01 (1996)
48. C. J. Horowitz and H. O. Meyer: Polarizing stored beams by interaction with polarized electrons. *Phys. Rev. Lett.* 72(25):3981 (1994)
49. D. P. Barber: Prospects for polarized protons at HERA. In *conference on the spin structure of the nucleon at Erice in 1995*, World Scientific (1998)
50. F. Rathmann, C. Montag, D. Fick, J. Tonhäser, W. Brückner, *et al*: New method to polarize protons in a storage ring and implications to polarize antiprotons. *Phys. Rev. Lett.* 71(9):1379–1382 (1993)
51. C. Montag: Beschleunigerphysikalische Untersuchungen zum FILTEX-Protonen-Testexperiment im Heidelberger Testspeicherring TSR. Diploma thesis, Philipps-Universität, Marburg (1993)
52. F. Z. Khiari, P. R. Cameron, G. R. Court, D. G. Crabb, *et al*: Acceleration of polarized protons to 22 GeV/c and the measurement of spin-spin effects in $\boldsymbol{p} + \boldsymbol{p} \to p + p$. *Phys. Rev.* D 39:45–85 (1989)
53. A. S. Belov, V. E. Kuzik, Yu. V. Plokhinskii, V. P. Yakushev, and V. G. Dudnikov: A source of polarized negative hydrogen ions with deuterium plasma ionizer. *Nucl. Instr. Meth.* A(333):256–259 (1993)
54. A. Belov: Atomic beam type polarized ion sources. In [24].
55. A. Zelenski: Optically pumped polarized ion sources (OPPIS). In [24].
56. A. N. Zelenski, C. D. P. Levy, K. Jayamanna, M. McDonald, *et al*: The TRIUMF high current DC optically pumped polarized H^- ion source. In *TRIUMF-PP-95-44 and Proceedings of PAC95*, Dallas (1995)
57. A. N. Zelenski, S. A. Kokhanovskii, V. M. Lobashev, and V. G. Polushkin: A laser source of polarized protons and H^- ions. *Nucl. Instr. Meth.* A(245):223–229 (1986)
58. L. Buchmann: A proton polarimeter for beam energies below 300-keV. *Nucl. Instr. Meth.* A(301):383–388 (1991)
59. K. Kurita: Proton-Carbon CNI polarimeter for RHIC. In S. D. Bass, A. De Roeck, A. Deshpande, editors, *Proceedings of the Workshop at Trento, Italy on Spin Structure of the Proton and Polarized Collider Physics, Nuclear Physics B (Proc. Suppl.)* 105 (2002)
60. G. Bunce: Proton polarimetry for RHIC. In [24].
61. A. D. Krisch: A polarized jet for RHIC polarimetry. In [24].
62. H. Huang et al.: Commissioning CNI Proton Polarimeters in RHIC. In *Proceedings to EPAC02*, Paris (2002)
63. H. Huang, I. Alekseev, G. Bunce, A. Deshpande, *et al*: Commissioning of RHIC p-Carbon CNI Polarimeter. In *Proceedings of SPIN00*, Osaka (2000)
64. M. Vogt: Bounds on the maximum attainable equilibrium spin polarization of protons in HERA. *Dissertation, Universität Hamburg*, DESY–THESIS–2000–054 (December 2000)
65. A. Lehrach: Calculation of the invariant spin field by adiabatically blowing up the beam with an rf dipole. In [24].

2 Spin Dynamics

2.1 The Equation of Spin Motion

The expectation value of the vector operator representing the spin of a particle in its instantaneous rest frame satisfies the equation of motion of a classical spin vector. The direction of this expectation value will be denoted here by *the spin* $\boldsymbol{s}$ with $|\boldsymbol{s}| = 1$ whence $\boldsymbol{s}$ is $\frac{2}{\hbar}$ times the expectation value. The polarization P of a beam is defined as the absolute value of the average spin taken over all N particles of the beam,

$$P = |\frac{1}{N}\sum_{j=1}^{N} \boldsymbol{s}_j| = |\langle \boldsymbol{s} \rangle_N| \ . \tag{2.1}$$

The spin $\boldsymbol{s}$ changes with the time t of the laboratory frame according to the Thomas-Bargmann-Michel-Telegdi (T-BMT) equation [1, 2, 3, 4],

$$\frac{\mathrm{d}}{\mathrm{d}t}\boldsymbol{s} = \boldsymbol{\Omega}_{BMT}(\boldsymbol{r}, \boldsymbol{p}, t) \times \boldsymbol{s} \ , \tag{2.2}$$

$$\begin{aligned} \boldsymbol{\Omega}_{BMT}(\boldsymbol{r}, \boldsymbol{p}, t) = &-\frac{q}{m\gamma}[(1 + G\gamma)\boldsymbol{B} \\ &-\frac{G\boldsymbol{p}\cdot\boldsymbol{B}}{(\gamma+1)m^2c^2}\boldsymbol{p} - \frac{1}{mc^2}(G + \frac{1}{1+\gamma})\boldsymbol{p}\times\boldsymbol{E}] \ , \end{aligned} \tag{2.3}$$

where the electric and magnetic fields $\boldsymbol{E}(\boldsymbol{r}, t)$ and $\boldsymbol{B}(\boldsymbol{r}, t)$ in the laboratory frame are functions of the particle's position $\boldsymbol{r}$ and the time t. The quantities $\boldsymbol{p}$ and γ are the particle's momentum and the relativistic factor in the laboratory frame, q and mc^2 are the charge and the rest energy, and $G = (g - 2)/2$ is the particle's anomalous gyro-magnetic g-factor, which is 1.793 for protons and 0.00116 for electrons.

2.1.1 Spin Motion in Flat Circular Accelerators

In terms of the components $\boldsymbol{B}_\perp$ and $\boldsymbol{B}_\|$ of the magnetic field, which are perpendicular and parallel to the particle's momentum, the Lorentz force equation and the T-BMT equation in purely magnetic fields show some similarities,

$$\frac{\mathrm{d}}{\mathrm{d}t}\boldsymbol{p} = -\frac{q}{m\gamma}\{ \qquad \boldsymbol{B}_\perp \qquad \} \times \boldsymbol{p}\,, \tag{2.4}$$

$$\frac{\mathrm{d}}{\mathrm{d}t}\boldsymbol{s} = -\frac{q}{m\gamma}\{(G\gamma+1)\boldsymbol{B}_\perp + (1+G)\boldsymbol{B}_\parallel\} \times \boldsymbol{s}\,. \tag{2.5}$$

In a solenoid magnet, $\boldsymbol{B}_\parallel$ produces a spin rotation around the longitudinal direction. In transverse magnetic fields, where $\boldsymbol{B}_\parallel = 0$ as in the vertical magnetic fields in the center plane of a flat circular accelerator, several conclusions can immediately be drawn from these equations.

- In such a transverse magnetic field, the momentum $\boldsymbol{p}$ rotates in the plane perpendicular to the field. If $\boldsymbol{s}_p$ describes the spin in a coordinate system that rotates with the particle's momentum, the equation of spin motion relative to the particle motion becomes $\frac{\mathrm{d}}{\mathrm{d}t}\boldsymbol{s}_p = -\frac{q}{m}G\boldsymbol{B}_\perp \times \boldsymbol{s}_p$. The spin rotation relative to the orbit motion is therefore independent of energy, in contrast with the orbit deflection, which varies like $1/\gamma$. For protons with velocity v close to the speed of light, a fixed field integral of $\int B\mathrm{d}l = \pi\frac{mcv}{qG} \approx 5.48$ Tm leads to a spin rotation of π. Electrons require a field integral of 4.62 Tm for a rotation angle of π. For fixed orbit deflections and thus fixed ratio $\boldsymbol{B}_\perp/\gamma$, the spin precession rate, however, increases with energy.
- If the orbit is deflected by an angle ϕ in a transverse magnetic field, then the spin is rotated by an angle $G\gamma\phi$ relative to the orbit. A 1 mrad orbit kick for a proton with 920 GeV energy produces 100° of spin rotation. For electrons with 27.5 GeV in HERA-e, such an orbit kick produces 3.6° of spin rotation.
- In a flat ring without solenoids, the orbit deflection angle of 2π during one turn leads to $G\gamma$ full spin rotations around the vertical direction relative to the particle's direction. For 920 GeV, there are approximately 1756 such rotations, and at about 27.5 GeV, an electron in HERA-e performs 62.5 such rotations.
- Whenever the energy of a proton is increased by 523 MeV, the spin rotates once more per revolution around the ring. For an electron, the corresponding energy increase is 441 MeV.

2.1.2 Spin Motion in the Curvilinear Coordinate System

The design trajectory of a particle accelerator is described by a space curve $\boldsymbol{R}(l)$ with $|\mathrm{d}\boldsymbol{R}(l)| = \mathrm{d}l$. Particle motion can then be described in a coordinate system defined relative to this curve. The second unit vector is chosen tangential to the curve, and the first and third unit vectors are chosen to obtain a right-handed orthonormal set of vectors to form a coordinate system. The first and third unit vectors therefore lie in a plane perpendicular to the curve. The orientation of the unit vectors in that plane is arbitrary and can change along the curve. A common choice for fixing this orientation leads to the following unit vectors:

$$\boldsymbol{t}_2 = \frac{\mathrm{d}}{\mathrm{d}l}\boldsymbol{R}(l) \ , \quad \frac{1}{\rho} = |\frac{\mathrm{d}}{\mathrm{d}l}\boldsymbol{t}_2| \ , \quad \boldsymbol{t}_1 = -\rho\frac{\mathrm{d}}{\mathrm{d}l}\boldsymbol{t}_2 \ , \quad \boldsymbol{t}_3 = \boldsymbol{t}_1 \times \boldsymbol{t}_2 \ , \tag{2.6}$$

where $T = -\boldsymbol{t}_3 \cdot \frac{\mathrm{d}}{\mathrm{d}l}\boldsymbol{t}_1$ is the torsion of the space curve $\boldsymbol{R}(l)$. This set of unit vectors is called the Frenet-Serret coordinate system. From these definitions and with $\frac{\mathrm{d}}{\mathrm{d}l}(\boldsymbol{t}_1 \cdot \boldsymbol{t}_2) = \boldsymbol{t}_2 \cdot \frac{\mathrm{d}}{\mathrm{d}l}\boldsymbol{t}_1 - \frac{1}{\rho} = 0$ it follows that

$$\frac{\mathrm{d}}{\mathrm{d}l}\boldsymbol{t}_1 = -T\boldsymbol{t}_3 + \frac{1}{\rho}\boldsymbol{t}_2 \ , \quad \frac{\mathrm{d}}{\mathrm{d}l}\boldsymbol{t}_3 = -\boldsymbol{t}_2 \times \frac{\mathrm{d}}{\mathrm{d}l}\boldsymbol{t}_1 = T\boldsymbol{t}_1 \ . \tag{2.7}$$

A space vector $\boldsymbol{r}$ is parameterized by l and by the two coordinates x and y via

$$\boldsymbol{r} = \boldsymbol{R}(l) + x\boldsymbol{t}_1(l) + y\boldsymbol{t}_3(l) \ . \tag{2.8}$$

A space curve is then specified by the two functions $x(l)$ and $y(l)$. The derivative with respect to l of such a space curve $\boldsymbol{r}(l)$ is given by the relation

$$\frac{\mathrm{d}}{\mathrm{d}l}\boldsymbol{r}(l) = (\frac{\mathrm{d}}{\mathrm{d}l}x + Ty)\boldsymbol{t}_1 + (\frac{\mathrm{d}}{\mathrm{d}l}y - Tx)\boldsymbol{t}_3 + (1 + \frac{x}{\rho})\boldsymbol{t}_2 \ . \tag{2.9}$$

To simplify the equations of motion, one can remove the torsion T. For this one introduces the orthonormal coordinate vectors $\boldsymbol{e}_x$, $\boldsymbol{e}_l$, $\boldsymbol{e}_y$ by winding back the rotation produced by the torsion,

$$\vartheta = \int_{l_0}^{l} T(\tilde{l})d\tilde{l} \ , \quad \boldsymbol{e}_x + i\boldsymbol{e}_y = \mathrm{e}^{\mathrm{i}\vartheta}(\boldsymbol{t}_1 - \mathrm{i}\boldsymbol{t}_3) \ , \quad \boldsymbol{e}_l = \boldsymbol{t}_2 \ . \tag{2.10}$$

The coordinate system with the unit vectors $\boldsymbol{e}_x$, $\boldsymbol{e}_l$, $\boldsymbol{e}_y$ is shown in Fig. 2.1 and is called the curvilinear coordinate system. It follows that

$$\frac{\mathrm{d}}{\mathrm{d}l}\boldsymbol{e}_x + \mathrm{i}\frac{\mathrm{d}}{\mathrm{d}l}\boldsymbol{e}_y = \mathrm{e}^{\mathrm{i}\vartheta}\{-T\boldsymbol{t}_3 + \frac{1}{\rho}\boldsymbol{t}_2 - \mathrm{i}T\boldsymbol{t}_1 + \mathrm{i}T(\boldsymbol{t}_1 - \mathrm{i}\boldsymbol{t}_3)\} = \frac{\mathrm{e}^{\mathrm{i}\vartheta}}{\rho}\boldsymbol{e}_l \ . \tag{2.11}$$

For the right-handed orthonormal set of unit vectors $[\boldsymbol{e}_x, \boldsymbol{e}_l, \boldsymbol{e}_y]$ of the curvilinear coordinate system [5, 6], one obtains

$$\frac{\mathrm{d}}{\mathrm{d}l}\boldsymbol{R}(l) = \boldsymbol{e}_l \ , \quad \boldsymbol{r} = \boldsymbol{R}(l) + x\boldsymbol{e}_x + y\boldsymbol{e}_y \ , \tag{2.12}$$

$$\frac{\mathrm{d}}{\mathrm{d}l}\boldsymbol{e}_x = \frac{\cos\vartheta}{\rho}\boldsymbol{e}_l \ , \quad \frac{\mathrm{d}}{\mathrm{d}l}\boldsymbol{e}_y = \frac{\sin\vartheta}{\rho}\boldsymbol{e}_l \ , \tag{2.13}$$

$$\frac{\mathrm{d}}{\mathrm{d}l}\boldsymbol{e}_l = -\frac{1}{\rho}\boldsymbol{t}_1 = -\frac{1}{\rho}(\cos\vartheta\boldsymbol{e}_x + \sin\vartheta\boldsymbol{e}_y) \ , \tag{2.14}$$

$$\frac{\mathrm{d}}{\mathrm{d}l}\boldsymbol{r} = \boldsymbol{e}_x\frac{\mathrm{d}}{\mathrm{d}l}x + \boldsymbol{e}_y\frac{\mathrm{d}}{\mathrm{d}l}y + (1 + \frac{x\cos\vartheta + y\sin\vartheta}{\rho})\boldsymbol{e}_l \ . \tag{2.15}$$

For convenience, one can define the position vector $\boldsymbol{x} = (x, y)^T$, the curvature vector $\boldsymbol{\kappa} = (\cos\vartheta, \sin\vartheta)^T/\rho$, and the path length factor $h = 1 + \boldsymbol{x}\cdot\boldsymbol{\kappa}$. Vectors like $\boldsymbol{p}$ that have a component in the $\boldsymbol{e}_l$ direction are described by the equation

$$\boldsymbol{p} = p_x\boldsymbol{e}_x + p_y\boldsymbol{e}_y + p_l\boldsymbol{e}_l \tag{2.16}$$

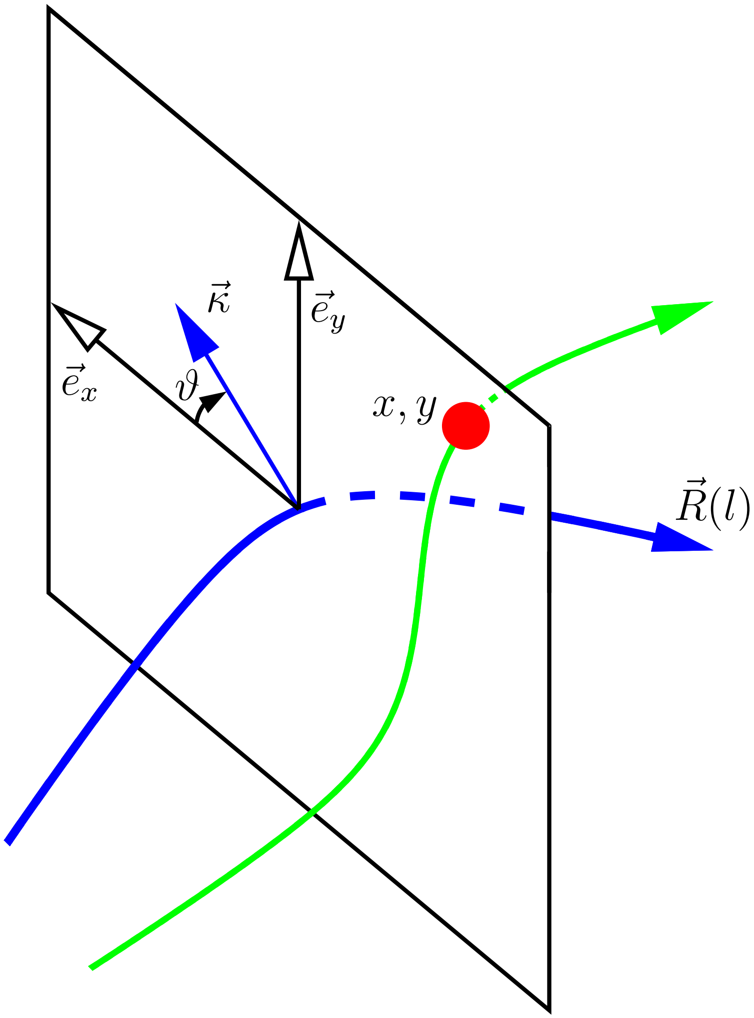

Fig. 2.1. The unit vectors $\boldsymbol{e}_x$ and $\boldsymbol{e}_y$, the curvature vector $\boldsymbol{\kappa}$ of the design curve $\boldsymbol{R}(l)$, and the generalized coordinates x, y, and l of the curvilinear coordinate system. This system is rotated by θ with respect to the Frenet-Serret coordinate system.

and have the derivative

$$\frac{\mathrm{d}}{\mathrm{d}l}\boldsymbol{p} = (\frac{\mathrm{d}}{\mathrm{d}l}p_x - p_l\kappa_x)\boldsymbol{e}_x + (\frac{\mathrm{d}}{\mathrm{d}l}p_y - p_l\kappa_y)\boldsymbol{e}_y + (\frac{\mathrm{d}}{\mathrm{d}l}p_l + p_x\kappa_x + p_y\kappa_y)\boldsymbol{e}_l \ . \quad (2.17)$$

To find the equations of particle motion in the curvilinear coordinate system, the independent coordinate in the equations of motion is changed from time t to arc length l by using

$$\frac{\mathrm{d}t}{\mathrm{d}l} = (\boldsymbol{e}_l \cdot \frac{\mathrm{d}}{\mathrm{d}l}\boldsymbol{r})/(\boldsymbol{e}_l \cdot \frac{\mathrm{d}}{\mathrm{d}t}\boldsymbol{r}) = \frac{h}{v}\frac{p}{p_l} \ , \quad (2.18)$$

where v is the velocity and $p = |\boldsymbol{p}|$ is the momentum. Properties of a reference particle moving on the design trajectory are indicated by subscripts 0, and we define the coordinates of all other particles relative to this reference particle through

$$x \ , \quad a = \frac{p_x}{p_0} \ , \quad y \ , \quad b = \frac{p_y}{p_0} \ , \quad \tau = (t_0 - t)\frac{K_0}{p_0} \ , \quad \delta = \frac{K - K_0}{K_0} \quad (2.19)$$

where $K = mc^2(\gamma - 1)$ is the kinetic energy. These six phase space variables are denoted by the phase space vector $\boldsymbol{z}$. The coordinate pairs (x, a), (y, b), and (τ, δ) are canonically conjugate [7, 8]. Because $\boldsymbol{R}(l)$ is the path of the reference particle, the particle transport in these variables is origin preserving, because a particle with $\boldsymbol{z} = 0$ will continue to travel along the design trajectory. The equation of motion for these phase space coordinates with l as independent variable is obtained by transforming the Lorentz force equation. Here the Stern-Gerlach forces are neglected because they are very small in comparison with the Lorentz force. In [9, 10, 11, 12] it is pointed out that at orbital resonances the small perturbations due to the Stern-Gerlach force can become relevant, because they can turn integrable motion into non-integrable motion, preventing the use of action angle variables, and because they can lead to a secular growth of the orbital amplitudes. But because no practical schemes for using Stern-Gerlach force in accelerators have been found so far [13, 14], we do not consider them here. Furthermore, many of the derivations will be restricted to motion that does not have orbital resonances.

To transform the equations of spin motion into the curvilinear coordinate system, the relation $\frac{\mathrm{d}}{\mathrm{d}l}t = \frac{h}{v}\frac{p}{p_l}$ from (2.18) is used. The spin direction $\boldsymbol{s}$ can be expressed by its components in the curvilinear coordinate system, and the column vector of these components is written as $\boldsymbol{S}$. A potential torsion of the reference curve does not enter the equations of particle motion in this coordinate system and it also does not enter the equation of spin motion,

$$\boldsymbol{s} = S_x\boldsymbol{e}_x + S_y\boldsymbol{e}_y + S_l\boldsymbol{e}_l \ , \quad (2.20)$$

$$\begin{aligned}\frac{\mathrm{d}}{\mathrm{d}l}\boldsymbol{s} &= (\frac{\mathrm{d}}{\mathrm{d}l}S_x - S_l\kappa_x)\boldsymbol{e}_x + (\frac{\mathrm{d}}{\mathrm{d}l}S_y - S_l\kappa_y)\boldsymbol{e}_y + (\frac{\mathrm{d}}{\mathrm{d}l}S_l + S_x\kappa_x + S_y\kappa_y)\boldsymbol{e}_l \\ &= \frac{h}{v}\frac{p}{p_l}\boldsymbol{\Omega}_{BMT}(\boldsymbol{r}, \boldsymbol{p}, l) \times \boldsymbol{s} \ . \quad (2.21)\end{aligned}$$

For the column vector $\boldsymbol{S}$, the equation of motion is therefore

$$\frac{\mathrm{d}}{\mathrm{d}l}\boldsymbol{S} = \{\boldsymbol{\Omega}_{BMT}(\boldsymbol{r},\boldsymbol{p},l)\frac{hp}{vp_l} - \boldsymbol{\kappa}\times\boldsymbol{e}_l\}\times\boldsymbol{S}\ . \tag{2.22}$$

The precession vector depends on the position and the momentum. This can be expressed as a dependence on l and on the 6-dimensional phase space variable $\boldsymbol{z}$.

2.1.3 Equations of Motion for Spins and Spin Fields

In a circular accelerator with circumference L, it is convenient to choose the azimuth $\theta = 2\pi l/L$ as independent variable, rather than the arc length l of the design trajectory. The coordinate vectors are not changed. All fields are then 2π-periodic in θ. The equation of particle motion is therefore 2π-periodic,

$$\frac{\mathrm{d}}{\mathrm{d}\theta}\boldsymbol{z} = \boldsymbol{v}(\boldsymbol{z},\theta)\ ,\quad \boldsymbol{v}(\boldsymbol{z},\theta+2\pi) = \boldsymbol{v}(\boldsymbol{z},\theta)\ , \tag{2.23}$$

$$\frac{\mathrm{d}}{\mathrm{d}\theta}\boldsymbol{S} = \boldsymbol{\Omega}(\boldsymbol{z},\theta)\times\boldsymbol{S}\ ,\quad \boldsymbol{\Omega}(\boldsymbol{z},\theta+2\pi) = \boldsymbol{\Omega}(\boldsymbol{z},\theta)\ , \tag{2.24}$$

where the precession vector is obtained from (2.22) as

$$\boldsymbol{\Omega}(\boldsymbol{z},\theta) = \frac{L}{2\pi}(\boldsymbol{\Omega}_{BMT}(\boldsymbol{r},\boldsymbol{p},l)\frac{hp}{vp_l} - \boldsymbol{\kappa}\times\boldsymbol{e}_l)\ . \tag{2.25}$$

A particle starting with an initial phase space coordinate $\boldsymbol{z}_i$ and with an initial spin $\boldsymbol{S}_i$ propagates around an accelerator according to the equations of spin-orbit motion (2.24). After it has traveled from azimuth θ_0 to θ, it will have the coordinates $\boldsymbol{z}(\theta) = \boldsymbol{M}(\boldsymbol{z}_i,\theta_0;\theta)$ and $\boldsymbol{S}(\theta) = \mathsf{R}(\boldsymbol{z}_i,\theta_0;\theta)\boldsymbol{S}_i$, where $\boldsymbol{M}(\boldsymbol{z}_i,\theta_0;\theta)$ is called the transport map and the orthogonal matrix $\mathsf{R}(\boldsymbol{z}_i,\theta_0;\theta)$ is called the spin transport matrix.

This rotation matrix can be computed by tracking three linearly independent spins along the phase space trajectory starting with $\boldsymbol{z}_i$ at azimuth θ_0. Transporting the nine real components of these vectors is however not an efficient way of simulating spin motion, because a rotation can be described by three real numbers. Furthermore, the orthogonal structure of R does not change the angle between two spins that travel along the same trajectory and it does not change the length of a spin. These properties can be violated either by numerical errors or by computational approximations when individual spins are propagated. Therefore, more efficient methods will be introduced below.

A particle beam consists of particles at different phase space positions. Each particle can have a different spin direction. The function $\boldsymbol{f}(\boldsymbol{z},\theta)$ with $|\boldsymbol{f}| = 1$ describing the spin direction for a particle at phase space point $\boldsymbol{z}$ at azimuth θ is called a spin field. The equation of motion for a spin field is thus

$$\frac{\mathrm{d}}{\mathrm{d}\theta}\boldsymbol{f} = \partial_\theta\boldsymbol{f} + [\boldsymbol{v}(\boldsymbol{z},\theta)\cdot\partial_{\boldsymbol{z}}]\boldsymbol{f} = \boldsymbol{\Omega}(\boldsymbol{z},\theta)\times\boldsymbol{f}\ . \tag{2.26}$$

2.1.4 Equation of Motion for the Spin Transport Matrix

In the following sections, I will investigate various methods for describing the propagation of spins and spin fields along particle trajectories. Inserting the relation $\boldsymbol{S}(\theta) = \mathsf{R}(\boldsymbol{z}_i, \theta_0; \theta)\boldsymbol{S}_i$ into the equation of motion (2.24) leads to the equation of motion for the spin transport matrix

$$\partial_\theta \mathsf{R}(\boldsymbol{z}_i, \theta_0; \theta) = \begin{pmatrix} 0 & -\Omega_3 & \Omega_2 \\ \Omega_3 & 0 & -\Omega_1 \\ -\Omega_2 & \Omega_1 & 0 \end{pmatrix} \mathsf{R}(\boldsymbol{z}_i, \theta_0; \theta) \;, \tag{2.27}$$

with the initial condition that $\mathsf{R}(\boldsymbol{z}_i, \theta_0; \theta_0)$ is the 3×3 unit matrix. The spin rotation matrix through a set of optical elements for a trajectory with the coordinates $\boldsymbol{z}_{n-1}$ at the entrance of the nth element is computed by multiplying the spin transport matrices $\mathsf{R}_n(\boldsymbol{z}_{n-1})$ of the individual elements [15, 16]. This method has the same disadvantage as the transport of three individual spins. Nine real components are transported, where three could already describe a rotation. Furthermore, computational inaccuracies in solving (2.27) can again lead to violations of the orthogonal structure of the matrix, which therefore has to be orthogonalized whenever such violations become problematic.

Using the transport matrix, a spin is propagated according to the relation $\boldsymbol{S}(\theta) = \mathsf{R}(\boldsymbol{z}_i, \theta_0; \theta)\boldsymbol{S}_i$ and a spin field $\boldsymbol{f}(\boldsymbol{z}, \theta)$ can be propagated using the relation

$$\boldsymbol{f}(\boldsymbol{z}, \theta) = \mathsf{R}(\boldsymbol{z}_i, \theta_0; \theta)\boldsymbol{f}(\boldsymbol{z}_i, \theta_0) \quad \text{with} \quad \boldsymbol{z}_i = \boldsymbol{M}(\boldsymbol{z}, \theta; \theta_0) \;, \tag{2.28}$$

where $\boldsymbol{M}(\boldsymbol{z}, \theta; \theta_0) = \boldsymbol{M}^{-1}(\boldsymbol{z}, \theta_0; \theta)$ is the inverse transport map describing the reverse motion from θ back to θ_0.

2.1.5 Equation of Motion for the Spin Transport Quaternion

As will now be demonstrated, it is more efficient to use an SU(2) representation rather than the SO(3) matrices when describing the rotations of spins. The matrix R of (2.27) describes the rotation of an initial spin $\boldsymbol{S}_i$ around a unit rotation vector $\boldsymbol{e}$ by an angle α. Splitting the spin into components parallel and perpendicular to $\boldsymbol{e}$, one obtains

$$\boldsymbol{S}(\theta) = \boldsymbol{e}(\boldsymbol{S}_i \cdot \boldsymbol{e}) + \cos\alpha[\boldsymbol{S} - \boldsymbol{e}(\boldsymbol{S}_i \cdot \boldsymbol{e})] + \sin\alpha\, \boldsymbol{e} \times \boldsymbol{S}_i \;. \tag{2.29}$$

With the Euler parameters $a_0 = \cos\frac{\alpha}{2}$ and $\boldsymbol{a} = \sin\frac{\alpha}{2}\boldsymbol{e}$, the matrix R can therefore be written as [17, 18]

$$R_{ij} = (a_0^2 - \boldsymbol{a}^2)\delta_{ij} + 2a_i a_j - 2a_0 \epsilon_{ijk} a_k \;, \tag{2.30}$$

where the vector product is expressed using the totally antisymmetric tensor ϵ_{ijk}. The SU(2) matrix representing a rotation around $\boldsymbol{e}$ by the angle α is given by the quaternion

$$A = \exp(-\mathrm{i}\frac{\alpha}{2}\boldsymbol{e}\cdot\boldsymbol{\sigma}) = a_0 1_2 - \mathrm{i}\boldsymbol{a}\cdot\boldsymbol{\sigma}\ , \quad a_0^2 + \boldsymbol{a}^2 = 1\ . \tag{2.31}$$

Here the elements of the vector $\boldsymbol{\sigma}$ are the three Pauli matrices with $\sigma_i\sigma_j = i\epsilon_{ijk}\sigma_k + \delta_{ij}1_2$ and $Tr(\sigma_i) = 0$. Using this, the matrix elements R_{ij} can be expressed by

$$R_{ij} = \frac{1}{2}Tr\left(\sigma_i \mathsf{A}\sigma_j\mathsf{A}^{-1}\right) \tag{2.32}$$

because this is equal to

$$\begin{aligned}
&\frac{1}{2}Tr\left(\sigma_i[a_0 - \mathrm{i}a_k\sigma_k]\sigma_j\mathsf{A}^{-1}\right) \qquad (2.33)\\
&= \frac{1}{2}Tr\left([\sigma_i\sigma_j a_0 - \mathrm{i}\sigma_i a_k\{\mathrm{i}\epsilon_{kjm}\sigma_m + \delta_{kj}\}]\mathsf{A}^{-1}\right)\\
&= \frac{1}{2}Tr\left([\{\mathrm{i}\epsilon_{ijk}\sigma_k + \delta_{ij}\}a_0 + \{\mathrm{i}\epsilon_{imn}\sigma_n + \delta_{im}\}a_k\epsilon_{kjm} - \mathrm{i}\sigma_i a_j]\mathsf{A}^{-1}\right)\\
&= -\epsilon_{ijk}a_k a_0 + \delta_{ij}a_0^2 - a_k(\delta_{nk}\delta_{ij} - \delta_{ik}\delta_{nj})a_n + a_k\epsilon_{kji}a_0 + a_i a_j\\
&= (a_0^2 - \boldsymbol{a}^2)\delta_{ij} + 2a_i a_j - 2a_0\epsilon_{ijk}a_k\ .
\end{aligned}$$

Therefore, $\boldsymbol{S}_i\cdot\boldsymbol{\sigma}$ is transported to $\boldsymbol{S}_f\cdot\boldsymbol{\sigma} = \mathsf{A}(\boldsymbol{S}_i\cdot\boldsymbol{\sigma})\mathsf{A}^{-1}$.

If a particle traverses an optical element that rotates the spin according to the quaternion A and then passes through an element that rotates the spin according to the quaternion B, the total rotation of the spin is given by

$$\begin{aligned}
C &= c_0 1_2 - \mathrm{i}\boldsymbol{c}\cdot\boldsymbol{\sigma} = (b_0 1_2 - \mathrm{i}\boldsymbol{b}\cdot\boldsymbol{\sigma})(a_0 1_2 - \mathrm{i}\boldsymbol{a}\cdot\boldsymbol{\sigma})\\
&= (b_0 a_0 - \boldsymbol{b}\cdot\boldsymbol{a})1_2 - \mathrm{i}(b_0\boldsymbol{a} + \boldsymbol{b}a_0 + \boldsymbol{b}\times\boldsymbol{a})\cdot\boldsymbol{\sigma}\ .
\end{aligned} \tag{2.34}$$

This concatenation of quaternions can be written in matrix form as

$$\boldsymbol{C} = \begin{pmatrix} c_0\\ \boldsymbol{c}\end{pmatrix} = \mathsf{B}\begin{pmatrix} a_0\\ \boldsymbol{a}\end{pmatrix}\ , \quad \mathsf{B} = \begin{pmatrix} b_0 & -b_1 & -b_2 & -b_3\\ b_1 & b_0 & -b_3 & b_2\\ b_2 & b_3 & b_0 & -b_1\\ b_3 & -b_2 & b_1 & b_0\end{pmatrix}\ . \tag{2.35}$$

Sometimes it is useful to have the quaternions appear in reversed order, even though particles travel first through the optical element corresponding to A,

$$\boldsymbol{C} = \begin{pmatrix} c_0\\ \boldsymbol{c}\end{pmatrix} = \tilde{\mathsf{A}}\begin{pmatrix} b_0\\ \boldsymbol{b}\end{pmatrix}\ , \quad \tilde{\mathsf{A}} = \begin{pmatrix} a_0 & -a_1 & -a_2 & -a_3\\ a_1 & a_0 & a_3 & -a_2\\ a_2 & -a_3 & a_0 & a_1\\ a_3 & a_2 & -a_1 & a_0\end{pmatrix}\ . \tag{2.36}$$

Because any vector of Euler parameters has unit length, the matrices B and $\tilde{\mathsf{A}}$ are both orthogonal.

It has turned out to be useful to represent rotations in terms of a_0 and $\boldsymbol{a}$ for the following three reasons:

1. Only 4 real components are needed to describe and concatenate the rotation of spins,

2. Even when numerical inaccuracies cause a small error in the computation of this representation, one can always normalize so that $a_0^2 + \boldsymbol{a}^2 = 1$, which then always leads to an orthogonal spin transport matrix,
3. Only 28 floating point operations are required to compute the combined spin transport quaternion of two particle optical elements from their individual quaternions. The multiplication of the spin transport matrices requires 45 floating point operations.

While particles are propagating along the design curve by a distance $\mathrm{d}\theta$, spins are rotated by an angle $|\boldsymbol{\Omega}|\mathrm{d}\theta$ around the vector $\boldsymbol{\Omega}$. After having been propagated to θ by the quaternion A, a spin gets propagated from θ to $\theta + \mathrm{d}\theta$ by the quaternion B with $b_0 = 1$ and $\boldsymbol{b} = \frac{1}{2}\boldsymbol{\Omega}\mathrm{d}\theta$. The resulting total rotation is given by $A + \mathrm{d}\theta\frac{\mathrm{d}}{\mathrm{d}\theta}A$ and one obtains the differential equation

$$\frac{\mathrm{d}}{\mathrm{d}\theta}\begin{pmatrix} a_0 \\ \boldsymbol{a} \end{pmatrix} = \frac{1}{2}\begin{pmatrix} 0 & -\Omega_1 & -\Omega_2 & -\Omega_3 \\ \Omega_1 & 0 & -\Omega_3 & \Omega_2 \\ \Omega_2 & \Omega_3 & 0 & -\Omega_1 \\ \Omega_3 & -\Omega_2 & \Omega_1 & 0 \end{pmatrix}\begin{pmatrix} a_0 \\ \boldsymbol{a} \end{pmatrix} . \tag{2.37}$$

Writing the vector of Euler parameters as $\boldsymbol{A}$ and the matrix as Ω, the equations of spin-orbit motion take the form

$$\frac{\mathrm{d}}{\mathrm{d}\theta}\boldsymbol{z} = \boldsymbol{v}(\boldsymbol{z},\theta) , \quad \frac{\mathrm{d}}{\mathrm{d}\theta}\boldsymbol{A} = \frac{1}{2}\Omega(\boldsymbol{z},\theta)\boldsymbol{A} . \tag{2.38}$$

The starting conditions at the initial azimuth θ_0 are $\boldsymbol{z} = \boldsymbol{z}_i$, $a_0 = 1$, and $\boldsymbol{a} = 0$. Sometimes, an equation of motion for the quaternion A itself is used instead,

$$\frac{\mathrm{d}}{\mathrm{d}\theta}A = -\mathrm{i}\frac{1}{2}\boldsymbol{\Omega}\cdot\boldsymbol{\sigma}A , \tag{2.39}$$

with the starting condition $A = 1_2$. When $\boldsymbol{A}(\boldsymbol{z}_i, \theta_0; \theta)$ is known, $\mathsf{R}(\boldsymbol{z}_i, \theta_0; \theta)$ can be constructed using (2.30) and one can again propagate an initial spin $\boldsymbol{S}_i$ and a spin field $\boldsymbol{f}(\boldsymbol{z}_i, \theta_0)$ by (2.28).

2.1.6 Equation of Motion for Spinors

In the SU(2) representation of rotations, a spin $\boldsymbol{S}$ is written in terms of the spinor $\Psi = (\psi_1, \psi_2)^T$ as $\boldsymbol{S} = \Psi^\dagger\boldsymbol{\sigma}\Psi$ where ψ_1 and ψ_2 are two complex numbers [17]. To have $|\boldsymbol{S}| = 1$, it is required that $|\psi_1|^2 + |\psi_2|^2 = 1$. The components of a spinor can be conveniently expressed in terms of polar coordinates ϑ and ϕ of the corresponding spin direction. This is illustrated by the fact that the following spinor and the following vector describe the same spin:

$$\Psi = \begin{pmatrix} \psi_1 \\ \psi_2 \end{pmatrix} = \begin{pmatrix} \cos\frac{\vartheta}{2}\mathrm{e}^{\mathrm{i}\phi_1} \\ \sin\frac{\vartheta}{2}\mathrm{e}^{\mathrm{i}\phi_2} \end{pmatrix} \iff \boldsymbol{S} = \begin{pmatrix} \sin\vartheta\cos(\phi_2 - \phi_1) \\ \sin\vartheta\sin(\phi_2 - \phi_1) \\ \cos\vartheta \end{pmatrix} . \tag{2.40}$$

The equation of motion for the spinor is

$$\frac{\mathrm{d}}{\mathrm{d}\theta}\Psi = -\mathrm{i}\frac{1}{2}(\boldsymbol{\Omega}\cdot\boldsymbol{\sigma})\Psi \ , \tag{2.41}$$

which leads back to the vector form of the differential equation of spin motion,

$$\begin{aligned}\frac{\mathrm{d}}{\mathrm{d}\theta}\boldsymbol{S} &= (\frac{\mathrm{d}}{\mathrm{d}\theta}\Psi^\dagger)\boldsymbol{\sigma}\Psi + \Psi^\dagger\boldsymbol{\sigma}(\frac{\mathrm{d}}{\mathrm{d}\theta}\Psi) \\ &= i\frac{1}{2}\Psi^\dagger[(\boldsymbol{\Omega}\cdot\boldsymbol{\sigma})\boldsymbol{\sigma} - \boldsymbol{\sigma}(\boldsymbol{\Omega}\cdot\boldsymbol{\sigma})]\Psi = \Psi^\dagger[\boldsymbol{\Omega}\times\boldsymbol{\sigma}]\Psi = \boldsymbol{\Omega}\times\boldsymbol{S} \ .\end{aligned} \tag{2.42}$$

If a spin rotates by an angle α around a θ independent unit rotation vector $\boldsymbol{e}$ while the particle travels to θ, then (2.41) leads to the spinor propagation relation $\Psi(\theta) = \exp(-\mathrm{i}\frac{\alpha}{2}\boldsymbol{e}\cdot\boldsymbol{\sigma})\Psi_i$. A spinor is therefore propagated by the spin transport quaternion of (2.31),

$$\Psi(\theta) = (a_0 1_2 - \mathrm{i}\boldsymbol{a}\cdot\boldsymbol{\sigma})\Psi_i \ . \tag{2.43}$$

If a spin is parallel to the rotation vector $\boldsymbol{e}$, it is not changed during the rotation. But the corresponding spinor Ψ_e is changed by a phase factor. To show this, the polar coordinates ϑ and ϕ of the vector $\boldsymbol{e}$ are used and the free phase factor of the spinor is indicated by $\mathrm{e}^{\mathrm{i}\xi}$,

$$\Psi_e = \mathrm{e}^{\mathrm{i}\xi}\begin{pmatrix}\cos\frac{\vartheta}{2} \\ \sin\frac{\vartheta}{2}\mathrm{e}^{\mathrm{i}\phi}\end{pmatrix} \ , \tag{2.44}$$

$$\begin{aligned}\Psi(\theta) &= \exp(-\mathrm{i}\frac{\alpha}{2}\boldsymbol{e}\cdot\boldsymbol{\sigma})\Psi_e = (\cos\frac{\alpha}{2} - \mathrm{i}\sin\frac{\alpha}{2}\boldsymbol{\sigma}\cdot\boldsymbol{e})\Psi_e \\ &= \begin{pmatrix}\cos\frac{\alpha}{2} - \mathrm{i}\sin\frac{\alpha}{2}\cos\vartheta & -\mathrm{i}\mathrm{e}^{-\mathrm{i}\phi}\sin\frac{\alpha}{2}\sin\vartheta \\ -\mathrm{i}\mathrm{e}^{\mathrm{i}\phi}\sin\frac{\alpha}{2}\sin\vartheta & \cos\frac{\alpha}{2} + \mathrm{i}\sin\frac{\alpha}{2}\cos\vartheta\end{pmatrix}\begin{pmatrix}\cos\frac{\vartheta}{2} \\ \sin\frac{\vartheta}{2}\mathrm{e}^{\mathrm{i}\phi}\end{pmatrix}\mathrm{e}^{\mathrm{i}\xi} \\ &= \mathrm{e}^{-\mathrm{i}\frac{\alpha}{2}}\Psi_e \ .\end{aligned} \tag{2.45}$$

In the spinor formalism, the phase change of the special spinor Ψ_e that describes the rotation vector $\boldsymbol{e}$ can therefore be used to determine the rotation angle α.

Once Ψ_i at θ_0 has been propagated to Ψ at θ, the spin of the particle can be computed as $\boldsymbol{S} = \Psi^\dagger\boldsymbol{\sigma}\Psi$. Alternatively, one can propagate the spinor $\Psi_i = (1,0)^T$ to obtain $\Psi = (a_0 - \mathrm{i}a_3, -\mathrm{i}a_1 + a_2)^T$ from (2.43). From the real and imaginary parts one then obtains the spin transport quaternion, which makes this method equivalent to the transportation of quaternions in Sect. 2.1.5.

A spin field $\boldsymbol{f}(\boldsymbol{z},\theta)$ can be represented by the phase space function $\Psi_{\boldsymbol{f}}(\boldsymbol{z},\theta)$ with $|\psi_1|^2 + |\psi_2|^2 = 1$. Then $\Psi_{\boldsymbol{f}}$ satisfies the equation of motion

$$\begin{aligned}\frac{\mathrm{d}}{\mathrm{d}\theta}\Psi_{\boldsymbol{f}}(\boldsymbol{z},\theta) &= \partial_\theta\Psi_{\boldsymbol{f}}(\boldsymbol{z},\theta) + [\boldsymbol{v}(\boldsymbol{z},\theta)\cdot\partial_{\boldsymbol{z}}]\Psi(\boldsymbol{z},\theta) \\ &= -\mathrm{i}\frac{1}{2}[\boldsymbol{\Omega}(\boldsymbol{z},\theta)\cdot\boldsymbol{\sigma}]\Psi(\boldsymbol{z},\theta) \ .\end{aligned} \tag{2.46}$$

In analogy to (2.28), such a spinor field is transported from azimuth θ_0 to θ by the spin transport quaternion $A(\boldsymbol{z}_i,\theta_0,\theta)$,

$$\Psi(\boldsymbol{z},\theta)=A(\boldsymbol{z}_i,\theta_0;\theta)\Psi(\boldsymbol{z}_i,\theta_0) \quad \text{with} \quad \boldsymbol{z}_i=\boldsymbol{M}(\boldsymbol{z},\theta;\theta_0)\ . \tag{2.47}$$

A useful collection of equations for the description of spin motion can be found in [19].

2.2 Spin Motion in Circular Accelerators

2.2.1 Spin Motion on the Closed Orbit and Imperfection Resonances

Before I analyze spin motion on a general particle trajectory in a circular accelerator, I will examine spin motion on the closed orbit. If no field errors, misaligned elements, or energy deviations are present, this orbit is the design trajectory of the accelerator. After particles with different spins have traveled one turn along the closed orbit from azimuth θ_0 to azimuth $\theta_0+2\pi$, all spins have rotated around some effective unit rotation axis $\boldsymbol{n}_0(\theta_0)$ by a rotation angle $2\pi\nu_0$. The angle of rotation around $\boldsymbol{n}_0$ divided by 2π is called the closed-orbit spin tune ν_0 and does not depend on the azimuth θ_0 at which $\boldsymbol{n}_0$ is determined. In the following discussion, θ_0 is an arbitrary but fixed azimuth that will no longer be indicated in the argument of $\boldsymbol{n}_0$. This spin rotation for the closed orbit $\boldsymbol{z}=0$ is described by the spin transport matrix $\mathsf{R}(0,\theta_0;\theta_0+2\pi)$. In a flat accelerator without solenoids and field errors and misaligned elements, the closed orbit is in the horizontal plane and passes only through vertical magnetic fields. Therefore, $\boldsymbol{n}_0$ is vertical and $\nu_0=G\gamma$ according to Sect. 2.1.1. When ν_0 is close to an integer, a case that is referred to as being near an *imperfection resonance*, the rotation matrix is close to the identity and spin directions have hardly changed after one turn. Misalignments distort the closed orbit of a flat ring and create horizontal field components on it, which produce spin precessions away from the vertical direction. For small misalignments, these rotations around the horizontal might be very small but they can still dominate spin motion when the main fields hardly produce any net spin rotation during one turn, i.e., close to integer values of ν_0. Thus, the rotation axis $\boldsymbol{n}_0$ for spins is almost vertical away from imperfection resonances but it can be nearly horizontal in their vicinity. At a fixed azimuth θ_0, the rotation axis $\boldsymbol{n}_0$ changes smoothly with ν_0 in between these extremes.

When a particle is accelerated such that ν_0 crosses an integer value, the rotation vector $\boldsymbol{n}_0$ can change strongly with energy. When the rate of spin rotation is much greater than the rate of change of the rotation vector, a spin that is nearly parallel to $\boldsymbol{n}_0$ is dragged along with the changing $\boldsymbol{n}_0$. The projection of a spin on $\boldsymbol{n}_0$ hardly changes during this procedure and will be shown to be an adiabatic invariant. To understand this fact, imagine that the spin rotates around $\boldsymbol{n}_0$ so that the changing $\boldsymbol{n}_0$ shifts alternately toward and away from the spin. Due to this rapid rotation, both cases happen in quick succession and the total effect averages out. This causes the spin to follow the slow change of $\boldsymbol{n}_0$.

Because it is inadvisable to let misalignments dominate spin motion, imperfection resonances ought to be avoided. However, because $\nu_0 = G\gamma$ in a flat ring, the closed-orbit spin tune changes during acceleration and the crossing of imperfection resonances is unavoidable. There are three possible regimes for resonance crossing [20].

- If the effects of misalignments are very small, the resonance can be crossed so rapidly that the spins hardly react and the beam's polarization is hardly changed.
- When the effect of misalignments is very strong, the rotation axis $\boldsymbol{n}_0$ changes very slowly during acceleration because the precession around the horizontal fields of misaligned elements starts to dominate already far from an imperfection resonance. Then the spins can follow the slow change of $\boldsymbol{n}_0$. But while the average $\langle \boldsymbol{S} \rangle_N$ of the spin directions changes, the change of the polarization $P = |\langle \boldsymbol{S} \rangle_N|$ is very limited. The change of a spin's projection on $\boldsymbol{n}_0$ as $\boldsymbol{n}_0$ changes slowly will be discussed in the next section.
- When the effect of misalignments has an intermediate strength, the angle between each spin and the $\boldsymbol{n}_0$ axis will have changed after the resonance is crossed. Because all spins subsequently rotate around $\boldsymbol{n}_0$, this reduces the time-averaged polarization.

The following two strategies can therefore be used to limit the reduction of polarization when imperfection resonances are crossed:

- Careful correction of the closed orbit to limit horizontal field components [20].
- Increasing the horizontal field components, for example by introducing a solenoid magnet. Devices that are deliberately used to increase the effect of imperfection resonances are referred to as partial snakes [21, 22, 23]. A solenoid magnet has been installed in the AGS that rotates spins by about 10° and very effectively avoids polarization loss at integer resonances of the closed-orbit spin tune. To avoid coupling between horizontal and vertical motion by the solenoid, a helical dipole partial snake has been constructed for the AGS [24, 26] and operates successfully [27], and the AGS can routinely produce 45% to 50% of polarization.

Because the closed orbit is not very well controlled in DESY III, use of a solenoid partial snake for overcoming the $\nu_0 = G\gamma = 8$ imperfection resonance at 4.08 GeV/c can probably not be avoided. However, it would suffice to have it rotate spins by 14° around the longitudinal direction [28]. Figure 2.2 (left) shows the results of a numerical simulation of how the spin of a particle on the closed orbit would change under the influence of a solenoid that rotates the spins by 0.8° while it is accelerated from $G\gamma = 7.97$ to $G\gamma = 8.03$. No misalignments are considered. A realistic acceleration rate of 5 keV/turn was assumed. Figure 2.2 (right) shows that while s_3 changes sign, the product $s_3 = \boldsymbol{S} \cdot \boldsymbol{n}_0$ hardly changed during the slow acceleration. Obviously, $\boldsymbol{n}_0$ has also smoothly changed from pointing vertically up to vertically down.

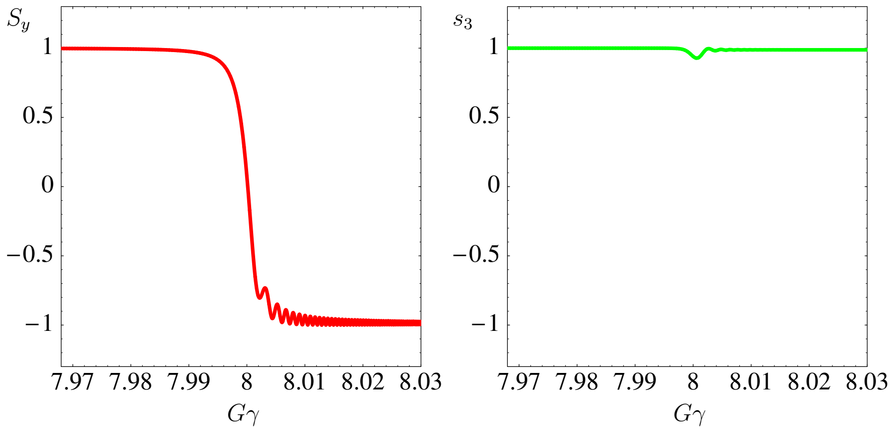

Fig. 2.2. The change of $S_y = \boldsymbol{S} \cdot \boldsymbol{e}_y$ (*left*) and the change of $s_3 = \boldsymbol{S} \cdot \boldsymbol{n}_0$ (*right*) during the acceleration from $G\gamma = 7.97$ to $G\gamma = 8.03$ for particles on the closed orbit in DESY III in the presence of a 0.8° solenoid partial snake.

Although the rotation vector $\boldsymbol{n}_0$ is only unique up to a sign, it is here not helpful to change the sign convention because $\boldsymbol{n}_0$ would then not be changing smoothly during the acceleration process. A small change close to $G\gamma = 8$ disappears after the resonance is crossed. The small reduction of polarization for $G\gamma = 8$ is due to the fact that the adiabatic invariant is not an exact invariant but can change by small amounts. The subsequent recovery of polarization is due to the symmetry of spin motion above and below the resonance. The adiabatic following of $\boldsymbol{n}_0$ shown in this figure illustrates how a reduction of polarization at imperfection resonances can be avoided. An analysis of the small reduction followed by a partial recovery of the s_3 needs more detailed computations of spin dynamics and is not a general consequence of adiabatic invariance.

For the acceleration process in a simple accelerator model, the change of $\boldsymbol{S} \cdot \boldsymbol{n}_0$ at a fixed azimuth θ_0 is described by the Froissart-Stora formula as will be seen in Sect. 2.2.10. This formula allows a quantitative computation of the limited reduction of polarization when either crossing a weak resonance relatively quickly or when crossing a strong resonance relatively slowly.

2.2.2 The Adiabatic Spin Invariant on the Closed Orbit

It was conjectured above that spins that are nearly parallel to $\boldsymbol{n}_0$ will follow slow changes of this net rotation vector at θ_0. In this section, I will prove this property by showing that $\boldsymbol{S}(\theta) \cdot \boldsymbol{n}_0(\theta)$ is an adiabatic invariant of motion. For simplicity, a coordinate system is introduced that has $\boldsymbol{n}_0(\theta)$ as one of its coordinate vectors and in which the spin motion on the closed orbit is as simple as possible.

A particle that travels along the closed orbit $\boldsymbol{z} = 0$ with its spin initially parallel to $\boldsymbol{n}_0$ at θ_0 will always have $\boldsymbol{S}(\theta_0) = \boldsymbol{n}_0$ whenever it passes the azimuth θ_0. Thus, for this particle not only the orbit but also the spin motion is 2π-periodic. Therefore at every θ, this periodic spin must be parallel to the net rotation vector $\boldsymbol{n}_0(\theta) = \boldsymbol{S}(\theta)$. The rotation axis $\boldsymbol{n}_0(\theta)$ of the one turn spin transport matrix is therefore sometimes called the spin closed orbit [18] and it satisfies the equation of spin motion on the closed orbit. Then, denoting the precession vector $\boldsymbol{\Omega}(\boldsymbol{z},\theta)$ on the closed orbit by $\boldsymbol{\Omega}_0(\theta)$,

$$\frac{\mathrm{d}}{\mathrm{d}\theta}\boldsymbol{n}_0(\theta) = \boldsymbol{\Omega}_0(\theta) \times \boldsymbol{n}_0(\theta) \ , \quad \boldsymbol{n}_0(\theta) = \boldsymbol{n}_0(\theta + 2\pi) \ . \tag{2.48}$$

Such a 2π-periodic vector $\boldsymbol{n}_0(\theta)$ always exists on the closed orbit; it is the rotation axis of the spin rotation matrix $\mathsf{R}_0(\theta) = \mathsf{R}(0,\theta;\theta + 2\pi)$ for one turn along the closed orbit. When introducing $\boldsymbol{n}_0$, the emphasis was on flat rings with vertical $\boldsymbol{n}_0$. But rings are frequently designed so that $\boldsymbol{n}_0$ is not vertical everywhere. For example, in rings where spin rotators are used to provide longitudinal polarization for experiments, $\boldsymbol{n}_0$ is longitudinal at the injection point.

Two unit vectors $\boldsymbol{m}_0(\theta)$ and $\boldsymbol{l}_0(\theta)$ are now chosen that at θ_0 make up the right-handed coordinate system $[\boldsymbol{m}_0(\theta_0), \boldsymbol{l}_0(\theta_0), \boldsymbol{n}_0(\theta_0)]$ and propagate around the ring according to the T-BMT equation on the closed orbit,

$$\frac{\mathrm{d}}{\mathrm{d}\theta}\boldsymbol{m}_0 = \boldsymbol{\Omega}_0(\theta) \times \boldsymbol{m}_0 \ , \quad \frac{\mathrm{d}}{\mathrm{d}\theta}\boldsymbol{l}_0 = \boldsymbol{\Omega}_0(\theta) \times \boldsymbol{l}_0 \ . \tag{2.49}$$

The three unit vectors will always constitute a right-handed coordinate system, because all three get rotated by the same precession equation. Whereas $\boldsymbol{n}_0$ is periodic around the ring, the vectors $\boldsymbol{m}_0$ and $\boldsymbol{l}_0$ have rotated around $\boldsymbol{n}_0$ by the angle $2\pi\nu_0$ after one turn and the unit vectors are therefore in general not 2π-periodic in θ. Now a 2π-periodic coordinate system is defined by rotating $\boldsymbol{m}_0$ and $\boldsymbol{l}_0$ back uniformly by $2\pi\nu_0$ during one turn [29, 30, 31],

$$\boldsymbol{m} + \mathrm{i}\boldsymbol{l} = \mathrm{e}^{\mathrm{i}\nu_0\theta}(\boldsymbol{m}_0 + \mathrm{i}\boldsymbol{l}_0) \ , \quad \frac{\mathrm{d}}{\mathrm{d}\theta}(\boldsymbol{m} + \mathrm{i}\boldsymbol{l}) = (\boldsymbol{\Omega}_0 - \nu_0\boldsymbol{n}_0) \times (\boldsymbol{m} + \mathrm{i}\boldsymbol{l}) \ . \tag{2.50}$$

In this coordinate system, a spin can be written as

$$\boldsymbol{S}(\theta) = s_1(\theta)\boldsymbol{m}(\theta) + s_2(\theta)\boldsymbol{l}(\theta) + s_3(\theta)\boldsymbol{n}_0(\theta) \ , \quad s_1^2 + s_2^2 + s_3^2 = 1 \ . \tag{2.51}$$

The equation of spin motion

$$\boldsymbol{\Omega}_0 \times \boldsymbol{S} = \frac{\mathrm{d}}{\mathrm{d}\theta}\boldsymbol{S} = \boldsymbol{m}\frac{\mathrm{d}}{\mathrm{d}\theta}s_1 + \boldsymbol{l}\frac{\mathrm{d}}{\mathrm{d}\theta}s_2 + \boldsymbol{n}_0\frac{\mathrm{d}}{\mathrm{d}\theta}s_3 + (\boldsymbol{\Omega}_0 - \nu_0\boldsymbol{n}_0) \times \boldsymbol{S} \tag{2.52}$$

can be decomposed into its components parallel to $\boldsymbol{m}$, $\boldsymbol{l}$, and $\boldsymbol{n}_0$. This gives

$$\frac{\mathrm{d}}{\mathrm{d}\theta}(s_1 + \mathrm{i}s_2) = i\nu_0(s_1 + \mathrm{i}s_2) \ , \quad \frac{\mathrm{d}}{\mathrm{d}\theta}s_3 = 0 \ , \tag{2.53}$$

which describes a uniform rotation around $\boldsymbol{n}_0$, which keeps s_3 invariant. It has been conjectured above that s_3 does not change much when parameters of the system are slowly varied. To show this, the definition of an adiabatic invariant given in [32, Sect. 8.1] is used.

Definition (Adiabatic invariant): *Consider an ordinary differential equation* $\frac{\mathrm{d}}{\mathrm{d}\theta}\boldsymbol{x} = \boldsymbol{g}(\boldsymbol{x}, \tau)$ *with* $\tau = \varepsilon\theta$ *and* $\boldsymbol{x} \in I\!R^n$ *for a small parameter* ε *so that* $\boldsymbol{g}$ *defines a slowly varying vector field. A function* $\boldsymbol{A}(\boldsymbol{x}, \tau)$ *is said to be an adiabatic invariant of this system if its variation on the interval* $\theta \in [0, 1/\varepsilon]$ *(which implies* $\tau \in [0, 1]$*) is small together with* ε*, except perhaps for a set of initial conditions whose measure goes to zero with* ε*; that is, for "most" initial conditions:*

$$\lim_{\varepsilon\to 0} \mathrm{Sup}_{\theta\in[0,1/\varepsilon]} |\boldsymbol{A}(\boldsymbol{x}(\theta), \varepsilon\theta) - \boldsymbol{A}(\boldsymbol{x}(0), 0)| = 0 \ . \tag{2.54}$$

The symbol Sup *denotes the supremum over the interval* $[0, 1/\varepsilon]$.

Sometimes a distinction is made between adiabatic invariants that satisfy (2.54) for *all* initial conditions and so-called almost adiabatic invariants that satisfy this equation for most initial conditions, where the exceptional initial conditions are from a set that has a measure that tends to 0 with ε [33, Sect. 4]. This distinction will not be made here.

To analyze whether $s_3 = \boldsymbol{S} \cdot \boldsymbol{n}_0$ is an adiabatic invariant, I consider a precession vector $\boldsymbol{\Omega}_0(\theta, \tau)$ that depends on a slowly changing parameter τ. For fixed τ, the rotation matrix for one turn has a unit rotation vector $\boldsymbol{n}_0(\theta, \tau)$ and one can again define the 2π-periodic coordinate system using this vector together with the unit vectors $\boldsymbol{m}(\theta, \tau)$ and $\boldsymbol{l}(\theta, \tau)$. Because these vectors have unit length and constitute a right-handed orthogonal coordinate system for all values of τ, their variation with τ can only be a rotation around some vector $\boldsymbol{\eta}(\theta, \tau)$,

$$\partial_\tau \boldsymbol{n}_0 = \boldsymbol{\eta}(\theta, \tau) \times \boldsymbol{n}_0 \ , \quad \partial_\tau(\boldsymbol{m} + \mathrm{i}\boldsymbol{l}) = \boldsymbol{\eta}(\theta, \tau) \times (\boldsymbol{m} + \mathrm{i}\boldsymbol{l}) \ . \tag{2.55}$$

These equations can be rearranged to compute $\boldsymbol{\eta}$ as

$$\boldsymbol{\eta} = \frac{1}{2}(\boldsymbol{m} \times \partial_\tau \boldsymbol{m} + \boldsymbol{l} \times \partial_\tau \boldsymbol{l} + \boldsymbol{n}_0 \times \partial_\tau \boldsymbol{n}_0) \ . \tag{2.56}$$

Now putting $\tau = \varepsilon\theta$, the spin of a particle that travels on the closed orbit while the parameter τ varies slowly is analyzed,

$$\begin{aligned} \boldsymbol{\Omega}_0(\theta, \tau) \times \boldsymbol{S} &= \frac{\mathrm{d}}{\mathrm{d}\theta}\boldsymbol{S} \\ &= \boldsymbol{m}\frac{\mathrm{d}}{\mathrm{d}\theta}s_1 + \boldsymbol{l}\frac{\mathrm{d}}{\mathrm{d}\theta}s_2 + \boldsymbol{n}_0\frac{\mathrm{d}}{\mathrm{d}\theta}s_3 \\ &\quad +(\boldsymbol{\Omega}_0 - \nu_0\boldsymbol{n}_0) \times \boldsymbol{S} + (\frac{\mathrm{d}}{\mathrm{d}\theta}\tau)\boldsymbol{\eta} \times \boldsymbol{S} \ . \end{aligned} \tag{2.57}$$

The term with $\frac{\mathrm{d}}{\mathrm{d}\theta}\tau = \varepsilon$ appears because the unit vectors' dependence on τ has been taken into account. The spin coordinates then fulfill the following equation of motion:

$$\frac{\mathrm{d}}{\mathrm{d}\theta}\begin{pmatrix} s_1 \\ s_2 \\ s_3 \end{pmatrix} = \begin{pmatrix} \{[\nu_0(\tau)\boldsymbol{n}_0 - \varepsilon\boldsymbol{\eta}] \times \boldsymbol{S}\} \cdot \boldsymbol{m} \\ \{[\nu_0(\tau)\boldsymbol{n}_0 - \varepsilon\boldsymbol{\eta}] \times \boldsymbol{S}\} \cdot \boldsymbol{l} \\ \{\qquad\qquad - \varepsilon\boldsymbol{\eta} \;\times \boldsymbol{S}\} \cdot \boldsymbol{n}_0 \end{pmatrix} \tag{2.58}$$

$$= \begin{pmatrix} \varepsilon(\eta_3 s_2 - \eta_2 s_3) - \nu_0(\tau)s_2 \\ \varepsilon(\eta_1 s_3 - \eta_3 s_1) + \nu_0(\tau)s_1 \\ \varepsilon(\eta_2 s_1 - \eta_1 s_2) \end{pmatrix} , \tag{2.59}$$

with $\tau = \varepsilon\theta$ and $\boldsymbol{\eta} = \eta_1\boldsymbol{m} + \eta_2\boldsymbol{l} + \eta_3\boldsymbol{n}_0$. For $1 - s_3^2 \geq \Delta$, $(\Delta \in I\!R^+)$, s_1 and s_2 can be written in terms of an angle ϕ as $s_1 = \sqrt{1-s_3^2}\cos\phi$ and $s_2 = \sqrt{1-s_3^2}\sin\phi$. And because $\sqrt{1-s_3^2}\frac{\mathrm{d}}{\mathrm{d}\theta}\phi = -\sin\phi\frac{\mathrm{d}}{\mathrm{d}\theta}s_1 + \cos\phi\frac{\mathrm{d}}{\mathrm{d}\theta}s_2$, one obtains

$$\frac{\mathrm{d}}{\mathrm{d}\theta}\begin{pmatrix} s_3 \\ \phi \end{pmatrix} = \begin{pmatrix} \varepsilon\,(\eta_2\cos\phi - \eta_1\sin\phi)\sqrt{1-s_3^2} \\ \nu_0(\tau) + \varepsilon[(\eta_2\sin\phi + \eta_1\cos\phi)\frac{s_3}{\sqrt{1-s_3^2}} - \eta_3] \end{pmatrix} . \tag{2.60}$$

For small ε and when $|\nu_0|$ is much larger than order ε, this system has the slowly varying coordinate s_3 and a quickly varying phase ϕ. It is therefore suitable for averaging methods. To bring this equation into standard form for averaging theorems, where frequencies only depend on slowly changing variables, I make use of the slowly changing variable τ with $\frac{\mathrm{d}}{\mathrm{d}\theta}\tau = \varepsilon$. In addition, I define $\tilde{\theta} = \theta$ and add the equation $\frac{\mathrm{d}}{\mathrm{d}\theta}\tilde{\theta} = 1$. For the spin motion on the closed orbit, this then leads to an autonomous differential equation as used in the previous definition of an adiabatic invariant,

$$\frac{\mathrm{d}}{\mathrm{d}\theta}\begin{pmatrix} s_3 \\ \tau \\ \phi \\ \tilde{\theta} \end{pmatrix} = \begin{pmatrix} 0 \\ 0 \\ \nu_0(\tau) \\ 1 \end{pmatrix} + \varepsilon\begin{pmatrix} f_3(s_3,\phi,\tau,\tilde{\theta}) \\ 1 \\ f_\phi(s_3,\phi,\tau,\tilde{\theta}) \\ 0 \end{pmatrix} , \tag{2.61}$$

$$f_3(s_3,\phi,\tau,\tilde{\theta}) = [\eta_2(\tilde{\theta},\tau)\cos\phi - \eta_1(\tilde{\theta},\tau)\sin\phi]\sqrt{1-s_3^2}\ , \tag{2.62}$$

$$f_\phi(s_3,\phi,\tau,\tilde{\theta}) = [\eta_2(\tilde{\theta},\tau)\sin\phi + \eta_1(\tilde{\theta},\tau)\cos\phi]\frac{s_3}{\sqrt{1-s_3^2}} - \eta_3(\tilde{\theta},\tau) \tag{2.63}$$

This system of ordinary differential equations has two slowly changing and two quickly changing variables for small ε. It is written in the standard form of averaging theorems for two frequency systems [33, Sect. 1.8], [32, Chap. 4].

To illustrate the basic idea of two-phase averaging, it is noted that $f_3(s_3,\phi,\tau,\tilde{\theta})$ is a 2π-periodic function of $\tilde{\theta}$ and that it is linear in trigonometric functions of ϕ, therefore

$$\overline{f} = \frac{1}{(2\pi)^2}\int_0^{2\pi}\int_0^{2\pi} f_3(s_3,\phi,\tau,\tilde{\theta})d\phi d\tilde{\theta} = 0\ . \tag{2.64}$$

One can simplify the equation of motion by transforming to a coordinate $\bar{s}_3 = s_3 + \varepsilon u(s_3,\phi,\tau,\tilde{\theta})$ with a function u that should have the same periodicity properties as f_3 with respect to ϕ and $\tilde{\theta}$. These functions, f_3 and u, are now Fourier expanded,

$$f_3(s_3,\phi,\tau,\tilde{\theta}) = \sum_{k=-\infty}^{\infty} (f_k^+(s_3,\tau)\mathrm{e}^{\mathrm{i}(k\tilde{\theta}+\phi)} + f_k^-(s_3,\tau)\mathrm{e}^{\mathrm{i}(k\tilde{\theta}-\phi)} \ , \tag{2.65}$$

$$u(s_3,\phi,\tilde{\theta},\varepsilon) = \sum_{k=-\infty}^{\infty} (u_k^+(s_3,\tau)\mathrm{e}^{\mathrm{i}(k\tilde{\theta}+\phi)} + u_k^-(s_3,\tau)\mathrm{e}^{\mathrm{i}(k\tilde{\theta}-\phi)} \ , \tag{2.66}$$

whence

$$\begin{aligned}\frac{\mathrm{d}}{\mathrm{d}\theta}\bar{s}_3 = \varepsilon \sum_{k=-\infty}^{\infty} &\{ \ [f_k^+ + u_k^+\mathrm{i}(k+\frac{\mathrm{d}}{\mathrm{d}\theta}\phi)]\mathrm{e}^{\mathrm{i}(k\tilde{\theta}+\phi)} \\ &+ [f_k^- + u_k^-\mathrm{i}(k-\frac{\mathrm{d}}{\mathrm{d}\theta}\phi)]\mathrm{e}^{\mathrm{i}(k\tilde{\theta}-\phi)} \ \} \\ = \varepsilon \sum_{k=-\infty}^{\infty} &\{ \ [f_k^+ + u_k^+\mathrm{i}(k+\nu_0)]\mathrm{e}^{\mathrm{i}(k\tilde{\theta}+\phi)} \\ &+ [f_k^- + u_k^-\mathrm{i}(k-\nu_0)]\mathrm{e}^{\mathrm{i}(k\tilde{\theta}-\phi)}\} + O(\varepsilon^2) \ .\end{aligned} \tag{2.67}$$

If $\nu_0(\tau)$ is not an integer, then one can choose $u_k^\pm(s_3,\tau) = if_k^\pm/(k \pm \nu_0(\tau))$ for all k and all first-order terms are eliminated leaving $\frac{\mathrm{d}}{\mathrm{d}\theta}\bar{s}_3 = O(\varepsilon^2)$. Such a transformation removes all terms that are first-order in ε except $\varepsilon\overline{f}$. Therefore, the differential equation after the transformation is called the averaged system. For the case under consideration, the average of f_3 is zero, and for $\theta \in [0,1/\varepsilon]$, changes of the variable $\bar{s}_3$ of the averaged system are of order ε. Changes of s_3 are of the same order, because the difference $\bar{s}_3 - s_3 = \varepsilon u$ is of order ε. This shows that $s_3 = \boldsymbol{S}\cdot\boldsymbol{n}_0$ is an adiabatic invariant as defined above. However, in this argument it was assumed that $\nu_0(\tau)$ never takes on integer values. Because the closed-orbit spin tune changes with energy ($\nu_0 = G\gamma$ in a flat ring), ν_0 might become an integer during the acceleration process. Phenomena due to resonance between the frequencies of the two quickly changing phases ϕ and $\tilde{\theta}$ could then occur.

I will therefore now state an averaging theorem for systems with two quickly changing phases that allows for the crossing of resonances and apply it to spin motion on the closed orbit. Various multi-phase averaging theorems could be used [32, Chaps.4-6], [33]. Here theorem 3 of [32, Sect. 4.1] is used, which is attributed to [34]. The application of two-phase averaging to the simple problem of spin motion on the closed orbit might seem more complicated than necessary but we have already seen that $\boldsymbol{S}\cdot\boldsymbol{n}_0$ deviates from 1 at $\nu_0 = G\gamma = 8$ in Fig. 2.2, indicating that the effects of resonances cannot be ignored. Moreover, by going into considerable detail here while dealing with the closed orbit, the stage is set for adiabatic invariants in the case of spin motion on a general trajectory.

Theorem (Averaging for two frequency systems): *Consider a system of the form*

$$\frac{\mathrm{d}}{\mathrm{d}\theta}\boldsymbol{I} = \varepsilon\boldsymbol{f}(\boldsymbol{I},\phi,\tilde{\theta},\varepsilon) \ , \tag{2.68}$$

$$\frac{\mathrm{d}}{\mathrm{d}\theta}\phi = \nu(\boldsymbol{I}) + \varepsilon g(\boldsymbol{I},\phi,\tilde{\theta},\varepsilon)\ , \tag{2.69}$$

$$\frac{\mathrm{d}}{\mathrm{d}\theta}\tilde{\theta} = 1\ , \tag{2.70}$$

where $\boldsymbol{I}$ belongs to a regular compact subset of Euclidean $I\!R^m$. Each function on the right-hand side is real, C^1 (first-order differentials exist and are continuous) in $\boldsymbol{I}$ and ε, periodic with period 2π in ϕ and $\tilde{\theta}$, and each possesses an analytic extension for $\phi \in \mathbb{C}$, $\Im\{\phi\} < \sigma$ and $\tilde{\theta} \in \mathbb{C}$, $\Im\{\tilde{\theta}\} < \sigma$ with $\sigma > 0$. The associated averaged system is

$$\frac{\mathrm{d}}{\mathrm{d}\theta}\bar{\boldsymbol{I}} = \varepsilon\bar{\boldsymbol{f}}(\bar{\boldsymbol{I}})\ ,\quad \bar{\boldsymbol{f}}(\bar{\boldsymbol{I}}) = \frac{1}{(2\pi)^2}\int_0^{2\pi}\int_0^{2\pi}\boldsymbol{f}(\bar{\boldsymbol{I}},\phi,\tilde{\theta},0)d\phi d\tilde{\theta}\ , \tag{2.71}$$

with the starting condition $\bar{\boldsymbol{I}}(0) = \boldsymbol{I}(0)$. Let every trajectory of the exact (not the averaged) system for which $\boldsymbol{I}$ stays in the range of definition for $\theta \in [0, 1/\varepsilon]$ have a strictly monotonic variation of $\nu(\boldsymbol{I})$ with θ, $|\frac{\mathrm{d}}{\mathrm{d}\theta}\nu| > c_1\varepsilon$ for some $c_1 \in R^+$. Then: On all these trajectories there exists $c \in R^+$ so that for sufficiently small ε

$$\mathrm{Sup}_{\theta\in[0,1/\varepsilon]}|\boldsymbol{I}(\theta) - \bar{\boldsymbol{I}}(\theta)| < c\sqrt{\varepsilon}\ . \tag{2.72}$$

In general, the solution of the averaged system does not approximate the original system well if $\tilde{\theta}$ and ϕ are in resonance, which means here that the closed-orbit spin tune $\nu_0(\tau)$ is an integer m. A simple example is the system $\frac{\mathrm{d}}{\mathrm{d}\theta}s_3 = \varepsilon\cos(\phi - m\tilde{\theta})$ and $\frac{\mathrm{d}}{\mathrm{d}\theta}\phi = \nu_0$. The averaged system leads to the relation $\bar{s}_3 = s_3(0)$, whereas the solution for an integer $\nu_0 = m$ is given by the relation $s_3 = s_3(0) + \varepsilon\theta\cos[\phi(0)]$. The change in s_3 for $\theta \in [0, 1/\varepsilon]$ does not tend to zero for the limit $\varepsilon \to 0$ and s_3 is therefore not an adiabatic invariant.

This example illustrates that large changes of slowly changing variables can build up at resonances. The simplest way of avoiding this behavior at resonances is to consider only systems in which resonances are passed quickly so that capture in resonances is avoided. This is the reason why the averaging theorem for two frequency systems requires $|\frac{\mathrm{d}}{\mathrm{d}\theta}\nu| > c_1\varepsilon$, which is often called condition A. This condition excludes systems where trajectories pass arbitrarily slowly through a resonance or cross the same resonance several times.

For spin motion on the closed orbit we choose $I_1(\theta) = s_3(\theta)$, so that the averaged system includes the equation $\frac{\mathrm{d}}{\mathrm{d}\theta}\bar{I}_1 = \bar{f}_3 = 0$ and leads to $\bar{I}_1(\theta) = \bar{I}_1(0) = s_3(0)$. If $|\frac{\mathrm{d}}{\mathrm{d}\theta}\nu_0(\varepsilon\theta)| > c_1\varepsilon$, the theorem then guarantees the relation

$$\lim_{\varepsilon\to 0}\mathrm{Sup}_{\theta\in[0,1/\varepsilon]}|s_3(\theta) - s_3(0)| = 0\ . \tag{2.73}$$

Cases where $\boldsymbol{S}$ is nearly parallel to $\boldsymbol{n}_0$ had to be excluded before (2.60) by the condition $1 - s_3^2 \geq \Delta$. For initial conditions with $1 - s_3(0)^2 \geq 2\Delta$, there is an ε^* so that $1 - s_3(\theta)^2 \geq \Delta$ for all $\varepsilon < \varepsilon^*$ according to (2.73). This is true for all $\Delta \in I\!R^+$. With the limit $\varepsilon^* \to 0$, the set of excluded initial conditions tends to $s_3 \in \{1, -1\}$, which has measure 0. Such initial conditions are accommodated in the above definition of adiabatic invariants. The scalar product $s_3(\theta) = \boldsymbol{S}(\theta) \cdot \boldsymbol{n}_0(\theta)$ is therefore an adiabatic invariant.

The condition $|\partial_\tau \nu_0(\tau)| > c_1$ requires that the spin tune changes quickly enough during the slow change of the parameter under consideration to avoid that ν_0 remains at an integer value for a long time. When $\nu_0(\tau)$ has a finite distance to integers, s_3 is an adiabatic invariant even when $\partial_\tau \nu_0(\tau) = 0$, because then averaging theorems for non-resonant domains can be applied [33, Sect. 1.6].

2.2.3 Spin Motion for Phase Space Trajectories and Intrinsic Resonances

For uncoupled linearized orbital motion phase space, the particles appear to perform harmonic oscillations around the closed orbit with the frequencies Q_x, Q_y, and Q_τ for horizontal, vertical, and longitudinal motion when viewed at a fixed azimuth θ_0 of the accelerator. These are called the orbital tunes. The quadrupole fields experienced by a particle therefore oscillate with the orbital tunes. Then, even without a detailed analysis of resonance phenomena, which will be provided later, one expects a strong disturbance of spin motion whenever the non-integer part of the spin precession frequency is in resonance with these oscillation frequencies. For example in a flat ring with spins initially aligned along the vertical $\boldsymbol{n}_0$, the spins will be strongly affected by radial quadrupole fields when the spin precession frequency is in resonance with the vertical betatron frequency. This can happen during the acceleration process, where a severe reduction of polarization can occur. The spin precession frequency of particles moving on the closed orbit is determined by the closed-orbit spin tune ν_0. In general, the spin tune is denoted by ν and depends not only on parameters of the accelerator but also on the amplitudes of a particle's oscillation around the closed orbit. Whenever ν is a linear combination of the frequencies of the particle's coordinates, the resulting coherent perturbation can strongly disturb the spins' motion, which in turn can strongly reduce the beam's polarization,

$$\nu = j_0 P_s + j_1 Q_x + j_2 Q_y + j_3 Q_\tau \quad , \quad P_s, j_n, \in \mathbb{N} \; . \tag{2.74}$$

When this condition for the tunes holds, one speaks of an *intrinsic resonance* of order n for $n = |j_1| + |j_2| + |j_3|$. A super-periodicity P_s of a ring reduces the number of resonances. For $P_s > 1$, the tunes in (2.74) have to include their integer parts. The depolarizing effect of these resonances has been experimentally verified during acceleration in many low energy polarized proton accelerators [20, 35] and will be described in more detail later. The first-order intrinsic resonances are the dominant reason for a reduction of polarization after solenoids have been introduced to eliminate the effect of imperfection resonances. If the first-order resonances are avoided, however, higher-order resonances become dominant even for decoupled linear phase space motion, as will be shown for the case of HERA-p.

It has been explained in Sect. 2.2.1 that the spin motion can be strongly perturbed at imperfection resonances due the fact that field imperfections dominate the spin motion whenever the main guide fields produce an integer number of spin rotations and therefore no apparent spin rotation after one completed turn. The depolarizing effect at intrinsic resonances can be understood in similar terms. For phase space trajectories that deviate little from the closed orbit, the spin motion is dominated by the main guide fields on the closed orbit except close to an intrinsic resonance, where the coherent perturbations described above can dominate over the main guide fields.

Consider, for example, a flat ring with vertical $\boldsymbol{n}_0$ and vertical betatron oscillations. For sufficiently small oscillation amplitudes around the closed orbit, one has $\nu \approx \nu_0$ and all spins rotate around $\boldsymbol{n}_0$ by $2\pi\nu_0$ during one turn. Then in a new coordinate system that rotates during one turn by $2\pi Q_y$ relative to the radial direction, the main guide fields produce a rotation of the spins by $2\pi(\nu_0 - Q_y)$. Therefore at $\nu_0 = Q_y$, the net spin rotation due to the main guide fields vanishes and the remaining rotations are due to extra horizontal fields on the trajectory that oscillates vertically around the closed orbit. At intrinsic resonances these extra fields therefore dominate over the effect of the accelerator's main guide fields. Because the dominant rotation at an intrinsic resonance is produced by the fields along a particle's phase space trajectory, it is different for different particles and the beam can therefore loose polarization under the influence of an intrinsic resonance.

The averaging theorem for two frequency systems in Sect. 2.2.2 has been used to prove that, as long as the system does not remain at a resonance for too long, spins on the closed orbit follow any slow change of $\boldsymbol{n}_0$. Therefore, a severe reduction of polarization while accelerating through an imperfection resonance can be avoided by making the acceleration rate low enough or by making the change of $\boldsymbol{n}_0$ slow enough by means of a partial snake as discussed in Sect. 2.2.1.

At intrinsic resonances a reduction of polarization can be avoided by a similar mechanism. While an intrinsic resonance is crossed, particles with large oscillation amplitudes will experience perturbations of spin motion that slowly increase already before the resonance, and an adiabatic conservation of polarization can occur, which leads to a flip of the polarization direction, similar to the illustration in Fig. 2.2. But polarization in the core of the beam, where the oscillation amplitudes are small, will be only weakly influenced when crossing intrinsic resonances. Therefore, the average polarization of the beam is reduced. Such a reduction of polarization can be avoided by first slowly exciting the whole beam coherently at a frequency close to the orbital tune that causes the perturbation [36], so that all particles take on relatively large oscillation amplitudes. During the acceleration, all spins then follow the adiabatic change of the polarization direction and the resonance can be crossed with little loss of polarization but with an overall flip in the polarization direction. The coherent excitation amplitude is then reduced slowly so that the beam emittance does not change noticeably during the whole process. This mechanism has been tested successfully at the AGS [37, 26]. There, an RF dipole has been used to slowly excite the vertical amplitudes of all the particles coherently. Then the dominant resonances $0+Q_y$, $12+Q_y$, $36-Q_y$, and $36+Q_y$ were crossed with little loss of polarization. Finally, the RF dipole was slowly switched off. No noticeable increase of emittance was observed. An older technique of avoiding the reduction of polarization at strong intrinsic resonances utilizes pulsed quadrupoles to move the orbital tune, within a few microseconds just before a resonance, so that the resonance is crossed so quickly that the spin motion is hardly disturbed [20].

For the case of a single resonance with frequency κ that is crossed by changing the closed-orbit spin tune according to $\nu_0 = \kappa + \nu_0'\theta$, the final polarization can be calculated with the Froissart-Stora formula, which will be introduced in Sect. 2.2.11. This confirms that polarization can be preserved when an intrinsic resonance is crossed either very quickly or very slowly.

A third method of avoiding loss of polarization at intrinsic resonances uses radial magnetic fields. The closed-orbit spin tune ν_0 can then deviate from $G\gamma$, and in fact it can be made independent of energy and low-order resonances can then be avoided during the acceleration process. It was mentioned after (2.5) that in a fixed transverse magnetic field the deflection angle of high-energy particles depends on energy, whereas the spin rotation does not depend on energy. This therefore opens the possibility of devising a fixed field magnetic device that rotates spins by π whenever a high-energy particle travels through it at the changing energies of an acceleration cycle. Field arrangements that rotate spins by π while perturbing the orbit only moderately are called Siberian Snakes [38, 39, 40, 41, 42]. At low energies this rotation can be produced by solenoid magnets. But when the beam is accelerated, their strength must increase to keep the angle equal to π. At sufficiently high energy, an arrangement of transverse magnetic fields can be used to produce this rotation, and here the field strength is independent of the energy. As illustrated by Fig. 2.3, two Siberian Snakes can make the spin tune ν_0 independent of energy and equal to $\frac{1}{2}$ in a flat ring. Starting at the far side of the ring and traveling through one quadrant to the left side of the figure, spins are rotated around the vertical (dashed line) according to the relation $\Psi = G\gamma\frac{\pi}{2}$. The light arrow represents a spin that is rotated by Ψ, whereas the dark arrow is only rotated by the Siberian Snakes and not by the fields in the arcs. The difference between the light and the dark arrow therefore indicates the rotation due to the fields of the quadrants. A Siberian Snake with radial precession axis (radial snake) rotates all spins by π around the radial direction before the particles enter the second quadrant. Because the spins have now reversed their vertical orientation, the rotation due to the first quadrant is rewound during the second quadrant. The rotation of the third quadrant is rewound during the fourth, due to the Siberian Snake with longitudinal precession axis (longitudinal snake) between these quadrants. The rotations

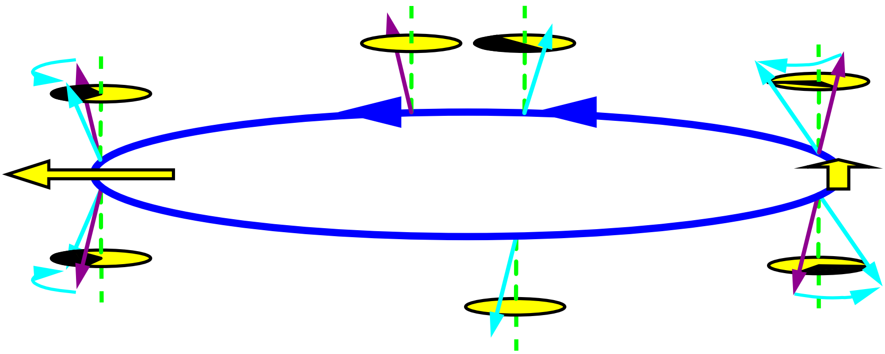

Fig. 2.3. Schematic spin motion in a flat ring with a symmetric arrangement of a longitudinal and a radial Siberian Snake. The one turn spin motion has $\nu_0 = \frac{1}{2}$ and $\boldsymbol{n}_0$ vertical for all energies.

of different quadrants cancel for all energies. As indicated by the dark area, all spins have in total rotated by π around the vertical by the time they have returned to the far side of the ring. No net rotation due to the arcs remains, and the dark arrow and the light arrow therefore coincide.

To be more general, one can consider N Siberian Snakes in a ring where a spin rotation angle Ψ_j around the vertical is produced between the jth and the $j+1$th Siberian Snake. These angles are in general energy dependent. The rotation axis of a snake is called the snake axis, and the angle of this axis to the radial direction is referred to as the snake angle φ_j. The spin transport quaternion of one snake is therefore $i[\cos(\varphi_j)\sigma_1 + \sin(\varphi_j)\sigma_2]$ and the total rotation during one turn is given by

$$A = \prod_{j=1}^{N} i\mathrm{e}^{-\mathrm{i}\frac{\Psi_j}{2}\sigma_3}[\cos(\varphi_j)\sigma_1 + \sin(\varphi_j)\sigma_2] \tag{2.75}$$

$$= i^N \mathrm{e}^{-\mathrm{i}\frac{\Delta\Psi}{2}\sigma_3} \prod_{j=1}^{N}[\cos(\varphi_j)\sigma_1 + \sin(\varphi_j)\sigma_2] \; . \tag{2.76}$$

Because σ_3 anti-commutes with the other two Pauli matrices, the exponent is given by $\Delta\Psi = \Psi_N - \Psi_{N-1} \pm \ldots \pm \Psi_1$. The total spin rotation is independent of energy when the snake locations are chosen to let $\Delta\Psi = 0$. A pair of snakes then produces a rotation around a vertical axis described by

$$\begin{aligned} &[\cos(\varphi_1)\sigma_1 + \sin(\varphi_1)\sigma_2] \cdot [\cos(\varphi_2)\sigma_1 + \sin(\varphi_2)\sigma_2] \cdot \\ &= \cos(\varphi_1 - \varphi_2) - \mathrm{i}\sin(\varphi_1 - \varphi_2)\sigma_3 \; . \end{aligned} \tag{2.77}$$

An even number of Siberian Snakes therefore produces a vertical rotation vector $\boldsymbol{n}_0$. The periodic spin direction on the closed orbit is then vertical in the bending magnets of the ring and is not deflected in these magnets.

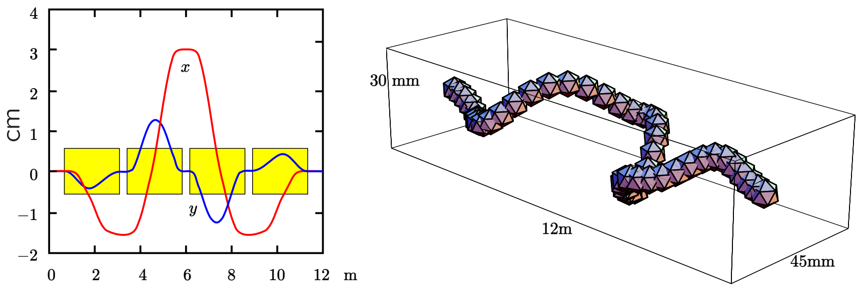

Fig. 2.4. Orbit motion in a helical snake designed for RHIC.

For an odd number of Siberian Snakes, $\boldsymbol{n}_0$ is in the horizontal plane and rotates by an energy dependent angle in each bending magnet. In high-energy accelerators with a large number of spin rotations inside the bending magnets, it is advisable to avoid this energy dependence. For this, $\boldsymbol{n}_0$ should be vertical in the arcs, which requires an even number N of Siberian Snakes. In this case, the total rotation is given by

$$A = i^N \mathrm{e}^{-\mathrm{i}(\frac{\Delta\Psi}{2}+\Delta\varphi)\sigma_3} , \tag{2.78}$$

with $\Delta\varphi = \varphi_N - \varphi_{N-1} \pm \ldots - \varphi_1$. For N Siberian Snakes in a ring with spin rotations otherwise only around the vertical, the following three conditions are required:

- $\Delta\Psi = 0$, to make ν_0 independent of energy.
- N is even, to make $\boldsymbol{n}_0$ vertical in the arcs of the ring.
- $\Delta\varphi = \frac{\pi}{2}$, to make $\nu_0 = \frac{1}{2}$.

As long as the amplitude-dependent spin tune ν does not change too strongly over the orbital amplitudes, all imperfection resonances and, because the orbital tunes cannot be 1/2, also all first-order intrinsic resonances are avoided by the insertion of such Siberian Snakes [43], and polarized beam acceleration to very high energy could become possible. Siberian Snakes with transverse fields can only be used at sufficiently high energies because their fields are not changed during acceleration of the beam and they produce orbit distortions that are too big for energies below approximately 8 GeV [44].

The orbit deviation in the Siberian Snakes built for RHIC [45, 46] is up to 3 cm at the injection momentum of about 25 GeV/c as shown in Fig. 2.4 (left). The orbit motion outside the Siberian Snake, however, is hardly changed by the insertion of this device. One such snake is made of 4 helical dipole magnets of about 2.4 m length [47]. Figure 2.4 (right) depicts the design orbit in a RHIC Siberian Snake in three dimensions. It is obvious why these devices, first suggested in Novosibirsk [38], received their name.

Because DESY III, the first synchrotron in the HERA-p accelerator chain, has a super-periodicity 8, only 4 strong intrinsic first-order resonances have to be crossed. They are at momenta of 1.69 GeV/c, 2.05 GeV/c, 6.05 GeV/c, and 6.37 GeV/c where the closed-orbit spin tune $\nu_0 = G\gamma$ is $8 - Q_y$, $0 + Q_y$, $16 - Q_y$, and $8 + Q_y$ for $Q_y = 4.3$. The polarization can be conserved by jumping the orbital tune with pulsed quadrupoles in a few microseconds or by excitation of a resonance with an RF dipole, whereas a solenoid partial snake would be used to cross the one strong imperfection resonance at $G\gamma = 8$ as mentioned in Sect. 2.2.1. All these methods have been successful at the AGS, and it is likely that a highly polarized proton beam could be extracted from the DESY III synchrotron at 7.5 GeV/c.

In PETRA, it would be very cumbersome to cross all resonances with the aid of the tune jumping technique or by RF dipole excitation. Because Siberian Snakes can be constructed for the injection energy of PETRA [28, 44], the best choice will be to avoid all first-order resonances by means of two such devices. There is space for Siberian Snakes in the east and the west section of PETRA [48, 28].

2.2.4 Changes to the Accelerator Chain for HERA-p

HERA-p is a very complex accelerator and a brief look already indicates 4 reasons why producing a polarized beam in HERA-p is more difficult than in a conventional flat ring with some super-periodicity.

1. HERA-p has no exact super-periodicity and only an approximate mirror symmetry between the north and south halves of the ring. Therefore, $P_s = 1$ in (2.74) and more resonances appear than in a ring with some higher super-periodicity. Furthermore, special schemes for canceling resonances in symmetric lattices [49] are not very effective in such a ring.
2. The proton ring of HERA-p is located above the electron ring in the arcs. The proton beam is bent down to the level of the electron ring on both sides of the three experiments H1, HERMES, and ZEUS in the north, east, and south straight sections. Figure 2.5 (left) shows schematically the dipole magnets that bend the proton beam into the plane of the electron beam. On entering a vertical bend section from the arc, a beam first encounters a super-conducting magnet called BV that bends vertically downward. This is followed by 4 identical magnets that are called BH in this tract and that bend the beam toward the ring center. Finally, the beam is brought back to the horizontal by three identical vertical bend magnets called BU. The combined effect of the BV and BU magnets surrounding a straight section is only a local change in the vertical position of the beam. Nevertheless, the spin motion is strongly affected as shown by the number of spin rotations performed in each magnet:

Magnet	Bend	Bending direction	Spin rotations at 920 GeV
BV	5.7 mrad	Vertically downward	1.6
BU	1.9 mrad	Vertically upward (3×)	0.5
BH	15.1 mrad	Horizontal (4×)	4.2

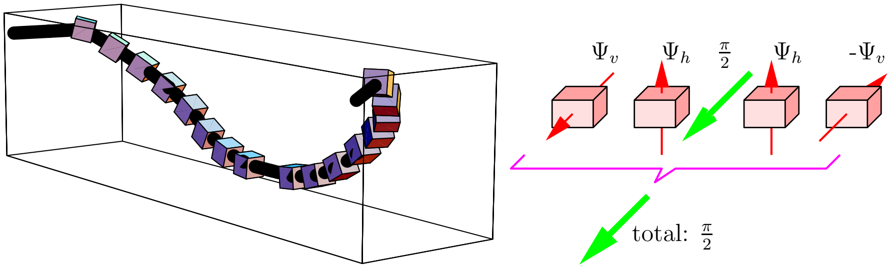

Fig. 2.5. Left: Interleaved horizontal and vertical magnets in HERA-p that direct the proton beam into the plane of the electron beam. **Right**: The radial Siberian Snakes in between the vertical magnets are called flattening snakes. Every non-flat region with a flattening snake rotates spins by π around the radial direction.

HERA-p is therefore not a flat ring and $\boldsymbol{n}_0$ is in general not vertical and will depend on the particles' energy. This can lead to a loss of polarization during the acceleration cycle and during the energy oscillation in every synchrotron period. This destructive effect of the vertical bends can, however, be eliminated by so-called flattening snakes [50, 51], which make $\boldsymbol{n}_0$ vertical outside the non-flat sections of HERA-p. These are radial Siberian Snakes, with a spin rotation characterized by $i\sigma_1$, which are inserted at the center of the horizontal rotation between the BV and the BU magnets. If the BV magnet rotates spins by the angle Ψ_v and a pair of BH magnets produce the angle Ψ_h, then the total spin rotation of the non-flat region is given by the quaternion

$$\mathrm{e}^{\mathrm{i}\frac{\Psi_v}{2}\sigma_1}\mathrm{e}^{-\mathrm{i}\frac{\Psi_h}{2}\sigma_3} i\sigma_1 \mathrm{e}^{-\mathrm{i}\frac{\Psi_h}{2}\sigma_3}\mathrm{e}^{-\mathrm{i}\frac{\Psi_v}{2}\sigma_1} = \mathrm{e}^{-\mathrm{i}\frac{\Psi_v}{2}\sigma_1} i\sigma_1 \mathrm{e}^{\mathrm{i}\frac{\Psi_v}{2}\sigma_1} = i\sigma_1 \; ; \quad (2.79)$$

which means that one non-flat region then rotates spins by π around the radial direction. Two non-flat regions, one to the right and one to the left of a collision point, compensate each other's spin rotation so that particles on the closed orbit leave these two non-flat regions with the spin direction that they had on entry. Because the rest of HERA-p has a horizontal flat design orbit, the flattening snakes create an effectively flat ring with vertical $\boldsymbol{n}_0$ in the arcs and $\nu_0 = G\gamma - 6\Psi_h/\pi$. The closed-orbit spin tune ν_0 is less than $G\gamma$ because the horizontal bends in the 6 non-flat regions in the north, east, and south do not contribute to the spin rotation during one turn.

3. There is space for spin rotators to make $\boldsymbol{n}_0$ and the polarization parallel to the beam direction inside the collider experiments while keeping it vertical in the arcs, and there is space for a flattening snake in the center of each non-flat region. There is also space for 4 Siberian Snakes. But installing more than 4 Siberian Snakes would involve a lot of costly construction work. Simulations have shown that 8 snakes would be desirable. However, it turned out to be important to optimize the 8 snake angles because four-

snake schemes can be better than eight-snake schemes when the snake angles are not properly chosen [52].
4. The relevant energies, and thus the magnetic fields, are very high and therefore the spin rotates rapidly and spin perturbations are large.

If HERA-p had been designed for polarized proton acceleration, several parts of the ring would probably have been constructed differently.

The changes required in the pre-accelerator chain and in HERA-p itself are summarized in Fig. 2.6. This shows the polarized H^- source and the polarimeters mentioned in Chap. 1 as well as the partial snake for DESY III and Siberian Snakes for PETRA. For HERA-p, the flattening snakes and spin rotators, which make the spin longitudinal in the experiment, are indicated. Both the 4 or 8 Siberian Snake options for HERA-p are indicated.

2.2.5 The Invariant Torus

The synchrotron radiation in proton synchrotrons that can be built today is so weak that particle motion can usually be described by a Hamiltonian. It is then often convenient to consider canonical phase space coordinates $\boldsymbol{z}$ in one Poincaré section [54] at azimuth θ_0 of the ring. I assume that action variables $J_j(\boldsymbol{z})$ and angle variables $\Phi_j(\boldsymbol{z})$ for each of the three degrees of freedom indicated by j can be introduced in a domain of the 6-dimensional phase space of (2.19). The actions do not change over one turn around the ring and the angles advance by an action dependent phase advance $2\pi Q_j(\boldsymbol{J})$ during one 2π-period in θ. In accelerator physics, the functions Q_j are the amplitude-dependent tunes. A particle starting with an initial phase space coordinate $\boldsymbol{z}_i$ will arrive at the final coordinate $\boldsymbol{z}_f = \boldsymbol{M}(\boldsymbol{z}_i)$ after one turn around the ring, where $\boldsymbol{M}(\boldsymbol{z}) = \boldsymbol{M}(\boldsymbol{z}, \theta_0; \theta_0+2\pi)$ is the transport map for one turn starting at θ_0. The action-angle variables after one turn are described by

$$\boldsymbol{J}(\boldsymbol{M}(\boldsymbol{z})) = \boldsymbol{J}(\boldsymbol{z}) \ , \quad \boldsymbol{\Phi}(\boldsymbol{M}(\boldsymbol{z})) = \boldsymbol{\Phi}(\boldsymbol{z}) + 2\pi\boldsymbol{Q}(\boldsymbol{J}(\boldsymbol{z})) \ , \tag{2.80}$$

so that the motion has the topology of a 3-torus. Because it will be clear from the context which Poincaré section is under consideration, the dependence on θ_0 of the one turn transport map and of the transformation to action-angle variables is not indicated.

A particle with initial action variables $\boldsymbol{J}_i$ will travel on the torus determined by the relation $\boldsymbol{J}(\boldsymbol{z}) = \boldsymbol{J}_i$ at azimuth θ_0. If the three tunes and 1 are incommensurable so that there are no resonances $\boldsymbol{j} \cdot \boldsymbol{Q} = j_0$ for any set of integers $\{j_n | n \in \{0, \ldots, 3\}\}$, the particle will come arbitrarily close to every phase space point of the torus. Because the set of phase space points on the torus is mapped onto itself by the one turn transport map, one speaks of an invariant torus. This means that particles starting on an invariant torus get redistributed in phase space during one turn around the ring, but they stay on the same torus. Similarly, one calls $I(\boldsymbol{z})$ an invariant function of motion

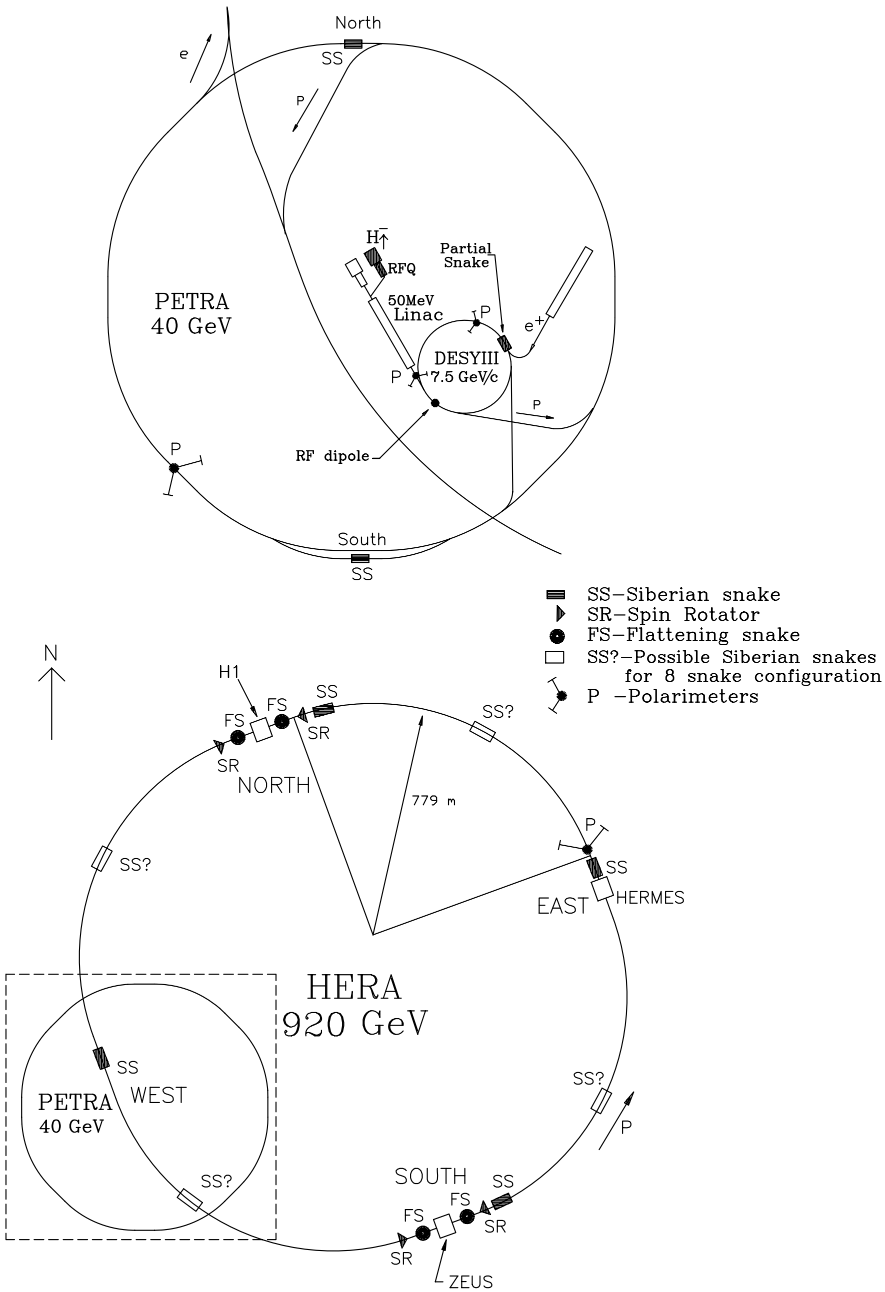

Fig. 2.6. The required changes in the pre-accelerator chain and in HERA-p (Drawing taken from [28, 53]).

if $I(\boldsymbol{M}(\boldsymbol{z})) = I(\boldsymbol{z})$. For horizontal linear orbit motion, an example is the Courant Snyder invariant [7] $I_x(x,a,\theta) = \beta(\theta)a^2 + 2\alpha(\theta)ax + \gamma(\theta)x^2$. The invariant curve $I_x(x,a,\theta_0) = \epsilon_x$ encloses the area $\pi\epsilon_x$ in the Poincaré section at θ_0. These rather well-known concepts are mentioned here because there are much less known analogous concepts for spin motion.

2.2.6 The Invariant Spin Field

In order to maximize the number of collisions of particles inside the experimental detectors of a storage ring system, one tries to maximize the total number of particles in the bunches and tries to minimize the emittances so that the particle distribution across phase space is narrow and the phase space density is high. If the beam is spin polarized, one additionally requires that the polarization is high and that it does not change much with time.

If all particles of a beam are initially completely polarized parallel to each other, the polarization state of the beam is in general not 2π-periodic and the beam polarization can change from turn to turn. Spin fields are propagated by (2.28). A special spin field $\boldsymbol{n}(\boldsymbol{z},\theta)$ that is 2π-periodic in θ is called an invariant spin field,

$$\boldsymbol{n}(\boldsymbol{z},\theta) = \mathsf{R}(\boldsymbol{z}_i,\theta_0;\theta)\boldsymbol{n}(\boldsymbol{z}_i,\theta_0)\ , \quad \boldsymbol{n}(\boldsymbol{z},\theta+2\pi) = \boldsymbol{n}(\boldsymbol{z},\theta)\ . \tag{2.81}$$

If the spin of each particle in a beam is initially parallel to $\boldsymbol{n}(\boldsymbol{z},\theta_0)$, particles get redistributed in phase space during one turn, but their spins will stay parallel to the invariant spin field. The spin field of the beam is then in an equilibrium state. During one turn, particles change their location in phase space from some initial phase space coordinate $\boldsymbol{z}_i$ in the Poincaré section at azimuth θ_0 to some final coordinate $\boldsymbol{z}_f = \boldsymbol{M}(\boldsymbol{z}_i)$ according to the one turn map. In addition a spin has changed its direction according to the one turn spin transport matrix $\mathsf{R}(\boldsymbol{z}_i) = \mathsf{R}(\boldsymbol{z}_i,\theta_0;\theta_0+2\pi)$, but it is now parallel to the invariant spin field at the particle's new phase space coordinate $\boldsymbol{z}_f$, and (2.81) is therefore equivalent to the periodicity condition

$$\boldsymbol{n}(\boldsymbol{M}(\boldsymbol{z})) = \mathsf{R}(\boldsymbol{z})\boldsymbol{n}(\boldsymbol{z})\ . \tag{2.82}$$

The invariant spin field was first introduced by Derbenev and Kondratenko [55] in the theory of radiative electron polarization and is often called the Derbenev-Kondratenko $\boldsymbol{n}$-axis. Note that $\boldsymbol{n}(\boldsymbol{z})$ is usually not an eigenvector of the spin transport matrix $\mathsf{R}(\boldsymbol{z})$ at some phase space point because the spin of a particle has changed after one turn around the ring, but the eigenvector does not change when it is transported by $\mathsf{R}(\boldsymbol{z})$.

The guide fields in storage rings are produced by dipole and quadrupole magnets. The dipole fields constrain the particles to almost circular orbits and the quadrupole fields focus the beam, thus ensuring that the particles do not drift too far away from the central orbit. In these fields, spins precess according to the T-BMT equation (2.22).

In horizontally bending dipoles, spins precess only around the vertical field direction. The quadrupoles have vertical and horizontal fields and additionally cause the spins to precess away from the vertical direction. The strength of the spin precession and the precession axis in machine magnets depends on the trajectory and the energy of the particle. Thus in one turn around the ring, the effective precession axis can deviate from the vertical and can strongly depend on the initial position of the particle in the 6-dimensional phase space of (2.19). From this it is clear that if an invariant spin field $\boldsymbol{n}(\boldsymbol{z})$ exists, it can vary across the orbital phase space. Several examples will illustrate that this variation can be large.

At very high energy, as for example in the HERA-p [56, 48, 57], it can happen that $\boldsymbol{n}(\boldsymbol{z})$ for particles with realistic phase space amplitudes deviates by tens of degrees from the beam average $\langle\boldsymbol{n}\rangle$ at azimuth θ_0. Thus even if each point in phase space were 100% polarized parallel to $\boldsymbol{n}(\boldsymbol{z})$, the beam-average polarization, which would be $|\langle\boldsymbol{n}\rangle|$, could be much smaller than 100%. This was first pointed out in [58] for the Super-conducting Super Collider (SSC) and in [56] for HERA-p. Clearly it is very important to have accurate and efficient methods for calculating $\boldsymbol{n}(\boldsymbol{z})$ and for ensuring that the spread of $\boldsymbol{n}(\boldsymbol{z})$ is as small as possible.

However, although it has been straightforward to define $\boldsymbol{n}(\boldsymbol{z},\theta)$, it is not easy to calculate this spin field in general, and much effort has been expended on this topic [59, 60, 61, 62, 63, 64, 65, 66], but mainly for electrons at energies up to 46 GeV. All algorithms developed before the polarized proton project at HERA-p rely on perturbation methods at some stage and either do not go to high enough order [29, 30, 66] or have problems with convergence at high order and high proton energies [62, 67]. In Chap. 4, several new methods for obtaining $\boldsymbol{n}(\boldsymbol{z},\theta)$ will be described and compared. But before that, some properties of the invariant spin field will have to be derived.

2.2.7 The Amplitude-dependent Spin Tune and the Uniqueness of $\boldsymbol{n}(\boldsymbol{z})$

The closed-orbit spin tune ν_0 has been introduced as the spin rotation angle divided by 2π for particles that have traveled one turn on the closed orbit. For particles that oscillate around the closed orbit, this rotation angle can depend on the amplitude of their oscillation. For the case that the orbit motion can be described in terms of action and angle variables $\boldsymbol{J}$ and $\boldsymbol{\Phi}$, as is always the case for stable linear motion, and the tunes Q_j are not in resonance on the invariant torus described by $\boldsymbol{J}$, it will now be shown how to define a spin rotation angle that is independent of $\boldsymbol{\Phi}$ on that torus.

Assuming that an $\boldsymbol{n}$-axis exists at an azimuth θ_0, one can introduce two unit vectors $\tilde{\boldsymbol{u}}_1(\boldsymbol{z})$ and $\tilde{\boldsymbol{u}}_2(\boldsymbol{z})$ to create a right-handed coordinate system $[\tilde{\boldsymbol{u}}_1, \tilde{\boldsymbol{u}}_2, \boldsymbol{n}]$. The vectors $\tilde{\boldsymbol{u}}_1$ and $\tilde{\boldsymbol{u}}_2$ are therefore defined up to a rotation around the $\boldsymbol{n}$-axis by an arbitrary phase space dependent angle $\phi(\boldsymbol{z})$. The spin direction $\boldsymbol{S}$ is expressed in terms of this coordinate system by the relation

$\boldsymbol{S} = s_1\tilde{\boldsymbol{u}}_1 + s_2\tilde{\boldsymbol{u}}_2 + J_S\boldsymbol{n}$. The coefficient J_S is called the spin action and does not change during the particle motion around the ring because the particle transport matrix $\mathsf{R}(\boldsymbol{z})$ is orthogonal and ensures that $J_S = \boldsymbol{S}\cdot\boldsymbol{n}$ is invariant. This property can be used to define the invariant function of spin-orbit motion $J_S(\boldsymbol{z},\boldsymbol{S}) = \boldsymbol{S}\cdot\boldsymbol{n}(\boldsymbol{z})$. If $(\boldsymbol{z}_i,\boldsymbol{S}_i)$ are the initial phase space point and the initial spin of a particle, then after one turn around the ring

$$\begin{aligned} J_S(\boldsymbol{z}_f,\boldsymbol{S}_f) &= J_S(\boldsymbol{M}(\boldsymbol{z}_i),\mathsf{R}(\boldsymbol{z}_i)\boldsymbol{S}_i) = [\mathsf{R}(\boldsymbol{z}_i)\boldsymbol{S}_i]\cdot\boldsymbol{n}(\boldsymbol{M}(\boldsymbol{z}_i)) \\ &= [\mathsf{R}(\boldsymbol{z}_i)\boldsymbol{S}_i]\cdot[\mathsf{R}(\boldsymbol{z}_i)\boldsymbol{n}(\boldsymbol{z}_i)] = \boldsymbol{S}_i\cdot\boldsymbol{n}(\boldsymbol{z}_i) = J_S(\boldsymbol{z}_i,\boldsymbol{S}_i)\ . \end{aligned} \tag{2.83}$$

For one turn, the spin motion in the coordinate system with $[\tilde{\boldsymbol{u}}_1,\tilde{\boldsymbol{u}}_2,\boldsymbol{n}]$ is a rotation around the $\boldsymbol{n}$-axis by a phase space dependent angle $2\pi\tilde{\nu}(\boldsymbol{z})$,

$$\begin{pmatrix} s_{f1} \\ s_{f2} \\ J_S \end{pmatrix} = \begin{pmatrix} \cos(2\pi\tilde{\nu}(\boldsymbol{z})) & -\sin(2\pi\tilde{\nu}(\boldsymbol{z})) & 0 \\ \sin(2\pi\tilde{\nu}(\boldsymbol{z})) & \cos(2\pi\tilde{\nu}(\boldsymbol{z})) & 0 \\ 0 & 0 & 1 \end{pmatrix} \begin{pmatrix} s_{i1} \\ s_{i2} \\ J_S \end{pmatrix}\ . \tag{2.84}$$

The first two rows can be written as

$$s_{f1} + \mathrm{i}s_{f2} = \mathrm{e}^{\mathrm{i}2\pi\tilde{\nu}(\boldsymbol{z})}(s_{i1} + \mathrm{i}s_{i2})\ . \tag{2.85}$$

By re-expressing this in terms of the complex quantity $\hat{s} = \mathrm{e}^{\mathrm{i}\phi(\boldsymbol{z})}(s_1 + \mathrm{i}s_2)$ where $\phi(\boldsymbol{z})$ is the arbitrary angle of $\tilde{\boldsymbol{u}}_1$ and $\tilde{\boldsymbol{u}}_2$, one obtains

$$\mathrm{e}^{-\mathrm{i}\phi(\boldsymbol{M}(\boldsymbol{z}))}\hat{s}_f = \mathrm{e}^{\mathrm{i}[2\pi\tilde{\nu}(\boldsymbol{z})-\phi(\boldsymbol{z})]}\hat{s}_i\ . \tag{2.86}$$

The one turn transport of phase space motion is described by $\boldsymbol{J}_f = \boldsymbol{J}_i$ and $\boldsymbol{\Phi}_f = \boldsymbol{\Phi}_i + 2\pi\boldsymbol{Q}$. Using the symbols $2\pi\tilde{\nu}_{\boldsymbol{J}}(\boldsymbol{\Phi})$ and $\phi_{\boldsymbol{J}}(\boldsymbol{\Phi})$ to indicate the spin rotation angle and the free phase of the coordinate system for motion on the invariant torus characterized by $\boldsymbol{J}$,

$$\hat{s}_f = \mathrm{e}^{\mathrm{i}(2\pi\tilde{\nu}_{\boldsymbol{J}}(\boldsymbol{\Phi})-\phi_{\boldsymbol{J}}(\boldsymbol{\Phi})+\phi_{\boldsymbol{J}}(\boldsymbol{\Phi}+2\pi\boldsymbol{Q}))}\hat{s}_i\ . \tag{2.87}$$

The goal of the subsequent manipulation is to choose $\phi_{\boldsymbol{J}}(\boldsymbol{\Phi})$ so that the spin motion characterized by the exponent is simplified to the extent that the rotation angle becomes independent of $\boldsymbol{\Phi}$. As with any function of phase space, the rotation $\mathrm{e}^{\mathrm{i}2\pi\tilde{\nu}_{\boldsymbol{J}}(\boldsymbol{\Phi})}$ is 2π-periodic in all components Φ_j. Therefore, the rotation angle can have a 2π-periodic contribution and a contribution linear in the phases

$$2\pi\tilde{\nu}_{\circ\boldsymbol{J}}(\boldsymbol{\Phi}) + \boldsymbol{j}\cdot\boldsymbol{\Phi}\ , \tag{2.88}$$

with some vector $\boldsymbol{j}$ that has integer components. We may just as well choose the rotation angle

$$2\pi\tilde{\nu}_{\boldsymbol{J}}(\boldsymbol{\Phi}) = \mathrm{Mod}(2\pi\tilde{\nu}_{\circ\boldsymbol{J}}(\boldsymbol{\Phi}) + \boldsymbol{j}\cdot\boldsymbol{\Phi}, 2\pi) \tag{2.89}$$

that is 2π-periodic and can thus be Fourier expanded. The rotation $\mathrm{e}^{\mathrm{i}\phi_{\boldsymbol{J}}(\boldsymbol{\Phi})}$ is also 2π-periodic in all components Φ_j. Therefore, the rotation angle $\phi_{\boldsymbol{J}}(\boldsymbol{\Phi})$ can also have a 2π-periodic contribution $\phi_{\circ\boldsymbol{J}}(\boldsymbol{\Phi})$ and a contribution linear in the phases

$$\phi_{\boldsymbol{J}}(\boldsymbol{\Phi}) = \phi_{\circ\boldsymbol{J}}(\boldsymbol{\Phi}) + \boldsymbol{j} \cdot \boldsymbol{\Phi} \; . \tag{2.90}$$

If the orbit tunes $\boldsymbol{Q}$ are not in resonance, then $\phi_{\boldsymbol{J}}(\boldsymbol{\Phi})$ can be chosen to eliminate the phase dependence of the exponent in (2.87) completely. This can be seen by Fourier transforming the periodic functions $\tilde{\nu}_{\boldsymbol{J}}(\boldsymbol{\Phi})$ and $\phi_{\circ\boldsymbol{J}}(\boldsymbol{\Phi})$ to obtain the following exponent in (2.87):

$$2\pi\boldsymbol{j} \cdot \boldsymbol{Q} + \sum_{\boldsymbol{k}}[2\pi\breve{\nu}_{\boldsymbol{J}}(\boldsymbol{k}) - \breve{\phi}_{\circ\boldsymbol{J}}(\boldsymbol{k})(1 - \mathrm{e}^{\mathrm{i}2\pi\boldsymbol{k}\cdot\boldsymbol{Q}})]\mathrm{e}^{\mathrm{i}\boldsymbol{k}\cdot\boldsymbol{\Phi}} \; . \tag{2.91}$$

By choosing the Fourier coefficients $\breve{\phi}_{\circ\boldsymbol{J}}(\boldsymbol{k})$ so that $\breve{\phi}_{\circ\boldsymbol{J}}(\boldsymbol{k}) = 2\pi\breve{\nu}_{\boldsymbol{J}}(\boldsymbol{k})/(1 - \mathrm{e}^{\mathrm{i}2\pi\boldsymbol{k}\cdot\boldsymbol{Q}})$, one can eliminate all Fourier coefficients $\breve{\nu}_{\boldsymbol{J}}(\boldsymbol{k})$ except for those with $\boldsymbol{k} = 0$. For this special choice of $\phi(\boldsymbol{z})$, the one turn spin rotation angle becomes $2\pi\nu(\boldsymbol{J}) = 2\pi[\breve{\nu}_{\boldsymbol{J}}(0)+\boldsymbol{j}\cdot\boldsymbol{Q}]$ and does not depend on $\boldsymbol{\Phi}$ but only on the action variables $\boldsymbol{J}$. Therefore, this rotation angle is the same for all particles on one invariant torus and thus does not change during particle motion. This spin precession rate $\nu(\boldsymbol{J})$ is a characteristic of the torus and allows the degree of coherence between spin and orbital motion to be quantified. In particular we expect coherent excitations of spin motion when the amplitude-dependent spin tune $\nu(\boldsymbol{J})$ is in resonance with the orbital tunes as in (2.74). Other angles that might be alternatively proposed [19, 68] do not correlate with resonance effects [69, 70, 71, 72].

To guarantee the convergence of the Fourier series of $\phi(\boldsymbol{z})$, I require the orbit tunes and 1 to be strongly incommensurable [33, Sect. 1.5], which implies that they are strongly non-orbit-resonant, defined as follows using the distance to the nearest integer $[\ldots]_d$ and the 1 norm $|\boldsymbol{k}|_1 = \sum_{n=1}^{3}|k_n|$:

Strongly non-orbit-resonant: *The particle motion is said to be strongly non-orbit-resonant if* $C, r \in I\!R^+$ *exist with* $[\boldsymbol{k}\cdot\boldsymbol{Q}]_d \geq C|\boldsymbol{k}|_1^{-r}$ *for all vectors* $\boldsymbol{k}$ *of integers.*

Strong incommensurability is a common requirement in perturbation theories, and for $r > \dim(\boldsymbol{k}) - 1$ (here $\dim(\boldsymbol{k})$=3) the set of $\boldsymbol{Q}$ for which there is no C has measure 0 [73, 74], [32, appendix 4].

The denominator $1 - \mathrm{e}^{\mathrm{i}2\pi\boldsymbol{k}\cdot\boldsymbol{Q}}$ then decreases with a power law, $|1 - \mathrm{e}^{\mathrm{i}2\pi\boldsymbol{k}\cdot\boldsymbol{Q}}| = 2|\sin(\pi\boldsymbol{k}\cdot\boldsymbol{Q})| \geq 4[\boldsymbol{k}\cdot\boldsymbol{Q}]_d \geq 4C|\boldsymbol{k}|_1^{-r}$. I further require that the spin rotation angle $2\pi\tilde{\nu}_{\boldsymbol{J}}(\boldsymbol{\Phi})$ has an analytic extension and therefore that its Fourier coefficients fall off exponentially with $|\boldsymbol{k}|_1$ [32, appendix 1.1], so as to counterbalance the denominator and to lead to a converging Fourier series. Alternatively, one could have required sufficient differentiability of $\tilde{\nu}_{\boldsymbol{J}}(\boldsymbol{\Phi})$, which would lead to a sufficiently strong power law fall-off for the $\breve{\phi}_{\boldsymbol{J}}(\boldsymbol{k})$ [32, appendix 1.2].

The coordinate vectors $\tilde{\boldsymbol{u}}_1$ and $\tilde{\boldsymbol{u}}_2$ for this special choice of $\phi(\boldsymbol{z})$ are referred to as $\boldsymbol{u}_1$ and $\boldsymbol{u}_2$. The exponent reduces to $\nu(\boldsymbol{J}) = \breve{\nu}_{\boldsymbol{J}}(0) + \boldsymbol{j}\cdot\boldsymbol{Q}$ and the spin rotation of (2.87) simplifies to

$$\hat{s}_f = \mathrm{e}^{\mathrm{i}2\pi\nu(\boldsymbol{J})}\hat{s}_i \; . \tag{2.92}$$

The goal of constructing a spin rotation depending only on orbital actions but not on the angle variables $\boldsymbol{\Phi}$ has now been achieved. The function $\nu(\boldsymbol{J})$ is called the amplitude-dependent spin tune. It is not unique, because one can add an integer j_0 and a linear combination $\boldsymbol{j}\cdot\boldsymbol{Q}$ of the orbit tunes by choosing different integers in (2.91). It is interesting to note that for action variables $\boldsymbol{J}$ where the integer components of $\boldsymbol{j}$ can be chosen so that

$$\nu(\boldsymbol{J}) + \boldsymbol{j}\cdot\boldsymbol{Q} = 0 \bmod 1 \ , \tag{2.93}$$

one can eliminate the spin rotation completely. These are the resonances described in equation 2.74. Several of the subsequent statements will be restricted to cases where this resonance condition is not satisfied. Furthermore, when $-\boldsymbol{n}(\boldsymbol{z})$ is chosen as the $\boldsymbol{n}$-axis for defining the spin tune on a torus, the spin tune ν also changes sign and $-\nu + j_0 + \boldsymbol{j}\cdot\boldsymbol{Q}$ could alternatively be chosen as the spin tune. This leads to the following conclusion:

Existence of $\nu(\boldsymbol{J})$: *Given that an $\boldsymbol{n}$-axis exists, that the system is strongly non-orbit-resonant, and that the above-mentioned analytic extension of the spin rotation angle $2\pi\tilde{\nu}$ exists, then a coordinate system $[\boldsymbol{u}_1, \boldsymbol{u}_2, \boldsymbol{n}]$ can be specified that defines an amplitude-dependent spin tune $\nu(\boldsymbol{J})$. This choice is not unique, because $\pm\nu + j_0 + \boldsymbol{j}\cdot\boldsymbol{Q}$ can also be chosen as the spin tune.*

Usually the integers are chosen so that the limit for small amplitudes is equal to the closed-orbit spin tune ν_0, which is $G\gamma$ for a unperturbed flat ring without solenoids.

Note that the free rotation angle of the coordinate system ϕ cannot eliminate all phase dependence of the spin rotation angle $2\pi\tilde{\nu}$ when the orbital tunes are resonant. To make this distinction clear, we speak of a phase space dependent spin rotation angle in this case, rather than of the amplitude-dependent spin tune.

To analyze the uniqueness of the $\boldsymbol{n}$-axis, the periodicity condition (2.82) is written in the coordinate system $[\boldsymbol{u}_1, \boldsymbol{u}_2, \boldsymbol{n}]$,

$$\boldsymbol{n}(\boldsymbol{M}(\boldsymbol{z})) = \begin{pmatrix} \cos(2\pi\nu) & -\sin(2\pi\nu) & 0 \\ \sin(2\pi\nu) & \cos(2\pi\nu) & 0 \\ 0 & 0 & 1 \end{pmatrix} \cdot \boldsymbol{n}(\boldsymbol{z}) \ , \tag{2.94}$$

with the obvious solution $\boldsymbol{n}(\boldsymbol{z}) = (0,0,1)^T$ for all $\boldsymbol{z}$. If another $\boldsymbol{n}$-axis $\boldsymbol{n}_2(\boldsymbol{z})$ exists, then $\boldsymbol{n}_2 - \boldsymbol{n}(\boldsymbol{n}\cdot\boldsymbol{n}_2)$ is non-zero at least at one phase space point and on all iterates of this point that can be reached during particle motion. This difference vector at these phase space points is normalized and written as $\cos(\alpha(\boldsymbol{z}))\boldsymbol{u}_1 + \sin(\alpha(\boldsymbol{z}))\boldsymbol{u}_2$ or as $\mathrm{e}^{\mathrm{i}\alpha(\boldsymbol{z})}$. In orbital action-angle variables, the function $\alpha_{\boldsymbol{J}}(\boldsymbol{\Phi}) = \alpha_{\circ\boldsymbol{J}}(\boldsymbol{\Phi}) + \boldsymbol{j}\cdot\boldsymbol{\Phi}$ has a 2π-periodic contribution and a linear contribution, and in complex notation, the periodicity condition (2.94) reads as

$$\mathrm{e}^{\mathrm{i}\alpha_{\boldsymbol{J}}(\boldsymbol{\Phi}+2\pi\boldsymbol{Q})} = \mathrm{e}^{\mathrm{i}[2\pi\nu(\boldsymbol{J})+\alpha_{\boldsymbol{J}}(\boldsymbol{\Phi})]} \ . \tag{2.95}$$

This requires that all Fourier coefficients of $\alpha_{\circ \boldsymbol{J}}(\boldsymbol{\Phi})$ vanish except $\breve{\alpha}_{\circ \boldsymbol{J}}(0)$. The resulting equation $\nu(\boldsymbol{J}) = \boldsymbol{j} \cdot \boldsymbol{Q}$ mod 1 shows that the periodicity condition (2.95) for $\boldsymbol{n}_2(\boldsymbol{z})$ can only be satisfied when a spin-orbit resonance occurs. Otherwise the invariant spin field is unique. This is summarized as follows.

Uniqueness of $\boldsymbol{n}(\boldsymbol{z})$: no spin-orbit resonance: *If an $\boldsymbol{n}$-axis and basis vectors $\boldsymbol{u}_1$, $\boldsymbol{u}_2$ exist and the spin rotation angle in one turn is not a linear combination of orbit phase advances modulo 2π, then the $\boldsymbol{n}$-axis is unique up to a sign.*

If the orbital tunes are rational, one can also formulate some statements about the uniqueness of the $\boldsymbol{n}$-axis. Given that the phase space motion can be described by action-angle variables and that the orbital tunes on an invariant torus in the Poincaré section at azimuth θ_0 are rational numbers, $Q_j = \frac{n_j}{m_j}$ where the smallest possible denominators are used, let N be the smallest common multiple of these denominators. Then $\boldsymbol{M}^N(\boldsymbol{z})$ is the identity map whereas $\boldsymbol{M}^n(\boldsymbol{z})$ is not the identity map for any $n < N$ and the following conclusions can be drawn:

Uniqueness of $\boldsymbol{n}(\boldsymbol{z})$: rational tunes: *If for some $N \in \mathbb{N}$, the N turn spin transport matrix on an invariant torus is not the identity matrix but the N turn orbital transport map is the identity, then an $\boldsymbol{n}$-axis exists on this invariant torus and is unique up to a sign at each phase space point.*

To show this, the spin transport matrix $\mathsf{R}_N(\boldsymbol{z})$ for N turns around the ring starting at θ_0 is used. Because it is not the identity matrix, it describes a rotation around a vector $\boldsymbol{e}_N(\boldsymbol{z})$ that is unique up to a sign. After N turns, the phase space transport map is the identity map and the periodicity condition of (2.82) for an $\boldsymbol{n}$-axis $\boldsymbol{n}_N(\boldsymbol{z})$ of the N turn spin-orbit system becomes $\boldsymbol{n}_N(\boldsymbol{z}) = \mathsf{R}_N(\boldsymbol{z})\boldsymbol{n}_N(\boldsymbol{z})$. The rotation vector $\boldsymbol{e}_N(\boldsymbol{z})$ is therefore the $\boldsymbol{n}$-axis $\boldsymbol{n}_N(\boldsymbol{z})$, unique up to a sign. The rotation vector $\boldsymbol{e}_N(\boldsymbol{M}(\boldsymbol{z}))$ of $\mathsf{R}_N(\boldsymbol{M}(\boldsymbol{z}))$ is given by $\pm\mathsf{R}(\boldsymbol{z})\boldsymbol{e}_N(\boldsymbol{z})$ because

$$\mathsf{R}_N(\boldsymbol{M}(\boldsymbol{z}))\mathsf{R}(\boldsymbol{z})\boldsymbol{e}_N(\boldsymbol{z}) = \mathsf{R}(\boldsymbol{M}^N(\boldsymbol{z}))\mathsf{R}_N(\boldsymbol{z})\boldsymbol{e}_N(\boldsymbol{z}) = \mathsf{R}(\boldsymbol{z})\boldsymbol{e}_N(\boldsymbol{z}) \; , \tag{2.96}$$

where the fact that $\boldsymbol{M}^N(\boldsymbol{z})$ is the identity map was used. The rotation vectors are unique up to a sign, and $\boldsymbol{e}_N(\boldsymbol{z})$ satisfies the periodicity condition (2.82) of an $\boldsymbol{n}$-axis up to a possible sign change,

$$\boldsymbol{e}_N(\boldsymbol{M}(\boldsymbol{z})) = \pm\mathsf{R}(\boldsymbol{z})\boldsymbol{e}_N(\boldsymbol{z}) \; . \tag{2.97}$$

Because $\boldsymbol{M}^N(\boldsymbol{z})$ is the identity map, a particle with initial phase space point $\boldsymbol{z}_i$ can only reach the N phase space points $Z(\boldsymbol{z}_i) = \{\boldsymbol{z}|\boldsymbol{M}^n(\boldsymbol{z}_i), n \in \{1, \ldots, N\}\}$, which will be called the trajectory through $\boldsymbol{z}_i$. Given that the sign for $\boldsymbol{e}_N(\boldsymbol{z}_i)$ has been chosen, then the sign of the rotation vectors on the trajectory through $\boldsymbol{z}_i$ is chosen so that the + sign in (2.97) is obtained. This equation is then the periodicity condition of (2.82) for $\boldsymbol{e}_N(\boldsymbol{z})$ and shows that $\boldsymbol{n}(\boldsymbol{z}) = \boldsymbol{e}_N(\boldsymbol{z})$ is an invariant spin field that is unique up to a sign for each trajectory.

A note on smoothness is in place. When N is the smallest integer for which $\boldsymbol{M}^N(\boldsymbol{z})$ is the identity map, then a connected phase space A_1 area can be found which can be iterated under the map $N-1$ times so that it covers all of the invariant torus. This means that the N iterations A_n with $A_n = \{\boldsymbol{M}(\boldsymbol{z})|\boldsymbol{z} \in A_{n-1}\}$ for $n \in \{2, N\}$ cover the invariant torus. An example for A_1 would be the part of the invariant torus for which $\Phi_1 \in [0, \frac{2\pi}{N})$. Assuming sufficient smoothness of $\mathsf{R}_N(\boldsymbol{z})$, the rotation vector $\boldsymbol{e}_N(\boldsymbol{z})$ will also vary smoothly over phase space, and the signs on each trajectory are chosen so that $\boldsymbol{n}(\boldsymbol{z}) = \boldsymbol{e}_N(\boldsymbol{z})$ is a smooth function on A_1. The so-defined $\boldsymbol{n}$-axis is continuous in each section A_n but does not have to be continuous at the surface of these sections, see examples in [75]. Because the section A_1 is not unique, the locations of these discontinuities are not unique. At these points of discontinuity, however, $\boldsymbol{n}$ only changes sign, not direction.

Even though it is straightforward to find an $\boldsymbol{n}$-axis for such a system with rational orbital tunes, it is important to note that an amplitude-dependent spin tune can in general not be computed for this $\boldsymbol{n}$-axis because the dependence of the spin rotation angle $2\pi\tilde{\nu}_{\boldsymbol{J}}(\boldsymbol{\Phi})$ on $\boldsymbol{\Phi}$ can in general only be eliminated in (2.91) when there is no resonance for the orbital tunes. When the phase dependence cannot be eliminated, we refer to the phase space dependent spin rotation angle.

Non-uniqueness of $\boldsymbol{n}(\boldsymbol{z})$: *If for some $N \in I\!N$, the N turn spin transport matrix on the invariant torus and also the N turn orbital transport map are the identity, then an $\boldsymbol{n}$-axis exists but it is not unique.*

In such a system all orbital tunes are rational and for each tune Q_j, the smallest possible denominator is denoted here by m_j. Let the angle variables $\boldsymbol{\Phi}_0 = 0$ correspond to the point $\boldsymbol{z}_0$ in phase space at some azimuth θ_0. There is a number k of turns after which a particle, starting at $\boldsymbol{z}_0$, will have reached the phase space point $\boldsymbol{z}_k$ which has the angle variables $\Phi_j = \frac{2\pi}{m_j}$. We introduce the set of phase space points $P_1 = \{\boldsymbol{z}|\Phi_j \in [0, \frac{2\pi}{m_j})$ for all $j\}$ and note that the complete torus is covered by the sets $P_n = \{\boldsymbol{z}|\Phi_j - nQ_j \in [0, \frac{2\pi}{m_j}]$ for all $j\}$ which are obtained by transporting the phase space points of P_1 through the one turn transport map $\boldsymbol{M}$ for n times. At the fixed azimuth θ_0 the trajectory $Z(\boldsymbol{z}_i)$ through a point $\boldsymbol{z}_i$ contains N points each of which is located in one of the P_n.

Consider a spin field $\boldsymbol{f}(\boldsymbol{z})$ which is arbitrarily chosen for all $\boldsymbol{z} \in P_1$. For all points $\boldsymbol{M}^n(\boldsymbol{z}) \in P_{n+1}$ it is chosen to satisfy $\boldsymbol{f}(\boldsymbol{M}^n(\boldsymbol{z})) = \mathsf{R}^n(\boldsymbol{z})\boldsymbol{f}(\boldsymbol{z})$ for $n \in \{1, \ldots, N-1\}$. This defines the spin field on the complete torus.

Due to this definition, the periodicity condition $\boldsymbol{f}(\boldsymbol{M}(\boldsymbol{z})) = \mathsf{R}(\boldsymbol{z})\boldsymbol{f}(\boldsymbol{z})$ is satisfied for all $\boldsymbol{z} \in P_n$ with $n \in \{1, \ldots, N-1\}$. But due to the assumption that $\boldsymbol{M}^N$ and $\boldsymbol{R}^N$ are the identity, it is also satisfied for P_N and thus for all of the torus. Therefore, $\boldsymbol{f}(\boldsymbol{z})$ is an invariant spin field, and because it was chosen arbitrarily for a set of points on the torus, it is not unique.

2.2.8 Maximum Time-Average Polarization

If two particles travel with the same phase space point along the same trajectory, the angle between their spins does not change. This is a consequence of the vector product in the T-BMT equation (2.28) and has already been stated in Sect. 2.2.7. Because $\boldsymbol{n}(\boldsymbol{z})$ is a spin field on the Poincaré section at θ_0 and is therefore propagated according to the T-BMT equation, the angle ϑ between a spin and $\boldsymbol{n}(\boldsymbol{z})$ will be the same every time a particle comes back to θ_0. Whenever, after some number of turns, a particle that started at $\boldsymbol{z}_i$ comes back to θ_0 with a phase space coordinate that is close to $\boldsymbol{z}_i$, the spin will again have an angle of approximately ϑ with respect to $\boldsymbol{n}(\boldsymbol{z}_i)$, assuming $\boldsymbol{n}(\boldsymbol{z})$ is sufficiently continuous. Because the components perpendicular to the $\boldsymbol{n}$-axis average to zero after many turns, the time-averaged polarization at $\boldsymbol{z}_i$ will be parallel to $\boldsymbol{n}(\boldsymbol{z}_i)$, and it can only have the magnitude 1 if the spin was initially parallel to the invariant spin field. However, even if all particles are initially polarized parallel to $\boldsymbol{n}(\boldsymbol{z})$, the beam polarization is not 1 but it is given by the beam average $|\langle\boldsymbol{n}\rangle|$, and this quantity can be small as stated in Sect. 2.2.6. In summary, the maximum time-average beam polarization that can be stored in an accelerator at a given fixed energy is therefore $P_{lim} = |\langle\boldsymbol{n}\rangle|$.

To prove in a formal way that the time-average polarization is parallel to $\boldsymbol{n}(\boldsymbol{z})$ if an invariant spin field exists and if the phase space coordinates stay on an invariant torus, I assume the beam initially has some spin field $\boldsymbol{f}(\boldsymbol{z})$ on the Poincaré section at θ_0 and perform the time average in the coordinate system $[\boldsymbol{u}_1, \boldsymbol{u}_2, \boldsymbol{n}]$ introduced in Sect. 2.2.7. Action-angle variables are used and the initial spin field in this coordinate system is written as $\boldsymbol{f}_0(\boldsymbol{\Phi})$. The action variables $\boldsymbol{J}$ are constant during a particle's motion and will not be indicated in the following derivation.

It is assumed that $\boldsymbol{f}_0(\boldsymbol{\Phi})$ possesses an analytic extension for $\Phi_j \in \mathbb{C}$, $\Im\{\Phi_j\} < \sigma$ with $\sigma > 0$, and it is assumed that the system is strongly non-orbit-resonant, implying $[\boldsymbol{j} \cdot \boldsymbol{Q}]_d \geq C|\boldsymbol{j}|_1^{-r}$ for some $C, r \in \mathbb{R}^+$. As with the requirement of an analytic extension and of strong incommensurability in Sect. 2.2.7, these conditions will be needed to guarantee the convergence of a Fourier series with resonance denominators. Furthermore, it is assumed that the motion is strongly non-spin-orbit-resonant in the following sense:

Strongly non-spin-orbit-resonant: *The particle motion is said to be strongly non-spin-orbit-resonant if $C, r \in \mathbb{R}^+$ exist with $[\nu + \boldsymbol{k} \cdot \boldsymbol{Q}]_d \geq C|\boldsymbol{k}|_1^{-r}$ for all vectors $\boldsymbol{k}$ of integers. Note that this is a weaker condition than strong* *incommensurability of the spin-orbit tunes and 1 because ν is not multiplied by an integer.*

As in Sect. 2.2.7, the set of spin and orbit tunes for which there is no C, given that $r > 2$, has measure 0.

As described in (2.28), the spin field is transported once around the ring by the one turn spin transport matrix, which has an especially simple form in the chosen coordinate system,

$$\boldsymbol{f}_j(\boldsymbol{\Phi}) = \begin{pmatrix} \cos(2\pi\nu) & -\sin(2\pi\nu) & 0 \\ \sin(2\pi\nu) & \cos(2\pi\nu) & 0 \\ 0 & 0 & 1 \end{pmatrix} \boldsymbol{f}_{j-1}(\boldsymbol{\Phi} - 2\pi\boldsymbol{Q}) \ , \tag{2.98}$$

where $\boldsymbol{f}_j(\boldsymbol{\Phi})$ is the spin field on the Poincaré section at θ_0 after j turns around the ring. The average at θ_0 after N turns in this coordinate system is therefore

$$\{\boldsymbol{f}\}_N(\boldsymbol{\Phi}) = \sum_{j=0}^{N} \begin{pmatrix} \cos(j2\pi\nu) & -\sin(j2\pi\nu) & 0 \\ \sin(j2\pi\nu) & \cos(j2\pi\nu) & 0 \\ 0 & 0 & 1 \end{pmatrix} \frac{\boldsymbol{f}_0(\boldsymbol{\Phi} - j2\pi\boldsymbol{Q})}{N+1} \ . \tag{2.99}$$

The third component of $\{\boldsymbol{f}\}_N$ is $\sum_{j=0}^{N} f_{0,3}(\boldsymbol{\Phi} - j2\pi\boldsymbol{Q})/(N+1)$ and the first and second components in complex notation are

$$\{\hat{f}\}_N = \{f\}_{N,1} + \mathrm{i}\{f\}_{N,2} = \frac{1}{N+1}\sum_{j=0}^{N} \mathrm{e}^{\mathrm{i}j2\pi\nu} \hat{f}_0(\boldsymbol{\Phi} - j2\pi\boldsymbol{Q}) \ , \tag{2.100}$$

where $\hat{f}_0(\boldsymbol{\Phi}) = f_{0,1}(\boldsymbol{\Phi}) + \mathrm{i}f_{0,2}(\boldsymbol{\Phi})$. In terms of the Fourier coefficients $\breve{f}_0(\boldsymbol{k})$ of $\hat{f}_0(\boldsymbol{\Phi})$ one obtains the inequality

$$\begin{aligned} |\{\hat{f}\}_N| &= |\frac{1}{N+1}\sum_{\boldsymbol{k}}\sum_{j=0}^{N} \mathrm{e}^{\mathrm{i}j2\pi(\nu - \boldsymbol{k}\cdot\boldsymbol{Q})} \breve{f}_0(\boldsymbol{k})\mathrm{e}^{\mathrm{i}\boldsymbol{k}\cdot\boldsymbol{\Phi}}| \\ &= \frac{1}{N+1}|\sum_{\boldsymbol{k}} \frac{1 - \mathrm{e}^{\mathrm{i}(N+1)2\pi(\nu - \boldsymbol{k}\cdot\boldsymbol{Q})}}{1 - \mathrm{e}^{\mathrm{i}2\pi(\nu - \boldsymbol{k}\cdot\boldsymbol{Q})}} \breve{f}_0(\boldsymbol{k})\mathrm{e}^{\mathrm{i}\boldsymbol{k}\cdot\boldsymbol{\Phi}}| \\ &\leq \frac{1}{N+1}\sum_{\boldsymbol{k}} \frac{2}{|1 - \mathrm{e}^{\mathrm{i}2\pi(\nu - \boldsymbol{k}\cdot\boldsymbol{Q})}|}|\breve{f}_0(\boldsymbol{k})| \ . \end{aligned} \tag{2.101}$$

The sum over $\boldsymbol{k}$ is finite. This is because $\boldsymbol{f}_0(\boldsymbol{\Phi})$ was assumed to have an analytic extension so that its Fourier coefficients fall off exponentially with $|\boldsymbol{k}|_1$ and because the denominator only falls off with a power law in $\boldsymbol{k}$ because the motion is strongly non-spin-orbit-resonant, $|1 - \mathrm{e}^{\mathrm{i}2\pi(\nu - \boldsymbol{k}\cdot\boldsymbol{Q})}| = 2|\sin(\pi(\nu - \boldsymbol{k}\cdot\boldsymbol{Q}))| \geq 4[\nu - \boldsymbol{k}\cdot\boldsymbol{Q}]_d \geq C|\boldsymbol{k}|_1^{-r}$. As an alternative to requiring an analytic extension of $\boldsymbol{f}_0(\boldsymbol{\Phi})$, one could require sufficient differentiability that would lead to a sufficiently strong power law fall-off for the $\breve{f}_0(\boldsymbol{k})$ [32, appendix 1].

Similarly for the third component of $\{\boldsymbol{f}\}_N$ one obtains

$$\{f\}_{N,3} = \breve{f}_{0,3}(0) + \frac{1}{N+1} \sum_{\boldsymbol{k} \neq 0} \frac{1 - \mathrm{e}^{-\mathrm{i}2\pi(N+1)\boldsymbol{k}\cdot\boldsymbol{Q}}}{1 - \mathrm{e}^{-\mathrm{i}2\pi\boldsymbol{k}\cdot\boldsymbol{Q}}} \breve{f}_{0,3}(\boldsymbol{k})\mathrm{e}^{\mathrm{i}\boldsymbol{k}\cdot\boldsymbol{\Phi}} , \quad (2.102)$$

where the sum over $\boldsymbol{k}$ converges for the given strongly non-orbit-resonant motion. For large N, $\{\boldsymbol{f}\}_N$ therefore converges linearly with $1/N$ to $\breve{f}_{0,3}\boldsymbol{n}$. The time-average polarization $\{\boldsymbol{f}\}(\boldsymbol{z}) = \lim_{N\to\infty}\{\boldsymbol{f}\}_N(\boldsymbol{z})$ at a phase space point $\boldsymbol{z}_i$ is parallel to $\boldsymbol{n}(\boldsymbol{z}_i)$ and can only be 1 if the initial spin state was already parallel to this $\boldsymbol{n}$-axis at every phase space point from which a particle can travel to $\boldsymbol{z}_i$. If $\{\boldsymbol{f}\}(\boldsymbol{z})$ is zero, there is no time-average polarization usable for the particle physics experiment. This proves the following conclusion:

Time-averaged polarization: *If the motion is strongly non-orbit-resonant and strongly non-spin-orbit-resonant and an invariant spin field $\boldsymbol{n}(\boldsymbol{z})$ exists on an invariant torus, then any initial spin field (which satisfies some requirement about analytic extensibility given above) has a time-average polarization at a phase space point $\boldsymbol{z}$ that is parallel to $\boldsymbol{n}(\boldsymbol{z})$. The maximum time-average polarization of a particle beam is the beam average $P_{lim} = |\langle\boldsymbol{n}\rangle|$, which is only realized when the spins of all particles are initially parallel to $\boldsymbol{n}(\boldsymbol{z})$.*

2.2.9 The Adiabatic Spin Invariant on Phase Space Trajectories

As explained in the previous section, the maximum time-average polarization attainable in a storage ring at a fixed energy can be small when $\boldsymbol{n}(\boldsymbol{z})$ has a large divergence over the beam, thereby leading to a small beam average $|\langle\boldsymbol{n}\rangle|$. It is however often possible, as will be seen for HERA-p in later sections, to choose an operation energy where the spread of the invariant spin field over the beam is acceptably small. But how can a polarized proton beam be transported with little loss of polarization from low energy through regions with small $P_{lim} = |\langle\boldsymbol{n}\rangle|$, and therefore small beam polarization, to a suitable energy where P_{lim} is acceptable? Can the beam polarization recover to large values at this suitable energy after it was much smaller, at least as small as P_{lim}, at lower energies?

This is possible if the spins that are initially parallel to $\boldsymbol{n}(\boldsymbol{z})$ remain close to the invariant spin field along their trajectories even when parameters of particle motion, for example the particles' energy, are slowly changed. In general, the invariant spin field on the Poincaré section at θ_0 changes when parameters such as the beam energy or quadrupole settings are changed. In other words, if the variable τ describes one of these parameters, then $\boldsymbol{n}(\boldsymbol{z},\tau)$ changes when τ varies from the initial setting $\tau_i = 0$. Of course it is assumed that an $\boldsymbol{n}$-axis exists for every value that this parameter might take. A beam that is polarized according to the invariant spin field and initially has the polarization $|\langle\boldsymbol{n}(\boldsymbol{z},0)\rangle|$ will remain polarized closely parallel to $\boldsymbol{n}(\boldsymbol{z},\tau)$ while τ is changed, as long as the change is slow enough and no very strong resonance effects diminish the polarization. For example while the beam is accelerated slowly, the beam polarization can be low when $P_{lim} = |\langle \boldsymbol{n} \rangle|$ is small, but when the spins follow the slow change of $\boldsymbol{n}(\boldsymbol{z}, \tau)$ with the energy parameter τ, the beam can have high polarization later, when the energy has reached a value where P_{lim} is large.

I will now prove that spins follow slow changes of the invariant spin field by showing that the product $J_S = \boldsymbol{S} \cdot \boldsymbol{n}(\boldsymbol{z})$ is an adiabatic invariant. On the closed orbit, the invariant spin field $\boldsymbol{n}(\boldsymbol{z})$ is parallel to the one turn rotation vector $\boldsymbol{n}_0$. It was shown in Sect. 2.2.1 that the angle between $\boldsymbol{n}_0(\theta)$ and the spin $\boldsymbol{S}(\theta)$ of a particle traveling on the closed orbit changes little when the system changes slowly, and $s_3(\theta) = \boldsymbol{S}(\theta) \cdot \boldsymbol{n}_0(\theta)$ was thereby proven to be an adiabatic invariant. This proof will now be generalized to show that $J_S = \boldsymbol{S} \cdot \boldsymbol{n}(\boldsymbol{z}, \tau)$ changes little along a particle trajectory while the spin motion $\boldsymbol{S}$ and the phase space motion $\boldsymbol{z}$ are subjected to equations of motion that change slowly with the parameter $\tau = \varepsilon\theta$,

$$\frac{\mathrm{d}}{\mathrm{d}\theta}\boldsymbol{z} = \boldsymbol{v}(\boldsymbol{z}, \theta, \tau) \ , \quad \frac{\mathrm{d}}{\mathrm{d}\theta}\boldsymbol{S} = \boldsymbol{\Omega}(\boldsymbol{z}, \theta, \tau) \times \boldsymbol{S} \ . \tag{2.103}$$

It is assumed that action-angle variables $\boldsymbol{J}$, $\boldsymbol{\Phi}$ and an invariant spin field $\boldsymbol{n}(\boldsymbol{z}, \tau)$ exist for all fixed parameters $\tau \in [0, 1]$ at some azimuth θ_0. Because the $\boldsymbol{n}$-axis is a spin field, it is propagated around the ring like $\boldsymbol{S}$ in (2.103). Furthermore, it is assumed that a coordinate system $[\boldsymbol{u}_1, \boldsymbol{u}_2, \boldsymbol{n}]$ exists at θ_0 for all fixed parameters $\tau \in [0, 1]$. To obtain a 2π-periodic coordinate system, we propagate $\boldsymbol{u}_1$ and $\boldsymbol{u}_2$ by

$$\frac{\mathrm{d}}{\mathrm{d}\theta}\boldsymbol{u}_i = (\boldsymbol{\Omega} - \nu\boldsymbol{n}) \times \boldsymbol{u}_i \ . \tag{2.104}$$

This lets spins rotate uniformly around $\boldsymbol{n}$ during one turn, after which their rotation is described by (2.94). This leads to an amplitude-dependent spin tune $\nu(\boldsymbol{J}, \tau)$, which in general depends on τ. These are non-trivial assumptions, because during the analysis of the existence of $\nu(\boldsymbol{J})$ in Sect. 2.2.7, the existence of $\boldsymbol{u}_1$ and $\boldsymbol{u}_2$ was only guaranteed when the system is strongly non-orbit-resonant. It is also taken into account that the tunes $\boldsymbol{Q}(\boldsymbol{J}, \tau)$ of phase space motion depend on the action variables and on the parameter τ, which slowly changes the system.

Using the phase space dependent 2π-periodic coordinate system, the spin of a particle with phase space coordinate $\boldsymbol{z}$ at azimuth θ is described by $\boldsymbol{S} = s_1\boldsymbol{u}_1 + s_2\boldsymbol{u}_2 + J_S\boldsymbol{n}$. The periodic unit vectors depend on τ and, when τ is changed, their variation with τ can only be a rotation around some vector $\boldsymbol{\eta}(\boldsymbol{z}, \theta, \tau)$,

$$\partial_\tau \boldsymbol{n} = \boldsymbol{\eta}(\boldsymbol{z}, \theta, \tau) \times \boldsymbol{n} \ , \quad \partial_\tau(\boldsymbol{u}_1 + \mathrm{i}\boldsymbol{u}_2) = \boldsymbol{\eta}(\boldsymbol{z}, \theta, \tau) \times (\boldsymbol{u}_1 + \mathrm{i}\boldsymbol{u}_2) \ . \tag{2.105}$$

In analogy to (2.56) $\boldsymbol{\eta}$ can be computed by the relation

$$\boldsymbol{\eta} = \frac{1}{2}(\boldsymbol{u}_1 \times \partial_\tau \boldsymbol{u}_1 + \boldsymbol{u}_2 \times \partial_\tau \boldsymbol{u}_2 + \boldsymbol{n} \times \partial_\tau \boldsymbol{n}) \ . \tag{2.106}$$

When the parameter $\tau = \varepsilon\theta$ changes slowly, the equation of spin motion can be written as

$$\begin{aligned}\boldsymbol{\Omega}(\boldsymbol{z},\theta,\tau)\times\boldsymbol{S} &= \frac{\mathrm{d}}{\mathrm{d}\theta}\boldsymbol{S} \\ &= \boldsymbol{u}_1\frac{\mathrm{d}}{\mathrm{d}\theta}s_1+\boldsymbol{u}_2\frac{\mathrm{d}}{\mathrm{d}\theta}s_2+\boldsymbol{n}\frac{\mathrm{d}}{\mathrm{d}\theta}J_S \\ &\quad +(\boldsymbol{\Omega}-\nu\boldsymbol{n})\times\boldsymbol{S}+(\frac{\mathrm{d}}{\mathrm{d}\theta}\tau)\boldsymbol{\eta}\times\boldsymbol{S}\ .\end{aligned} \tag{2.107}$$

The spin coordinates then have the following equations of motion:

$$\begin{aligned}\frac{\mathrm{d}}{\mathrm{d}\theta}\begin{pmatrix} s_1 \\ s_2 \\ J_S\end{pmatrix} &= \begin{pmatrix} \{[\nu(\boldsymbol{J},\tau)\boldsymbol{n}-\varepsilon\boldsymbol{\eta}]\times\boldsymbol{S}\}\cdot\boldsymbol{u}_1 \\ \{[\nu(\boldsymbol{J},\tau)\boldsymbol{n}-\varepsilon\boldsymbol{\eta}]\times\boldsymbol{S}\}\cdot\boldsymbol{u}_2 \\ \{\qquad\qquad -\varepsilon\boldsymbol{\eta}\ \times\boldsymbol{S}\}\cdot\boldsymbol{n}\end{pmatrix} \\ &= \begin{pmatrix} \varepsilon(\ \eta_3 s_2\ -\eta_2 J_S\ )-\nu(\boldsymbol{J},\tau)s_2 \\ \varepsilon(\ \eta_1 J_S\ -\eta_3 s_1\ )+\nu(\boldsymbol{J},\tau)s_1 \\ \varepsilon(\ \eta_2 s_1\ -\eta_1 s_2\ )\end{pmatrix}\ ,\end{aligned} \tag{2.108}$$

with $\boldsymbol{\eta} = \eta_1\boldsymbol{u}_1+\eta_2\boldsymbol{u}_2+\eta_3\boldsymbol{n}$ and $\tau = \varepsilon\theta$. This equation is obviously very similar to (2.59) for particles on the closed orbit, and for $1-J_S^2 \geq \Delta \in I\!R^+$ one writes $s_1 = \sqrt{1-J_S^2}\cos\phi$ and $s_2 = \sqrt{1-J_S^2}\sin\phi$ and obtains

$$\frac{\mathrm{d}}{\mathrm{d}\theta}\begin{pmatrix} J_S \\ \phi\end{pmatrix} = \begin{pmatrix} \varepsilon\ (\eta_2\cos\phi-\eta_1\sin\phi)\sqrt{1-J_S^2} \\ \nu(\boldsymbol{J},\tau)+\ \varepsilon[(\eta_2\sin\phi+\eta_1\cos\phi)\frac{J_S}{\sqrt{1-J_S^2}}-\eta_3]\end{pmatrix}\ , \tag{2.109}$$

where the vector $\boldsymbol{\eta}$ depends on the orbit variables $\boldsymbol{J}$ and $\boldsymbol{\Phi}$ and on θ. A similar equation for the change of J_S with slowly changing particle energy has been derived in [58]. This system has the slowly varying coordinates $\boldsymbol{J}$ and J_S and the quickly varying phases $\boldsymbol{\Phi}$ and ϕ. It is therefore suitable for averaging methods. To bring it into standard form, where the frequencies only depend on slowly changing variables and the right-hand side is 2π-periodic in all phases, the slowly changing variable τ with $\frac{\mathrm{d}}{\mathrm{d}\theta}\tau = \varepsilon$ is used and $\tilde{\theta}$ is introduced as a phase variable with $\frac{\mathrm{d}}{\mathrm{d}\theta}\tilde{\theta} = 1$. To simplify notations, the functions

$$f_{J_S}(\boldsymbol{J},\boldsymbol{\Phi},J_S,\phi,\tau,\tilde{\theta}) = [\eta_2\cos\phi-\eta_1\sin\phi]\sqrt{1-J_S^2}\ , \tag{2.110}$$

$$f_\phi(\boldsymbol{J},\boldsymbol{\Phi},J_S,\phi,\tau,\tilde{\theta}) = [\eta_2\sin\phi+\eta_1\cos\phi]\frac{J_S}{\sqrt{1-J_S^2}}-\eta_3\ , \tag{2.111}$$

with $\tau = \varepsilon\tilde{\theta}$ are defined. The equation of spin-orbit motion then becomes

$$\frac{\mathrm{d}}{\mathrm{d}\theta}\begin{pmatrix} \boldsymbol{J} \\ J_S \\ \tau \\ \boldsymbol{\Phi} \\ \phi \\ \tilde{\theta}\end{pmatrix} = \begin{pmatrix} 0 \\ 0 \\ 0 \\ \boldsymbol{Q}(\boldsymbol{J},\tau) \\ \nu(\boldsymbol{J},\tau) \\ 1\end{pmatrix} + \varepsilon\begin{pmatrix} p_J(\boldsymbol{J},\boldsymbol{\Phi},\tau,\tilde{\theta}) \\ f_{J_S}(\boldsymbol{J},\boldsymbol{\Phi},J_S,\phi,\tau,\tilde{\theta}) \\ 1 \\ p_\Phi(\boldsymbol{J},\boldsymbol{\Phi},\tau,\tilde{\theta}) \\ f_\phi(\boldsymbol{J},\boldsymbol{\Phi},J_S,\phi,\tau,\tilde{\theta}) \\ 0\end{pmatrix}\ . \tag{2.112}$$

The perturbations p_J and p_{Φ} to the motion of the action and angle variables are due to the variation of the equation of phase space motion (2.103) with the parameter τ. The average over the angle variable $\boldsymbol{\Phi}$ of the perturbation p_J vanishes for Hamiltonian systems, because there $\langle p_J\rangle_{\boldsymbol{\Phi}} =\langle\partial_{\boldsymbol{\Phi}} H(\boldsymbol{J},\boldsymbol{\Phi},\tau,\tilde{\theta})\rangle_{\boldsymbol{\Phi}}=$ 0, where the fact is used that the derivative of a periodic function has zero mean. Here H is the Hamiltonian of the system with varying τ. It can depend on $\boldsymbol{J}$ and $\boldsymbol{\Phi}$, while the Hamiltonian for constant τ does not depend on the angle variables $\boldsymbol{\Phi}$. The average over the phase ϕ of the perturbation f_{J_S} also vanishes due to the trigonometric functions in (2.110). For accelerators, with the 6-dimensional phase space of (2.19), this system of ordinary differential equations therefore has 5 slowly and 5 quickly changing variables for small ε. It is written in the standard form of multi-phase averaging theorems [33, Sect. 1.9], [32, Chap. 6].

To illustrate which kind of resonances can disturb the coupled spin-orbit motion, I perform a coordinate transformation leading to the averaged system in first order of ε. This procedure is very similar to the averaging transformation for the two frequency system obtained for particles on the closed orbit in Sect. 2.2.1. Here $f_{J_S}(\boldsymbol{J},\boldsymbol{\Phi},J_S,\phi,\tau,\tilde{\theta})$ is linear in trigonometric functions of ϕ and one can try to find a transformation $\bar{J}_S = J_S+\varepsilon u(\boldsymbol{J},\boldsymbol{\Phi},J_S,\phi,\tau,\tilde{\theta})$, which leads to simpler equations of motion. These functions u and f_{J_S} are Fourier expanded,

$$f_{J_S} = \sum_{j_0,\boldsymbol{j}}[f_j^+(\boldsymbol{J},J_S,\tau)\mathrm{e}^{\mathrm{i}(\boldsymbol{j}\cdot\boldsymbol{\Phi}+j_0\tilde{\theta}+\phi)} + f_j^-(\boldsymbol{J},J_S,\tau)\mathrm{e}^{\mathrm{i}(\boldsymbol{j}\cdot\boldsymbol{\Phi}+j_0\tilde{\theta}-\phi)}]\ , \quad (2.113)$$

$$u = \sum_{\boldsymbol{j},j_0}[u_j^+(\boldsymbol{J},J_S,\tau)\mathrm{e}^{\mathrm{i}(\boldsymbol{j}\cdot\boldsymbol{\Phi}+j_0\tilde{\theta}+\phi)} + u_j^-(\boldsymbol{J},J_S,\tau)\mathrm{e}^{\mathrm{i}(\boldsymbol{j}\cdot\boldsymbol{\Phi}+j_0\tilde{\theta}-\phi)}]\ , \quad (2.114)$$

where the subscript j subsumes the labels $\boldsymbol{j}$ and j_0. This in turn leads to

$$\begin{aligned}\frac{\mathrm{d}}{\mathrm{d}\theta}\bar{J}_S &= \varepsilon\sum_{\boldsymbol{j},j_0}\{[f_j^+ + u_j^+\mathrm{i}(\boldsymbol{j}\cdot\frac{\mathrm{d}}{\mathrm{d}\theta}\boldsymbol{\Phi}+j_0+\frac{\mathrm{d}}{\mathrm{d}\theta}\phi)]\mathrm{e}^{\mathrm{i}(\boldsymbol{j}\cdot\boldsymbol{\Phi}+j_0\tilde{\theta}+\phi)}\\ &+ \quad [f_j^- + u_j^-\mathrm{i}(\boldsymbol{j}\cdot\frac{\mathrm{d}}{\mathrm{d}\theta}\boldsymbol{\Phi}+j_0-\frac{\mathrm{d}}{\mathrm{d}\theta}\phi)]\mathrm{e}^{\mathrm{i}(\boldsymbol{j}\cdot\boldsymbol{\Phi}+j_0\tilde{\theta}-\phi)}\}\\ &= \varepsilon\sum_{\boldsymbol{j},j_0}\{[f_j^+ + u_j^+\mathrm{i}(\boldsymbol{j}\cdot\boldsymbol{Q}+j_0+\nu)]\mathrm{e}^{\mathrm{i}(\boldsymbol{j}\cdot\boldsymbol{\Phi}+j_0\tilde{\theta}+\phi)}\\ &+ \quad [f_j^- + u_j^-\mathrm{i}(\boldsymbol{j}\cdot\boldsymbol{Q}+j_0-\nu)]\mathrm{e}^{\mathrm{i}(\boldsymbol{j}\cdot\boldsymbol{\Phi}+j_0\tilde{\theta}-\phi)}\} + O(\varepsilon^2)\ .\end{aligned}$$

If there is no spin-orbit resonance, then one can choose $u_j^\pm = if_j^\pm/(\boldsymbol{j}\cdot\boldsymbol{Q} + j_0 \pm \nu)$ and all first-order terms are eliminated except the zeroth Fourier coefficient, leaving the averaged system

$$\frac{\mathrm{d}}{\mathrm{d}\theta}\bar{J}_S = \frac{1}{(2\pi)^5}\int_0^{2\pi}\cdots\int_0^{2\pi} f_{J_S}(\boldsymbol{J},\boldsymbol{\Phi},J_S,\phi,\tau,\tilde{\theta})d\boldsymbol{\Phi}d\phi d\tilde{\theta}+O(\varepsilon^2)\ . \quad (2.115)$$

For the case under consideration, the average of f_{J_S} is zero, and for $\theta \in [0, 1/\varepsilon]$, changes of the variable $\bar{J}_S$ of the averaged system are of order ε. Changes of J_S are of the same order, because the difference $\bar{J}_S - J_S = \varepsilon u$ is of order ε, so that $J_S = \boldsymbol{S}\cdot\boldsymbol{n}$ is an adiabatic invariant as defined in Sect. 2.2.2. However, for this argument it was assumed that $\boldsymbol{j}\cdot\boldsymbol{Q} + \nu$ does not become integer. But often this cannot be avoided, and resonance phenomena between the 5 frequencies of the 5 quickly changing phases can occur. In the following, a multi-phase averaging theorem that includes the crossing of resonances will be applied to the spin-orbit motion. Here I use theorem 2 of [32, Sect. 6.1] which is attributed to [76].

Theorem (Averaging for N frequency systems): *Consider a system of the form*

$$\frac{\mathrm{d}}{\mathrm{d}\theta}\boldsymbol{I} = \varepsilon \boldsymbol{f}(\boldsymbol{I}, \boldsymbol{\phi}, \varepsilon)\ , \tag{2.116}$$

$$\frac{\mathrm{d}}{\mathrm{d}\theta}\boldsymbol{\phi} = \boldsymbol{\nu}(\boldsymbol{I}) + \varepsilon g(\boldsymbol{I}, \boldsymbol{\phi}, \varepsilon)\ , \tag{2.117}$$

where $\boldsymbol{I}$ belongs to a regular compact subset of Euclidean $\mathbb{R}^m$ and $\boldsymbol{\phi} \in \mathbb{R}^n$. Each function on the right-hand side is real, C^1 in $\boldsymbol{I}$ and ε, periodic with period 2π in all ϕ_j, and each possesses an analytic extension for $\phi_j \in \mathbb{C}$, $\Im\{\phi_j\} < \sigma$ with $\sigma > 0$. The associated averaged system is

$$\frac{\mathrm{d}}{\mathrm{d}\theta}\bar{\boldsymbol{I}} = \varepsilon \bar{\boldsymbol{f}}(\bar{\boldsymbol{I}})\ , \quad \bar{\boldsymbol{f}}(\bar{\boldsymbol{I}}) = \frac{1}{(2\pi)^n}\int_0^{2\pi} \boldsymbol{f}(\bar{\boldsymbol{I}}, \boldsymbol{\phi}, 0)d\boldsymbol{\phi}\ , \tag{2.118}$$

with $\bar{\boldsymbol{I}}(0) = \boldsymbol{I}(0)$. Let the following non-degeneracy condition (called Arnold's condition) be satisfied: "Assuming the frequency $\nu_n(\boldsymbol{I}) \neq 0$ (with no loss of generality, because in every region at least one frequency will be non-zero), then the map $\boldsymbol{I} \to (\nu_1(\boldsymbol{I}), \ldots, \nu_{n-1}(\boldsymbol{I}))/\nu_n(\boldsymbol{I})$ has maximal rank, equal to $n-1$." Then: for every continuous function $\rho(\varepsilon)$ with $C_1\sqrt{\varepsilon} \leq \rho(\varepsilon) \leq C_2$, $C_1, C_2 \in \mathbb{R}^+$, the set of allowed initial conditions V is partitioned as $V = V'(\varepsilon, \rho(\varepsilon)) \bigcup V''(\varepsilon, \rho(\varepsilon))$ for sufficiently small ε such that

$$\mathrm{Sup}_{\theta\in[0,1/\varepsilon]}|\boldsymbol{I}(\theta) - \bar{\boldsymbol{I}}(\theta)| < \rho(\varepsilon) \tag{2.119}$$

for $(\boldsymbol{I}(0), \boldsymbol{\phi}(0)) \in V'$, i.e., for initial conditions in V', the separation between the exact solution and the solution of the averaged system is less than $\rho(\varepsilon)$. Moreover, the measure of $V''(\varepsilon, \rho(\varepsilon))$ is smaller than $C\sqrt{\varepsilon}/\rho(\varepsilon)$ for some $C \in \mathbb{R}^+$.

I now apply this averaging theorem for N frequency systems to (2.112) of spin-orbit motion. The frequency of the variable $\tilde{\theta}$ is 1 and can therefore be used as ν_n of Arnold's condition. The 4 frequencies $(\boldsymbol{Q}(\boldsymbol{J}, \tau), \nu(\boldsymbol{J}, \tau))$ depend on 4 of the 5 slowly changing variables, and I assume that the rank is 4 so that the Jacobi matrix of the 4 frequencies has non-vanishing determinant, $\det[\partial_{(\boldsymbol{J},\tau)}(\boldsymbol{Q}, \nu)] \neq 0$. A more detailed analysis of the requirement on the function involved is possible, as mentioned in [77]. The authors of [77] are working on a proof of adiabatic invariance for spin motion on the closed orbit and for spin motion in phase space that does not rely on the here used general averaging theorems and therefore gives more direct access to required properties.

When the frequencies are in resonance, the slowly changing variables $\boldsymbol{I}$ can accumulate large changes and the solution of the averaged system does not approximate the original system well. In the above theorem, Arnold's condition ensures that no slowly changing variable I_j can change at a resonance without moving the system out of this resonance.

Choosing $\rho(\varepsilon) = \varepsilon^{1/4}$, one finds for Hamiltonian systems, where $\bar{\boldsymbol{J}} = \boldsymbol{J}(0)$ because $\bar{\boldsymbol{p}}_{\boldsymbol{J}} = 0$, that the set of initial conditions for which $\mathrm{Sup}_{\theta\in[0,1/\varepsilon]}|\boldsymbol{J}(\theta) - \boldsymbol{J}(0)| \geq \varepsilon^{1/4}$ has a measure smaller than $C\varepsilon^{1/4}$. The variation of the action variables $\boldsymbol{J}$ for $\theta \in [0, 1/\varepsilon]$ therefore tends to 0 with ε, except for initial conditions from a set with a measure that also tends to 0 with ε. The action variables are therefore adiabatic invariants as defined in Sect. 2.2.2, which is a well-known fact. In addition it is found with $\bar{f}_{J_S} = 0$ that the set of initial conditions for which $\mathrm{Sup}_{\theta\in[0,1/\varepsilon]}|J_S(\theta) - J_S(0)| \geq \varepsilon^{1/4}$ has a measure smaller than $C\varepsilon^{1/4}$. Furthermore, the condition $1 - J_S^2 \geq \Delta$ above (2.109) excludes a set of initial conditions with a measure that tends to 0 with $\varepsilon \to 0$, as argued after (2.73). Therefore, $J_S = \boldsymbol{S} \cdot \boldsymbol{n}(\boldsymbol{z})$ is an adiabatic invariant as defined in Sect. 2.2.2.

Here I have simply relied on general theorems to show that the derived equations of spin-orbit motion give rise to adiabatic invariants. But even without (2.72) and without the theorem on averaging for two-frequency systems it is quite straightforward to prove the adiabatic invariance of $s_3 = \boldsymbol{S} \cdot \boldsymbol{n}_0$ directly. With significantly more effort, but less than proving the above theorem on averaging for N frequency systems, also the adiabatic invariance of $J_S = \boldsymbol{S} \cdot \boldsymbol{n}(\boldsymbol{z})$ can be proven directly [77, 78]. In addition, this will give more insight into spin dynamics.

2.2.10 The Single Resonance Model (SRM)

In the previous sections, $\boldsymbol{n}$, $\boldsymbol{u}_1$, $\boldsymbol{u}_2$, and ν have been introduced and the adiabatic invariance of J_S has been established for a very general class of systems. Now these quantities will be computed for an analytically solvable model, and the adiabatic invariance will be illustrated by letting a parameter of this model change.

The spin precession vector for particles that oscillate around the closed orbit can be decomposed into the closed-orbit contribution $\boldsymbol{\Omega}_0$ and a part $\boldsymbol{\omega}$ due to the particles' oscillations, $\boldsymbol{\Omega}(\boldsymbol{z},\theta) = \boldsymbol{\Omega}_0(\theta) + \boldsymbol{\omega}(\boldsymbol{z},\theta)$. The one turn rotation axis $\boldsymbol{n}_0$ precesses around $\boldsymbol{\Omega}_0$ and the 2π-periodic vectors $\boldsymbol{m}$ and $\boldsymbol{l}$, which were introduced in Sect. 2.2.2 precess according to (2.50), $\frac{\mathrm{d}}{\mathrm{d}\theta}(\boldsymbol{m}+\mathrm{i}\boldsymbol{l}) = (\boldsymbol{\Omega}_0 - \nu_0\boldsymbol{n}_0) \times (\boldsymbol{m} + \mathrm{i}\boldsymbol{l})$. In this coordinate system I now write

$$\boldsymbol{S} = s_1\boldsymbol{m} + s_2\boldsymbol{l} + s_3\boldsymbol{n}_0 \ , \quad \boldsymbol{\omega} = \omega_1\boldsymbol{m} + \omega_2\boldsymbol{l} + \omega_3\boldsymbol{n}_0 \tag{2.120}$$

and introduce the complex notation $\hat{s} = s_1 + \mathrm{i}s_2$ and $\omega = \omega_1 + \mathrm{i}\omega_2$. The equation of spin motion is then

$$\boldsymbol{\Omega} \times \boldsymbol{S} = \boldsymbol{m}\frac{\mathrm{d}}{\mathrm{d}\theta}s_1 + \boldsymbol{l}\frac{\mathrm{d}}{\mathrm{d}\theta}s_2 + \boldsymbol{n}_0\frac{\mathrm{d}}{\mathrm{d}\theta}s_3 + (\boldsymbol{\Omega}_0 - \nu_0\boldsymbol{n}_0) \times \boldsymbol{S} \tag{2.121}$$

and the equation of motion for $\hat{s}$ is obtained by multiplication with $\boldsymbol{m} + \mathrm{i}\boldsymbol{l}$, and taking into account that $s_3 = \sqrt{1 - |\hat{s}|^2}$,

$$\frac{\mathrm{d}}{\mathrm{d}\theta}\hat{s} = i(\nu_0 + \omega_3)\hat{s} - \mathrm{i}\omega\sqrt{1 - |\hat{s}|^2} \ . \tag{2.122}$$

In the coordinate system $[\boldsymbol{m}_0, \boldsymbol{l}_0, \boldsymbol{n}_0]$ of (2.49), which is rotated with respect to the $[\boldsymbol{m}, \boldsymbol{l}, \boldsymbol{n}_0]$ system by $\nu_0\theta$, this equation becomes

$$\hat{s}_0 = \mathrm{e}^{-\mathrm{i}\nu_0\theta}\hat{s} \ , \quad \frac{\mathrm{d}}{\mathrm{d}\theta}\hat{s}_0 = i\omega_3\hat{s}_0 - \mathrm{i}\mathrm{e}^{-\mathrm{i}\nu_0\theta}\omega\sqrt{1 - |\hat{s}|^2} \ . \tag{2.123}$$

If the motion in phase space can be transformed to action-angle variables, the spin precession vector $\boldsymbol{\omega}(\boldsymbol{J}, \boldsymbol{\Phi}, \theta)$ for particles that oscillate around the closed orbit is a 2π-periodic function of $\boldsymbol{\Phi}$ and θ. The Fourier spectrum of ω has frequencies $j_0 + \boldsymbol{j} \cdot \boldsymbol{Q}$. The integer contributions j_0 are due to the 2π periodicity of $\boldsymbol{\omega}$ in θ, and the contributions $\boldsymbol{j} \cdot \boldsymbol{Q}$ of integer multiples of the orbit tunes are due to the 2π periodicity of $\boldsymbol{\omega}$ in Φ_k. When one of the Fourier frequencies is nearly in resonance with ν_0, one component of $\mathrm{e}^{-\mathrm{i}\nu_0\theta}\omega$ is nearly constant. Then it can be a good approximation to drop all other Fourier components because their influence on spin motion can average to zero so that they are in effect less dominant. This is referred to as the single resonance approximation. However, this is not always a good approximation as will become apparent when HERA-p is analyzed in Sect. 3.2.1; it can only be good when the domains of influence of individual resonances are well separated. This model corresponds to the rotating field approximation often used to discuss spin resonance in solid state physics [79]. For a conventional flat ring, the first-order resonances due to vertical motion dominate and therefore the Fourier components with frequencies $\kappa = j_0 \pm Q_y$ are often of most interest.

The amplitude of a single Fourier contribution is sometimes called the resonance strength. This is misleading because generally it cannot be used in the Froissart-Stora formula to be introduced in Sect. 2.2.11, which describes depolarization due to resonance strength. Only for first-order resonances, where $\sum_{n=1}^{3} |j_n| = 1$, this strength can be used in the Froissart-Stora formula. For this case, the strength will be computed in Sect. 3.2.1. A method for computing higher-order resonance strength, where $\sum_{n=1}^{3} |j_n| > 1$, is presented for the first time in Sect. 2.2.12.

The single resonance approximation leads to the analytically solvable model advertised above, which is usually called the single resonance model (SRM). It has $\boldsymbol{\Omega}_0 = \nu_0\boldsymbol{n}_0$ and an $\boldsymbol{\omega}$ that only has one Fourier contribution, $\boldsymbol{\omega} = \epsilon_\kappa(\boldsymbol{m}\cos\Phi + \boldsymbol{l}\sin\Phi)$, with $\Phi = j_0\theta + \boldsymbol{j} \cdot \boldsymbol{\Phi} + \Phi_0$. This $\boldsymbol{\omega}$ is perpendicular to $\boldsymbol{n}_0$ and tilts spins away from $\boldsymbol{n}_0$. The SRM can for example be used to approximate a flat ring where $\boldsymbol{n}_0$ is vertical and the $\boldsymbol{\omega}$ describes the effect of the dominant harmonic in horizontal fields, which is due to vertical betatron motion. Because $\frac{\mathrm{d}}{\mathrm{d}\theta}\boldsymbol{\Phi} = \boldsymbol{Q}$, the frequency is $\kappa = j_0 + \boldsymbol{j}\cdot\boldsymbol{Q}$ and the equation of motion (2.122) becomes

$$\frac{\mathrm{d}}{\mathrm{d}\theta}\hat{s} = i\nu_0\hat{s} - \mathrm{i}\epsilon_\kappa \mathrm{e}^{\mathrm{i}(\kappa\theta+\Phi_0)}\sqrt{1-|\hat{s}|^2}\ . \tag{2.124}$$

When the coordinates in the $[\boldsymbol{m}, \boldsymbol{l}, \boldsymbol{n}_0]$ system are arranged in column vectors [80, 81], one obtains

$$\frac{\mathrm{d}}{\mathrm{d}\theta}\Phi = \kappa\ ,\quad \frac{\mathrm{d}}{\mathrm{d}\theta}\boldsymbol{S} = \boldsymbol{\Omega}(\Phi)\times\boldsymbol{S}\ ,\quad \boldsymbol{\Omega} = \begin{pmatrix}\epsilon_\kappa\cos\Phi\\ \epsilon_\kappa\sin\Phi\\ \nu_0\end{pmatrix}\ . \tag{2.125}$$

Initial coordinates $\boldsymbol{z}_i$ are taken into final coordinates $\boldsymbol{z}_f$ after one turn according to the relation $\boldsymbol{\Phi}_f = \boldsymbol{\Phi}_i + 2\pi\boldsymbol{Q}$ whence $\Phi_f = \Phi_i + 2\pi\kappa$. Now the orthogonal matrix $\mathsf{T}(\boldsymbol{e},\varphi)$ is introduced to describe a rotation around a unit vector $\boldsymbol{e}$ by an angle φ. Transforming the spin components of $\boldsymbol{S}$ into a rotating frame using the relation $\boldsymbol{S}_R = \mathsf{T}(\boldsymbol{n}_0, -\Phi)\cdot\boldsymbol{S}$, one obtains the simplified equation of spin motion

$$\frac{\mathrm{d}}{\mathrm{d}\theta}\boldsymbol{S}_R = \boldsymbol{\Omega}_R\times\boldsymbol{S}_R\ ,\quad \boldsymbol{\Omega}_R = \begin{pmatrix}\epsilon_\kappa\\ 0\\ \delta\end{pmatrix}\ ,\quad \delta = \nu_0 - \kappa\ . \tag{2.126}$$

If a spin field is oriented parallel to $\boldsymbol{\Omega}_R$ in this frame, it does not change from turn to turn. Therefore, $\boldsymbol{n}_R = \boldsymbol{\Omega}_R/|\boldsymbol{\Omega}_R|$ is an $\boldsymbol{n}$-axis. In the original frame, this $\boldsymbol{n}$-axis is

$$\boldsymbol{n}(\Phi) = \mathrm{sig}(\delta)\frac{1}{\Lambda}\begin{pmatrix}\epsilon_\kappa\cos\Phi\\ \epsilon_\kappa\sin\Phi\\ \delta\end{pmatrix}\ ,\quad \Lambda = \sqrt{\delta^2+\epsilon_\kappa^2}\ , \tag{2.127}$$

where the "sign factor" $\mathrm{sig}(\delta)$ has been chosen so that on the closed orbit ($\epsilon_\kappa = 0$) the $\boldsymbol{n}$-axis $\boldsymbol{n}(\Phi)$ coincides with $\boldsymbol{n}_0 = (0,0,1)^T$. As required, $\boldsymbol{n}$ is both a solution of the T-BMT equation (2.125), $\frac{\mathrm{d}}{\mathrm{d}\theta}\boldsymbol{n} = \mathrm{sig}(\delta)\frac{\kappa\epsilon_\kappa}{\Lambda}(-\sin\Phi,\cos\Phi,0)^T = \boldsymbol{\Omega}\times\boldsymbol{n}$ and, as with any function of phase space, a 2π-periodic function of the angle variables $\boldsymbol{\Phi}$ and of θ.

This analytically solvable model can also be used to illustrate the construction of a phase independent but amplitude-dependent spin tune $\nu(\boldsymbol{J})$, which was introduced in Sect. 2.2.7. Once an $\boldsymbol{n}$-axis has been obtained, one can transform the components of $\boldsymbol{S}$ into a coordinate system $[\boldsymbol{n}, \tilde{\boldsymbol{u}}_1, \tilde{\boldsymbol{u}}_2]$. With the simple choice

$$\tilde{\boldsymbol{u}}_2(\Phi) = \frac{\boldsymbol{n}_0\times\boldsymbol{n}}{|\boldsymbol{n}_0\times\boldsymbol{n}|} = \mathrm{sig}(\delta)\begin{pmatrix}-\sin\Phi\\ \cos\Phi\\ 0\end{pmatrix}\ , \tag{2.128}$$

$$\tilde{\boldsymbol{u}}_1(\Phi) = \frac{1}{\Lambda}\begin{pmatrix} \delta\cos\Phi \\ \delta\sin\Phi \\ -\epsilon_\kappa \end{pmatrix} , \tag{2.129}$$

$\tilde{\boldsymbol{u}}_1$ is equal to $\tilde{\boldsymbol{u}}_2 \times \boldsymbol{n}$ and the basis vectors are clearly 2π-periodic in $\boldsymbol{\Phi}$ and in θ as required. Because $\boldsymbol{n}$ and the basis vectors $\tilde{\boldsymbol{u}}_1$ and $\tilde{\boldsymbol{u}}_2$ comprise an orthogonal coordinate system for all θ, and because $\boldsymbol{n}$ precesses around $\boldsymbol{\Omega}$, one has, in analogy to (2.50), $\frac{\mathrm{d}}{\mathrm{d}\theta}\tilde{\boldsymbol{u}}_2 = (\boldsymbol{\Omega} - \tilde{\nu}\boldsymbol{n}) \times \tilde{\boldsymbol{u}}_2$ with the rotation rate $\tilde{\nu}$ which was already used in (2.84). It can be computed by the relation

$$\begin{aligned} \tilde{\nu} &= (\frac{\mathrm{d}}{\mathrm{d}\theta}\tilde{\boldsymbol{u}}_2 - \boldsymbol{\Omega} \times \tilde{\boldsymbol{u}}_2) \cdot \tilde{\boldsymbol{u}}_1 = \mathrm{sig}(\delta)[\begin{pmatrix} -\kappa\cos\Phi + \nu_0\cos\Phi \\ -\kappa\sin\Phi + \nu_0\sin\Phi \\ -\epsilon_\kappa \end{pmatrix}] \cdot \tilde{\boldsymbol{u}}_1 \\ &= \mathrm{sig}(\delta)\Lambda . \end{aligned} \tag{2.130}$$

In Sect. 2.2.7, an additional rotation of $\tilde{\boldsymbol{u}}_1$ and $\tilde{\boldsymbol{u}}_2$ around $\boldsymbol{n}$ was used to make $\tilde{\nu}$ independent of the angle variables $\boldsymbol{\Phi}$ and to define the amplitude-dependent spin tune. Here however, $\tilde{\nu}$ is already independent of $\boldsymbol{\Phi}$. In the SRM, $\epsilon_\kappa = |\boldsymbol{\omega}(\boldsymbol{z})|$, and therefore $\tilde{\nu}$ depends on the orbital amplitude. The amplitude-dependent spin tune $\nu(\boldsymbol{J})$ can be changed by multiples of the orbit tune, as stated in Sect. 2.2.7. This freedom can be used to obtain a ν which reduces to ν_0 on the design orbit ($\epsilon_\kappa = 0$) by letting $\tilde{\boldsymbol{u}}_1$ and $\tilde{\boldsymbol{u}}_2$ rotate around $\boldsymbol{n}$ by $-\Phi$, to give the amplitude-dependent spin tune

$$\nu = \mathrm{sig}(\delta)\Lambda + \kappa . \tag{2.131}$$

The corresponding uniformly rotating basis vectors $\boldsymbol{u}_1$ and $\boldsymbol{u}_2$ become

$$\boldsymbol{u}_1 = \tilde{\boldsymbol{u}}_1\cos\Phi - \tilde{\boldsymbol{u}}_2\sin\Phi , \quad \boldsymbol{u}_2 = \tilde{\boldsymbol{u}}_2\cos\Phi + \tilde{\boldsymbol{u}}_1\sin\Phi . \tag{2.132}$$

On the closed orbit, the coordinate system now reduces to

$$\boldsymbol{n} \to \boldsymbol{n}_0 , \quad \boldsymbol{u}_1 \to \mathrm{sig}(\delta)\boldsymbol{m} , \quad \boldsymbol{u}_2 \to \mathrm{sig}(\delta)\boldsymbol{l} , \quad \nu \to \nu_0 . \tag{2.133}$$

This model leads to the average polarization

$$P_{lim} = |\langle\boldsymbol{n}(\boldsymbol{z})\rangle| = \frac{|\delta|}{\sqrt{\delta^2 + \epsilon_\kappa^2}} = \sqrt{1 - \left(\frac{\epsilon_\kappa}{\Delta}\right)^2} , \tag{2.134}$$

$$\Delta = \nu - \kappa , \ \delta = \nu_0 - \kappa , \tag{2.135}$$

where the distance of the amplitude-dependent spin tune ν from resonance has been denoted by Δ, which is equivalent to $\mathrm{sig}(\delta)\Lambda$. In Fig. 2.7 (top), P_{lim} is plotted versus ν_0. It drops to 0 at $\nu_0 = \kappa$ because according to (2.127) the cone of vectors $\{\boldsymbol{n}(\Phi)|\Phi \in [0, 2\pi]\}$ opens up for small values of $|\delta|$. This strong reduction of P_{lim} occurs when ν approaches κ, i.e., close to spin-orbit resonances. According to (2.131) ν is never exactly equal to κ, but it jumps by $2\epsilon_\kappa$ across the resonance condition $\nu = \kappa$, which is shown in Fig. 2.7 (bottom). This jump of the spin tune could in principle be transformed away because the sign of the spin tune is not uniquely determined, as described in Sect. 2.2.7. This however requires a change of the sign of $\boldsymbol{n}$. Here the sign of $\boldsymbol{n}$ in (2.127)

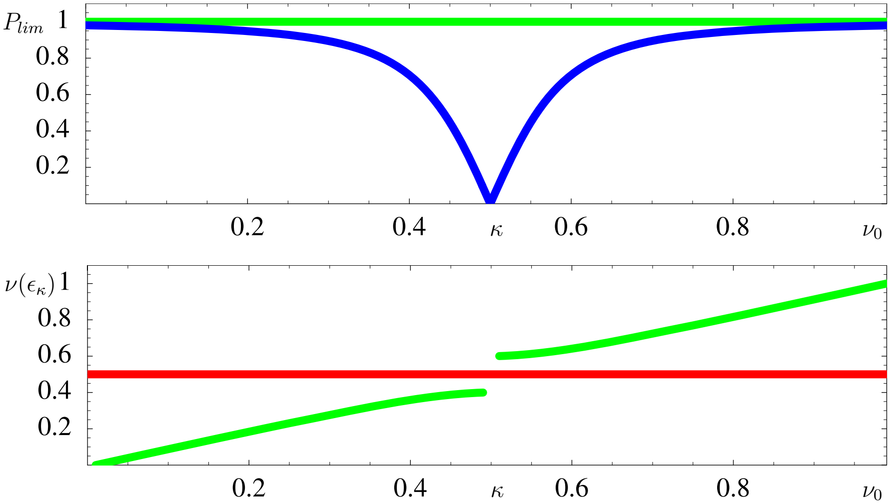

Fig. 2.7. P_{lim} and the amplitude-dependent spin tune $\nu(\epsilon_\kappa)$ for the SRM in the vicinity of $\nu_0 = \kappa$, for $\kappa = 0.5$ and $\epsilon_\kappa = 0.1$.

has been fixed by choosing $\boldsymbol{n}_0 \cdot \boldsymbol{n} > 0$, and the tune jump can therefore not be transformed away.

The SRM is the simplest nontrivial model for which analytical solutions have been found. In [82] the spin precession frequency has been computed for a single resonance strength with one or more point-like Siberian Snakes. In [83], the Fourier expansion of the $\boldsymbol{n}$-axis has been computed for these model storage rings with Siberian Snakes. These models and their solution are very instructive, but their derivation is rather lengthy, even the two nicely streamlined derivations in [84], and they will not be covered here.

Now, for the SRM, we will go through the steps that were used in Sect. 2.2.9 to describe spin motion when a parameter τ of the system is being slowly changed, i.e., $\frac{\mathrm{d}}{\mathrm{d}\theta}\tau = \varepsilon$. In particular, this allows the study of an acceleration where ν_0 crosses the frequency κ. To avoid confusion with ϵ_κ and to use the conventional notation of the SRM, we will subsequently use the symbol $\tilde{\alpha}$ instead of ε. To obtain the equation of motion in standard form of averaging theorems, the spin motion is described in the coordinate system $[\boldsymbol{u}_1, \boldsymbol{u}_2, \boldsymbol{n}]$. In order to take account of the change of the basis vectors with the parameter τ, the vector $\boldsymbol{\eta}$ is introduced as in (2.106),

$$\boldsymbol{\eta} = \frac{1}{2}(\boldsymbol{u}_1 \times \partial_\tau \boldsymbol{u}_1 + \boldsymbol{u}_2 \times \partial_\tau \boldsymbol{u}_2 + \boldsymbol{n} \times \partial_\tau \boldsymbol{n}) \ . \tag{2.136}$$

Because $\nu_0 = G\gamma$ in a flat ring, the acceleration process in the SRM is usually described by a slowly changing $\nu_0 = \kappa + \tau$ with $\tau = \tilde{\alpha}\theta$ while assuming that κ and ϵ_κ do not change with energy. This leads to the following expressions for the variation of the basis vectors and for $\boldsymbol{\eta}$:

$$\partial_\tau \boldsymbol{u}_1 = \mathrm{sig}(\delta)\frac{\epsilon_\kappa}{\Lambda^2}\boldsymbol{n}\cos\Phi \;, \tag{2.137}$$

$$\partial_\tau \boldsymbol{u}_2 = \mathrm{sig}(\delta)\frac{\epsilon_\kappa}{\Lambda^2}\boldsymbol{n}\sin\Phi \;, \tag{2.138}$$

$$\partial_\tau \boldsymbol{n} = -\mathrm{sig}(\delta)\frac{\epsilon_\kappa}{\Lambda^2}\tilde{\boldsymbol{u}}_1 \;, \tag{2.139}$$

$$\boldsymbol{\eta} = \mathrm{sig}(\delta)\frac{\epsilon_\kappa}{\Lambda^2}\frac{1}{2}(-\tilde{\boldsymbol{u}}_2 - \boldsymbol{u}_2\cos\Phi + \boldsymbol{u}_1\sin\Phi) = -\mathrm{sig}(\delta)\frac{\epsilon_\kappa}{\Lambda^2}\tilde{\boldsymbol{u}}_2 \;. \tag{2.140}$$

In a general system, the equations of motion for the components of $\boldsymbol{S} = \boldsymbol{u}_1 s_1 + \boldsymbol{u}_2 s_2 + \boldsymbol{n} J_S$ are described as in (2.108) by

$$\frac{\mathrm{d}}{\mathrm{d}\theta}\begin{pmatrix} s_1 \\ s_2 \\ J_S \end{pmatrix} = \begin{pmatrix} \tilde{\alpha}(\ \eta_3 s_2 \ - \eta_2 J_S\ ) - \nu(\boldsymbol{J},\tau)s_2 \\ \tilde{\alpha}(\ \eta_1 J_S \ - \eta_3 s_1\ ) + \nu(\boldsymbol{J},\tau)s_1 \\ \tilde{\alpha}(\ \eta_2 s_1 \ - \eta_1 s_2\ ) \end{pmatrix} . \tag{2.141}$$

In complex notation with $\hat{s} = s_1 + \mathrm{i}s_2$, $\eta = \eta_1 + \mathrm{i}\eta_2$, and $J_S = \sqrt{1-|\hat{s}|^2}$, this gives

$$\frac{\mathrm{d}}{\mathrm{d}\theta}\hat{s} = i[\nu(\boldsymbol{J},\tau) - \tilde{\alpha}\eta_3]\hat{s} + \mathrm{i}\tilde{\alpha}\eta\sqrt{1-|\hat{s}|^2} \;. \tag{2.142}$$

For the SRM, the equations (2.140) and (2.132) lead to $\eta = -\mathrm{i}\frac{\epsilon_\kappa}{\Lambda^2}\mathrm{e}^{\mathrm{i}(\kappa\theta+\Phi_0)}$, $\eta_3 = 0$, and

$$\frac{\mathrm{d}}{\mathrm{d}\theta}\hat{s} = i[\mathrm{sig}(\delta)\Lambda + \kappa]\hat{s} + \tilde{\alpha}\frac{\epsilon_\kappa}{\Lambda^2}\mathrm{e}^{\mathrm{i}(\kappa\theta+\Phi_0)}\sqrt{1-|\hat{s}|^2} \;. \tag{2.143}$$

The spin tune $\mathrm{sig}(\delta)\Lambda + \kappa$ in this equation jumps by $2\epsilon_\kappa$ at $\nu_0 = \kappa$.

It has been proven in Sect. 2.2.9 that spins follow $\boldsymbol{n}$ under adiabatic changes of parameters and that J_S is an adiabatic invariant. Therefore, this equation of motion for the SRM must describe this adiabatic following of $\boldsymbol{n}$ except at the point $\nu_0 = \kappa$ where the sign of $\boldsymbol{n}$ is changed by the convention (2.127). Thus (2.143) does not lead to an exact invariance of $J_S = \sqrt{1-|\hat{s}|^2}$, but it describes its adiabatic invariance. And this equation also applies when the change of ν_0 is not adiabatic so that one can compute how an initial $J_S(0) = 1$ is reduced when the condition $\nu_0 = \kappa$ is crossed.

Note again that the coordinate system $[\boldsymbol{u}_1, \boldsymbol{u}_2, \boldsymbol{n}]$ has a discontinuity at $\delta = 0$ where $\boldsymbol{n}$ and $\tilde{\boldsymbol{u}}_2$ change sign. This leads to a discontinuity of J_S at this point, but if $\tilde{\alpha}$ is very small, J_S changes only very slowly at all other positions due to its adiabatic invariance. If the unit vectors just below the resonance are denoted by the subscript $-$ and just above the resonance by a subscript $+$, the discontinuity at $\delta = 0$ in the basis vectors is reflected in a discontinuity in $\hat{s}$,

$$\boldsymbol{S} = \boldsymbol{u}_{1-}s_{1-} + \boldsymbol{u}_{2-}s_{2-} + \boldsymbol{n}_- J_{S-} = \boldsymbol{u}_{1+}s_{1+} + \boldsymbol{u}_{2+}s_{2+} + \boldsymbol{n}_+ J_{S+} \;. \tag{2.144}$$

Thus due to the choice of sign for the $\boldsymbol{n}$-axis, $J_{S+} = -J_{S-}$ and a particle with its initial spin parallel to $\boldsymbol{n}_0$ at large negative δ will have a flipped spin once a large positive δ is reached. When propagating a spin with initial condition $\hat{s}_i$ by (2.143), one has to solve the equation up to the point $\delta = 0$, where the spin coordinate is denoted by $\hat{s}_-$. Equation (2.144) then leads to $\hat{s}_+$, which is subsequently used as the initial condition for a further propagation of the spin.

For proving the adiabatic invariance of J_S in a general system an advanced theorem of N frequency averaging was applied for which the frequencies were allowed to pass through resonance conditions. Note that simpler theorems would have sufficed for the SRM, because here the frequency ν never passes through the resonance condition $\nu = \kappa$ but obeys the constraint $|\nu - \kappa| \geq \epsilon_\kappa$.

2.2.11 The Froissart-Stora Formula

The adiabatic spin invariant for general systems was established in Sect. 2.2.9. For the analytically solvable SRM, the change of this adiabatic invariant can be computed explicitly. When the design-orbit spin tune changes during the acceleration process, intrinsic resonances and imperfection resonances will be encountered, where ν jumps from $\kappa \pm \epsilon_\kappa$ to $\kappa \mp \epsilon_\kappa$ while the spin is under the strong influence of an approximately resonant Fourier contribution of ω. It is then found that for some speeds of the spin tune change, parameterized by $\tilde{\alpha}$, a reduction of polarization can occur that does not recover after the energy has increased and the resonance is crossed.

To describe the reduction of polarization during resonance crossing, (2.143) can be used but the usual approach is to insert a changing closed-orbit spin tune ν_0 into the equation of motion (2.125). The method of solution depends on the form of the function $\nu_0(\theta)$ [85, 86, 18, 87]. If the closed-orbit spin tune changes like $\nu_0 = \kappa + \tilde{\alpha}\theta$, the corresponding spinor equation of motion (2.41) can be solved in terms of confluent hypergeometric functions. The equations for arbitrary initial conditions are quite complicated, but when at $\theta \to -\infty$ a vertical spin $s_3(-\infty) = 1$ is chosen as the initial condition, then the vertical component at $\theta \to +\infty$ is given by the well-known and regularly used Froissart-Stora formula [85],

$$s_3(\infty) = 2\mathrm{e}^{-\pi\frac{\epsilon_\kappa^2}{2\tilde{\alpha}}} - 1 \, . \tag{2.145}$$

In the case of a strong perturbation ϵ_κ, or when the acceleration is very slow, spins follow the change of $\boldsymbol{n}(\Phi)$. The $\boldsymbol{n}$-axis in (2.127) has a discontinuity from $\boldsymbol{n}_- = -\epsilon_\kappa(\cos\Phi, \sin\Phi, 0)^T$ just below resonance to $\boldsymbol{n}_+ = -\boldsymbol{n}_-$ just above resonance. Spins do not follow this instantaneous change of sign, but they then follow $-\boldsymbol{n}$ adiabatically after the resonance has been crossed. Therefore, $s_3(\infty)$ is close to -1 for a slow change of ν_0. When the perturbation is weak or crossed very quickly, then spin motion is hardly affected and $s_3(\infty)$ is close to 1 in (2.145). In intermediate cases, $|s_3|$ is reduced. In the first case, the time-averaged polarization is preserved but the spins are reversed. In the second case, the time-averaged polarization is preserved without reversal. In the third case, the time-averaged polarization is reduced. These are the phenomena alluded to in Sect. 2.2.3 in the discussion on crossing first-order intrinsic resonances.

While the Froissart-Stora formula only applies to a single resonance, an approximation for small resonance strength has been formulated and extended to the case of two overlapping resonances in [88].

2.2.12 The Froissart-Stora Formula for Higher-Order Resonances

The Froissart-Stora formula is regularly used to describe the reduction of polarization due to vertical betatron motion during resonance crossing in accelerators where the closed-orbit spin tune ν_0 changes with energy. These descriptions were normally restricted to flat rings and $\nu_0 = G\gamma$. The single resonance approximation (2.122) of spin motion leads to a resonance at some Fourier frequency $\kappa = j_0 + \boldsymbol{j} \cdot \boldsymbol{Q}$ of $\omega(\boldsymbol{z}(\theta), \theta)$. Therefore, not only first-order resonances but also higher-order resonances can appear in the SRM and can be described by the Froissart-Stora formula. However, when only linear orbital motion is considered and $\boldsymbol{\omega}$ is linearized in $\boldsymbol{z}$, then $\boldsymbol{\omega}$ can only have Fourier components at the first-order frequencies $j_0 \pm Q_k$. But due to the nonlinear character of spin motion, higher-order resonances can still appear even for such linearized systems [62, 89, 90, 18]. This was already pointed out at (2.74) and will be exhibited by examples in this tract that were all computed for linear phase space motion and linearized magnetic fields in $\boldsymbol{\omega}$. For such systems the single resonance approximation of (2.122) would lead to no higher-order resonances at all. Before the following investigations, it was not clear whether a Froissart-Stora formula with some resonance strength ϵ_κ could be applied to crossing such higher-order resonances. But even if it can be applied, it is clear that the resonance strength cannot be obtained from a Fourier coefficient of $\boldsymbol{\omega}$ in (2.122).

Because Siberian Snakes are unavoidable for polarized beam acceleration in HERA-p, the design-orbit spin tune is $\frac{1}{2}$ in most cases that will be considered here and it does not change during acceleration. Because the orbital tunes are never chosen to be $\frac{1}{2}$, first-order resonances with $\nu = j_0 \pm Q_k$ are avoided and higher-order resonances can become dominant. But because the strength of such resonances cannot be obtained as a Fourier coefficient of $\omega(\boldsymbol{z}(\theta), \theta)$, a method for obtaining the strength of the higher-order resonances is required in order to use the Froissart-Stora formula when Siberian Snakes are in use.

When spin motion in a ring is approximated by a single resonance with $\kappa = j_0 \pm Q_y$ and then Siberian Snakes are included in the ring, it has often been noted that only odd-order resonances with $\kappa = j_0 + j_y Q_y$ appear, i.e., j_y is odd. However, it can be shown by nonlinear normal form theory that this is a feature of any ring with midplane symmetric spin-orbit motion and is not peculiar to rings with Siberian Snakes [72]. For rings without midplane symmetry, resonances of even order can appear also.

HERA-p has non-flat regions, and rings with closed-orbit distortions in general do not have midplane symmetric motion. Then, resonances with even

j_y can also appear and be destructive. In fact, the resonances with $j_y = 2$ are the most destructive spin-orbit resonances in HERA-p after Siberian Snakes are included.

As mentioned in Sect. 2.2.4, HERA-p will require flattening snakes. In addition at least 4 Siberian Snakes are required. The snake angles φ_j of these 4 snakes can be chosen quite arbitrarily, except for the restriction $\Delta\varphi = \varphi_4 - \varphi_3 + \varphi_2 - \varphi_1 = \frac{\pi}{2}$ derived in Sect. 2.2.3. Because the performance of HERA-p for polarized beam acceleration and storage depends on the choices of snake angles, Sect. 4.1.3 will be dedicated to finding an optimal choice for these snake angles. But to illustrate the main concepts and to discuss crossing higher-order resonances, two different example schemes having 1 snake in each of the 4 straight sections will now be presented. In the following, I will characterize snake schemes by their snake angles starting with the Siberian Snake in the south and going east around the ring. The two example schemes are denoted by $(\frac{\pi}{4}0\frac{\pi}{4}0)$ and $(\frac{3\pi}{4}\frac{3\pi}{8}\frac{3\pi}{8}\frac{\pi}{4})$. A pair of non-flat regions is located in the south, east, and north straight sections of HERA-p and therefore 6 flattening snakes are required. Nevertheless, it can be useful to symmetrize HERA-p by adding two extra flattening snakes in the west section. When referring to snake schemes, the number of flattening snakes will be denoted by *6fs* or *8fs*. The two example schemes are shown in:

Figure 2.8 (left): Scheme $(\frac{\pi}{4}0\frac{\pi}{4}0)6fs$ with snake angles south: 45°, east: 0°, north: 45°, west: 0°. Such a scheme and similar symmetric schemes were originally considered advantageous by popular opinion [91], mostly due to their symmetry.

Figure 2.8 (right): Scheme $(\frac{3\pi}{4}\frac{3\pi}{8}\frac{3\pi}{8}\frac{\pi}{4})8fs$ with snake angles south: 135°, east: 67.5°, north: 67.5°, west: 45°. This scheme was found by the optimization described in Sect. 4.1.3.

In Fig. 2.9, the amplitude-dependent spin tune (green) and P_{lim} (blue) are plotted versus the reference momentum for a vertical amplitude of 70π mm mrad for the HERA-p luminosity upgrade optics that is used in the year 2004 [92]. This shows that many higher-order resonances can be observed in HERA-p. The ring was made effectively flat by flattening snakes and 4 Siberian Snakes were included with the snake arrangement $(\frac{\pi}{4}0\frac{\pi}{4}0)8fs$. The curves for P_{lim} and $\nu(\boldsymbol{J})$ were computed with the non-perturbative algorithm described in Sect. 4.1.1 using the spin-orbit dynamics program SPRINT [93, 81]. The $\boldsymbol{n}$-axis and also P_{lim} are in general different at different azimuth θ_0. For this figure and for all following plots of P_{lim}, the $\boldsymbol{n}$-axis was observed at the interaction point of the ZEUS experiment in the south of HERA.

While the design-orbit spin tune remains at $\frac{1}{2}$, the amplitude-dependent spin tune $\nu(J_y)$ changes with energy and is in resonance with $2Q_y$ at the second line (red) and with $5Q_y - 1$ at the bottom line at several energies. In both cases a clear change of P_{lim} can be observed. The fall of P_{lim} at some resonances is similar to the behavior for the single resonance approximation shown in (2.135) where P_{lim} is reduced at those resonances. The drop

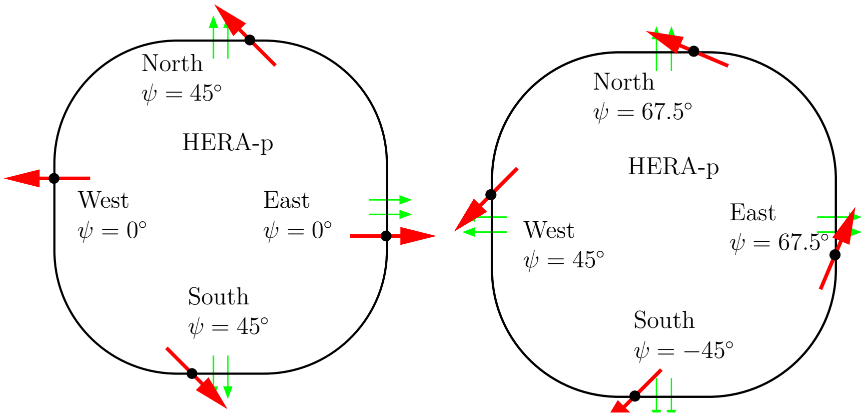

Fig. 2.8. A traditional snake scheme (*left*) and a snake scheme after the optimizations described in Sect. 4.1.3 (*right*). The flattening snakes (*small arrows*) and 4 Siberian Snakes (*large arrows*), together with their snake angle, are indicated.

of P_{lim} at 811.2 GeV/c is due to the $2 - 5Q_y$ resonance, which lies a little below the $2Q_y$ line. At all other energies where this resonance is crossed, no influence on P_{lim} can be observed because the corresponding fifth-order resonance strength is very small. At some second-order resonances, P_{lim} increases resonantly. Presumably, two resonant effects are in constructive interference at these energies. Nonetheless, polarization can be reduced when these resonance positions are crossed during acceleration because a sudden increase of $P_{lim} = \langle \boldsymbol{n} \rangle$ might be due to a change of $\boldsymbol{n}(\boldsymbol{z})$ that is too sudden for the adiabatic invariance of $J_S = \boldsymbol{n}(\boldsymbol{z}) \cdot \boldsymbol{S}$ to be maintained. In addition, one can see in Fig. 2.9 that the spin tune $\nu(J_y)$ has discontinuities at some of the resonances.

When a parameter τ is being varied, the spin motion is described in the coordinate system $[\boldsymbol{u}_1, \boldsymbol{u}_2, \boldsymbol{n}]$ by (2.142),

$$\frac{\mathrm{d}}{\mathrm{d}\theta}\hat{s} = i(\nu(\boldsymbol{J},\tau) - \tilde{\alpha}\eta_3)\hat{s} + i\tilde{\alpha}\eta\sqrt{1 - |\hat{s}|^2} \ , \quad \tilde{\alpha} = \frac{\mathrm{d}}{\mathrm{d}\theta}\tau \ . \tag{2.146}$$

If τ is taken to be the reference energy of the ring, this equation implicitly describes the change of $J_S = \sqrt{1 - |\hat{s}|^2}$ during acceleration. Even when the average $\langle J_S \rangle_N$ of J_S taken over all N particles of a bunch is large, the polarization of the bunch $P = |\langle \boldsymbol{s} \rangle_N|$ will be small if P_{lim} is small. But P can in principle always be reinstated to a large value close to $\langle J_S \rangle_N$. For this purpose, the invariant spin field would need to be changed slowly enough to allow the spins to follow it to a state in which its divergence over the phase space of the beam is small so that P_{lim} is close to 1. A small average beam polarization during acceleration is therefore not destructive as long as J_S stays large for each particle. On the other hand, a reduction of $\langle J_S \rangle_N$

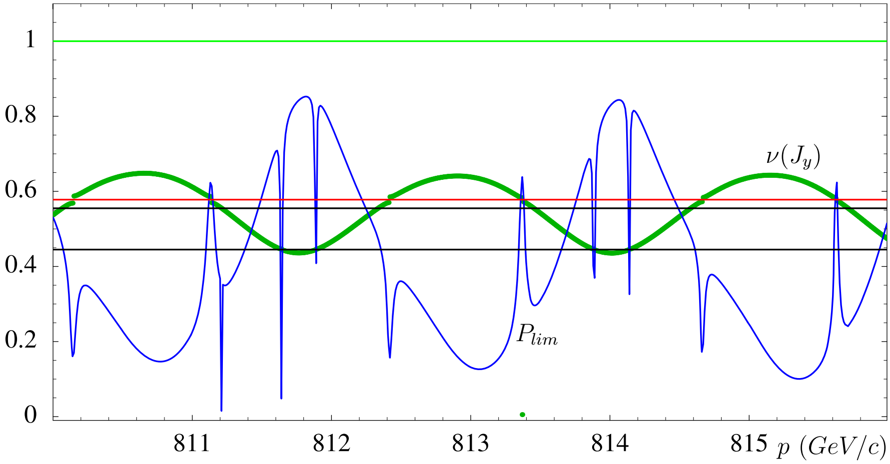

Fig. 2.9. P_{lim} (*blue*) and $\nu(J_y)$ (*green*) for particles with a 4.2σ vertical amplitude of 70π mm mrad in HERA-p with the $(\frac{\pi}{4}0\frac{\pi}{4}0)8fs$ snake scheme and $Q_y = 0.289$. Three resonance lines cross ν, and at each crossing P_{lim} exhibits a large variation and there are jumps in ν, bottom: $\nu = 5Q_y - 1$, middle: $\nu = 2 - 5Q_y$, and top $\nu = 2Q_y$.

describes a reduction of polarization that is not reversible by a slow change of the invariant spin field [94].

In the following, I will show that (2.146) has some characteristics of the equation of spin motion (2.143) of the SRM. If the spin tune ν has a discontinuity from ν_- to ν_+ at some energy, then I define the center frequency $\kappa^* = \frac{1}{2}(\nu_- + \nu_+)$. To take the jump of ν into account, I introduce $\Lambda^* = |\nu - \kappa^*|$, which does not have a discontinuity, and I express the spin tune as $\nu = \mathrm{sig}(\nu - \kappa^*)\Lambda^* + \kappa^*$.

Because $\boldsymbol{\eta}$ is related to the basis vectors by (2.106), it is a 2π-periodic function of $\boldsymbol{\Phi}$ and θ, and (2.146) has a structure similar to that of the equation of motion (2.122) in the coordinate system $[\boldsymbol{m}, \boldsymbol{l}, \boldsymbol{n}_0]$ to which the single resonance approximation was applied. The jump of ν across κ^* can be produced by a Fourier component of η if there is a set of integers so that $\boldsymbol{j} \cdot \boldsymbol{Q} + j_0 = \kappa^*$. This was the case in all instances of spin tune jumps found so far. Accordingly, one can analyze what happens when the Fourier component $\eta_{\kappa^*} \mathrm{e}^{\mathrm{i}(\kappa^*\theta + \Phi_0)}$ of η dominates the motion of $\hat{s}$. For that analysis, all other Fourier components of η are ignored. When $\tilde{\alpha}$ is small, spins that are initially almost parallel to the $\boldsymbol{n}$-axis remain close to $\boldsymbol{n}$ so that $\hat{s}$ is small and $\tilde{\alpha}\eta_3\hat{s}$ can therefore be ignored. This leads to

$$\frac{\mathrm{d}}{\mathrm{d}\theta}\hat{s} = i(\mathrm{sig}(\nu - \kappa^*)\Lambda^* + \kappa^*)\hat{s} + I\tilde{\alpha}\eta_{\kappa^*}\mathrm{e}^{\mathrm{i}\kappa^*\theta + \Phi_0}\sqrt{1 - |\hat{s}|^2}\,. \tag{2.147}$$

Due to its similarity with (2.143), this equation will produce the observed spin tune jump by $2\epsilon_{\kappa^*} = |\nu_+ - \nu_-|$ if $\eta_{\kappa^*} = \frac{\epsilon_{\kappa^*}}{\Lambda^{*2}} = \frac{\epsilon_{\kappa^*}}{(\nu-\kappa^*)^2}$ in the vicinity of the energy where the jump occurs. Otherwise (2.147) would not reproduce this jump. One is then left with a relation that has exactly the structure of the equation of motion (2.143) for the SRM. Therefore, the Froissart-Stora formula can be applied to estimate how much polarization is lost when a polarized beam is accelerated through the energy region where the spin tune jumps by $2\epsilon_\kappa$. In the following, we will check whether, for some higher-order resonances in HERA-p, all assumptions leading to the approximation (2.147) are satisfied to the extent that the Froissart-Stora formula describes the reduction of polarization well.

The basis vectors $\boldsymbol{n}$, $\boldsymbol{u}_1$, and $\boldsymbol{u}_2$, and the amplitude-dependent spin tune ν can in general only be computed by computationally intensive methods that will be described in later sections. The perturbing function η is then obtained from

$$\begin{aligned}\eta &= \boldsymbol{\eta} \cdot (\boldsymbol{u}_1 + \mathrm{i}\boldsymbol{u}_2) = \boldsymbol{\eta} \cdot (-\boldsymbol{n} \times \boldsymbol{u}_2 + \mathrm{i}\boldsymbol{n} \times \boldsymbol{u}_1) \\ &= (\boldsymbol{\eta} \times \boldsymbol{n}) \cdot (-\boldsymbol{u}_2 + \mathrm{i}\boldsymbol{u}_1) = i(\boldsymbol{u}_1 + \mathrm{i}\boldsymbol{u}_2) \cdot (\partial_\tau \boldsymbol{n}) \, ,\end{aligned} \tag{2.148}$$

but the required differentiation is prone to numerical inaccuracies. However, when $\boldsymbol{n}$ is computed by perturbative normal form theory using differential algebra (DA) [67], the differentiation with respect to τ can be performed automatically. After η is computed, the Fourier integral over the complete ring would finally be required in order to compute ϵ_κ.

If (2.146) can be approximated well by a SRM, there is however a different and much less cumbersome method for determining the relevant resonance strength and the resonant frequency. Observation of the amplitude-dependent spin tune $\nu(\boldsymbol{J})$ allows the determination of all parameters that are required to evaluate the Froissart-Stora formula for higher-order resonances whenever a SRM for η is applicable: The spin tune jumps by $2\epsilon_\kappa$, the center of the jump is located at the frequency κ itself, and the rate of change of ν with changing energy is used to determine the parameter $\tilde{\alpha}$ for (2.145). In the SRM, this parameter is $\frac{\nu_0-\kappa}{\theta}$ where ν_0 is the frequency of spin rotations when the resonance strength vanishes. Here the corresponding frequency, which would be observed if no perturbation η were present, is not directly computed. But it can be approximately inferred from the slope $\partial_\tau \nu$ at some distance from the resonance.

It is important to note again that the discontinuity of the spin tune could in general be transformed away because its sign can be changed by choosing $-\boldsymbol{n}$ as the $\boldsymbol{n}$-axis to which the spin tune refers, as shown in Sect. 2.2.7. If the sign of $\boldsymbol{n}$ is fixed so that the $\boldsymbol{n}$-axis $\boldsymbol{n}_-$ just below and $\boldsymbol{n}_+$ just above the resonance have $\boldsymbol{n}_- \cdot \boldsymbol{n}_+ < 0$, then the discontinuity of ν at the resonance cannot be transformed away.

According to (2.135), $\langle \boldsymbol{n} \rangle$ is given by $P_{lim}^{SRM} = \sqrt{1 - (\frac{\epsilon_\kappa}{\nu-\kappa})^2}$ in the SRM. To check whether the observed drop of P_{lim} indeed shows the characteristics of the SRM, the width of the resonance dip in P_{lim}^{SRM} was obtained from the amplitude-dependent spin tune alone and then compared with the width of the dip in the actual P_{lim} of the system. This analysis was done for the resonance at approximately 812.4 GeV/c, and the results are shown in Fig. 2.10. The top left plot shows the dependence of P_{lim} and ν on the reference momentum for a vertical amplitude of 70π mm mrad, which, with HERA-p's current one sigma emittance of 4π mm mrad, corresponds to the amplitude of a 4.2σ vertical emittance. The momentum range is as in Fig. 2.9. The low P_{lim} shows that many perturbing effects interfere in this region. In units of π mm mrad, the vertical amplitude of the particles in the top left graph is 70, in the middle graphs it is 40 and 60, and in the bottom graphs 80 and 100. The horizontal scale displays the distance Δp in GeV/c from the momentum at the resonance.

In the 4 bottom graphs, P_{lim} and P_{lim}^{SRM} are plotted for different orbital amplitudes, and the different resonance strengths are obtained from the jump in $\nu(J_y)$. Only information about ν was used to compute P_{lim}^{SRM}. To allow better comparison, a linear change of P_{lim}^{SRM} with momentum was added as a background curve and the height of the dip was scaled to fit the actual P_{lim}. The width, however, was not changed. The distance between spin tune and resonance has been magnified by 10, $\nu^* = \kappa + 10(\kappa - \nu)$ in these graphs. The tune jump is symmetric around the resonance line $\nu = 2Q_y$, showing that a second-order resonance is excited.

As shown in Fig. 2.10 (top right), the tune jump scales approximately linearly with the orbital action variable J_y. This is consistent with the crossing of a second-order resonance, because a frequency of $2Q_y$ can be produced by monomials of $\sqrt{J_y}\mathrm{e}^{\pm \mathrm{i} Q_y \theta}$ with order larger or equal to 2. This linear scaling is not exact for two reasons: (1) The jump does not reduce to 0 at $J_y = 0$ but already at some finite amplitude at which $\nu(J_y)$ does not cross the resonance line. (2) When the amplitude is changed, the momentum at which the resonance occurs changes, and the resonance strength is in general different at different energies. Deviations from a linear dependence should therefore be expected. P_{lim} is already very low away from the resonance at $\nu = 2Q_y$, indicating that other strong perturbations distort the invariant spin field and can interfere with the resonance harmonic.

Thus I conclude that the resonance width computed in terms of the tune jump $2\epsilon_\kappa$ agrees surprisingly well with the actual drop in P_{lim}.

Because the higher-order resonances analyzed here show the established and characteristic relation between tune jump and reduction of P_{lim}, the applicability of the Froissart-Stora formula will now be tested. It would be of great significance for analyzing the acceleration of polarized beams through such higher-order resonances if the Froissart-Stora formula could be applied.

In Fig. 2.11 (top), P_{lim} and ν are shown for the HERA optics used in 2004 with 4 Siberian Snakes in the scheme $(\frac{\pi}{4}0\frac{\pi}{4}0)6fs$. P_{lim} is reduced at two resonances with $\nu = 2Q_y$. The vertical tune had been chosen as $Q_y =$

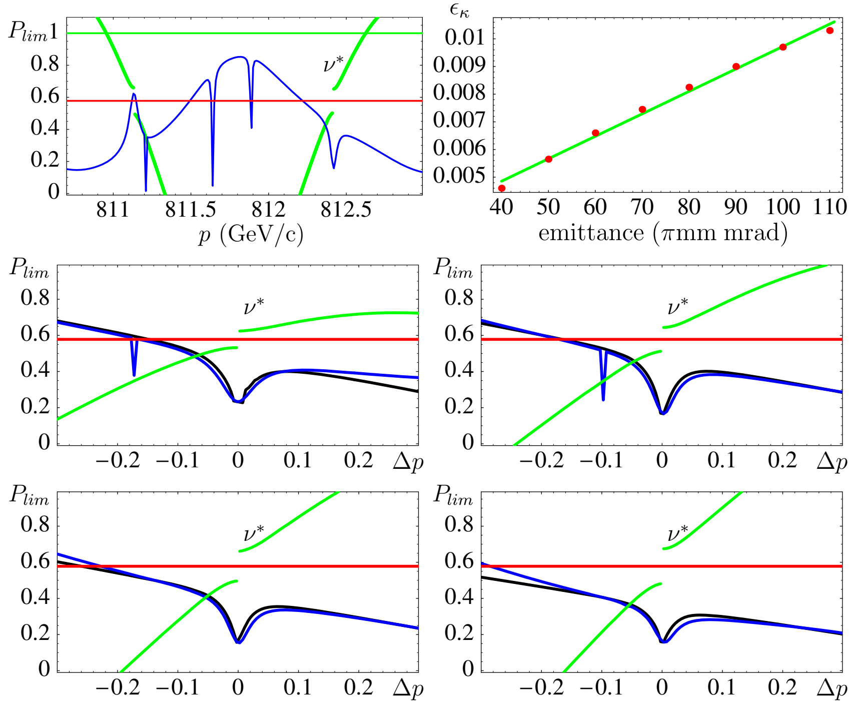

Fig. 2.10. Top left: P_{lim} and ν in the vicinity of the resonance at approximately 812.4 GeV/c for the $(\frac{\pi}{4}0\frac{\pi}{4}0)8fs$ snake scheme. The distance between ν and resonance has been magnified by 10, $\nu^* = \kappa + 10(\kappa - \nu)$. **Top right**: Proportionality between tune jump $2\epsilon_k$ and the amplitude $2J_y$ of a vertical emittance. **Middle and bottom**: Correlation between the width of the actual drop of P_{lim} and the predictions of the single resonance approximation using only the amplitude-dependent spin tune. Vertical amplitudes of particles in HERA-p in units of π mm mrad from top left to bottom right: 70, 40, 60, 80, and 100. Δp: distance from the momentum at resonance in GeV/c.

0.2725 so that these resonances are crossed already for the small 0.75σ vertical amplitude of 2.25π mm mrad. At this small amplitude, P_{lim} is reasonably large.

The spins of a set of particles were set parallel to the invariant spin field $\boldsymbol{n}(\boldsymbol{z})$ so that all had $J_S = 1$ at the momentum of 801 GeV/c. The $\boldsymbol{n}$-axis had been computed by stroboscopic averaging to be described in Sect. 4.2. Due to the rather large P_{lim} at that energy, the initial polarization was approximately 97%. Starting with this spin configuration, the beam was accelerated to 804 GeV/c at various rates. The average $\langle J_S \rangle_N$ over the tracked particles is plotted versus acceleration rate in Fig. 2.11 (bottom) together with the prediction of the Froissart-Stora formula. As already explained, the average

$\langle J_S \rangle_N$ describes the degree of beam polarization that could be recovered due to the adiabatic invariance of J_S when moving into an energy regime where $\boldsymbol{n}(\boldsymbol{z})$ is close to parallel to the vertical.

The resonance strength ϵ_{2Q_y} has been determined from the tune jump. The parameter $\tilde{\alpha}$ is proportional to the energy increase per turn d_E and is determined from the tune slope $\frac{\Delta\nu}{\Delta E}$ in Fig. 2.11 (top right) by the relation $\tilde{\alpha} = \frac{1}{2\pi}\frac{\Delta\nu}{\Delta E}d_E$.

The polarization obtained by accelerating particles through the second-order resonance agrees remarkably well with the Froissart-Stora formula. For the slow acceleration of about 50 keV per turn in HERA-p, the polarization would be completely reversed on the 0.75 sigma invariant torus. This would lead to a net reduction of beam polarization, because the spins in the center of the beam are not reversed.

This result on the applicability of (2.145) for the resonance strength and $\tilde{\alpha}$ obtained from the amplitude-dependent spin tune is so important for detailed analysis of the acceleration process that it will be checked in another case. In the next example, the HERA-p lattice of the year 2004 was used, the tune was adjusted to a realistic value of $Q_y = 0.289$ and a 4.2σ vertical amplitude of 70π mm mrad was chosen. At this large amplitude, the second- and fifth-order resonances already shown in Fig. 2.9 are observed. Particles were then accelerated from 812.2 GeV/c to 812.6 GeV/c with different acceleration rates. Note that the initial condition has a vertical polarization of only 60%. Nevertheless, this state of polarization corresponds to a completely polarized beam, and 100% polarization can potentially be recovered by changing the energy adiabatically into a region where $\boldsymbol{n}(\boldsymbol{z})$ is tightly bundled. These studies emphasize again the importance of choosing $\boldsymbol{n}(\boldsymbol{z})$ as the initial spin direction. For example, if the spins were initially polarized vertically, they would rotate around $\boldsymbol{n}(\boldsymbol{z})$ and that would lead to a fluctuating polarization, even without a resonance, and it would not be possible to establish a Froissart-Stora formula for higher-order resonances.

As shown in Fig. 2.12, P_{lim} is as low as 0.11 in the center of the displayed region. Obviously other strong effects beyond the second-order resonance are present and overlap with it. Therefore, it is again important that the particles that should be accelerated through the resonance are initially polarized parallel to the invariant spin field. The bottom figure shows $\langle J_S \rangle_N$ after the acceleration. The fact that $\langle J_S \rangle_N$ is again described very well by the Froissart-Stora formula (2.145) is an impressive confirmation of the conjecture.

The two data points at largest acceleration speed are lower than predicted by the Froissart-Stora formula. A possible explanation is the following: at very large acceleration speeds, the resonance region is crossed so quickly that the spin motion is hardly disturbed. But when the $\boldsymbol{n}$-axis $\boldsymbol{n}_-$ before the resonance region is not parallel to the $\boldsymbol{n}$-axis $\boldsymbol{n}_+$ after the resonance region, then the spins that initially had $J_S = 1$ will approximately have $J_S = \boldsymbol{n}_- \cdot \boldsymbol{n}_+$ after

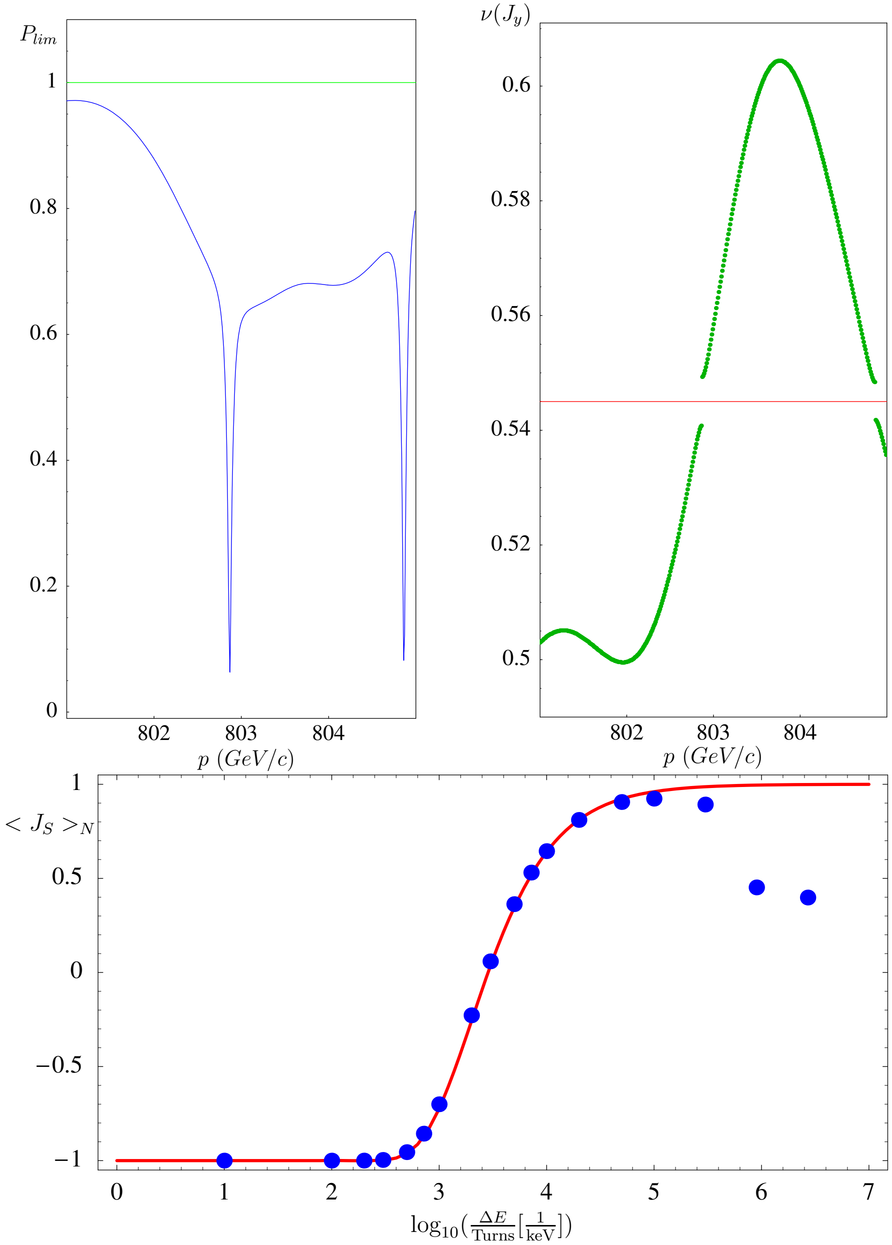

Fig. 2.11. Top: P_{lim} and ν for a second-order resonance of the HERA-p optics used in 2004 with a $(\frac{\pi}{4}0\frac{\pi}{4}0)6fs$ snake scheme for $Q_y = 0.2725$ and a 0.75σ vertical amplitude of 2.25π mm mrad. **Bottom**: $\langle J_S \rangle_N$ after acceleration from 801 GeV/c to 804 GeV/c with different acceleration rates (*points*) and the prediction of the Froissart-Stora formula (*curve*) using parameters ϵ_{2Q_y} and $\tilde{\alpha}$ obtained from ν.

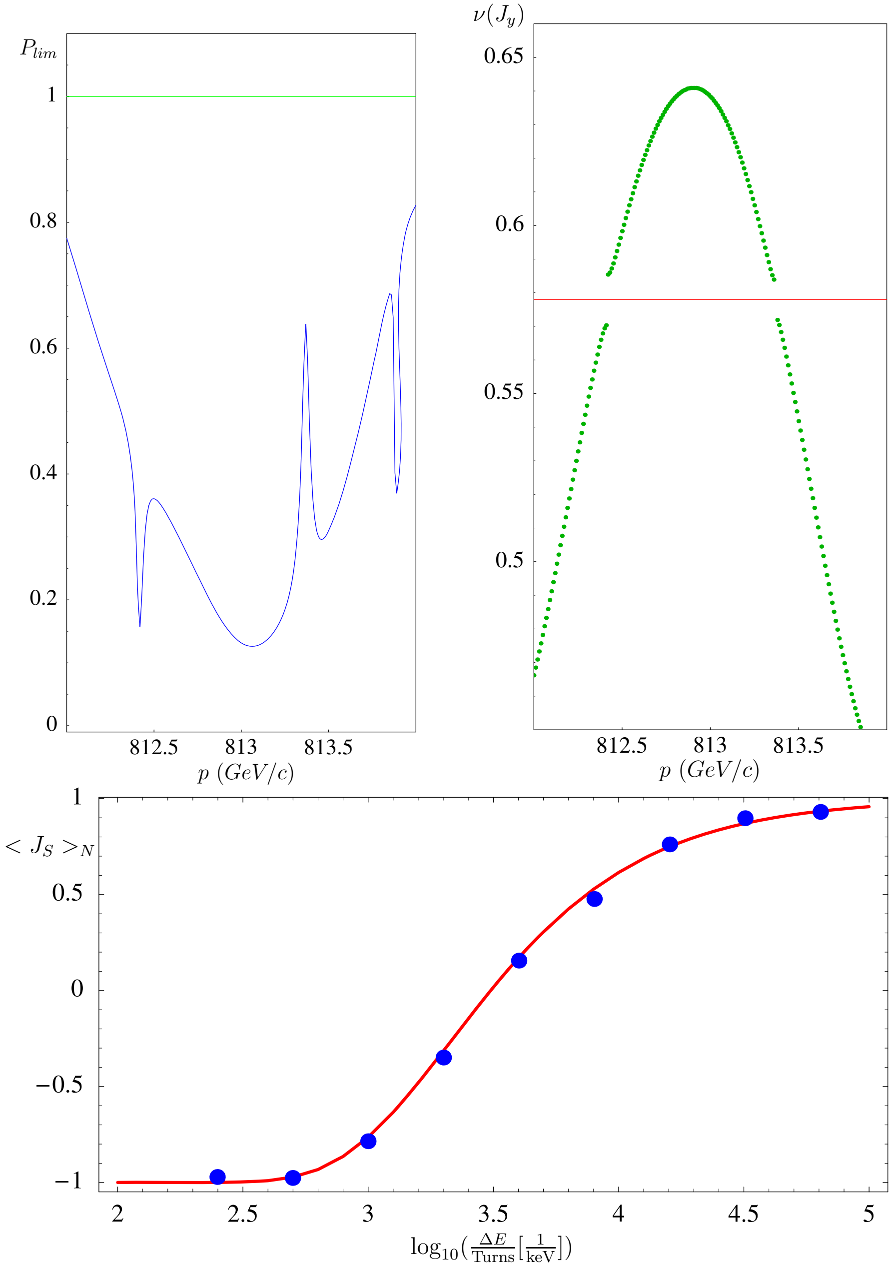

Fig. 2.12. Top: P_{lim} and ν for a second-order resonance of the HERA-p optics of the year 2004 with realistic tune of $Q_y = 0.289$ and a large 4.2σ vertical amplitude of 70π mm mrad with the $(\frac{\pi}{4}0\frac{\pi}{4}0)8fs$ snake scheme. **Bottom**: $\langle J_S \rangle_N$ after acceleration from 812.2 GeV/c to 812.6 GeV/c with different acceleration rates (*points*) and the prediction of the Froissart-Stora formula (*curve*) using parameters ϵ_{2Q_y} and $\tilde{\alpha}$ obtained from ν.

the resonance region is crossed, which is smaller than the Froissart-Stora prediction, which approaches 1 for large acceleration speeds.

Here the parameter τ was the slowly changing momentum. This generalized way of using the Froissart-Stora formula can however also be used when other system parameters change. An example can be found in Sect. 4.3, where the particle amplitude is changed artificially slowly in order to compute the invariant spin field at various orbital amplitudes. In [72], an example is displayed where the Froissart-Stora formula is successfully applied to a resonance that is encountered because of a slow variation of Q_y.

2.2.13 The Choice of Orbital Tunes

When the amplitude-dependent spin tune $\nu(\boldsymbol{J})$ of particles with the amplitude $\boldsymbol{J}$ crosses a resonance, for example during acceleration, the beam polarization is usually reduced. For example, if the acceleration is slow enough to allow for the adiabatic invariance of J_S, the spin on the torus given by $\boldsymbol{J}$ is reversed after the resonance, whereas it is unchanged at smaller phase space amplitudes so that polarization, which is an average over large and small amplitudes, is reduced. This latter conservation of the spin's direction can be either because the resonance is weaker at smaller amplitudes or because the $\nu(\boldsymbol{J})$ does not cross the resonance for particles in the core of the beam. The average polarization is then reduced. However, the polarization often recovers because ν usually varies with energy as shown in Figs. 2.9, 2.11, and 2.12 so that $\nu(\boldsymbol{J})$ will cross the resonance for a second time and the polarization for particles with amplitude $\boldsymbol{J}$ will be flipped back.

Nevertheless, there is some reduction of polarization involved, even after two successive resonance crossings. There are three reasons: First, there are amplitudes where the spin tune only comes into the vicinity of a resonance and then moves away with energy before the resonance has been crossed completely. Second, even though the spin tune might cross the same resonance condition when returning back to $\frac{1}{2}$ at a higher energy, the strength of the two resonances is usually different. If the first resonance was sufficiently strong on the torus $\boldsymbol{J}$ to reverse the sign of spins, the second resonance might not be strong enough to reverse it again. Third, there are amplitudes where the resonance has intermediate strength and polarization is neither reversed nor conserved, but reduced.

Because of these problems occurring at resonance crossings, it is important to find suitable orbital tunes so that low-order spin-orbit resonances are far away from the operating point. The dominant effects are due to radial fields on vertical betatron trajectories. Thus Fig. 2.13 (right) shows the resonance lines $\nu = j_0 + jQ_y$ up to order 10 in the ν-Q_y plane. If the spin tune on the closed orbit is fixed to $\nu_0 = \frac{1}{2}$ by Siberian Snakes, the orbital tune can be chosen to avoid resonance lines. However, the dynamic aperture of proton motion should not be reduced and the tunes have to be far away from low-order orbital resonances. Figure (2.13) (left) shows the Q_x-Q_y tune diagram

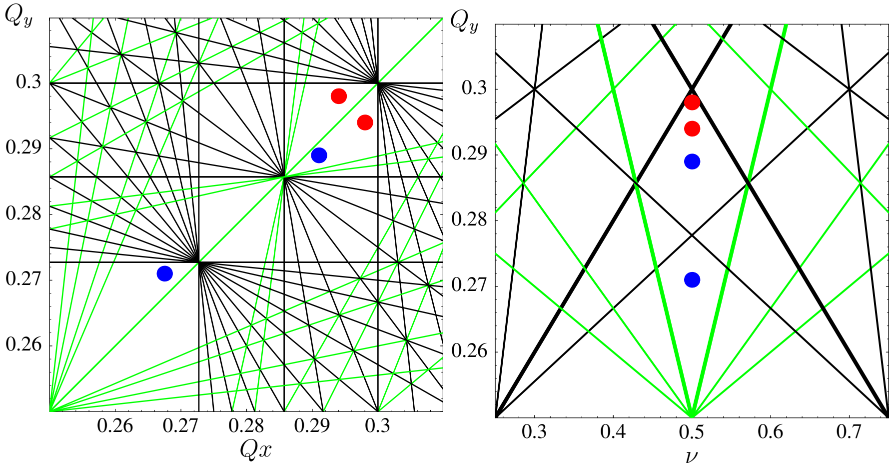

Fig. 2.13. Left: the current orbit tunes ($Q_x = 0.294$,$Q_y = 0.298$) or ($Q_x = 0.298$,$Q_y = 0.294$) (*red*) and the new orbit tunes for polarized proton operation ($Q_x = 0.291$,$Q_y = 0.289$) or ($Q_x = 0.2675$, $Q_y = 0.271$) (*blue*) in the x-y resonance diagram. All resonances up to order 11 are shown. Difference resonances are indicated in green. **Right**: The current vertical tunes (*red*) and the new vertical tunes (*blue*) in the spin-orbit resonance diagram. The odd spin-orbit resonances (*black*) and the even spin-orbit resonances (*green*) are shown up to order 10 in the vicinity of closed-orbit spin tune $\nu_0 = \frac{1}{2}$. For HERA-p, the resonances of second order (*fat green*) and of fifth order (*fat black*) are most destructive.

with resonance lines up to order 11. The operating point has to stay away from these resonance lines.

The established tunes of the 2004 HERA-p operation $Q_x = 0.294$, $Q_y = 0.298$ or $Q_x = 0.298$, $Q_y = 0.294$ (red points) would be unfortunate choices due to their closeness to the resonance $\nu = j_0 \pm 5Q_y$. For the IUCF cooler ring with a partial snake running, second-order resonances have been observed experimentally [95]. For HERA-p with Siberian Snakes, several simulations have shown that the resonances of second order and of fifth order are most destructive. This is supported by Fig. 2.9. Therefore, two new tunes (blue points) are suggested that have an optimal distance from low-order spin-orbit resonances. For the simulations of this tract, the orbit tunes for polarized proton operation were chosen to be ($Q_x = 0.291$,$Q_y = 0.289$). The working point ($Q_x = 0.2675$,$Q_y = 0.271$) would also be a good choice.

To test whether HERA-p could operate with these tunes, Q_y was slowly shifted from the current working point in the direction of the seventh-order resonance to the first choice of polarization tunes. No increase of the beam-loss rates near collimators or of any other beam-loss monitor rate was observed during this procedure.

Moreover, the second choice for polarization with somewhat lower tunes could be reached. Crossing the seventh-order resonance at $Q_y \approx 0.286$ did not cause any problems. However, when crossing the 11th-order resonance at $Q_y = 0.273$, the beam-loss rates close to collimators increased from about 250 Hz to up to 14 kHz. After this resonance had been crossed, the rates fell to about 1.5 kHz. Whereas the working point close to the seventh-order resonance would seem unproblematic, more work would have to be invested in establishing good tunes in the vicinity of $\frac{3}{11}$.

2.2.14 The Importance of the Invariant Spin Field for HERA-p

After having discussed many properties and several applications of the invariant spin field in this chapter, I want to summarize why knowledge of the invariant spin field is essential when analyzing polarized proton beams in HERA-p.

First, when the invariant spin field is known, a much clearer simulation of spin motion is possible than with simple spin-orbit tracking alone. Figure 2.14 shows the average vertical polarization of 100 particles that execute purely vertical betatron motion with the same normalized amplitude of 4π mm mrad but different initial angle variables. These particles have been tracked for 500 turns through the HERA-p lattice of the year 2004 while the beam was initially polarized 100% parallel to $\boldsymbol{n}_0$. Similar kinds of tracking results have been presented in [96]. Because the spins of these particles are not parallel to the invariant spin field, and because the spread of $\boldsymbol{n}$ over the angle variable is large in this case, the averaged polarization exhibits a strong beat. This figure also shows that when particles at a phase space coordinate $\boldsymbol{z}$ are initially parallel to $\boldsymbol{n}(\boldsymbol{z})$, the averaged polarization stays constant, namely at $P_{lim} = 0.765$. Therefore, by starting simulations with spins parallel to the $\boldsymbol{n}$-axis one can perform a much cleaner analysis of beam polarization in accelerators.

After acceleration in HERA-p, the polarized beam has to be stored over several hours during which the polarization should be constant and high. Therefore, each particle should be polarized parallel to the invariant spin field $\boldsymbol{n}(\boldsymbol{z})$ at its phase space position $\boldsymbol{z}$. To have a high time-average beam polarization, every phase space point must have a polarization direction $\boldsymbol{n}(\boldsymbol{z})$ that is almost parallel to the beam average $\langle\boldsymbol{n}\rangle$. Figure 2.15 (top left) shows the energy dependence of $P_{lim} = |\langle\boldsymbol{n}\rangle|$ for vertical betatron motion. At some energies, the invariant spin field at different phase space points can be rather parallel but it suddenly diverges at critical energies leading to diminished polarization, even though only first-order effects have been considered in this figure by using linearized spin-orbit motion described in Sect. 3.1. The invariant spin field then becomes parallel again at higher energies. The critical energies correspond to first order spin-orbit resonances $\nu = j_0 \pm Q_y$.

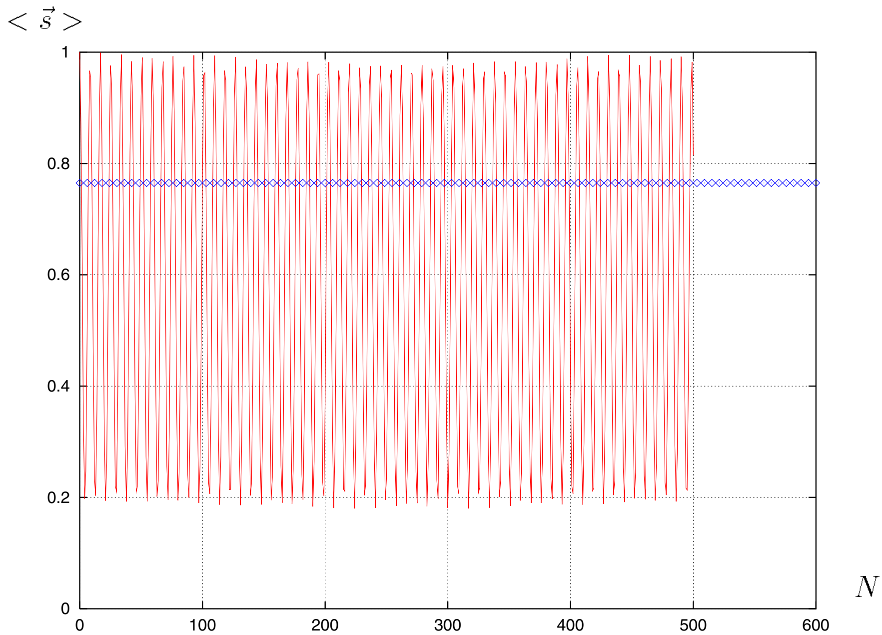

Fig. 2.14. Propagation of a beam that is initially completely polarized parallel to $\boldsymbol{n}_0$ leads to a fluctuating average polarization (*curve*). For another beam that is initially polarized parallel to the invariant spin field $\boldsymbol{n}$, the average polarization stays constant (*diamands*), in this case equal to $P_{lim} = 0.765$.

When the spread of $\boldsymbol{n}$ across phase space is large and therefore particles at different phase space points in the beam are polarized in significantly different directions, three problems occur:

1. The divergence of the polarization direction reduces the time average polarization available to the particle physics experiments because $P_{lim} = |\langle \boldsymbol{n} \rangle|$ is the maximum time-average polarization that can be stored in a ring [97].
2. The polarization direction involved in each collision analyzed in a detector is strongly dependent on the phase space position of the interacting particle.
3. Polarimeters that measure the polarization of particles in the tails of the beam do not yield accurate values for the average polarization.

It is clear from Fig. 2.15 (top left) that in HERA-p, acceptable polarization could be obtained only over a very restricted part of the energy range even if a completely polarized beam were delivered at high energy.

The invariant spin field is important during storage of polarized beams but also during the acceleration cycle. When a change of the invariant spin

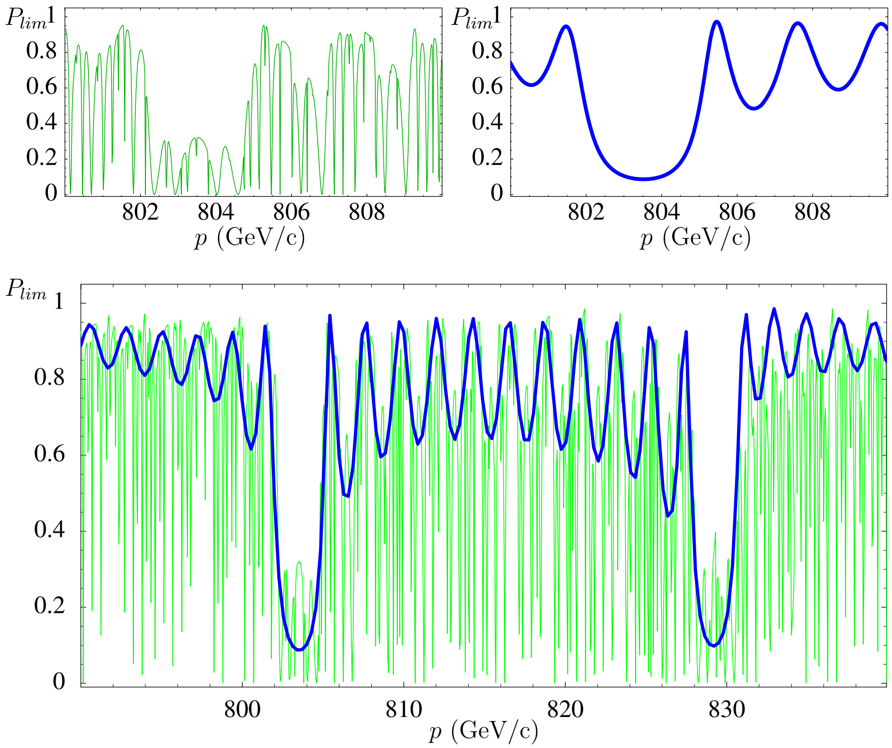

Fig. 2.15. The dependence of the maximum time-average polarization $P_{lim} = |\langle \boldsymbol{n} \rangle|$ on momentum for a vertical amplitude of 25π mm mrad, which corresponds to 2.5σ of the beam size, after HERA-p is made effectively flat for spin motion by flattening snakes. **Top left**: At numerous intrinsic resonances, P_{lim} drops to small values. **Top right**: P_{lim} after the insertion of Siberian Snakes. **Bottom**: P_{lim} with and without Siberian Snakes in a wider region of energy. (Snake scheme $(\frac{\pi}{4}0\frac{\pi}{4}0)6fs$.) Qualitatively similar curves are obtained at other positions in the ring.

field $\boldsymbol{n}(\boldsymbol{z})$ during acceleration from an originally parallel spin field to a divergent spin field and back to a parallel spin field $\boldsymbol{n}(\boldsymbol{z})$ is fast enough, the spins do not react strongly. If it is slow enough, the adiabatic invariance of $J_S = \boldsymbol{S} \cdot \boldsymbol{n}(\boldsymbol{z})$ implies that the spins follow the changing invariant spin field, keeping J_S nearly invariant. In both cases, the beam will recover its polarization after the critical energy region is crossed. The beam polarization is only reduced in intermediate cases. Therefore, Fig. 2.15 indicates regions in which polarization can easily be reduced during acceleration, even though the displayed P_{lim} is computed from the periodicity (2.82) for one turn at a fixed energy.

Strong divergence of the invariant spin field at critical energies can occur even when Siberian Snakes are present, as shown in Fig. 2.15 (top right), even though first-order resonances do not occur. In Fig. 2.15 (bottom), the energy dependences of P_{lim} with and without Siberian Snakes are overlaid, which shows that not all resonance effects are removed by Siberian Snakes, but that resonance structures remain even with Siberian Snakes, although on average P_{lim} is larger. This will be analyzed in detail in Sect. 4.1. Siberian Snakes smooth the variation of $P_{lim} =|\langle \boldsymbol{n}(\boldsymbol{z})\rangle|$ with energy. As a result $\boldsymbol{n}(\boldsymbol{z})$ changes more slowly during acceleration when Siberian Snakes are inserted and the spin can follow this change more easily, keeping changes of the adiabatic invariant J_S smaller.

Siberian Snakes not only help to increase P_{lim} for purely vertical betatron motion and fix the closed-orbit spin tune during acceleration, but they are also essential for countering effects of synchrotron motion. At 920 GeV in HERA-p, the synchrotron tune Q_τ is approximately 8.7×10^{-4} so that a full synchrotron oscillation cycle takes about 1150 turns. Then the energy change in one turn is very small, and in the absence of Siberian Snakes the system will to a large extent behave as if the closed-orbit spin tune oscillates very slowly at the synchrotron frequency. Moreover, the 1σ energy spread of $\frac{\Delta E}{E} = 1.1 \times 10^{-4}$ creates an associated spread in $G\Delta\gamma$ of 0.19 . Thus if there are no Siberian Snakes in the ring, the closed-orbit spin tune can easily cross the condition $\nu_0 = j_0 + Q_y$ during a synchrotron period. The disruptive effect of this periodic crossing is shown in Fig. 2.16 (left) for a particle that moves on a phase space torus with 1σ longitudinal amplitude and $\frac{1}{2}\sigma$ vertical amplitude of 1π mm mrad for a flat HERA-p at 920 GeV. The vertical spin component of a particle with this amplitude changes sign twice every synchrotron period, once for every crossing of the condition $G\gamma = 1758 + Q_y$. Thus the polarization of a beam of particles with a distribution of synchrotron phases will be very low. When the dependence of the closed-orbit spin tune on energy deviation is removed by Siberian Snakes, crossings are eliminated, and the variation of the vertical spin components is strongly suppressed. This is shown in Fig. 2.16 (right), which was computed with 4 Siberian Snakes. Thus Siberian Snakes are indispensable for nullifying effects of synchrotron oscillations.

These plots can also be interpreted in terms of the invariant spin field on 6-dimensional phase space. In Fig. 2.16, the beam is not accelerated so that $J_S = \boldsymbol{S} \cdot \boldsymbol{n}(\boldsymbol{z})$ is invariant and should not even change adiabatically slowly. The changing sign of the vertical spin component therefore reflects the fact that $\boldsymbol{n}(\boldsymbol{z})$ varies from nearly upward to nearly downward over the range of 2π for the longitudinal phase space angle. The resulting large spread of $\boldsymbol{n}(\boldsymbol{z})$ over the phase space torus results in a small $P_{lim} =|\langle \boldsymbol{n}\rangle|$, where the synchrotron motion is automatically included in the average over 6-dimensional phase space. The installation of Siberian Snakes drastically reduces this spread so that P_{lim} can be large.

Siberian Snakes are therefore necessary for three reasons:

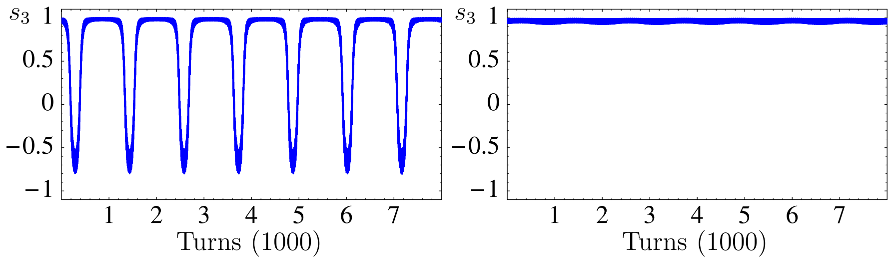

Fig. 2.16. The vertical spin component of one particle during 7 synchrotron periods in HERA-p with 0.5σ vertical amplitude (1π μm) and 1σ longitudinal amplitude (18π mm). While the energy of the particle oscillated due to the synchrotron motion, the reference energy of the ring remained constant. **Left**: Without Siberian Snakes. **Right**: With 4 Siberian Snakes in the $(\frac{\pi}{4}0\frac{\pi}{4}0)6fs$ scheme.

1. They increase P_{lim}, the maximum beam polarization usable at a fixed energy.
2. They smooth the dependence of the invariant spin field on the accelerator's reference energy and therefore improve the possibility to accelerate a beam while keeping the adiabatic invariant $J_S = \boldsymbol{S}\cdot\boldsymbol{n}(\boldsymbol{z})$ nearly constant.
3. They reduce the dependence of spin transport on the energy oscillations of synchrotron motion.

Figure 2.15 was used to show that, even with only first-order effects and with 4 Siberian Snakes in the $(\frac{\pi}{4}0\frac{\pi}{4}0)6fs$ snake scheme, acceptable polarization could not be obtained over the whole energy range. As a next step, I therefore tried to find better choices of snake positions and snake angles.

This search will be presented in Sect. 4.1.3. Figure 2.17 shows the resulting improvements in the variations of $P_{lim} = |\langle\boldsymbol{n}\rangle|$ and in the variations of ν obtained when going from the $(\frac{\pi}{4}0\frac{\pi}{4}0)8fs$ to the $(\frac{3\pi}{4}\frac{3\pi}{8}\frac{3\pi}{8}\frac{\pi}{4})8fs$ snake scheme of Fig. 2.8. Here the non-perturbative algorithm described in Sect. 4.1.1 was used to include higher-order effects and to analyze improvements in the variation of the amplitude-dependent spin tune.

In the following chapters, tools for reliable computation of the invariant spin field and for the selection of optimal snake schemes will be described. In Sect. 3.3.2, light will be shed on the reasons why certain snake schemes are favorable. Because special snake schemes lead to comparatively large P_{lim} and small spin tune spread, it is expected that the reduction of polarization during the acceleration process is comparatively small for these schemes. In fact, tracking simulations will show that the snake schemes that I have found allow the acceleration of a beam with significantly larger emittance than standard snake schemes.

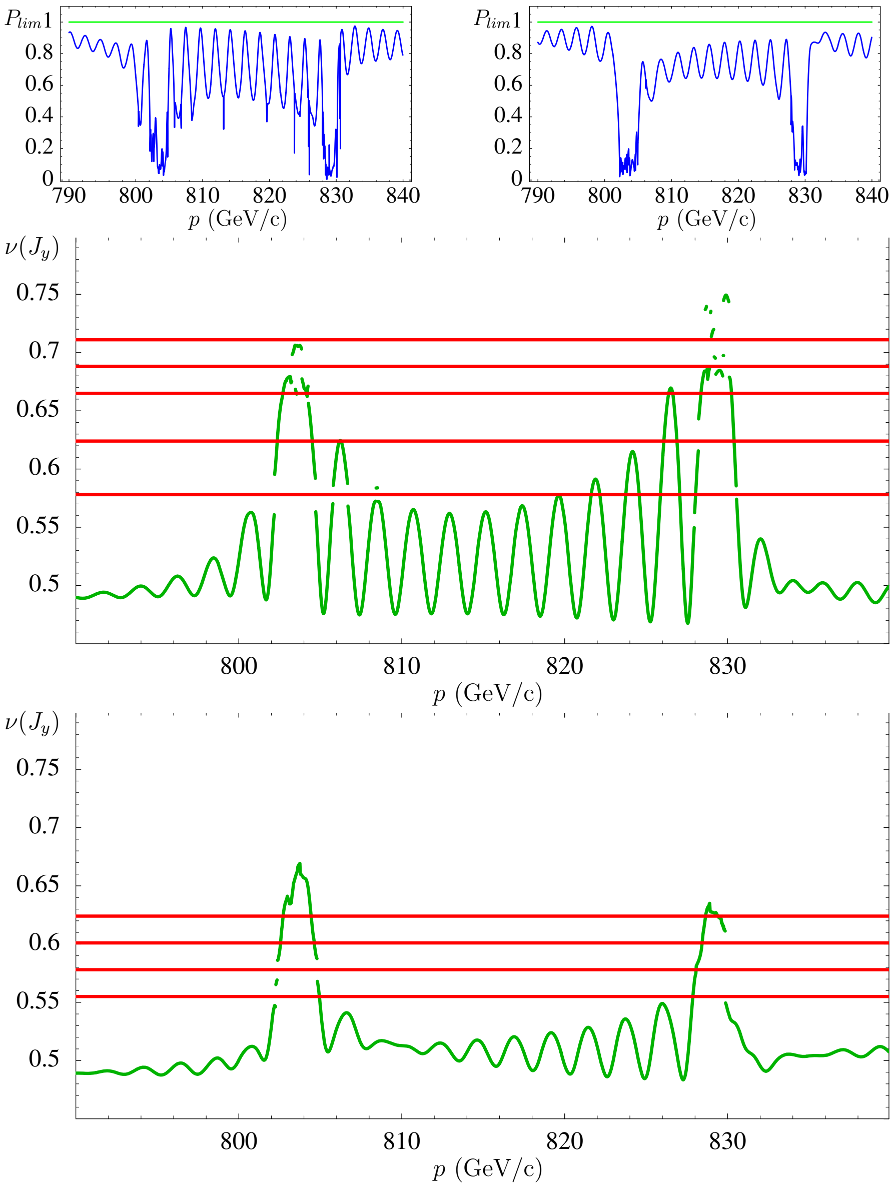

Fig. 2.17. The dependence of maximum time-average polarization P_{lim} on momentum for 2.5σ vertical motion (25π mm mrad) in HERA-p with a conventional snake scheme $(\frac{\pi}{4}0\frac{\pi}{4}0)8fs$ (*top left*) and an optimized scheme $(\frac{3\pi}{4}\frac{3\pi}{8}\frac{3\pi}{8}\frac{\pi}{4})8fs$ (*top right*). The amplitude-dependent but orbital phase independent spin tune ν is shown for $(\frac{\pi}{4}0\frac{\pi}{4}0)8fs$ (*middle*) and for $(\frac{3\pi}{4}\frac{3\pi}{8}\frac{3\pi}{8}\frac{\pi}{4})8fs$ (*bottom*). From top to bottom, the following resonance lines are drawn, **Middle**: $1-Q_y$, $3-8Q_y$, $5-15Q_y$, $16Q_y-4$, $2Q_y$ and **Bottom**: $\nu=16Q_y-4$, $\nu=9Q_y-2$, $\nu=2Q_y$, $\nu=2-5Q_y$. The strength of these higher-order resonances can be deduced from the tune jumps.

References

1. J. Frenkel: Die Elektrodynamik des rotierenden Elektrons. *Z. Phys.* 37:243–262 (1926)
2. L. H. Thomas: The kinematics of an electron with an axis. *Philos. Mag.* 3(13):1–20 (1927)
3. H. Mendlowitz and K. M. Case: *Phys. Rev.* 97:33 (1955)
4. V. Bargmann, L. Michel, and V. L. Telegdi: Precession of the polarization of particles moving in a homogeneous electro-magnetic field. *Phys. Rev. Lett.* 2(10):435–436 (1959)
5. H. Rose: Hamiltonian magnetic optics. *Nucl. Instr. Meth.* A258:374–401 (1987)
6. G. H. Hoffstaetter: Nonlinear dependence of synchrotron radiation on beam parameters. In *Proceedings of PAC95, Dallas* (1995)
7. E. D. Courant and H. S. Snyder: Theory of the alternating-gradient synchrotron. *Ann. Phys.* 3:1–48 (1958)
8. M. Berz: Computational aspects of optics design and simulation: COSY INFINITY. *Nucl. Instr. Meth.* A298:473-479 (1990)
9. Ya. S. Derbenev: The Stern-Gerlach method in charge particle storage rings (1) The double-resonance Stern-Gerlach effect. UM-HE-90-30, University of Michigan (1990)
10. Ya. S. Derbenev: The Stern-Gerlach method in charged particle storage rings (2) The neo-classical Stern-Gerlach effect. UM-HE-90-32, University of Michigan (1990)
11. Ya. S. Derbenev: Concepts for Stern-Gerlach polarization in storage rings. DESY Accelerator Physics Seminar (1995)
12. S. R. Mane: Exceptional orbits: a new class of spin trajectories in circular accelerators. *Nucl. Instr. Meth. A*498:52–89 (2003)
13. M. Conte, A. Penzo, and M. Pusterla: Spin splitting due to longitudinal Stern-Gerlach kicks. *Nuovo Cimento*, 108 A(1):127–136 (1995)
14. M. Conte, B. E. Norum, A. Penzo, M. Pusterla, and R. Rossmanith: A proposed test of the spin splitter effect in HERA-p. DESY–HERA-96-01 (1996)
15. A. Luccio: Numerical spin tracking in a synchrotron, computer code SPINK-examples and reference manual. BNL-52481, Brookhaven (1995)
16. V. Balandin, M. Berz, and N. Golubeva: Computation and analysis of spin dynamics. In *Fourth Computational Accelerator Physics Conference, AIP Conference Proceedings 391*, p. 276 (1996)
17. P. Nghiem and A. Tkatchenko: Simulation of proton spin motion in circular accelerators using one-turn spinor transfer maps. *Nucl. Instr. Meth.* A(335):3349–366 (1993)
18. S. Y. Lee: *Spin dynamics and Snakes in synchrotrons.* World Scientific (1997)
19. Bryan W. Montague: Polarized beams in high-energy storage rings. *Physics Reports*, 113(1):1–96 (1984)
20. F. Z. Khiari, P. R. Cameron, G. R. Court, D. G. Crabb, *et al*: Acceleration of polarized protons to 22 GeV/c and the measurement of spin-spin effects in $\boldsymbol{p}+\boldsymbol{p} \rightarrow p+p$. *Phys. Rev.* D 39:45–85 (1989)
21. H. Huang, L. Ahrens, J. G. Alessi, M. Beddo, K. A. Brown, *et al*: Preservation of proton polarization by a partial Siberian Snake. *Phys. Rev. Lett.* 73:2982–2985 (1994)

22. B. B. Blinov, C. M. Chu, E. D. Courant, D. A. Crandell, *et al*: First test of a partial Siberian Snake during polarized beam acceleration. *Phys. Rev. Lett.* 73(12):1621–1623 (1994)
23. R. A. Phelps, V. A. Anferov, C. M. Chu, E. D. Courant, *et al*: Adiabatic partial Siberian Snake turn-on with no beam depolarization. *Phys. Rev. Lett.* 72(10):1479–1481 (1994)
24. H. Huang, et al.: Polarized proton acceleration at the brookhaven AGS – an update. In *Proceedings of EPAC02*, Paris (2002)
25. D. P. Barber and A. De Roeck, editors: *Proceedings of Polarized Protons at High Energies*, DESY–Proceedings–1999–03 (1999)
26. T. Roser: RHIC spin program: machine aspects and recent progress. In [25].
27. T. Roser: private communication and "The Relativistic Heavy Ion Collidor Run-4 Polarized Proton Operation Web Log" (2004)
28. SPIN Collaboration and the DESY Polarization Team: Acceleration of polarized protons to 820 GeV at HERA. UM–HE–96–20, University of Michigan (1996)
29. A. W. Chao: Polarization of a stored electron beam. In *Conference proceedings 87*. US Particle Accelerator School, Batavia, USA, American Institute of Physics (1981)
30. A. W. Chao: Evaluation of radiative spin polarization in an electron storage ring. *Nucl. Instr. Meth.* 180:29 (1981)
31. H. Mais and G. Ripken: Theory of spin-orbit motion in electron-positron storage rings. DESY–83–062 (1983)
32. P. Lochak and C. Meunier: *Multiphase averaging for classical systems with applications to adiabatic theorems*, volume 72 of *Applied Mathematical sciences*. Springer (1988)
33. V. I. Arnold, editor: *Mathematical Aspects of Classical and Celestial Mechanics, Chapter 5*, volume Dynamical Systems III of *Encyclopedia of mathematical sciences; V*. Springer (1988)
34. A. I. Neistadt: Passage through resonance in a two-frequency problem. *Soviet Phys. Doklady*, 20(3):189–191, 1975. English translation of Doklady Akad. Nauk. SSSR Mechanics 221 (2), 301–304 (1975)
35. T. Roser: Polarized proton beam in the AGS. In *Proceedings of SPIN98*, Protvino (1998)
36. D. A. Crandell, V. A. Anferov, B. B. Bilinov, D. D. Caussyn, *et al*: Spin flipping through and intrinsic depolarizing resonance by strengthening it. *Phys. Rev. Lett.* 77(9):1763–1765 (1996)
37. M. Bai, L. Ahrens, J. Alessi, K. Brown, G. Bunce, P. Cameron, *et al*: Overcoming intrinsic spin resonances with an rf dipole. *Phys. Rev. Lett.* 80(21):4673–4676 (1998)
38. Ya. S. Derbenev and A. M. Kondratenko: Acceleration of polarized particles. *Sov. Phys. Doklady*, 20:562, 1976. also in Russian.: *Dokl. Akad. Nauk Ser. Fiz.* 223:830-833 (1975)
39. Ya. S. Derbenev, A. M. Kondratenko, S. I. Serednyakov, *et al*: Radiative polarization: obtaining, control, using. *Particle Accelerators*, 8:115–126 (1978)
40. Ya. S. Derbenev and A. M. Kondratenko: On the possibilities to obtain high-energy polarized particles in accelerators and storage rings. In G. H. Thomas, editor, *High-energy Physics with Polarized Beams and Polarized Targets*, AIP Conference Proceedings 51, p. 292 (1978)

41. A. D. Krisch, S. R. Mane, R. S. Raymond, T. Roser, *et al*: First test of the Siberian Snake magnet arrangement to overcome depolarizing resonances in a circular accelerator. *Phys. Rev. Lett.* 63(11):1137–1140 (1989)
42. A. Luccio and T. Roser, editors: Third workshop on Siberian Snakes and spin rotators. BNL–52453, Brookhaven (1994)
43. J. E. Goodwin, H-O. Meyer, M. G. Minty, P. V. Pancella, *et al*: Overcoming intrinsic and synchrotron depolarizing resonances with a Siberian Snake. *Phys. Rev. Lett.* 64(23):2779–2782 (1990)
44. V. Anferov: Siberian Snake design for a high-energy ring. In [25].
45. V. Ranjbar et al.: Snake calibration in RHIC. In *Proceedings to EPAC02*, Paris (2002)
46. V. Ranjbar et al.: Fitting helical snake and rotator field strength measurements in RHIC. In *Proceedings to PAC01*, Chicago (2001)
47. V. I. Ptitsin and Yu. M. Shatunov: Helical spin rotators and snakes. In *Proc. 3. Workshop on Siberian Snakes and Spin Rotators*, BNL-52453:15, Brookhaven (1994)
48. G. H. Hoffstaetter: Polarized protons in HERA. In DESY–96–05 (1996)
49. G. H. Hoffstaetter: Snake matching. In UM–HE 99–05, University of Michigan (1999)
50. K. Steffen: Strong spin matching with and without snakes, a scheme for preserving polarization in large ring accelerators. DESY–88–068 (1988)
51. V. A. Anferov: Spin transparent interaction regions for HERA. *Nucl. Instr. Meth.* A398(2-3):423–425 (1997)
52. D. P. Barber, G. H. Hoffstaetter, and M. Vogt: Spin motion at high energy in HERA-p. In UM–HE 99–05, University of Michigan (1999)
53. SPIN Collaboration and the DESY Polarization Team: Acceleration of polarized protons to 920 GeV at HERA. UM–HE–99–05, University of Michigan (1999)
54. H. Poincaré: *Les méthodes nouvelles de la méchanique céleste.* Gauthier-Villars, Paris, 1892, 1893, 1899. three volumes.
55. Ya. S. Derbenev and A. M. Kondratenko: Diffusion of particle spin in storage rings. *Sov. Phys. JETP*, 35:230 (1972)
56. D. P. Barber: Prospects for polarized protons at HERA. In *conference on the spin structure of the nucleon at Erice in 1995*, World Scientific (1998)
57. D. P. Barber, K. Heinemann, G. H. Hoffstaetter, and M. Vogt: The phase space dependent spin polarization direction in the HERA proton ring at high energy. In *Proceedings to EPAC96*, Siges/Spain and DESY–M–96–14 (1996)
58. K. Yokoya: On multiple Siberian Snakes. SSC–189, SSC Central Design Group (1988)
59. K. Yokoya: The action-angle variables of classical spin motion in circular accelerators. DESY–86–057 (1986)
60. K. Yokoya: Calculation of the equilibrium polarization of stored electron beams using Lie algebra. *Nucl. Instr. Meth.* A258:149–160 (1987)
61. K. Yokoya: Non-perturbative calculation of equilibrium polarization of stored electron beams. KEK–92–6, Tsukuba (1992)
62. S. R. Mane: Electron-spin polarization in high-energy storage rings. II. Evaluation of the equilibrium polarization. *Phys. Rev.* A(36):120–130 (1987)
63. S. R. Mane: Polarization of electron beams in high-energy storage rings. 1: convergence of perturbation theory. *Nucl. Instr. Meth.* A321:21–41 (1992)

64. D. P. Barber, K. Heinemann, and G. Ripken: Notes on spin dynamics in storage rings. DESY–M–92–04 (1992)
65. V. Balandin and N. Golubeva: Hamiltonian methods for the study of polarized proton beam dynamics in accelerators and storage rings. DESY–98–016 (1998)
66. Yu. Eidelman and V. Yakimenko: The application of Lie methods to the spin motion in nonlinear collider fields. *Particle Accelerators*, 45:17–35 (1994)
67. V. Balandin and N. Golubeva: Nonlinear spin dynamics. *Proceedings of the XV International Conference on High-energy Particle Accelerators, Hamburg*, p. 998–1000 (1992)
68. M. Berz: *Differential Algebraic Description and Analysis of Spin Dynamics*, volume 343 of *AIP Conference Proceedings*, p. 321–327 (1995)
69. D. P. Barber, G. H. Hoffstaetter and M. Vogt: Polarized protons in HERA. In *Proceedings to EPAC02*, Paris and DESY-M-02–01 (2002)
70. D. P. Barber, M. Vogt, and G. H. Hoffstaetter: The amplitude-dependent spin tune and the invariant spin field in high-energy proton accelerators. In *Proceedings EPAC98*, Stockholm (1998)
71. D. P. Barber, G. H. Hoffstaetter, and M. Vogt: The amplitude-dependent spin tune and the invariant spin field in high-energy proton accelerators. In *Proceedings SPIN98*, Protvino (1998)
72. M. Vogt: Bounds on the maximum attainable equilibrium spin polarization of protons in HERA. *Dissertation, Universität Hamburg*, DESY–THESIS–2000–054 (December 2000)
73. J. Moser: Lectures on Hamiltonian systems. *Mem. Am. Math. Soc. 81*, p. 60 (1968)
74. J. W. S. Cassels: *An introduction to the theory of Diophantine approximation.* Cambridge University Press, Cambridge U.K. (1957)
75. D. P. Barber, R. Jaganathan, M. Vogt: Spin tune in the single resonance model with a pair of Siberian Snakes. DESY–05–035 and ArXiv:physics/0502121 (2005)
76. A. I. Neistadt: Averaging in multi-frequency systems. *Soviet Phys. Doklady*, 20(7):492–494, 1976. English translation of Doklady Akad. Nauk. SSSR Mechanics 223 (2), 314–317 (1976)
77. G. H. Hoffstaetter, H. S. Dumas and J. A. Ellison: Adiabatic invariants for spin-orbit motion. In *Proceedings to EPAC02*, Paris and DESY-M-02–01 (2002)
78. G. H. Hoffstaetter, H. S. Dumas and J. A. Ellision Phys. Rev. ST-AB, 8, 014001 (2006)
79. K. Abragam: *The principles of nuclear magnetism.* Clarendon (1961)
80. S. R. Mane: Exact solution of the Derbenev-Kondratenko $\boldsymbol{n}$-axis for a model with one resonance. FERMILAB–TM–1515 (1988)
81. K. Heinemann and G. H. Hoffstaetter: A tracking algorithm for the stable spin polarization field in storage rings using stroboscopic averaging. *Phys. Rev.* E 54:4240–4255 (1996)
82. S. R. Mane: Exact solutions for the spin tune for model storate rings. *Nucl. Instr. Meth.* A480:328–338 (2002)
83. S. R. Mane: Analytical solutions for the invariant spin field for model storage rings. *Nucl. Instr. Meth.* A485:277–297 (2002)
84. S. R. Mane: MILES: a new nonperturbative formalism to calculate the invariant spin field in circular accelerators. *Nucl. Instr. Meth.* A498:1–15 (2003)

85. M. Froissart and R. Stora: Depolarisation d'un faisceau de protons polarises dans un synchrotron. *Nucl. Instr. Meth.* 7:297–305 (1960)
86. E. D. Courant and R. D. Ruth: The acceleration of polarized protons in circular accelerators. BNL–51270 and UC–28 and ISA–80–5 (1980)
87. M. F. Schlesinger: *The wonderful world of stochastics*. Studies in statistical mechanics 12. North-Holland, p. 382 (1985)
88. S. R. Mane: Approximate formula for the asymptotic polarization for passage across two overlapping spin resonances. *Nucl. Instr. Meth. A*524:80–91 (2004)
89. S. Y. Lee and S. Tepikian: Resonance due to a local spin rotator in high-energy accelerators. *Phys. Rev. Lett.* 56(16):1635–1638 (1986)
90. S. Y Lee: Spin-depolarization mechanisms due to overlapping spin resonances in synchrotrons. *Phys. Rev.* E 47(5):3631–3644 (1993)
91. V. Ptitsin and Yu. M. Shatunov: The investigation of spin resonances in an accelerator with Siberian Snakes. In C. W. de Jager, T. J. Ketel, P. J. Mulders, J. E. J. Oberski, and M. Oskam-Tamoezer, editors, *Proceedings SPIN96*, p. 516–518. World Scientific (1996)
92. G. H. Hoffstaetter, Future possibilities for HERA, In *Proceedings EPAC00*, Vienna (2000)
93. G. H. Hoffstaetter and M. Vogt: SPRINT users guide and reference manual. DESY (2002)
94. M. Vogt, D. P. Barber, and G. H. Hoffstaetter: Introduction to the invariant spin field and update on simulations with polarized protons at HERA-p. In DESY–HERA–98–04 (1998)
95. L. V. Alexeeva, V. A. Anferov, D. D. Caussyn, C. M. Chu, *et al*: Observation of a second-order spin-depolarizing resonance. *Phys. Rev. Lett.* 75(10):1931–1933 (1995)
96. V. Balandin, N. Golubeva, and D. P. Barber: Studies of the behavior of proton spin motion in HERA-p at high energies. DESY–M–96–04 (1996)
97. D. P. Barber, K. Heinemann, G. H. Hoffstaetter, and M. Vogt: The permissible equilibrium polarization distribution in a stored proton beam. In *ICFA Proceedings Quantum Aspects of Beam Physics*, World Scientific (1998)

3 First-Order Spin Motion

3.1 Linearized Spin-Orbit Motion

In this section, an approximate description of spin motion will be presented that includes first-order resonances but is complementary to the SRM and is valid even when resonances overlap. At azimuth θ, a spin can be described in terms of a complex coordinate α and the orthogonal coordinate system $[\boldsymbol{m}, \boldsymbol{l}, \boldsymbol{n}_0]$ of Sect. 2.2.2 as [1, 2, 4]

$$\boldsymbol{S} = \Re\{\alpha\}\boldsymbol{m}(\theta) + \Im\{\alpha\}\boldsymbol{l}(\theta) + \sqrt{1-|\alpha|^2}\boldsymbol{n}_0(\theta) \; . \tag{3.1}$$

According to (2.50), the coordinate vectors $\boldsymbol{m}$ and $\boldsymbol{l}$ satisfy the equation of motion

$$\frac{\mathrm{d}}{\mathrm{d}\theta}(\boldsymbol{m} + \mathrm{i}\boldsymbol{l}) = (\boldsymbol{\Omega}_0 - \nu_0 \boldsymbol{n}_0) \times (\boldsymbol{m} + \mathrm{i}\boldsymbol{l}) \; . \tag{3.2}$$

The spin of a particle that travels on the closed orbit precesses around $\boldsymbol{\Omega}_0$ and has rotated ν_0 times around $\boldsymbol{n}_0$ after one turn. According to (3.2), $\boldsymbol{m}$ and $\boldsymbol{l}$ also precess around $\boldsymbol{\Omega}_0$, but in addition a precession around $\boldsymbol{n}_0$ is subtracted, leaving no net rotation after one turn. Therefore, the coordinate system $[\boldsymbol{m}, \boldsymbol{l}, \boldsymbol{n}_0]$ is 2π-periodic in θ.

When the spin coordinate α and the phase space coordinates $\boldsymbol{z}$ are small so that the equation of spin-orbit motion can be linearized, then one approximates an initial spin of a particle at azimuth θ_0 by $\boldsymbol{S}_i \approx \Re\{\alpha_i\}\boldsymbol{m}(\theta_0) + \Im\{\alpha_i\}\boldsymbol{l}(\theta_0) + \boldsymbol{n}_0(\theta_0)$ and after the particle has traveled to azimuth θ, one has $\boldsymbol{S} = \Re\{\alpha\}\boldsymbol{m}(\theta) + \Im\{\alpha\}\boldsymbol{l}(\theta) + \boldsymbol{n}_0(\theta)$ where α is determined by the 7×7 spin-orbit transport matrix,

$$\begin{pmatrix} \boldsymbol{z} \\ \alpha \end{pmatrix} = \mathsf{M}_{77}(\theta_0;\theta) \begin{pmatrix} \boldsymbol{z}_i \\ \alpha_i \end{pmatrix} = \begin{pmatrix} \mathsf{M}(\theta_0;\theta) & \boldsymbol{0} \\ \boldsymbol{G}^T(\theta_0;\theta) & \mathrm{e}^{\mathrm{i}\nu_0(\theta-\theta_0)} \end{pmatrix} \begin{pmatrix} \boldsymbol{z}_i \\ \alpha_i \end{pmatrix} , \tag{3.3}$$

whereby $\mathsf{M}(\theta_0;\theta)$ is the 6×6-dimensional transport matrix for the phase space variables. For a particle on the closed orbit, the exponential describes the rotation of the spin component α around $\boldsymbol{n}_0$ with respect to $\boldsymbol{m}$ and $\boldsymbol{l}$. This rotation appears in (3.3) because spins precess around $\boldsymbol{\Omega}_0$ for $\boldsymbol{z} = 0$, while the coordinate vectors $\boldsymbol{m}$ and $\boldsymbol{l}$ rotate around $\boldsymbol{\Omega}_0 - \nu_0\boldsymbol{n}_0$. The complex row vector $\boldsymbol{G}^T(\theta_0;\theta)$ describes additional spin motion with respect to $\boldsymbol{m}$ and

$\boldsymbol{l}$ due to off closed-orbit fields. The 6-dimensional zero vector $\boldsymbol{0}$ shows that the effect of Stern-Gerlach forces on the orbit motion is not considered.

The linearized spin-orbit transport through two successive optical elements is described by the product of their 7×7 matrices. These matrices were derived long ago [2, 3] for all standard optical elements and were initially used for the description of polarized electron beams.

Alternatively, the spin transport can be described by a spin transport quaternion as discussed in Sect. 2.1.5. When linearizing with respect to phase space variables, indicated by $=_1$, a spin transport quaternion $\boldsymbol{C}$ is separated into the quaternion for closed-orbit motion $\boldsymbol{C}^0$ and a contribution $\boldsymbol{C}^1$ that is linear in the phase space variables, $\boldsymbol{C} =_1 \boldsymbol{C}^0 + \boldsymbol{C}^1(\boldsymbol{z})$. The spin-orbit transport through two successive optical elements is described by the action of first the quaternion $\boldsymbol{A}$ associated with the first element and then the quaternion $\boldsymbol{B}$ of the second element. The quaternion $\boldsymbol{C}$ describing the combined rotation is computed using the orthogonal 4×4 matrix $\tilde{\mathsf{A}}$ as described in (2.36),

$$\boldsymbol{C}^0 = \tilde{\mathsf{A}}^0 \boldsymbol{B}^0 \ , \quad \boldsymbol{C}^1 = \tilde{\mathsf{A}}^0 \boldsymbol{B}^1 + \tilde{\mathsf{A}}^1 \boldsymbol{B}^0 \ . \tag{3.4}$$

The spin transport quaternion of an optical element does not depend on the basis vectors $[\boldsymbol{m}, \boldsymbol{l}, \boldsymbol{n}_0]$ and is therefore the same for two identical optical elements that are at different locations of the ring. The 7×7 matrix of individual optical elements does not have this advantage. Furthermore, a generalization to quaternions that depend nonlinearly on the phase space coordinates is straightforward (see Sect. 4.1.4). Therefore, the quaternion method is used in the program SPRINT [5, 6] to describe spin transport.

The spin transport quaternion can be written as the concatenation of first the closed-orbit spin transport described by $\boldsymbol{C}^0$ and then a purely phase space dependent spin transport that does not change the spin of particles on the closed orbit. With the quaternion $\boldsymbol{e}_1 = (1, 0, 0, 0)^T$ describing the identity transformation and with a quaternion $\boldsymbol{D}^1$ that vanishes for particles on the closed orbit, the purely phase space dependent spin transport is described by $\boldsymbol{e}_1 + \boldsymbol{D}^1$,

$$\boldsymbol{C} = \tilde{\mathsf{C}}^0 (\boldsymbol{e}_1 + \boldsymbol{D}^1) \ , \quad \boldsymbol{D}^1 = \tilde{\mathsf{C}}^{0T} \boldsymbol{C}^1 \ . \tag{3.5}$$

Here advantage has been taken of the fact that the 4×4-dimensional matrix $\tilde{\mathsf{C}}^0$ is orthogonal, as has been pointed out after (2.36) so that it can be inverted by transposition. The 3×3 spin-rotation matrix on the closed orbit is written as R^0 and the rotation matrix corresponding to the concatenated quaternion in (3.5) is written as the product $\mathsf{R}^D \mathsf{R}^0$. The quaternion $\boldsymbol{e}_1 + \boldsymbol{D}^1$ with $\boldsymbol{D}^1 = (d_0^1, \boldsymbol{d}^{\,1})^T$ is related to the rotation matrix R^D via (2.30), and to first order it reads as

$$\begin{aligned} R_{ij}^D \ &= \ [(1 + d_0^1)^2 - (\boldsymbol{d}^{\,1})^2] \delta_{ij} + 2 d_i^1 d_j^1 - 2(1 + d_0^1) \epsilon_{ijk} d_k^1 \\ &=_1 \ (1 + 2 d_0^1) \delta_{ij} - 2 \epsilon_{ijk} d_k^1 \ . \end{aligned} \tag{3.6}$$

The total spin rotation $\mathsf{R}^D \mathsf{R}^0$ first transports the initial spin $\boldsymbol{S}_i = \boldsymbol{n}_0(\theta_0)$ to $\boldsymbol{n}_0(\theta) = \mathsf{R}^0 \boldsymbol{n}_0(\theta_0)$ and then to

$$\boldsymbol{S}_f = (1 + 2d_0^1)\boldsymbol{n}_0(\theta) + 2\boldsymbol{d}^1 \times \boldsymbol{n}_0(\theta) . \tag{3.7}$$

When a spin with $\boldsymbol{S}_i = \boldsymbol{n}_0$ is transported by the 7×7 spin-orbit transport matrix, then $\alpha_f = \boldsymbol{S}_f \cdot [\boldsymbol{m}(\theta) + \mathrm{i}\boldsymbol{l}(\theta)]$ is given by $\boldsymbol{G} \cdot \boldsymbol{z}$, which now equates to

$$\boldsymbol{G} \cdot \boldsymbol{z} = 2[\boldsymbol{d}^1 \times \boldsymbol{n}_0(\theta)] \cdot [\boldsymbol{m}(\theta) + \mathrm{i}\boldsymbol{l}(\theta)] = -\mathrm{i}2\boldsymbol{d}^1 \cdot [\boldsymbol{m}(\theta) + \mathrm{i}\boldsymbol{l}(\theta)] . \tag{3.8}$$

This illustrates how the spin-orbit transport matrix M_{77} can easily be computed when its spin transport quaternion is known.

3.1.1 The Invariant Spin Field for Linearized Spin-Orbit Motion

Although it is difficult to compute $\boldsymbol{n}$ in general, an approximation for $\boldsymbol{n}$ can easily be obtained [7, 8] for linearized spin-orbit motion on a Poincaré section at azimuth θ_0. Its components perpendicular to $\boldsymbol{n}_0(\theta_0)$ are written as a complex function $n_\alpha(\boldsymbol{z})$ and a 7-dimensional spin-orbit vector $\boldsymbol{n}_1$ is used to obtain the first-order expansion of $\boldsymbol{n}(\boldsymbol{z})$. Using the one turn matrix $\mathsf{M}_{7\times7} = M_{7\times7}(\theta_0; \theta_0 + 2\pi)$, the linearized periodicity condition (2.82) for the invariant spin field is

$$\boldsymbol{n}_1(\boldsymbol{z}) = \begin{pmatrix} \boldsymbol{z} \\ \alpha_n(\boldsymbol{z}) \end{pmatrix} , \quad \boldsymbol{n}_1(\mathsf{M}\boldsymbol{z}) = \mathsf{M}_{77}\boldsymbol{n}_1(\boldsymbol{z}) . \tag{3.9}$$

This equation can be solved for $\boldsymbol{n}_1$ after the matrices are diagonalized. Let A^{-1} be the column matrix of eigenvectors $\boldsymbol{v}_k^\pm$ of the one turn matrix M. The eigenvalues are $\mathrm{e}^{\pm i2\pi Q_k}$ with the orbital tunes Q_k. The matrix $\mathsf{\Lambda} = \mathsf{A}\ \mathsf{M}\ \mathsf{A}^{-1}$ is the diagonal matrix of these eigenvalues. Now the 7×6-dimensional matrix T is needed, which is the column matrix of the first 6 eigenvectors of M_{77} and has the form

$$\mathsf{T} = \begin{pmatrix} \mathsf{A}^{-1} \\ \boldsymbol{B}^T \end{pmatrix} , \quad \text{with} \quad \mathsf{T}\ \mathsf{\Lambda} = \mathsf{M}_{77}\mathsf{T} , \tag{3.10}$$

where the seventh components of the eigenvectors form a vector $\boldsymbol{B}$. If a linear function $\boldsymbol{n}_1(\boldsymbol{z}) = \mathsf{K}\boldsymbol{z}$ of the phase space coordinates can be found that satisfies the periodicity condition (3.9), then the seventh component of $\boldsymbol{n}_1$ describes an invariant spin field. Because the upper 6 components of $\boldsymbol{n}_1(\boldsymbol{z})$ are $\boldsymbol{z}$, the upper 6 rows of K form the identity matrix 1_6. Inserting $\boldsymbol{n}_1 = \mathsf{K}\boldsymbol{z}$ into (3.9) and multiplying the resulting condition $\mathsf{K}\ \mathsf{M} = \mathsf{M}_{77}\mathsf{K}$ by A^{-1} from the right leads to $\mathsf{K}\ \mathsf{A}^{-1}\mathsf{\Lambda} = \mathsf{M}_{77}\mathsf{K}\ \mathsf{A}^{-1}$. Therefore, the columns of $\mathsf{K}\ \mathsf{A}^{-1}$ are eigenvectors of $\mathsf{M}_{7\times7}$ and are therefore proportional to the columns of T. Because the upper 6 rows $1_6\mathsf{A}^{-1}$ agree with those of T, the 6 proportionality constants must be 1. Therefore, $\mathsf{K}\ \mathsf{A}^{-1} = \mathsf{T}$ and I conclude that there exists a unique linear invariant spin field given by

$$\boldsymbol{n}_1(\boldsymbol{z}) = \mathsf{T}\ \mathsf{A}\boldsymbol{z} , \quad \alpha_n = \boldsymbol{B} \cdot (\mathsf{A}\boldsymbol{z}) . \tag{3.11}$$

Now the steps that lead to the amplitude-dependent spin tune for a system that does not have an orbital resonance in Sect. 2.2.7 are repeated for linearized spin-orbit motion. In linear approximation the orthonormal coordinate system $[\boldsymbol{n}, \boldsymbol{u}_1, \boldsymbol{u}_2]$ at θ_0 is given by

$$\boldsymbol{n}(\boldsymbol{z}) =_1 \Re\{\alpha_n\}\boldsymbol{m} + \Im\{\alpha_n\}\boldsymbol{l} + \boldsymbol{n}_0 \ , \tag{3.12}$$

$$\boldsymbol{u}_1(\boldsymbol{z}) =_1 \boldsymbol{m} - \Re\{\alpha_n\}\boldsymbol{n}_0 \ , \quad \boldsymbol{u}_2(\boldsymbol{z}) =_1 \boldsymbol{l} - \Im\{\alpha_n\}\boldsymbol{n}_0 \ . \tag{3.13}$$

A spin $\boldsymbol{S}_i =_1 \Re\{\alpha_i\}\boldsymbol{m} + \Im\{\alpha_i\}\boldsymbol{l} + \boldsymbol{n}_0$ is transported to $\boldsymbol{S}_f =_1 \Re\{\boldsymbol{G}\cdot\boldsymbol{z} + \mathrm{e}^{\mathrm{i}2\pi\nu_0}\alpha_i\}\boldsymbol{m} + \Im\{\boldsymbol{G}\cdot\boldsymbol{z} + \mathrm{e}^{\mathrm{i}2\pi\nu_0}\alpha_i\}\boldsymbol{l} + \boldsymbol{n}_0$ after one turn, so that

$$\boldsymbol{u}_1(\mathsf{M}\boldsymbol{z}) =_1 \boldsymbol{m} - \Re\{\boldsymbol{G}\cdot\boldsymbol{z} + \mathrm{e}^{\mathrm{i}2\pi\nu_0}\alpha_n\}\boldsymbol{n}_0 \ , \tag{3.14}$$

$$\boldsymbol{u}_2(\mathsf{M}\boldsymbol{z}) =_1 \boldsymbol{l} - \Im\{\boldsymbol{G}\cdot\boldsymbol{z} + \mathrm{e}^{\mathrm{i}2\pi\nu_0}\alpha_n\}\boldsymbol{n}_0 \ . \tag{3.15}$$

At the initial phase space point this leads to the projections $\boldsymbol{S}_i\cdot(\boldsymbol{u}_1(\boldsymbol{z}_i) + \mathrm{i}\boldsymbol{u}_2(\boldsymbol{z}_i)) =_1 \alpha_i - \alpha_n$, and after one turn to $\boldsymbol{S}_f\cdot(\boldsymbol{u}_1(\boldsymbol{z}_f) + \mathrm{i}\boldsymbol{u}_2(\boldsymbol{z}_f)) =_1 \mathrm{e}^{\mathrm{i}2\pi\nu_0}(\alpha_i - \alpha_n)$. The amplitude dependent spin tune ν in linearized spin-orbit motion is therefore simply given by ν_0.

The eigenvector condition of (3.10),

$$\mathsf{M}_{77}\begin{pmatrix}\boldsymbol{v}_k^\pm \\ B_k^\pm\end{pmatrix} = \mathrm{e}^{\pm i2\pi Q_k}\begin{pmatrix}\boldsymbol{v}_k^\pm \\ B_k^\pm\end{pmatrix} \ , \tag{3.16}$$

leads to $\boldsymbol{G}\cdot\boldsymbol{v}_k^\pm + \mathrm{e}^{\mathrm{i}2\pi\nu_0}B_k^\pm = \mathrm{e}^{\pm i2\pi Q_k}B_k^\pm$. Therefore,

$$B_k^\pm = \boldsymbol{G}\cdot\boldsymbol{v}_k^\pm/(\mathrm{e}^{\pm i2\pi Q_k} - \mathrm{e}^{\mathrm{i}2\pi\nu_0}) \tag{3.17}$$

so that α_n diverges at first-order intrinsic resonances where $\nu = j_0 \pm Q_k$, with $\nu = \nu_0$ for linearized spin-orbit motion. This means that α_n becomes large so that the assumption of linear spin-orbit motion is no longer valid. In the normal form space belonging to the diagonal matrix Λ, the coordinates are given by the actions J_j and the angle variables Φ_j with

$$A\boldsymbol{z} = (\sqrt{J_1}\mathrm{e}^{\mathrm{i}\Phi_1}, \sqrt{J_1}\mathrm{e}^{-\mathrm{i}\Phi_1}, \dots, \sqrt{J_3}\mathrm{e}^{\mathrm{i}\Phi_3}, \sqrt{J_3}\mathrm{e}^{-\mathrm{i}\Phi_3})^T \ . \tag{3.18}$$

The average over all angle variables on an invariant torus is described by $\langle\dots\rangle_{\boldsymbol{\Phi}}$. It leads to the average opening angle of

$$\begin{aligned}\langle\vartheta(\boldsymbol{n}, \boldsymbol{n}_0)\rangle_{\boldsymbol{\Phi}} &\approx \mathrm{atan}(\sqrt{\langle|\alpha_n|^2\rangle_{\boldsymbol{\Phi}}}) \\ &= \mathrm{atan}\left(\sqrt{\sum_{k=1}^{3}(|B_k^+|^2 + |B_k^-|^2)J_k}\right) \ ,\end{aligned} \tag{3.19}$$

where the $B_k^\pm$ are the seventh components of the eigenvectors in (3.10) and (3.11) was used. The maximum time-average polarization is approximately

$$P_{lim} = \langle\cos(\vartheta(\boldsymbol{n}, \boldsymbol{n}_0))\rangle_{\boldsymbol{\Phi}} \approx [1 + \sum_{k=1}^{3}(|B_k^+|^2 + |B_k^-|^2)J_k]^{-\frac{1}{2}} \ . \tag{3.20}$$

These approximations for $\boldsymbol{n}(\boldsymbol{z})$, $\langle\vartheta\rangle$, and P_{lim} can only be accurate if $|\alpha_n|$ is small.

In a ring with midplane symmetry, the one turn spin-orbit matrix $\mathsf{M}_{7\times7}$ has a block structure with 2×2 matrix blocks and 2-dimensional zero and non-zero vectors,

$$\mathsf{M}_{7\times7} = \begin{pmatrix} * & \mathsf{0} & * & \mathbf{0} \\ \mathsf{0} & * & \mathsf{0} & \mathbf{0} \\ * & \mathsf{0} & * & \mathbf{0} \\ \mathbf{0}^T & \boldsymbol{*}^T & \mathbf{0}^T & * \end{pmatrix} . \tag{3.21}$$

The 6×6-dimensional phase space transport matrix has a checker board structure, because there is no coupling between vertical motion and the other two degrees of freedom in a midplane-symmetric ring. Furthermore, $\boldsymbol{G}$ only has contributions from vertical motion because a spin with $\boldsymbol{S}_i = \boldsymbol{n}_0$ ($\alpha_i = 0$) is not deflected out of the vertical unless the particle flies through horizontal magnetic field components, which only happens for particles with a vertical oscillation amplitude. The opening angle $\langle\vartheta\rangle$ and P_{lim} then only depend on the vertical action J_y.

3.1.2 Spin-Orbit-Coupling Integrals

Instead of computing the one turn matrix $M_{7\times7}$ as the product of spin-orbit transport matrices of individual elements or as the concatenation of their spin transport quaternions, one can also solve the linearized equation of motion for α directly. To obtain simplified formulas, the coordinate system $[\boldsymbol{m}_0, \boldsymbol{l}_0, \boldsymbol{n}_0]$, which was introduced in Sect. 2.2.2, is now used. The vectors $\boldsymbol{m}_0$ and $\boldsymbol{l}_0$ are perpendicular to $\boldsymbol{n}_0$, precess according to the T-BMT equation on the closed orbit and are related to the $\boldsymbol{m}$ and $\boldsymbol{l}$ by a rotation around $\boldsymbol{n}_0$ according to the relation $\boldsymbol{m} + \mathrm{i}\boldsymbol{l} = \mathrm{e}^{\mathrm{i}\nu_0(\theta-\theta_0)}(\boldsymbol{m}_0 + \mathrm{i}\boldsymbol{l}_0)$ as in (2.50). Here it is assumed that the two coordinate systems coincide at azimuth 0. Whereas the coordinate system $[\boldsymbol{m}, \boldsymbol{l}, \boldsymbol{n}_0]$ is 2π-periodic in θ, $[\boldsymbol{m}_0, \boldsymbol{l}_0, \boldsymbol{n}_0]$ is not.

The precession vector for spins can be separated into a part for particles on the closed orbit and a part due to oscillations around closed orbit, $\boldsymbol{\Omega}(\boldsymbol{z}, \theta) = \boldsymbol{\Omega}_0(\theta) + \boldsymbol{\omega}(\boldsymbol{z}, \theta)$. The spin direction and the phase space dependent part $\boldsymbol{\omega}$ of the precession vector will be written in complex notation in the coordinate system $[\boldsymbol{m}_0, \boldsymbol{l}_0, \boldsymbol{n}_0]$ as

$$\boldsymbol{S} = \Re\{\alpha_0\}\boldsymbol{m}_0 + \Im\{\alpha_0\}\boldsymbol{l}_0 + \boldsymbol{n}_0\sqrt{1 + |\alpha_0|^2} , \tag{3.22}$$

$$\boldsymbol{\omega} = \Re\{\omega_0\}\boldsymbol{m}_0 + \Im\{\omega_0\}\boldsymbol{l}_0 + \boldsymbol{n}_0\omega_3 . \tag{3.23}$$

The first equation differs from the equations (2.120) and (3.1) because α_0 refers to $\boldsymbol{m}_0$ and $\boldsymbol{l}_0$ whereas α referred to $\boldsymbol{m}$ and $\boldsymbol{l}$. Inserting this into the T-BMT equation (2.24), one obtains

$$\begin{aligned} \boldsymbol{\Omega} \times \boldsymbol{S} &= \frac{\mathrm{d}}{\mathrm{d}\theta}\boldsymbol{S} \\ &= \Re\{\frac{\mathrm{d}}{\mathrm{d}\theta}\alpha_0\}\boldsymbol{m}_0 + \Im\{\frac{\mathrm{d}}{\mathrm{d}\theta}\alpha_0\}\boldsymbol{l}_0 + \boldsymbol{n}_0\frac{\mathrm{d}}{\mathrm{d}\theta}\sqrt{1 - |\alpha_0|^2} + \boldsymbol{\Omega}_0 \times \boldsymbol{S} . \end{aligned} \tag{3.24}$$

This leads to a differential equation for α_0,

$$\begin{aligned}\frac{\mathrm{d}}{\mathrm{d}\theta}\alpha_0 &= (\boldsymbol{\omega}\times\boldsymbol{S})\cdot(\boldsymbol{m}_0+\mathrm{i}\boldsymbol{l}_0) = \boldsymbol{\omega}\cdot[\boldsymbol{S}\times(\boldsymbol{m}_0+\mathrm{i}\boldsymbol{l}_0)] \\ &= \boldsymbol{\omega}\cdot[i\alpha_0\boldsymbol{n}_0+\sqrt{1-|\alpha_0|^2}\;(\boldsymbol{l}_0-\mathrm{i}\boldsymbol{m}_0)] \\ &= -\mathrm{i}\omega_0\sqrt{1-|\alpha_0|^2}+\mathrm{i}\alpha_0\omega_3\ .\end{aligned} \tag{3.25}$$

Linearization with respect to $\boldsymbol{z}$ and α_0 leads to $\frac{\mathrm{d}}{\mathrm{d}\theta}\alpha_0 = -\mathrm{i}\omega_0^1$, where the superscript signals the first-order expansion of $\omega(\boldsymbol{z},\theta)$ with respect to $\boldsymbol{z}$. Because $\alpha=\alpha_0\mathrm{e}^{\mathrm{i}\nu_0(\theta-\theta_0)}$, and because $\alpha_f=\boldsymbol{G}\cdot\boldsymbol{z}_i$ after one turn if $\alpha_i=0$ at azimuth θ_0, one now obtains

$$\boldsymbol{G}\cdot\boldsymbol{z}_i = -\mathrm{i}\mathrm{e}^{\mathrm{i}2\pi\nu_0}\int_{\theta_0}^{\theta_0+2\pi}\omega_0^1(\boldsymbol{z}(\theta),\theta)\mathrm{d}\theta\ , \tag{3.26}$$

where the trajectory $\boldsymbol{z}(\theta)$ has started with $\boldsymbol{z}_i$ at azimuth θ_0.

In flat rings it is advantageous to use the co-moving coordinate system $[\boldsymbol{e}_x,\boldsymbol{e}_l,\boldsymbol{e}_y]$ introduced in Sect. 2.1.2 with $\boldsymbol{e}_y$ vertical and with $\boldsymbol{e}_l$ parallel to the closed orbit. In such a ring, $\boldsymbol{n}_0$ and $\boldsymbol{\Omega}_0=\Omega_0\boldsymbol{e}_y$ are vertical, and for a particle on the closed orbit, a spin rotates by the angle $\Psi=\int_{\theta_0}^{\theta}\Omega_0\mathrm{d}\theta$ between azimuth θ_0 and θ. Therefore, $\boldsymbol{m}_0+\mathrm{i}\boldsymbol{l}_0=\mathrm{e}^{-\mathrm{i}\Psi}(\boldsymbol{e}_x+\mathrm{i}\boldsymbol{e}_y)$ and $\omega_0^1=\mathrm{e}^{-\mathrm{i}\Psi}(\omega_x^1+\mathrm{i}\omega_l^1)$.

In a midplane-symmetric ring, there are no skew elements or solenoids and horizontal components of $\boldsymbol{\omega}$ only occur when a particle oscillates vertically around the closed orbit. When linearizing in $\boldsymbol{z}$, these components are produced by the quadrupole focusing strength k ($k>0$ for a horizontally focusing effect). The spin rotations in these fields are $(G\gamma+1)$ larger than the orbit deflections created by the quadrupoles, and one obtains $\omega_0^1\mathrm{d}\theta=(G\gamma+1)\mathrm{e}^{-\mathrm{i}\Psi}yk\mathrm{d}l$, where for the ring circumference L, $l=L\frac{\theta}{2\pi}$ is the path length of the design trajectory. In terms of the vertical betatron function β_y and the betatron phase Φ_y, one has $y=\sqrt{2J_y\beta_y}\cos(\Phi_y+\Phi_{yi})$. This has lead to the definition of the one turn spin-orbit-coupling integrals [9, 10, 11, 8]

$$I_y^{\pm} = -\mathrm{i}(G\gamma+1)\frac{1}{\sqrt{2}}\oint_{l_0}^{l_0+L}\mathrm{e}^{\mathrm{i}(-\Psi\pm\Phi_y)}\sqrt{\beta_y}k\mathrm{d}l\ , \tag{3.27}$$

where $\Psi(\theta_0)=0$ and the initial betatron phase is $\Phi_y(\theta_0)=0$. When the initial phase space coordinate $\boldsymbol{z}_i$ has the vertical phase Φ_{yi} and the Courant-Snyder invariant [12] $2J_y$, (3.26) is equivalent to the relation

$$\boldsymbol{G}\cdot\boldsymbol{z}_i = \mathrm{e}^{\mathrm{i}2\pi\nu_0}(I_y^+\mathrm{e}^{\mathrm{i}\Phi_{yi}}+I_y^-\mathrm{e}^{-\mathrm{i}\Phi_{yi}})\sqrt{J_y}\ . \tag{3.28}$$

With the eigenvectors $\boldsymbol{v}_2^{\pm}$ of (3.10) associated with vertical motion we have $\boldsymbol{z}_i=\sqrt{J_y}(\boldsymbol{v}_2^+\mathrm{e}^{\mathrm{i}\Phi_{yi}}+\boldsymbol{v}_2^-\mathrm{e}^{-\mathrm{i}\Phi_{yi}})$ and obtain $\boldsymbol{G}\cdot\boldsymbol{v}_2^{\pm}=\mathrm{e}^{\mathrm{i}2\pi\nu_0}I_y^{\pm}$. Spin-orbit-coupling integrals are therefore useful for analyzing linear spin-orbit motion in the case of a midplane-symmetric ring. They will be used in Sect. 3.3.2 for the optimization of Siberian Snake arrangements.

In a general setting, where $\boldsymbol{\omega}^{\,1}(\boldsymbol{z}(\theta),\theta)$ not only has radial components, generalized spin-orbit-coupling integrals at θ_0 are defined as $I_k^\pm = \mathrm{e}^{-\mathrm{i}2\pi\nu_0}\boldsymbol{G}\cdot\boldsymbol{v}_k^\pm$. This brings them into close relation with the components $B_k^\pm$ of the $\boldsymbol{n}$-axis, which by (3.11) and (3.18) can be written as

$$\alpha_n = \sum_{k=1}^{3}\sqrt{J_k}(B_k^+\mathrm{e}^{\mathrm{i}\Phi_k} + B_k^-\mathrm{e}^{-\mathrm{i}\Phi_k})\ , \quad B_k^\pm = \frac{I_k^\pm}{\mathrm{e}^{\mathrm{i}2\pi(\pm Q_k-\nu_0)}-1}\ . \tag{3.29}$$

So far eigenvectors of the one turn matrix have only been used at the initial azimuth θ_0. To get the trajectory $\boldsymbol{z}(\theta)$ for a particle which started with the initial phase variables Φ_{ki} at azimuth 0, one needs the eigenvectors $\boldsymbol{v}_k^\pm(\theta)$ of the one turn matrix at θ,

$$\boldsymbol{z}(\theta) = \sum_{k=1}^{3}\sqrt{J_k}[\boldsymbol{v}_k^+(\theta)\mathrm{e}^{i[Q_k(\theta-\theta_0)+\Phi_{ki}]} + \boldsymbol{v}_k^-(\theta)\mathrm{e}^{-\mathrm{i}[Q_k(\theta-\theta_0)+\Phi_{ki}]}]\ , \tag{3.30}$$

By inserting this into (3.26) and taking advantage of the linearity of ω_0^1 in $\boldsymbol{z}$, one obtains

$$\begin{aligned} I_k^\pm &= \mathrm{e}^{-\mathrm{i}2\pi\nu_0}\boldsymbol{G}\cdot\boldsymbol{v}_k^\pm \\ &= -\mathrm{i}\int_{\theta_0}^{\theta_0+2\pi}\boldsymbol{\omega}^1(\boldsymbol{v}_k^\pm(\theta),\theta)\cdot(\boldsymbol{m}+\mathrm{i}\boldsymbol{l})\mathrm{e}^{\mathrm{i}(\pm Q_k-\nu_0)(\theta-\theta_0)}\mathrm{d}\theta\ . \end{aligned} \tag{3.31}$$

It has been suggested ad hoc in [13, 14] that $|I_2^+|^2 + |I_2^-|^2$ be used as a quality factor for the optics of polarized proton synchrotrons. Due to the central importance of the invariant spin field for the acceleration process and for storage of polarized beams, it now becomes clear that the quality factor should in general rather be $\sum_{k=1}^3[\frac{|I_k^+|^2}{\sin^2(\pi(Q_k-\nu_0))} + \frac{|I_k^\pm|^2}{\sin^2(\pi(-Q_k-\nu_0))}]$. Close to intrinsic resonances where $\pm Q_k - \nu_0$ is integer for some k, the opening angle of the $\boldsymbol{n}$-axis diverges in the approximation of linearized spin-orbit motion.

3.1.3 Limitations of Linearized Spin-Orbit Motion

The approximation of linearized spin-orbit motion is no longer justified when P_{lim} is not close to 1, which happens close to intrinsic resonances in Fig. 3.1. Linearized spin-orbit motion can be applied even when the resonances are not well separated, but when computing the average polarization of a polarized beam, $|\alpha_n|$ must be small enough to justify the underlying approximation. If the the condition $|\alpha_n| \leq 0.5$ is accepted, the average polarization computed with linearized spin-orbit motion is only trustworthy as long as it is above about 87%.

Figure 3.1 shows for DESY III (top) and for PETRA (bottom), that in most of their energy range spin dynamics can be described well by linearized spin-orbit motion.

For the HERA-p optics of the year 2004 with non-flat regions as they are today, Fig. 3.2 (top) shows that linearized spin-orbit motion leads to a P_{lim}

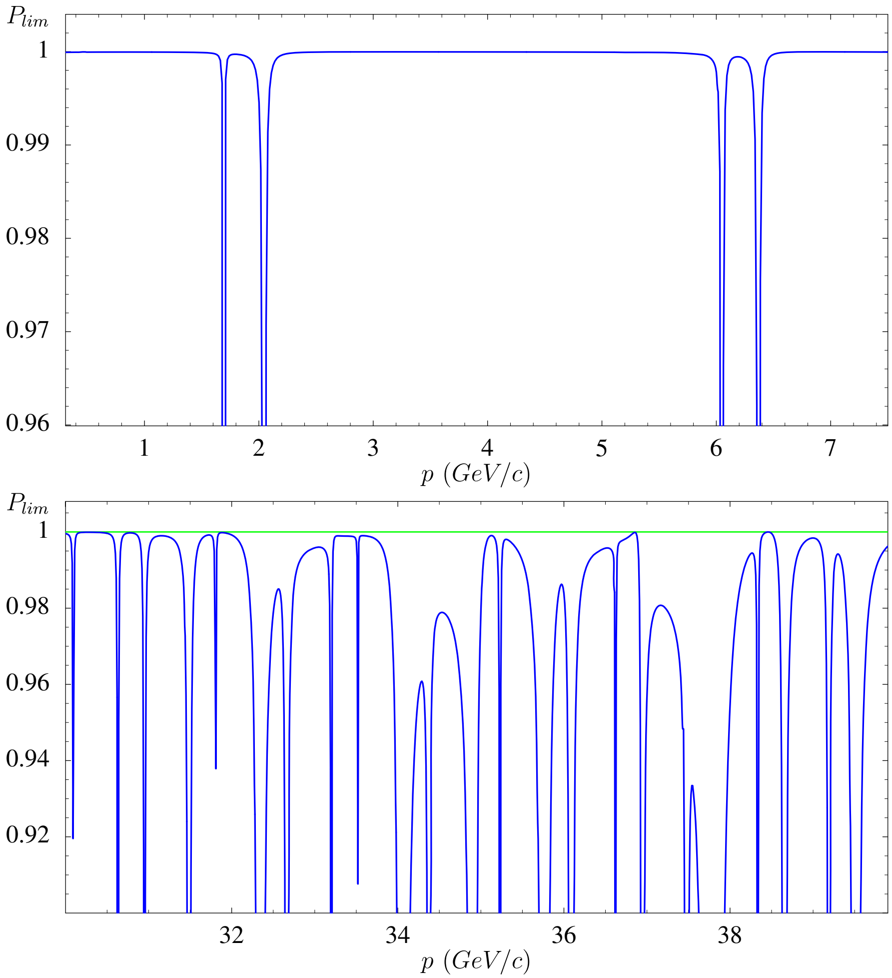

Fig. 3.1. P_{lim} versus momentum as approximated by linearized spin-orbit motion for DESY III (*top*) and for the high-energy end of PETRA (*bottom*) for vertical motion with normalized amplitude of 25π mm mrad. The dips have been cut in order to magnify the interesting region where $|\alpha_n|$ is small.

that deviates strongly from 1 over a wide range of energies, so that linearization in α cannot be applied. When the flattening snakes are introduced as described in Sect. 2.2.4, P_{lim} increases somewhat and a regular resonance structure can clearly be seen (bottom). Nevertheless, linearization cannot be accurate over many energy ranges.

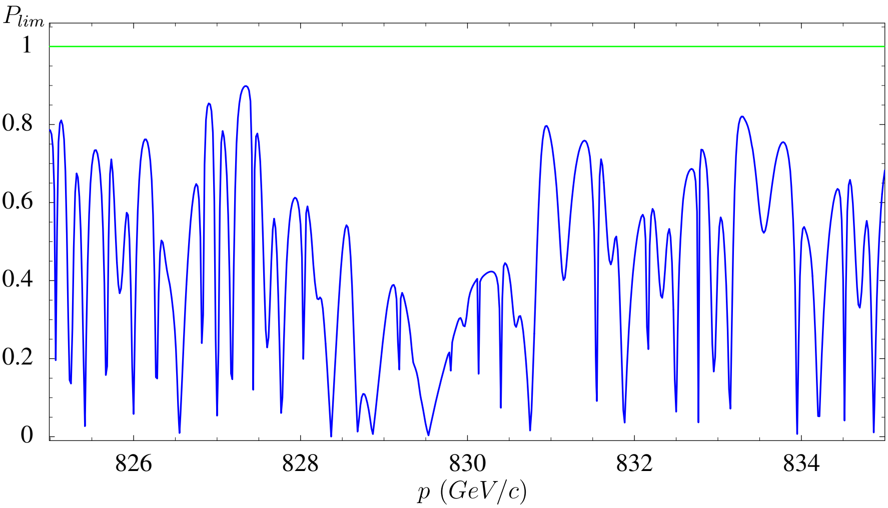

Fig. 3.2. P_{lim} versus momentum as approximated by linearized spin-orbit motion for high energies in HERA-p with non-flat regions as they are today (*top*) and after the installation of flattening snakes (*bottom*) for vertical motion with normalized amplitude of 25π mm mrad.

The decrease of P_{lim} at intrinsic resonances shows that Siberian Snakes have to be used to make the closed-orbit spin tune independent of energy, so that no first-order intrinsic resonances have to be crossed.

3.2 First-Order Resonance Spectrum

3.2.1 The Resonance Spectrum

While P_{lim} can only be computed for overlapping resonances by the approximation of linearized spin-orbit motion, this approach is only accurate when P_{lim} is close to 1. On the other hand, the SRM of Sect. 2.2.10 gives the exact value for P_{lim} for one chosen resonance, but it is only valid for well separated resonances. Similarly the advance models with point-like Siberian Snakes for which exact values of P_{lim} were found in [15, 16] can only be applied when resonances in the ring are well separated. The spin dynamics close to intrinsic resonances can be analyzed by Fourier expanding the field components $\boldsymbol{\omega}(\boldsymbol{z},\theta)$ that perturb the spin of a particle that oscillates around the closed orbit. For spins parallel to the rotation vector on the closed orbit $\boldsymbol{n}_0(\theta)$, only the components of $\boldsymbol{\omega}(\boldsymbol{z},\theta)$ that are perpendicular to $\boldsymbol{n}_0$ perturb the polarization.

As described in Sect. 2.2.10, spin motion is strongly disturbed when a Fourier component of $\boldsymbol{\omega}(\boldsymbol{z}(\theta),\theta)$ rotates with the same frequency around $\boldsymbol{n}_0$ as the spins so that there is a build up of the tilt away from $\boldsymbol{n}_0$. In the 2π-periodic coordinate system $[\boldsymbol{m},\boldsymbol{l},\boldsymbol{n}_0]$, the Fourier component $\tilde{\epsilon}_k$ of $\omega=\boldsymbol{\omega}\cdot(\boldsymbol{m}+\mathrm{i}\boldsymbol{l})$ for the frequency κ is

$$\tilde{\epsilon}_\kappa=\lim_{N\to\infty}\frac{1}{2\pi N}\int_0^{2\pi N}\omega(\boldsymbol{z}(\theta),\theta)\mathrm{e}^{-\mathrm{i}\kappa\theta}\mathrm{d}\theta\ . \tag{3.32}$$

A warning is needed. The picture of perturbing effects suggests that the beam is slowly depolarized after it has been injected with 100% polarization. In fact the spins get deflected from their initial polarization direction $\boldsymbol{n}_0$ during one turn, only because the $\boldsymbol{n}$-axis $\boldsymbol{n}(\boldsymbol{z})$ is tilted away from the closed-orbit spin direction $\boldsymbol{n}_0$. If, as already explained in Sect. 2.2.14 and in Fig. 2.14, an ensemble of particles had started with its spins parallel to the invariant spin field, no net deflection away from $\boldsymbol{n}$ due to the perturbing fields would have occurred and no reduction of polarization would be noticed after one turn. However, because $\boldsymbol{n}(\boldsymbol{z})$ is tilted away from $\boldsymbol{n}_0$, the average polarization $P_{lim}=|\langle\boldsymbol{n}(\boldsymbol{z})\rangle|$ for such an initial distribution is smaller than 1 to start with.

For each energy of the particle, there is in general a different Fourier spectrum for ω. Because at each energy the most important frequencies κ are those that are close to ν_0, it is customary to compute the resonance strength $\epsilon_{\nu_0(E)}=|\tilde{\epsilon}_{\nu_0(E)}|$ for all energies of the acceleration cycle. Obviously, $\epsilon_{\nu_0(E)}$ is zero, except when a Fourier frequency of $\omega(\boldsymbol{z}(\theta),\theta)$ at energy E is equal to

$\nu_0(E)$. The resulting line spectrum over E is called the depolarizing resonance spectrum of an accelerator.

These resonance strengths ϵ_{ν_0} for the three proton synchrotrons at DESY are shown in the top Figs. 3.3, 3.4, and 3.5. They were all computed for an oscillation amplitude of $\boldsymbol{z}(\theta)$ corresponding to the amplitude of a 2.5σ vertical emittance of 25π mm mrad. Additionally the average opening angles $\langle\vartheta(\boldsymbol{,n}_0)\rangle_{\boldsymbol{\Phi}}$ from (3.20) are shown.

It is possible to recover the first-order isolated resonance strength from the one turn spin-orbit transport matrix [17]. For a spin that was initially parallel to $\boldsymbol{n}_0$, (3.25) yields

$$\alpha_0(\theta) \approx -\mathrm{i}\int_0^\theta \omega_0 \mathrm{d}\theta\ ,\ \text{ with } \omega_0 = \boldsymbol{\omega}\cdot(\boldsymbol{m}_0+\mathrm{i}\boldsymbol{l}_0) = \mathrm{e}^{-\mathrm{i}\nu_0\theta}\boldsymbol{\omega}\cdot(\boldsymbol{m}+\mathrm{i}\boldsymbol{l})\ . \quad (3.33)$$

Comparing with (3.32), one can express the resonance strength as $\tilde{\epsilon}_{\nu_0} = i\lim_{N\to\infty}\frac{1}{2\pi N}\alpha_0(2\pi N)$. The resonance strength can therefore be computed from $\frac{1}{N}\mathsf{M}_{77}^N$ for large N. The computation becomes very efficient if one makes iterative use of the relation $\mathsf{M}_{77}^{2N} = (M_{77}^N)^2$.

The coordinate vectors $\boldsymbol{m}_0(2\pi)$ and $\boldsymbol{l}_0(2\pi)$ to which $\alpha_0(2\pi)$ refers have rotated by $2\pi\nu_0$, whereas the final spin coordinate α_f computed by M_{77} refers to the coordinate vectors $\boldsymbol{m}(0) = \boldsymbol{m}_0(0)$ and $\boldsymbol{l}(0) = \boldsymbol{l}_0(0)$. Therefore, $\alpha_0(2\pi N) = \alpha_f \exp(-\mathrm{i}2\pi N\nu_0)$. The resonance strength ϵ_{ν_0} can be most easily computed when the powers of the one turn matrix are evaluated in terms of its diagonal form Λ with the elements $\mathrm{e}^{\pm i2\pi Q_k}$. Using the simplifying notation $\breve{Q}_{2k-1} = Q_k$ and $\breve{Q}_{2k} = -Q_k$, one has

$$\begin{aligned}
\tilde{\epsilon}_{\nu_0} &= i\lim_{N\to\infty}\frac{1}{2\pi N}\alpha_0(2\pi N) \qquad (3.34)\\
&= i\lim_{N\to\infty}\frac{1}{2\pi N}(0,\mathrm{e}^{-\mathrm{i}N2\pi\nu_0})\begin{pmatrix}\mathsf{M} & 0\\ \boldsymbol{G}^T & \mathrm{e}^{\mathrm{i}2\pi\nu_0}\end{pmatrix}^N\begin{pmatrix}\boldsymbol{z}\\ 0\end{pmatrix}\\
&= i\lim_{N\to\infty}\mathrm{e}^{-\mathrm{i}N2\pi\nu_0}\frac{1}{2\pi N}\sum_{j=0}^{N-1}[\mathrm{e}^{\mathrm{i}(N-j-1)2\pi\nu_0}\boldsymbol{G}^T\mathsf{A}^{-1}\Lambda^j]\mathsf{A}\boldsymbol{z}\\
&= i\mathrm{e}^{-\mathrm{i}2\pi\nu_0}\sum_{k=1}^{6}G_l A_{lk}^{-1}A_{km}z_m\lim_{N\to\infty}\frac{1}{2\pi N}\sum_{j=0}^{N-1}\mathrm{e}^{\mathrm{i}2\pi j(\breve{Q}_k-\nu_0)}
\end{aligned}$$

where one has to sum over equal indexes l and m. This formula shows that the resonance strength is always zero, except when $\nu_0 = \kappa = j_0 \pm Q_k$. At such a closed-orbit spin tune, the resonance strength is given in terms of

$$\begin{aligned}
2\pi\epsilon_{\nu_0} &= |\boldsymbol{G}^T\mathsf{A}^{-1}\mathrm{diag}(0...1...0)\mathsf{A}\boldsymbol{z}| = |\boldsymbol{G}^T\mathsf{A}^{-1}(0...\sqrt{J_k}\mathrm{e}^{\pm i\Phi_k}...0)^T|\\
&= |\boldsymbol{G}\cdot\boldsymbol{v}_k^{\pm}|\sqrt{J_k} = |I_k^{\pm}|\sqrt{J_k} \qquad (3.35)
\end{aligned}$$

whence $\tilde{\epsilon}_{\nu_0} = \epsilon_{\nu_0}\mathrm{e}^{\mathrm{i}(\pm\Phi_k-2\pi\nu_0+\varphi)}$ with some constant phase φ. The 1 in the diagonal matrix is in position $2k-1$ for $\nu_0 = j_0 + Q_k$ and at position $2k$ for $\nu_0 = j_0 - Q_k$. Here $\mathsf{A}^{-1}(0...\sqrt{J_k}\mathrm{e}^{\pm i\Phi_k}...0)^T$ is the initial value for a phase space trajectory that has only Fourier components with frequencies $\pm Q_k$ plus integers and the eigenvector $\boldsymbol{v}_k^{\pm}$ of M has been used. The infinite Fourier integral in (3.32) has been reduced to the scalar product between the bottom row vector of M_{77} and an eigenvector of M. This happens to equal the absolute value of the spin-orbit-coupling integral in (3.29). This very simple formula is used in the program SPRINT [5, 6].

After the first-order resonance strength for a frequency κ has been computed, one can investigate the influence of just the corresponding Fourier contribution of ω to the spin motion. The resulting single resonance model (SRM) has been described in Sect. 2.2.10.

3.2.2 Limitations of the SRM

Approximations to the spin motion by the SRM are only accurate if the resonances are well separated so that one Fourier harmonic of ω dominates the dynamics. When a ring is not flat and has no exact super-periodicity, the first-order resonances appear when the spin tune comes close to $j_0 \pm Q_k$, where the tunes Q_k of all three degrees of motion can appear. HERA-p is not flat, but after the installation of flattening snakes, the first-order spin motion is very similar to that of a flat ring, where only resonances due to vertical motion appear. With a vertical orbit tune of approximately $\frac{1}{3}$ in HERA-p, the range of ν_0 between resonances is $\frac{1}{3}$ or $\frac{2}{3}$. The resonance strength is related to the width of the resonance as shown in Sect. 2.2.10, and to justify a single resonance approach, the resonance strength of two neighboring resonances should therefore be significantly less than $\frac{1}{3}$.

In linearized spin-orbit motion, the opening angle of the invariant spin field is given approximately by (3.20). In Fig. 3.3, the peaks in the resonance strength (top) are located exactly at the peaks of the opening angles computed with the linearized approach (bottom). Furthermore, the widths of the peaks in opening angle are correlated with the resonance strengths. The resonances are well separated and in DESY III, first-order theories for analyzing polarization dynamics along with classical means of controlling depolarizing effects [18] are therefore applicable.

The corresponding figure for PETRA shows again that large opening angles of linearized spin-orbit motion are correlated with large resonance strength. However, the first-order resonances are getting so close at the high-energy end of 39 GeV that several pairs of resonances are overlapping. It has been observed experimentally [19] that Siberian Snakes can stabilize spin motion in the presence of overlapping resonances. The resonance strengths are still far away from PETRA's fractional vertical tune of about 0.2, and therefore also in this energy regime, classical means of controlling depolarizing first-order resonances can be applied.

In HERA-p the situation changes even with flattening snakes as shown in Fig. 3.5. The first resonance that is stronger than $\frac{1}{3}$ for a normalized vertical amplitude of 25π mm mrad appears at about 150 GeV/c and resonances start

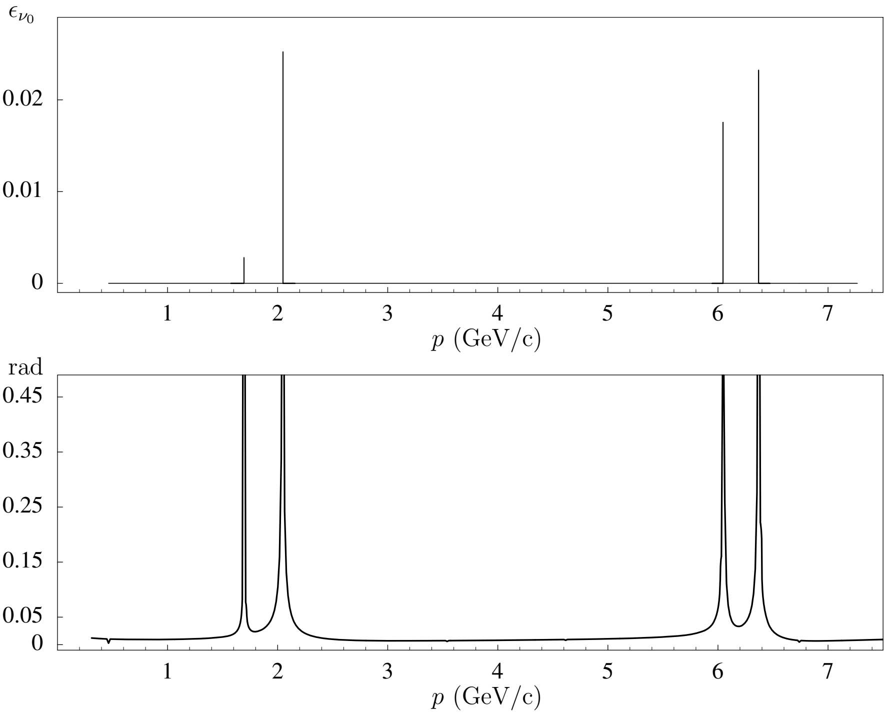

Fig. 3.3. Resonance strengths ϵ_{ν_0} (*top*) and opening angles $\langle\vartheta(\boldsymbol{n}, \boldsymbol{n}_0)\rangle$ of linearized spin-orbit motion (*bottom*) for particles with a normalized vertical amplitude of 25π mm mrad in DESY III. The number of resonances is very low due to a superperiodicity 8.

to overlap. Because there are over 3000 first-order resonances on the ramp of HERA-p from 39 to 920 GeV/c, this effect can only be seen clearly when looking at a smaller energy range as in Fig. 3.5. The resonances are strongly overlapping and the average opening angles of the invariant spin field are so big that linearized spin-orbit motion and the SRM for first-order resonances are not trustworthy anymore. Therefore, methods that include higher-order spin effects have to be applied.

The average polarization computed with either of these two models, linearized spin-orbit motion or the single resonance model with first order resonances, is in any case only accurate if there are only effects that are dominated by first-order resonances. Effects that are not related to first-order resonances cannot be simulated by a first-order resonance strength or by linearized spin-orbit motion and therefore the first-order theories cannot be used to decide whether non-first-order effects are small or not. In general, therefore, a higher-order extension is needed to decide about the validity of the first-order theories.

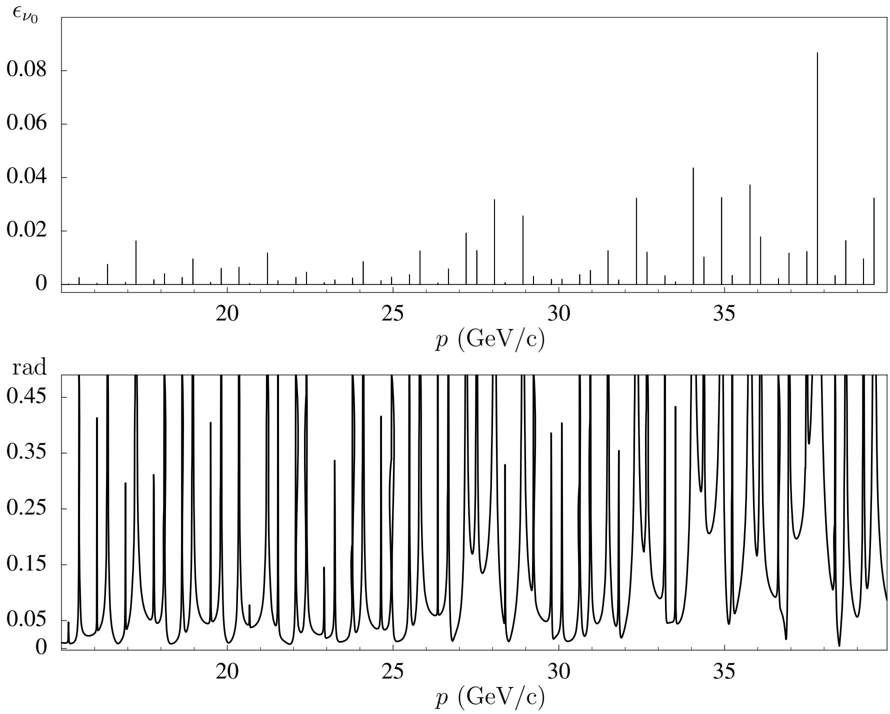

Fig. 3.4. Resonance strengths ϵ_{ν_0} (*top*) and opening angles $\langle\vartheta(\boldsymbol{n},\boldsymbol{n}_0)\rangle$ of linearized spin-orbit motion (*bottom*) for particles with normalized vertical amplitude of 25π mm mrad in PETRA.

3.2.3 First-Order Resonances in HERA-p

The general approach described in Sect. 3.2.1 can be applied to flat as well as to non-flat rings, but usually the single resonance model is used for midplane-symmetric rings, which have a vertical $\boldsymbol{n}_0$. There the resonance strength $\epsilon_{\nu_0} = \frac{\sqrt{J_k}}{2\pi}|\boldsymbol{G}\cdot\boldsymbol{v}_k^{\pm}|$ in (3.35) is only non-zero for the vertical degree of freedom due to the block structure described in (3.21). This reflects the fact that particles that stay in the midplane do not traverse horizontal fields and their spins are not deflected away from the vertical $\boldsymbol{n}_0$.

HERA-p is not midplane-symmetric. Its design trajectory does not even lie in a plane, due to the non-flat regions required to bend the proton beam to the level of the electron beam. This was already discussed in Sect. 2.2.4, together with flattening snakes that are inserted at the center of each non-flat region to make the spin motion effectively that of a flat ring by forcing $\boldsymbol{n}_0$ to be vertical outside the non-flat regions. Nevertheless, $\boldsymbol{n}_0$ is non-vertical inside these regions and the spin-orbit-coupling integrals for horizontal and longitudinal motion are not identically zero so that more resonances occur

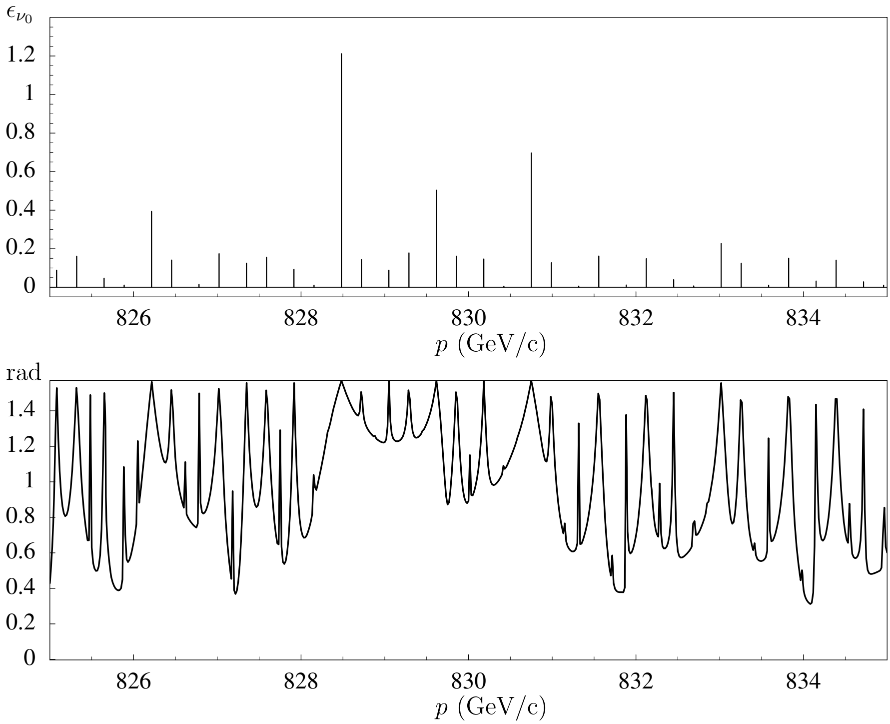

Fig. 3.5. Resonance strengths ϵ_{ν_0} (*top*) and opening angles $\langle\vartheta(\boldsymbol{n}, \boldsymbol{n}_0)\rangle$ of linearized spin-orbit motion (*bottom*) for particles with normalized vertical amplitude of 25π mm mrad in HERA-p.

in HERA-p than in other rings. Because the vertical motion leads to the dominant perturbations of spin dynamics, the resonances of this degree of freedom will be considered first.

A flat circular accelerator with a super-periodicity P_s has a betatron phase advance of $\frac{2\pi}{P_s}\hat{Q}_k$ and a spin phase advance of $\frac{2\pi}{P_s}G\gamma$ for each superperiod. Here $\hat{Q}_k$ is an orbital tune including the integer part. A resonance for linearized spin-orbit motion occurs whenever the non-integer part $\frac{1}{P_s}\hat{Q}_k - [\frac{1}{P_s}\hat{Q}_k]$ has a resonance condition with $\frac{1}{P_s}G\gamma$: $\frac{1}{P_s}G\gamma = j_0 \pm (\frac{1}{P_s}\hat{Q}_k - [\frac{1}{P_s}\hat{Q}_k])$, or $G\gamma = P_s n \pm \hat{Q}_k$ for some integers j_0 and n. The number of resonances is therefore reduced by a factor P_s.

HERA-p has no exact super-periodicity and therefore all resonances $G\gamma = n \pm Q_k$ can occur. There is only a very approximate super-periodicity 4 because the 4 arcs are identical. It is reasonable to make HERA-p as close to super-periodic as possible. Insertion of flattening snakes in the non-flat regions south, east, and north is a step in this direction, because this makes the regions more similar to the flat west section. This lattice with 6 flattening snakes is here referred to as the *6fs* snake scheme.

In this scheme, however, the spin rotation across the west quadrant is larger than the rotation across the other quadrants. The non-flat regions produce two spin rotation angles Ψ_h as shown in Fig. 2.5. The two non-flat regions around the interaction points, taken together, do not produce any net spin rotation, because they are compensated by the flattening snakes as shown in Sect. 2.2.4. While spins rotate by $\frac{\pi}{2}G\gamma$ across the west quadrant, they only rotate by $\frac{\pi}{2}G\gamma - 4\Psi_h$ across the other three quadrants. This violation of periodicity can be compensated by using two more flattening snakes in appropriate regions around the west interaction point. These two flattening snakes do not compensate a vertical bend; they simply reduce the spin rotation. This choice of 8 flattening snakes is here referred to as snake scheme *8fs*.

Figure 3.6 (top) shows, the resonance strength ϵ_{ν_0} with $\nu_0 = j_0 \pm Q_y$ for the *6fs* scheme. The middle figure shows the resonance strength of HERA-p from 40 to 1000 GeV/c for the *8fs* scheme. While the strongest resonances are somewhat smaller in the *6fs* scheme, there are more of these very strong resonances clustering together around critical energies, leading to more overlapping strong resonances. As in the previous figures, the resonance strength was computed for a 2.5σ vertical amplitude of 25π mm rad. For constancy, the figures of the following sections showing resonance strength, P_{lim}, and the amplitude dependent spin tune ν, are all computed for this orbital amplitude, except when stated otherwise.

In a completely four-fold symmetric model of HERA-p, where the south quadrant has been repeated 4 times, such a clustering of resonances does not appear, as shown in Fig. 3.6 (bottom). Each of the very strong resonances consists of only one line. So there is no interference of several very strong resonance effects. The red points show the sum of the resonances in the *6fs* scheme, which are very close to the critical energy. This sum is smaller in the *8fs* scheme (blue points) because there is some remnant periodicity recovered by the addition of the two Siberian Snakes in the west.

The very strong resonances which appear in all three figures at about 34 critical energies are very destructive for the acceleration of polarized proton beams. It is therefore important to understand how these very strong resonances are produced. To obtain a clearer picture of the structure of these resonances, the resonance spectrum is separated into the two spectra of Fig. 3.7. Those corresponding to a frequency $\kappa = \nu_0 = j_0 + Q_y$ (left) and those corresponding to $\kappa = \nu_0 = j_0 - Q_y$ (right) have both a regular structure of equally spaced very strong and medium strength resonances. In both graphs, the distance between two such resonances is 58.01 GeV/c. A bend of 60.42 mrad produces one complete extra spin rotation for every 58.01 GeV/c increase in momentum. Because the bend angle of one of the HERA-p FODO cells is 60.42 mrad, this indicates that the strong resonances are due to the con-

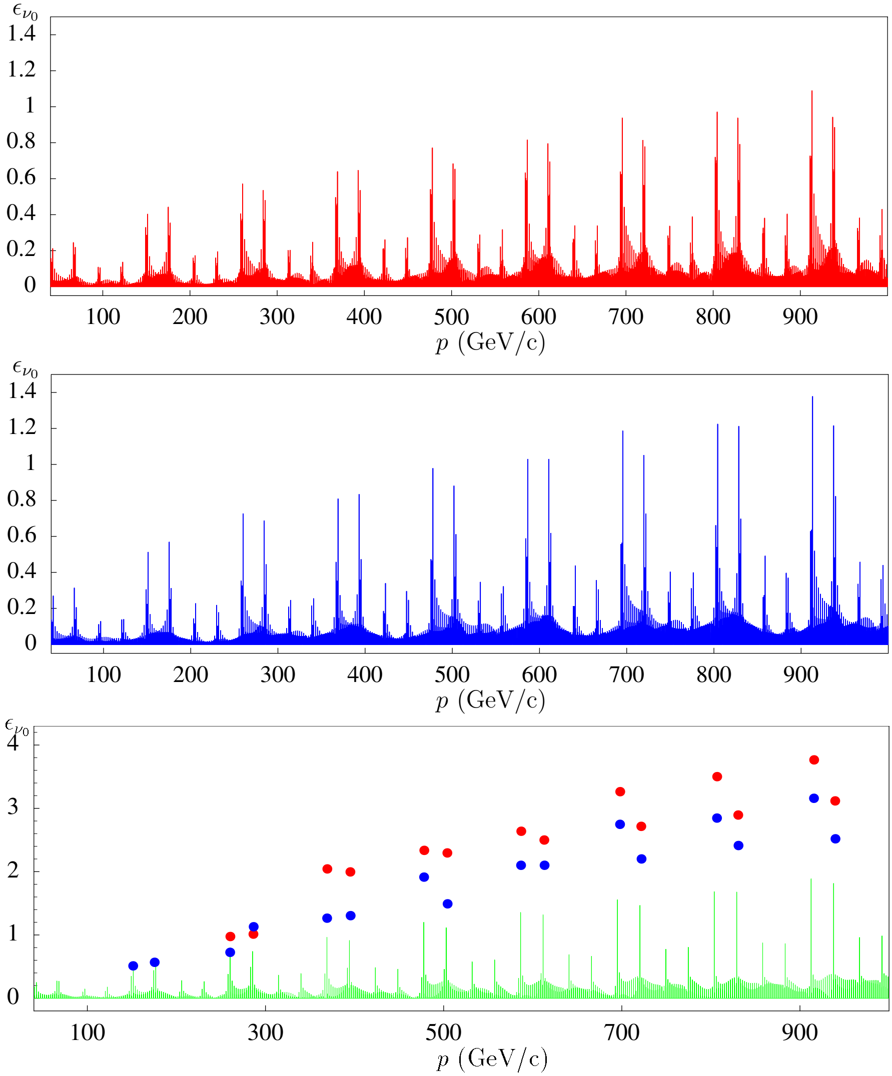

Fig. 3.6. Resonance strength for HERA-p. They are mostly due to vertical motion, which was chosen to have a normalized amplitude of 25π mm mrad. **Top**: The line spectrum of resonances for HERA-p with 6 flattening snakes, one for each non-flat region. **Middle**: The line spectrum of resonances for HERA-p when symmetrized by 8 flattening snakes (*8fs* scheme). **Bottom**: A model of HERA-p with super-periodicity 4 has only well separated, very strong resonances at critical energies, whereas for the realistic models *6fs* and *8fs*, several overlapping strong resonances cluster at these energies. The points show the sum of the resonance strengths, which are not well separated for these two models. For each resonance, the upper of two points corresponds to *6fs*, the lower *8fs* because this sum is larger for the *6fs* scheme than for *8fs*.

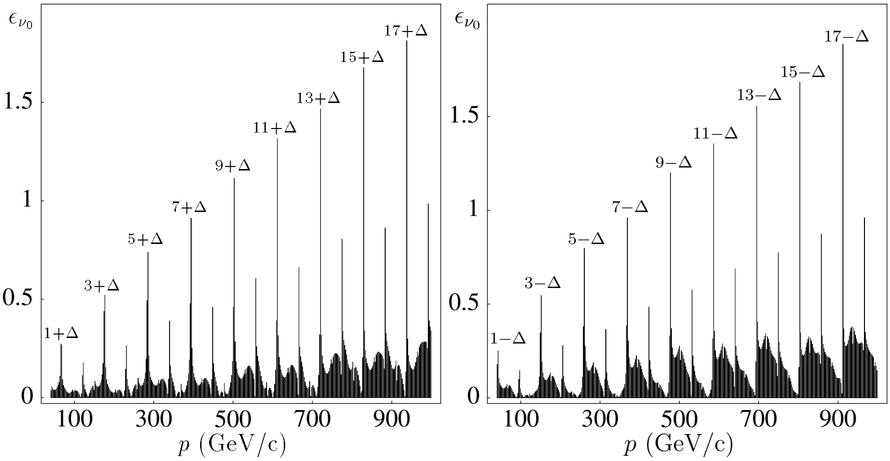

Fig. 3.7. The resonance strength ϵ_{ν_0} for a HERA-p model with super-periodicity 4 for $\nu_0 = j_0 + Q_y$ (*left*) and for $\nu_0 = j_0 - Q_y$ (*right*). The numbers $N_{odd} \pm \Delta$ labeling the very strong resonances indicate the spin phase advance in one FODO. The normalized amplitude of vertical oscillations was 25π mm mrad.

structive interference of spin perturbations in every FODO cell. Such an interference is seen in every circular accelerator built from identical elementary cells [20].

The mechanism leading to these very strong resonances is most easily understood in terms of the spin-orbit-coupling integral,

$$I_y^{\pm} \propto \int \sqrt{\beta_y} \mathrm{e}^{\mathrm{i}(-\Psi \pm \Phi_y)} k \mathrm{d}l \ . \tag{3.36}$$

The arc in HERA-p is a regular structure of identical FODO cells containing alternating focusing and defocusing quadrupoles QX and QY. In between these quadrupoles there are bends $\phi_B = 30.21$ mrad with weak quadrupole windings for adjusting the tunes. The relative spin phase advance over one FODO cell is $G\gamma\Delta_c$ with $\Delta_c = \frac{2\phi_B}{2\pi}$ and the relative orbit phase advance (phase/2π) in a HERA-p FODO cell is about $\Delta = \frac{1}{4}$. Whenever the phase advance $-G\gamma\Delta_c \pm \Delta$ in the spin-orbit-coupling integrals $I_y^{\pm}$ in a FODO cell is an integer, the perturbation of spin motion in each FODO cell directly adds to that of the previous one.

There are therefore strong resonances due to a large coupling integral I_y^+ around every energy with $\gamma = \frac{N+\Delta}{G\Delta_c}$ and due to a large coupling integral I_y^- around every energy with $\gamma = \frac{N-\Delta}{G\Delta_c}$. The FODO phase advance is not exactly $\frac{\pi}{2}$ for the HERA-p lattice used in 2004 but the actual Δ of 0.243 produces exactly the position of the observed very strong and medium strength resonances.

This however does not explain why these resonances come in alternating pairs of stronger and weaker resonances. This effect is due to an alternation of constructive and destructive interference of spin perturbations in the focusing and the defocusing quadrupoles. If a relative vertical phase advance of $\varDelta_1$ from QY to QX is given, the spin perturbation in the QY magnet is counteracted by that in the QX magnet when the phase advance $-\frac{1}{2}G\gamma\varDelta_c \pm \varDelta_1$ of the spin-orbit-coupling integral $I_y^{\pm}$ between these quadrupoles is an integer. This leads to a pair of weaker resonances. But at the other critical energies, where $-G\gamma\varDelta_c \pm \varDelta$ is approximately an odd integer, the spin perturbations of the QX and QY add to each other, leading to a pair of stronger resonances. When the FODO cell is symmetric, so that $\varDelta = 2\varDelta_1$, a cancellation occurs whenever $-G\gamma\varDelta_c \pm \varDelta = 2N$. However, the HERA-p FODO cell is not completely symmetric, due to a slight geometric asymmetry and due to two additional small quadrupoles of unequal strength for tune control. But the approximate symmetry is sufficient to cause the observed alternation between very strong and medium strength resonances. At each of the very strong resonances, the relative spin phase advance per FODO cell is therefore

$$-G\gamma\varDelta_c = N_{odd} \pm \varDelta \tag{3.37}$$

for odd integers N_{odd}. These values are indicated at each of the resonances associated with I_y^+ (left) and I_y^- (right) in Fig. 3.7.

When operating HERA-p with polarized beams, one should choose an energy in between two medium strength resonances to limit the influence of the very strong resonances during the many hours of storage time. A good momentum in that respect would be 870 GeV/c, where spins rotate 16 times in each FODO and the energy is just between the medium strength resonances at $G\gamma\varDelta_c = 16 \pm \varDelta$.

First-order resonances due to vertical motion can only occur at energies where $\nu_0 \pm Q_y$ is an integer. At these energies, the resonance condition for each FODO cell will in general not be satisfied exactly, but the resonances with $-G\gamma\varDelta_c \pm \varDelta \approx N_{odd}$ will be very strong. In the model with super-periodicity 4, the resonance strengths were shown as lines in Fig. 3.6 and only one resonance is very strong at each critical energy. Here the distance to the next resonance that is allowed by symmetry is 4 times larger than the distance in a ring without super-periodicity. This explains why several very strong and overlapping resonances cluster at critical energies in a realistic model of HERA-p.

As has been shown in Fig. 3.6, the number of these overlapping resonances can be reduced by adding two flattening snakes in the west. The advantage of symmetrizing HERA-p by these additional magnets is also apparent in the resonance effects that appear due to radial motion with the tune Q_x and due to longitudinal motion with the tune Q_τ. But these effects will not be discussed here.

3.3 Optimal Choices of Siberian Snakes

It has been pointed out several times that Siberian Snakes are indispensable if polarized proton beams are to be accelerated in a high-energy synchrotron such as HERA-p. This has the following reasons:

1. Siberian Snakes fix the design-orbit spin tune to $\frac{1}{2}$ during the acceleration cycle so that no first-order resonances have to be crossed. Crossing first-order resonances can lead to a severe reduction of polarization by an amount described by the Froissart-Stora formula in Sect. 2.2.11.
2. Siberian Snakes strongly reduce the influence of energy variations on spin motion within a synchrotron period as has been illustrated in Fig. 2.16.
3. Siberian Snakes reduce the variation of $\boldsymbol{n}(\boldsymbol{z})$ for particles that oscillate vertically and therefore pass through horizontal fields that perturb the spin motion. An example of this reduction and the associated increase in P_{lim} was shown in Fig. 2.15.
4. When $\boldsymbol{n}$ changes rapidly during acceleration, the adiabatic invariance of $J_S = \boldsymbol{n}(\boldsymbol{z}) \cdot \boldsymbol{S}$ might be violated and polarization would be reduced. It is therefore important that Siberian Snakes smoothen the rapid changes of $\boldsymbol{n}$ during the acceleration cycle as shown in Fig. 2.15.
5. Siberian Snakes can also compensate perturbing effects of misaligned optical elements [21, 22, 20] but this tract will not cover the effect of misalignments.

There will be little reduction of polarization during the acceleration process and all particles will be polarized in nearly the same direction at high energy if the accelerator has an invariant spin field $\boldsymbol{n}(\boldsymbol{z})$ that changes slowly during the acceleration process and that is nearly parallel for all relevant phase space points so that P_{lim} is large. Achieving this is one of the non-trivial tasks of Siberian Snakes. However, there is so far no reliable formula for determining the number of Siberian Snakes required for an accelerator [24, 25]. To make things worse, for any given number of Siberian Snakes there are very many different possible combinations of the snake angles that lead to an energy independent closed-orbit spin tune of $\frac{1}{2}$ and to a vertical $\boldsymbol{n}_0$ in the accelerator's arcs. And so far there is also no reliable formula for determining which of these snake schemes leads to the highest polarization.

There used to be a popular opinion that, owing to their symmetry, 5 standard choices of the snake angles for 4 Siberian Snakes are advantageous for HERA-p. These choices are not optimal, as will be shown. For reasons why these standard schemes were considered useful, see for example [26]. RHIC with its two snakes, is operated with a similar standard scheme [27]. The energy dependence of P_{lim} in HERA-p produced by these 5 snake schemes is shown in Fig. 3.8. They seem to produce rather similar but very low maximum time-average polarization P_{lim} in the critical energy regions where very strong resonances are excited. The observation of such rather small differences in the $\boldsymbol{n}$-axis for such different schemes suggests the following detailed investigation

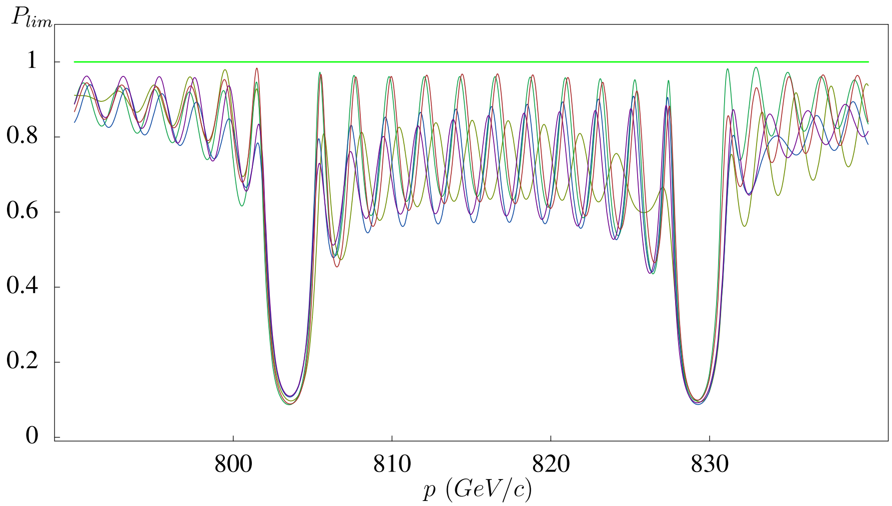

Fig. 3.8. P_{lim} of linearized spin-orbit motion for a 2.5σ vertical amplitude for 4 Siberian Snakes in a *6fs* scheme of HERA-p. Each curve corresponds to one of the 5 standard choices of snake schemes in the following table. The right column shows an obvious notation to describe the snake angles in a snake scheme:

Scheme	South	East	North	West
$(0\frac{\pi}{2}00)$	$0°$	$90°$	$0°$	$0°$
$(\frac{\pi}{4}0\frac{\pi}{4}0)$	$45°$	$0°$	$45°$	$0°$
$(\frac{3\pi}{4}0\frac{3\pi}{4}0)$	$-45°$	$0°$	$-45°$	$0°$
$(\frac{5\pi}{8}\frac{\pi}{8}\frac{5\pi}{8}\frac{\pi}{8})$	$-22.5°$	$22.5°$	$-22.5°$	$22.5°$
$(\frac{\pi}{8}\frac{5\pi}{8}\frac{\pi}{8}\frac{5\pi}{8})$	$22.5°$	$-22.5°$	$22.5°$	$-22.5°$

of the influence of snake schemes. Figure 3.9 (left) shows P_{lim} as computed for linearized spin-orbit motion by (3.20) for 4 other schemes with 4 Siberian Snakes that were chosen to demonstrate that very different values of P_{lim} can be obtained depending on the snake scheme. In the following, I will try to improve P_{lim} by investigating methods of determining the optimal snake arrangement for an accelerator. Initially, the approximation of linearized spin-orbit motion will be used and then higher-order effects with various snake schemes will be analyzed.

It turned out that large increases in P_{lim} can result from the choice of a suitable snake scheme. This is shown in Fig. 3.9 (right) where P_{lim} curves for the vertical motion with two different Siberian Snake arrangements in HERA-p are superimposed. For this figure, the betatron phase advances in the vertical optics had been specially tuned in a way to be described in Sect. 3.3.2. For this special optics, the snake scheme $(0\frac{\pi}{2}\frac{\pi}{2}\frac{\pi}{2})8fs$ leads to an especially favorable maximum time-average polarization (blue curve) even at critical energies. Another snake scheme that is not suitable produces a reduction of P_{lim} (red curve) at all critical energies during the ramp. This

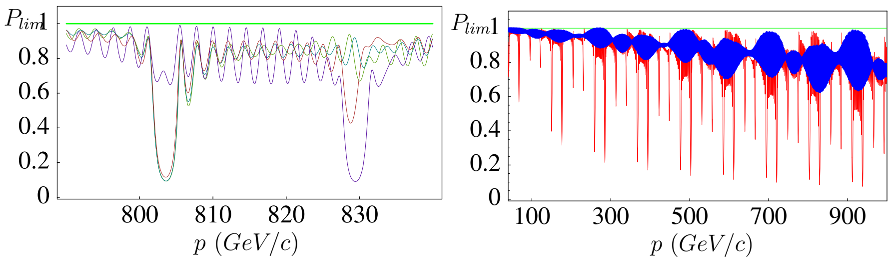

Fig. 3.9. Left: P_{lim} for 4 different snake schemes that lead to very different maximum time-average polarization for the standard HERA-p lattice. **Right**: P_{lim} for the standard scheme $(\frac{\pi}{4}0\frac{\pi}{4}0)6fs$ (*red*) and for the $(0\frac{\pi}{2}\frac{\pi}{2}\frac{\pi}{2})8fs$ scheme (*blue*) after the vertical optics in HERA-p has been changed so that the contribution of the arcs to the spin-orbit-coupling integrals cancel when the latter scheme is used.

example, given here to emphasize the point, is somewhat extreme because the vertical optics was custom designed for the $(0\frac{\pi}{2}\frac{\pi}{2}\frac{\pi}{2})8fs$ snake scheme, but nevertheless, it demonstrates how great the differences of P_{lim} for snake schemes can be.

By comparing Fig. 3.9 with the resonance strengths of HERA-p shown in Fig. 3.6, the residual resonance structure after the installation of Siberian Snakes, which was already mentioned in Sect. 2.2.14, can clearly be seen. Special snake schemes, however, are able to eliminate the influence even of the strongest resonances when only linearized spin-orbit motion is considered. In the following, the reason for these large differences between different snake schemes will be analyzed and optimal snake schemes for HERA-p will be investigated further.

3.3.1 Spin-Orbit-Coupling Integrals with Siberian Snakes

To introduce spin-orbit-coupling integrals in flat rings in Sect. 3.1.2, $\boldsymbol{n}_0$ was initially assumed to point vertically upward, and the coordinate system $[\boldsymbol{e}_x, \boldsymbol{e}_l, \boldsymbol{e}_y]$ was used. Now Siberian Snakes will be included, which rotate all spins (and also $\boldsymbol{n}_0$) by π around some axis in the horizontal plane. Then it is convenient to use the coordinate system $[\boldsymbol{e}_x, \boldsymbol{n}_0 \times \boldsymbol{e}_x, \boldsymbol{n}_0]$. The second vector $\boldsymbol{e}_2$ corresponds to $\boldsymbol{e}_l$ when $\boldsymbol{n}_0$ is vertical upward and to $-\boldsymbol{e}_l$ after a Siberian Snake has rotated $\boldsymbol{n}_0$ downward. In this new coordinate system, I again use the complex notation $\hat{s} = s_1 + \mathrm{i}s_2$. When a particle with spin parallel to $\boldsymbol{n}_0$ travels along the trajectory $y = \sqrt{2J_y\beta_y}\cos\Phi_y$ through a quadrupole of focusing strength k, then in first order the spin direction is deflected from $\boldsymbol{n}_0$ by the angle $(G\gamma+1)\int_{\mathrm{Quad}} yk\mathrm{d}l$, leaving a change $\Delta\hat{s}$ in the spin coordinates of

$$\Delta\hat{s} = -\mathrm{i}(G\gamma+1)\int_{\mathrm{Quad}} \sqrt{2J_y\beta_y}\cos\Phi_y k\mathrm{d}l \tag{3.38}$$

where positive values of k describe vertically defocusing quadrupoles. When $\boldsymbol{n}_0$ points vertically upward and a spin is initially parallel to $\boldsymbol{n}_0$, then a vertically defocusing quadrupole rotates the spin in the direction of $-\boldsymbol{e}_l = -\boldsymbol{e}_2$. When $\boldsymbol{n}_0$ points vertically downward, the spin rotates in the direction of $\boldsymbol{e}_l = -\boldsymbol{e}_2$ leaving (3.38) correct for both cases.

After the spin component $\hat{s}$ has been created by the deflection of a spin that was parallel to $\boldsymbol{n}_0$ when the particle entered a quadrupole, it subsequently rotates by $\Psi(\theta) = \int_{\theta_0}^{\theta} \Omega_{0y}(\tilde{\theta})d\tilde{\theta}$. This describes spin precession around the vertically upward direction, independently of the fact that $\boldsymbol{n}_0$ might be pointing downward. When $\boldsymbol{n}_0$ is pointing upward, the disturbed spin rotates to $\hat{s}\mathrm{e}^{\mathrm{i}\Psi}$, whereas it subsequently rotates to $\hat{s}\mathrm{e}^{-\mathrm{i}\Psi}$ when $\boldsymbol{n}_0$ is pointing downward.

The change of the spin away from $\boldsymbol{n}_0$ accumulated after a section of the ring from θ_0 to θ_1 in which there is no Siberian Snake is given by

$$\hat{s} = C\mathrm{e}^{\mathrm{i}\Psi(\theta_1)} \int_{\theta_0}^{\theta_1} k2\sqrt{J_y\beta_y}\cos\Phi_y \mathrm{e}^{-\mathrm{i}\Psi(\theta)}\mathrm{d}\theta \tag{3.39}$$

with $C = -\mathrm{i}(G\gamma+1)\frac{1}{\sqrt{2}}\frac{L}{2\pi}$, when $\boldsymbol{n}_0$ points upward. When $\boldsymbol{n}_0$ points downward, it is given by

$$\hat{s} = C\mathrm{e}^{-\mathrm{i}\Psi(\theta_1)} \int_{\theta_0}^{\theta_1} k2\sqrt{J_y\beta_y}\cos\Phi_y \mathrm{e}^{\mathrm{i}\Psi(\theta)}\mathrm{d}\theta \ . \tag{3.40}$$

To compute the spin change that accumulates over the whole ring, $\boldsymbol{n}_0$ is initially taken to be upward.

In Sect. 3.1.2, the spin-orbit-coupling integrals of the complete ring were defined. Here spin-orbit-coupling integrals of a subsection of the ring that does not contain a Siberian Snake are defined accordingly as

$$I_y^{\pm} = C\int_{\theta_0}^{\theta_1} k\sqrt{\beta_y}\mathrm{e}^{\mathrm{i}(-\Psi\pm\Phi_y)}\mathrm{d}\theta \ , \tag{3.41}$$

where the initial phases are chosen to be $\Psi(\theta_0) = 0$ and $\Phi_y(\theta_0) = 0$.

It is now assumed that there are n Siberian Snakes in the ring and that n is even, to make $\boldsymbol{n}_0$ vertical in the arcs of the ring. The azimuth at the position of a snake is denoted by θ_j and the spin phase advance around the vertically upward direction between snake j and $j+1$ is denoted by Ψ_j. The spin phase advance after the jth Siberian Snake is $\Psi_j(\theta)$ with $\Psi_j(\theta_j) = 0$. The deviation of the spin accumulated between just after the jth snake to just before the $(j+1)$th snake is denoted by $\hat{s}_j$.

For simplicity $\theta_0 = 0$ and $\theta_{n+1} = 2\pi$ is used, and the spin phase advance from azimuth θ_0 to the first Siberian Snake is Ψ_0. Because the vector $\boldsymbol{n}_0$ initially points vertically upward, one obtains

$$\hat{s}_0 = C\mathrm{e}^{\mathrm{i}\Psi_0} \int_{\theta_0}^{\theta_1} k\sqrt{\beta_y}\cos\Phi_y \mathrm{e}^{-\mathrm{i}\Psi_0(\theta)}\mathrm{d}\theta \ . \tag{3.42}$$

By considering the direction of $\boldsymbol{n}_0$ after the jth snake, one obtains

$$\hat{s}_j = C\mathrm{e}^{\mathrm{i}(-)^j\Psi_j}\int_{\theta_j}^{\theta_{j+1}} k\sqrt{\beta_y}\cos\Phi_y \mathrm{e}^{-\mathrm{i}(-)^j\Psi_j(\theta)}\mathrm{d}\theta \ . \tag{3.43}$$

In the following, a Siberian Snake with a snake axis that is in the horizontal plane will be referred to as a horizontal Siberian Snake, and for historical reasons a snake that rotates spins around the vertical by some rotation angle will be referred to as type III snake. A horizontal Siberian Snake with a snake angle φ is equivalent to a radial Siberian Snake followed by a type III snake with rotation angle $\alpha = 2\varphi$ because

$$-\mathrm{i}(\sigma_1\cos\varphi+\sigma_2\sin\varphi) = (\cos\varphi-\mathrm{i}\sigma_3\cos\varphi)(-\mathrm{i}\sigma_1) = \mathrm{e}^{-\mathrm{i}\frac{\alpha}{2}\sigma_3}(-\mathrm{i}\sigma_1) \ . \tag{3.44}$$

Thus a horizontal Siberian Snake with snake angle ϕ in effect introduces an extra spin phase advance of 2ϕ.

The radial Siberian Snake does not change $\hat{s}$, because it changes the axis $\boldsymbol{e}_2 = \boldsymbol{n}_0 \times \boldsymbol{e}_x$ along with the longitudinal component of the spin. The subsequent rotation around the vertical takes the spin from $\hat{s}$ to $\hat{s}\mathrm{e}^{-\mathrm{i}\alpha}$ for downward $\boldsymbol{n}_0$ after the snake and to $\hat{s}\mathrm{e}^{\mathrm{i}\alpha}$ for upward $\boldsymbol{n}_0$ after the snake.

The angle of the jth Siberian Snake is $\varphi_j = \frac{\alpha_j}{2}$, and the horizontal spin component accumulating over a complete turn from 0 to 2π is

$$\begin{aligned}
\hat{s} \;=\;& \hat{s}_n + \hat{s}_{n-1}\mathrm{e}^{\mathrm{i}(\alpha_n+\Psi_n)} + \hat{s}_{n-2}\mathrm{e}^{\mathrm{i}(-\alpha_{n-1}-\Psi_{n-1}+\alpha_n+\Psi_n)} \\
&+ \ldots + \hat{s}_1\mathrm{e}^{\mathrm{i}(\alpha_2+\Psi_2-\alpha_3-\Psi_3\pm\ldots)} + \hat{s}_0\mathrm{e}^{\mathrm{i}(-\alpha_1-\Psi_1+\alpha_2+\Psi_2-\alpha_3-\Psi_3\pm\ldots)} \\
=\;& \sum_{j=0}^{n}\hat{s}_j\mathrm{e}^{\mathrm{i}\sum_{k=j+1}^{n}(-)^k(\alpha_k+\Psi_k)} \qquad (3.45) \\
=\;& C\sum_{j=0}^{n}\mathrm{e}^{\mathrm{i}(-)^j\Psi_j}\int_{\theta_j}^{\theta_{j+1}} k\sqrt{\beta_y}\cos\Phi_y\mathrm{e}^{-\mathrm{i}(-)^j\Psi_j(\theta)}\mathrm{d}\theta\,\mathrm{e}^{\mathrm{i}\sum\limits_{k=j+1}^{n}(-)^k(\alpha_k+\Psi_k)}
\end{aligned}$$

with the convention $\sum_{k=n+1}^{n}(\ldots) = 0$.

As shown in Sect. 2.2.3, the spin phase advances between snakes must satisfy the condition $\sum_{k=0}^{n}(-)^k\Psi_k = 0$ to make the closed-orbit spin tune independent of energy and the snake angles must satisfy the condition $\sum_{k=1}^{n}(-)^k\varphi_k = \frac{\pi}{2}$ to make the closed-orbit spin tune ν_0 equal to $\frac{1}{2}$.

For simplicity $\alpha_0 = 0$ is used, although there is no Siberian Snake at θ_0. This leads to

$$\begin{aligned}
\hat{s} =\;& C\sum_{j=0}^{n}\mathrm{e}^{\mathrm{i}(\pi-\sum\limits_{k=0}^{j}(-)^k(\alpha_k+\Psi_k))}\mathrm{e}^{\mathrm{i}(-)^j\Psi_j}\int_{\theta_j}^{\theta_{j+1}} k\sqrt{\beta_y}\cos\Phi_y\mathrm{e}^{-\mathrm{i}(-)^j\Psi_j(\theta)}\mathrm{d}\theta \\
=& -C\sum_{j=0}^{n}\mathrm{e}^{-\mathrm{i}\sum\limits_{k=0}^{j-1}(-)^k(\alpha_k+\Psi_k)}\int_{\theta_j}^{\theta_{j+1}} k\sqrt{\beta_y}\cos\Phi_y\mathrm{e}^{-\mathrm{i}(-)^j(\Psi_j(\theta)+\alpha_j)}\mathrm{d}\theta. \qquad (3.46)
\end{aligned}$$

The spin-orbit-coupling integrals for a ring with horizontal Siberian Snakes are therefore defined as

$$I_y^{\pm} = -C \sum_{j=0}^{n} \mathrm{e}^{-\mathrm{i}\sum_{k=0}^{j-1}(-)^k(\alpha_k+\Psi_k)} \int_{\theta_j}^{\theta_{j+1}} k\sqrt{\beta_y}\mathrm{e}^{\mathrm{i}[-(-)^j(\Psi_j(\theta)+\alpha_j)\pm\Phi_y]}\mathrm{d}l \ . \tag{3.47}$$

In terms of the orbital phase advance Φ_{yj} between snake j and $j+1$, one obtains

$$I_y^{\pm} = -C \sum_{j=0}^{n} \mathrm{e}^{\mathrm{i}\sum_{k=0}^{j-1}[-(-)^k(\alpha_k+\Psi_k)\pm\Phi_{yk}]} \times \int_{\theta_j}^{\theta_{j+1}} k\sqrt{\beta_y}\mathrm{e}^{\mathrm{i}[-(-)^j(\Psi_j(\theta)+\alpha_j)\pm\Phi_{yj}(\theta)]}\mathrm{d}\theta \ . \tag{3.48}$$

A corresponding formula has been used in [13] to introduce so-called strong spin matching, where Siberian Snakes are used to produce a cancellation of spin perturbations in different FODO cells. It is expected that the spin motion on vertical betatron orbits will be relatively stable when in linear approximation a spin that is initially parallel to $\boldsymbol{n}_0$ comes back to that direction after one turn, i.e., $\hat{s}(2\pi) = 0$. This is achieved in linear approximation for all trajectories when both spin-orbit-coupling integrals vanish. The ring is then said to be spin matched or spin transparent for vertical betatron motion.

3.3.2 Snake Matching in Rings with Super-periodicity

The spin perturbations in different parts of the ring can compensate each other when these parts have similar spin-orbit-coupling integrals. This is achieved by using the Siberian Snakes to adjust the spin phase advances in such a way that spin-orbit-coupling integrals of similar parts of a ring cancel each other. In the following, the process of finding a snake scheme for which such a compensation occurs will be referred to as *snake matching*. After demonstrating the idea for type III snakes, which simply rotate spins around the vertical by some fixed angle with little influence on the orbit motion, I will demonstrate two quite general results:

1. A ring with super-periodicity 4 can be completely snake matched using 8 Siberian Snakes, i.e., a snake scheme can be found for which the spin-orbit-coupling integrals are zero due to a complete cancellation of spin perturbations in different parts of the ring. There are exactly two such possibilities that lead to energy independent snake angles.
2. Such a ring can also be snake matched using 4 Siberian Snakes. Then, however, the snake axes depend on energy and have to be changed during

the acceleration process. Such Siberian Snakes with variable snake axes can be constructed [28].

Snake Matching with Type III Snakes for Super-periodicity 4: For a flat ring without horizontal Siberian Snakes, the spin-orbit coupling integral for vertical motion was defined as

$$I^{\pm} = \int_0^L k\sqrt{\beta_y} e^{i(-\Psi \pm \Phi_y)} dl \ . \tag{3.49}$$

For ease of notation, the constant C in (3.41) is now dropped and the arc-length $l = L\frac{\theta}{2\pi}$ is used rather than the azimuth θ. Furthermore, the index y on the spin-orbit-coupling integral and on the vertical tune will no longer be indicated. In any case, the methods for canceling spin-orbit-coupling integrals by a special choice of snake angles that will now be derived can also be used for transverse and longitudinal motion. In this section, the notation will be further simplified by using the symbols ν_0 and Q to denote 2π times the spin tune 2π times the orbital tune. Then for a ring with super-periodicity 4, $I^{\pm}$ can be computed from

$$I^{\pm}_{\frac{1}{4}} = \int_0^{L/4} k\sqrt{\beta_y} e^{i(-\Psi \pm \Phi_y)} dl \ , \tag{3.50}$$

$$I^{\pm} = I^{\pm}_{\frac{1}{4}}[1 + e^{i(-\nu_0 \pm Q)/4} + e^{i2(-\nu_0 \pm Q)/4} + e^{i3(-\nu_0 \pm Q)/4}] \ . \tag{3.51}$$

Spin transparency requires that I^+ as well as I^- vanish. Thus the bracket in (3.51) must vanish. This is only possible when $e^{i(-\nu_0 \pm Q)/4}$ is either -1 or i. Choosing the first possibility to eliminate I^+ and the second to eliminate I^-, one obtains

$$e^{i(-\nu_0+Q)/4} = -1 \ , \quad e^{i(-\nu_0-Q)/4} = i \ . \tag{3.52}$$

This leads to the requirement $e^{iQ/2} = i$, which cannot be satisfied in a realistic ring. Therefore, a four-fold repetitive symmetry cannot lead to spin transparency at any energy. While the spin disturbance of two quadrants can therefore not cancel in I^+ as well as in I^-, one of these integrals can cancel whenever the spin phase advance between the quadrants is appropriate.

The situation changes if type III snakes are installed. As first found in [29], type III snakes can improve the spin dynamics in HERA-p by increasing $P_{lim} = |\langle \boldsymbol{n} \rangle|$. They can be used to manipulate the spin phase advance to make the spin-orbit-coupling integrals of different parts of the ring cancel. To demonstrate this, 4 type III snakes are installed regularly spaced around the ring.

There are three possibilities for canceling the spin disturbances between quadrants of the ring. The quadrants whose destructive effects cancel are connected by arrows in Fig. 3.10.

The spin-orbit-coupling integrals are

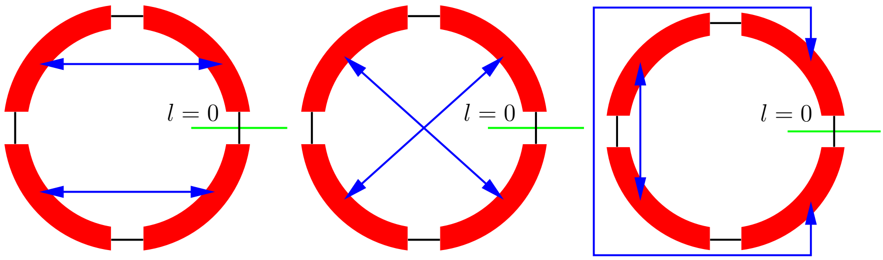

Fig. 3.10. The three possibilities for canceling the depolarizing effects of quadrants of a ring with super-periodicity 4. The arrows indicate which quadrants cancel.

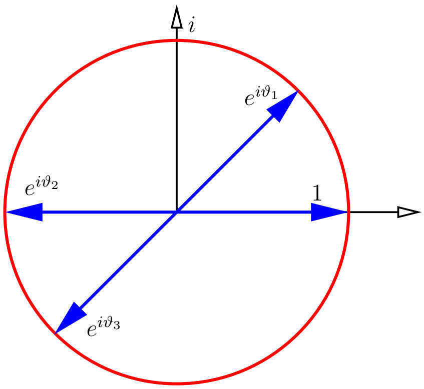

Fig. 3.11. Four complex numbers with modulus one can only add up to zero when they consist of two pairs that individually add up to zero.

$$
\begin{aligned}
I^{\pm} = I^{\pm}_{\frac{1}{4}}(1 &+ \mathrm{e}^{\mathrm{i}(-\nu_0 \pm Q)/4 - \psi_1} \\
&+ \mathrm{e}^{\mathrm{i}2(-\nu_0 \pm Q)/4 - \psi_1 - \psi_2} + \mathrm{e}^{\mathrm{i}3(-\nu_0 \pm Q)/4 - \psi_1 - \psi_2 - \psi_3}) \ ,
\end{aligned} \tag{3.53}
$$

where ψ_j is the spin rotation angle of the type III snake at $l = j\frac{L}{4}$. To snake match the ring, I^+ as well as I^- must vanish. Therefore, the bracket on the right hand side has to vanish in both cases. A sum of 4 complex numbers with unit modulus can only vanish when it consist of two pairs of numbers that cancel each other. This is shown in Fig. 3.11.

The three possibilities of cancellation demonstrated in Fig. 3.10 are given by the following three sets of equations:

1. $(-\nu_0 \pm Q)/4 - \psi_1 \mathrel{\hat{=}} \pi$ and $(-\nu_0 \pm Q)/4 - \psi_3 \mathrel{\hat{=}} \pi$,
2. $2(-\nu_0 \pm Q)/4 - \psi_1 - \psi_2 \mathrel{\hat{=}} \pi$ and $\psi_3 \mathrel{\hat{=}} \psi_1$,
3. $3(-\nu_0 \pm Q)/4 - \psi_1 - \psi_2 - \psi_3 \mathrel{\hat{=}} \pi$ and $(-\nu_0 \pm Q)/4 - \psi_2 \mathrel{\hat{=}} \pi$.

The symbol $\overset{\circ}{=}$ indicates equivalence modulo 2π. To snake match, one of these three conditions has to hold for $(-\nu_0+Q)$, which lets I^+ vanish, and another of the conditions has to hold for $(-\nu_0-Q)$, which lets I^- vanish. I^+ and I^- cannot vanish due to the same condition if restrictions on the allowed orbital phase advance Q are to be avoided. There are therefore three possibilities:

1. $I^+=0$ due to condition 2 and $I^-=0$ due to condition 3 requires
$$\psi_2 \overset{\circ}{=} \pi + 2(-\nu_0+Q)/4 - \psi_1 \ , \quad \psi_3 \overset{\circ}{=} \psi_1 \ , \tag{3.54}$$
$$\psi_2 \overset{\circ}{=} \pi + (-\nu_0-Q)/4 \ , \quad \psi_3 \overset{\circ}{=} 2(-\nu_0-Q)/4 - \psi_1 \ . \tag{3.55}$$
The first and the third of these equations require that $\psi_1 \overset{\circ}{=} (-\nu_0+3Q)/4$ whereas the second and the fourth equations require that $\psi_1 \overset{\circ}{=} (-\nu_0-Q)/4$. These two requirements are in general not compatible, and the ring cannot be made spin transparent in this way.
2. $I^+=0$ due to condition 1 and $I^-=0$ due to condition 3 requires
$$\psi_1 \overset{\circ}{=} \pi + (-\nu_0+Q)/4 \ , \quad \psi_3 \overset{\circ}{=} \psi_1 \ , \tag{3.56}$$
$$\psi_2 \overset{\circ}{=} \pi + (-\nu_0-Q)/4 \ , \quad \psi_3 \overset{\circ}{=} 2(-\nu_0-Q)/4 - \psi_1 \ . \tag{3.57}$$
The first and the last of these equations together require $\psi_3 \overset{\circ}{=} \pi-(3Q-\nu_0)/4$. This is in conflict with the second equation. Thus this way also cannot lead to a spin transparent ring.
3. $I^+=0$ due to condition 1 and $I^-=0$ due to condition 2 requires
$$\psi_1 \overset{\circ}{=} \pi + (-\nu_0+Q)/4 \ , \quad \psi_3 \overset{\circ}{=} \psi_1 \ , \tag{3.58}$$
$$\psi_2 \overset{\circ}{=} \pi + 2(-\nu_0-Q)/4 - \psi_1 \ , \quad \psi_3 \overset{\circ}{=} \psi_1 \ . \tag{3.59}$$
These 4 equations are compatible and lead to $\psi_1 \overset{\circ}{=} \psi_3 \overset{\circ}{=} \pi+(-\nu_0+Q)/4$ and $\psi_2 \overset{\circ}{=} (-\nu_0-3Q)/4$.

The type III snake at $l=0$ has the rotation angle ψ_4, which is chosen in such a way that the closed-orbit spin tune of the ring does not change due to the snakes, i.e., $\psi_1+\psi_2+\psi_3+\psi_4 \overset{\circ}{=} 0$. The required rotation angles are then
$$\psi_1 \overset{\circ}{=} \psi_3 \overset{\circ}{=} \pi+\frac{-\nu_0+Q}{4} \ , \quad \psi_2 \overset{\circ}{=} -\frac{\nu_0+3Q}{4} \ , \quad \psi_4 \overset{\circ}{=} \frac{Q-3-\nu_0}{4} \ . \tag{3.60}$$

Obviously, a change in sign of Q leads to $I^+=0$ due to condition 2 and to $I^-=0$ due to condition 1. There are therefore exactly two possibilities for making a ring with super-periodicity 4 spin transparent by means of 4 type III snakes. These possibilities are shown in Fig. 3.12. However, the scheme of 4 type III snakes presented here cannot be a practical snake scheme, because it does not make the closed-orbit spin tune independent of energy. But it illustrates how type III snakes can be used at fixed energy to make spin perturbations from different parts of the ring cancel each other. This feature can then be used in combination with the Siberian Snakes that are installed to make the closed-orbit spin tune independent of energy.

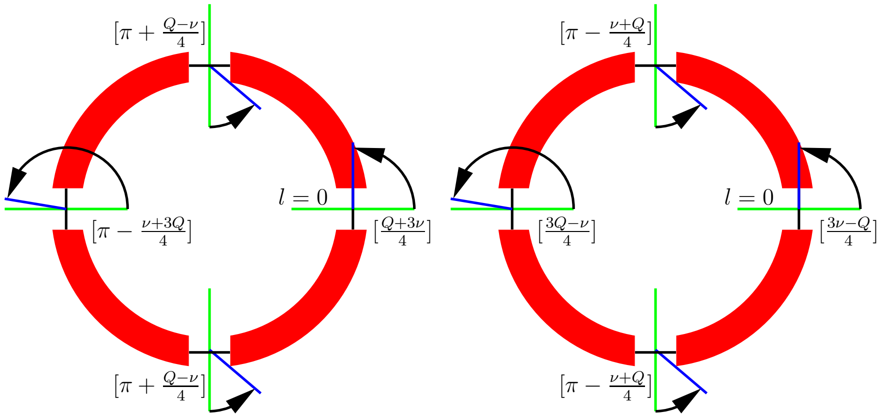

Fig. 3.12. The only two ways to snake match a ring with super-periodicity 4 by 4 type III snakes. The number $[x]$ denotes x mod 2π and lies in $[0, 2\pi)$. The vertical tune times 2π is denoted by Q and $\nu_0 = G\gamma 2\pi$.

Snake Matching with Type III Snakes for Super-periodicity 4 and Mirror Symmetry: In particle optical systems, mirror symmetries are often used to cancel perturbative effects [30, 31, 32, 33]. Therefore, it is interesting to see whether mirror symmetry can lead to vanishing of spin-orbit-coupling integrals when 4 Siberian Snakes are installed at the symmetry points of the ring. If one super-period is mirror symmetric, then

$$I^{\pm}_{\frac{1}{8}} = \int_0^{L/8} k\sqrt{\beta_y}\mathrm{e}^{\mathrm{i}(-\Psi\pm\Phi_y)}\mathrm{d}l\ , \tag{3.61}$$

$$\begin{aligned} I^{\pm}_{\frac{1}{4}} &= \int_0^{L/8} k(l)\sqrt{\beta_y(l)}\mathrm{e}^{\mathrm{i}(-\Psi(l)\pm\Phi_y(l))}\mathrm{d}l \\ &\quad + \int_{L/8}^{L/4} k(l)\sqrt{\beta_y(l)}\mathrm{e}^{\mathrm{i}(-\Psi(l)\pm\Phi_y(l))}\mathrm{d}l \\ &= \int_0^{L/8} k(l)\sqrt{\beta_y(l)}\mathrm{e}^{\mathrm{i}(-\Psi(l)\pm\Phi_y(l))}\mathrm{d}l \\ &\quad + \int_0^{L/8} k(\frac{L}{4}-l)\sqrt{\beta_y(\frac{L}{4}-l)}\mathrm{e}^{\mathrm{i}(-\Psi(\frac{L}{4}-l)\pm\Phi_y(\frac{L}{4}-l))}\mathrm{d}l \\ &= I^{\pm}_{\frac{1}{8}} + \int_0^{L/8} k(l)\sqrt{\beta_y(l)}\mathrm{e}^{\mathrm{i}(-(\Psi(\frac{L}{4})-\Psi(l))\pm(Q/4-\Phi_y(l)))}\mathrm{d}l \\ &= I^{\pm}_{\frac{1}{8}} + (I^{\pm}_{\frac{1}{8}})^*\mathrm{e}^{\mathrm{i}(-\nu_0\pm Q)/4}\ . \end{aligned} \tag{3.62}$$

With $\Sigma^{\pm} = (-\nu_0 \pm Q)/4$, one obtains for the complete ring

$$I^{\pm} = (I^{\pm}_{\frac{1}{8}} + (I^{\pm}_{\frac{1}{8}})^*\mathrm{e}^{\mathrm{i}\Sigma^{\pm}}) \cdot (1 + \mathrm{e}^{\mathrm{i}\Sigma^{\pm}} + \mathrm{e}^{\mathrm{i}2\Sigma^{\pm}} + \mathrm{e}^{\mathrm{i}3\Sigma^{\pm}})\ . \tag{3.63}$$

Thus snake matching the ring with super-periodicity 4 is not influenced by the fact that the ring might have a mirror symmetry because the bracket in (3.63) is equivalent to the corresponding bracket in (3.51) for rings without mirror symmetry.

In this tract, type III snakes will not be considered further, because a horizontal Siberian Snake with snake angle φ can be decomposed into a radial Siberian Snake and a type III snake with rotation angle 2φ, as pointed out in (3.44). A type III snake changes the difference between orbital phase Φ_y and spin phase, and that in turn changes the phase in the spin-orbit-coupling integral. This phase can be used to cancel the perturbation in one part of the accelerator against the perturbation in another part, but this can be achieved just as well and with less expense by a slight change of betatron phase advance Φ_y in the vertical optics of the ring. This technique will be used in Sect. 3.3.3.

Snake Matching of Siberian Snakes with Fixed Axes at All Energies for Super-periodicity 4: The snake matching technique with type III snakes has the great disadvantage that these snakes have to be ramped with the rest of the ring in order to snake match at each energy. But horizontal Siberian Snakes can also be used to manipulate the spin phase advance between parts of the ring, and the use of such snakes for snake matching will now be investigated.

Schemes with 4 Snakes: For 4 horizontal Siberian Snakes, the spin-orbit-coupling integral in (3.48) is

$$\begin{aligned} I^{\pm} = &\int_0^{l_1} k\sqrt{\beta_y}\mathrm{e}^{\mathrm{i}(-\Psi_0\pm\Phi_{y0})}\mathrm{d}l \\ &+\mathrm{e}^{\mathrm{i}(-\Psi_0\pm\Phi_{y0})}\int_{l_1}^{l_2} k\sqrt{\beta_y}\mathrm{e}^{\mathrm{i}(\Psi_1+\alpha_1\pm\Phi_{y1})}\mathrm{d}l \\ &+\mathrm{e}^{\mathrm{i}(-\Psi_0+\alpha_1+\Psi_1\pm(\Phi_{y0}+\Phi_{y1}))}\int_{l_2}^{l_3} k\sqrt{\beta_y}\mathrm{e}^{\mathrm{i}(-\Psi_2-\alpha_2\pm\Phi_{y2})}\mathrm{d}l \\ &+\mathrm{e}^{\mathrm{i}(-\Psi_0+\alpha_1+\Psi_1-\alpha_2-\Psi_2\pm(\Phi_{y0}+\Phi_{y1}+\Phi_{y2}))}\int_{l_3}^{L} k\sqrt{\beta_y}\mathrm{e}^{\mathrm{i}(\Psi_3+\alpha_3\pm\Phi_{y3})}\mathrm{d}l\ . \end{aligned} \tag{3.64}$$

For a ring with super-periodicity 4 and with 4 equally spaced horizontal Siberian Snakes, one obtains with $\nu_0 = \Psi(L)$, $\Psi_j = \Psi(L)/4$, and $\Phi_{yj} = Q/4$ the relation

$$I^{\pm}_{\frac{1}{4}} = \int_0^{\frac{L}{4}} k\sqrt{\beta_y}\mathrm{e}^{\mathrm{i}(-\Psi\pm\Phi_y)}\mathrm{d}l\ , \tag{3.65}$$

$$\begin{aligned} I^{\pm} &= I^{\pm}_{\frac{1}{4}}(1+\mathrm{e}^{\mathrm{i}(-\Psi_0+\alpha_1+\Psi_1-\alpha_2\pm(\Phi_{y0}+\Phi_{y1}))}) \\ &\quad+(I^{\mp}_{\frac{1}{4}})^*\mathrm{e}^{\mathrm{i}(-\Psi_0+\alpha_1\pm\Phi_{y0})}(1+\mathrm{e}^{\mathrm{i}(\Psi_1-\alpha_2-\Psi_2+\alpha_3\pm(\Phi_{y1}+\Phi_{y2}))}) \\ &= I^{\pm}_{\frac{1}{4}}(1+\mathrm{e}^{\mathrm{i}(\alpha_1-\alpha_2\pm 2Q/4)}) \end{aligned} \tag{3.66}$$

$$+(I^{\mp}_{\frac{1}{4}})^* \mathrm{e}^{\mathrm{i}((-\nu_0 \pm Q)/4+\alpha_1)}(1+\mathrm{e}^{\mathrm{i}(-\alpha_2+\alpha_3\pm 2Q/4)}) \, .$$

Spin transparency of the ring is therefore obtained when

$$\alpha_1 - \alpha_2 \pm 2Q/4 \overset{\circ}{=} \pi \text{ and } -\alpha_2 + \alpha_3 \pm 2Q/4 \overset{\circ}{=} \pi \, . \tag{3.67}$$

This cannot be achieved in general because the conditions $\alpha_1 - \alpha_2 + 2Q/4 \overset{\circ}{=} \pi$ and $\alpha_1 - \alpha_2 - 2Q/4 \overset{\circ}{=} \pi$ have to be satisfied simultaneously, which implies $Q \overset{\circ}{=} 0$.

In the case of mirror symmetry in the ring, $I^{+}_{\frac{1}{4}}$ and $I^{-}_{\frac{1}{4}}$ are related by (3.62),

$$I^{\pm}_{\frac{1}{4}} = I^{\pm}_{\frac{1}{8}} + (I^{\pm}_{\frac{1}{8}})^* \mathrm{e}^{\mathrm{i}(-\nu_0 \pm Q)/4} \, , \tag{3.68}$$

$$\begin{aligned} I^{\mp *}_{\frac{1}{4}} &= I^{\mp *}_{\frac{1}{8}} + I^{\mp}_{\frac{1}{8}} \mathrm{e}^{-\mathrm{i}(-\nu_0 \mp Q)/4} = (I^{\mp *}_{\frac{1}{8}} \mathrm{e}^{\mathrm{i}(-\nu_0 \mp Q)/4} + I^{\mp}_{\frac{1}{8}}) \mathrm{e}^{-\mathrm{i}(-\nu_0 \mp Q)/4} \\ &= I^{\mp}_{\frac{1}{4}} \mathrm{e}^{-\mathrm{i}(-\nu_0 \mp Q)/4} \, . \end{aligned} \tag{3.69}$$

With mirror symmetric quadrants, the spin-orbit-coupling integral then simplifies to

$$I^{\pm} = I^{\pm}_{\frac{1}{4}}(1+\mathrm{e}^{\mathrm{i}(\alpha_1-\alpha_2\pm 2Q/4)}) + I^{\mp}_{\frac{1}{4}}(1+\mathrm{e}^{\mathrm{i}(-\alpha_2+\alpha_3\pm 2Q/4)})\mathrm{e}^{\mathrm{i}(\alpha_1 \pm 2Q/4)} \tag{3.70}$$

and again this additional symmetry does not simplify the compensation of the spin-orbit integrals.

Schemes with 8 Snakes: The same procedure can now be repeated with 8 snakes. For that purpose, 4 more horizontal Siberian Snakes are placed at the locations $jL/4 + \Delta l$, $j \in \{0, 1, 2, 3\}$. In terms of the integrals

$$I^{\pm}_0 = \int_0^{\Delta l} k\sqrt{\beta_y} \mathrm{e}^{\mathrm{i}(-\Psi \pm \Phi_y)} \mathrm{d}l \, , \quad I^{\pm}_1 = \int_{\Delta l}^{\frac{L}{4}} k\sqrt{\beta_y} \mathrm{e}^{\mathrm{i}(\Psi \pm \Phi_y)} \mathrm{d}l \, , \tag{3.71}$$

the spin-orbit coupling integrals of (3.48) are then

$$\begin{aligned} I^{\pm} = {} & I^{\pm}_0 (1 + \mathrm{e}^{\mathrm{i}(-\Psi_0+\alpha_1+\Psi_1-\alpha_2\pm(\Phi_{y0}+\Phi_{y1}))} + \ldots \\ & + \mathrm{e}^{\mathrm{i}(-\Psi_0+\alpha_1+\Psi_1-\alpha_2\mp\ldots-\alpha_{n-2}\pm(\Phi_{y0}+\ldots+\Phi_{yn-3}))}) \\ & + I^{\pm}_1 \mathrm{e}^{\mathrm{i}(-\Psi_0+\alpha_1\pm\Phi_{y0})}(1 + \mathrm{e}^{\mathrm{i}(\Psi_1-\alpha_2-\Psi_2+\alpha_3\pm(\Phi_{y1}+\Phi_{y2}))} + \ldots \\ & + \mathrm{e}^{\mathrm{i}(\Psi_1-\alpha_2-\Psi_2+\alpha_3\pm\ldots+\alpha_{n-1}\pm(\Phi_{y1}+\ldots+\Phi_{yn-2}))}) \, . \end{aligned} \tag{3.72}$$

If there is an additional mirror symmetry and the snakes are all placed in the symmetry points, (3.62) implies $I^{\pm}_1 = (I^{\pm}_0)^* \mathrm{e}^{\mathrm{i}(-\nu_0 \pm Q)/4}$, which again does not lead to simplifications. The complete spin phase advance of the ring is $\sum_{j=0}^{n}(-)^j(\Psi_j + \alpha_j) = \pi$. Because this phase advance is required to be independent of energy, $\sum_{j=0}^{n}(-)^j\Psi_j$ has to vanish. Because of the superperiodicity this requires $\Psi_0 = \Psi_1$, and all the spin phases Ψ_j in the equations (3.73) cancel. Then in terms of the difference angles $\Delta_{jk} = \alpha_j - \alpha_k$, spin matching the ring requires

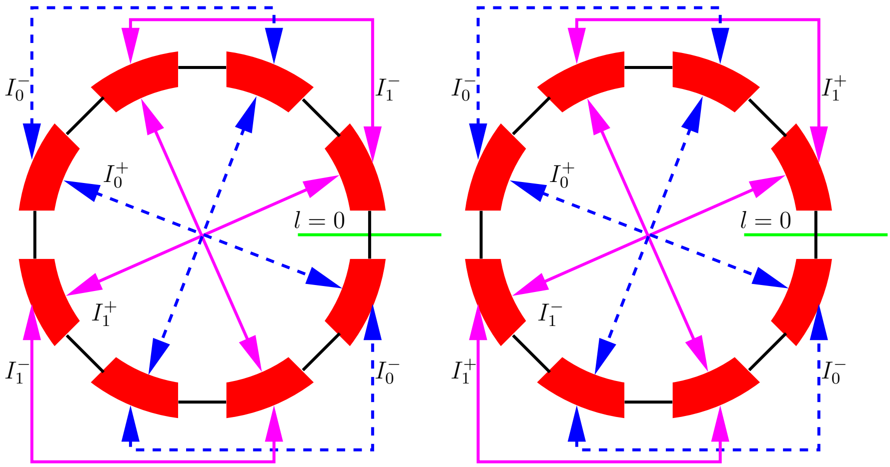

Fig. 3.13. The two possibilities by which the individual parts of the ring cancel the spin-orbit-coupling integrals. Changing the sign of Q leads to two corresponding snake schemes. The symbols I_0^+, I_0^-, I_1^+, and I_1^- indicate which part of the spin-orbit-coupling integrals are canceled.

$$1 + e^{i(\pm\frac{Q}{4}+\Delta_{12})} + e^{i(\pm 2\frac{Q}{4}+\Delta_{12}+\Delta_{34})} + e^{i(\pm 3\frac{Q}{4}+\Delta_{12}+\Delta_{34}+\Delta_{56})} = 0 \ , \quad (3.73)$$
$$1 + e^{i(\pm\frac{Q}{4}-\Delta_{23})} + e^{i(\pm 2\frac{Q}{4}-\Delta_{23}-\Delta_{45})} + e^{i(\pm 3\frac{Q}{4}-\Delta_{23}-\Delta_{45}-\Delta_{67})} = 0 \ . \quad (3.74)$$

Sets of 4 complex numbers with modulus 1 can only add up to zero by the three schemes shown in Fig. 3.10. The equations (3.73) and (3.74) have the same structure as the matching conditions of equations (3.53), and the relations (3.60) can therefore be used to obtain the following two ways to satisfy (3.73):

$$\Delta_{12} \stackrel{\circ}{=} \Delta_{56} \stackrel{\circ}{=} \pi - Q/4 \ , \quad \Delta_{34} \stackrel{\circ}{=} 3Q/4 \ , \quad (3.75)$$
$$\Delta_{12} \stackrel{\circ}{=} \Delta_{56} \stackrel{\circ}{=} \pi + Q/4 \ , \quad \Delta_{34} \stackrel{\circ}{=} -3Q/4 \ . \quad (3.76)$$

Equation (3.76) resulted from reversing the sign of Q in (3.75). There are also exactly two possibilities for solving (3.74),

$$\Delta_{23} \stackrel{\circ}{=} \Delta_{67} \stackrel{\circ}{=} \pi + Q/4 \quad , \quad \Delta_{45} \stackrel{\circ}{=} -3Q/4 \ , \quad (3.77)$$
$$\Delta_{23} \stackrel{\circ}{=} \Delta_{67} \stackrel{\circ}{=} \pi - Q/4 \quad , \quad \Delta_{45} \stackrel{\circ}{=} 3Q/4 \ . \quad (3.78)$$

There are now 4 possibilities to snake match the ring; these are obtained by combining the equations (3.75)&(3.77), (3.75)&(3.78), (3.76)&(3.77), or (3.76)&(3.78), where the last two possibilities also result from the first two by reversing the sign of Q. Figure 3.13 shows how parts of the ring cancel the depolarizing effects of other parts in these snake matching schemes.

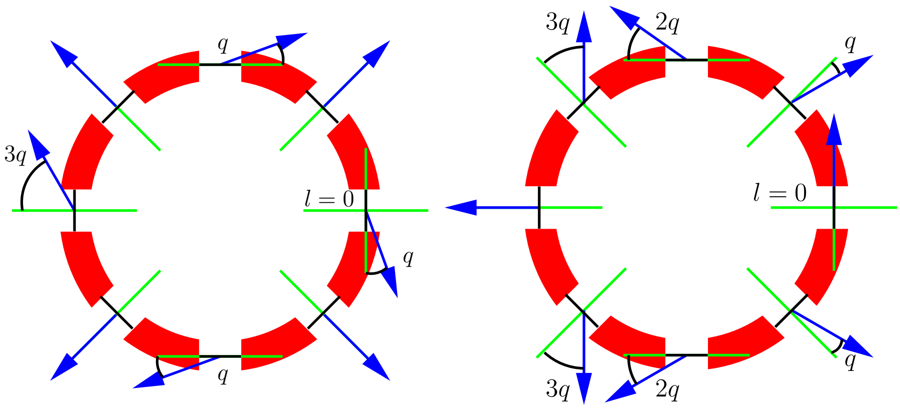

Fig. 3.14. Two of the 4 ways to snake match a ring with super-periodicity 4 using 8 horizontal Siberian Snakes. The number q denotes $Q/8 \bmod \pi$ and lies in $[0, \pi)$. The vertical tune times 2π is denoted by Q and $\nu = G\gamma 2\pi$. The other two possible snake schemes are obtained by reversing the sign of Q. When all snake angles are increased by the same amount, then the ring remains spin transparent. Note that the snake angle is independent of ν and thus of energy.

Because only differences in the snake angles appear, one of the angles can be chosen arbitrarily. This then fixes all other snake angles. For simplicity I choose $\alpha_1 = 0$. This leads to the following possibilities:

Combination of the equations (3.75) and (3.77):

$$\alpha_1 \overset{\circ}{=} 0\,,\ \alpha_2 \overset{\circ}{=} \pi + Q/4\,,\ \alpha_3 \overset{\circ}{=} 0\,,\ \alpha_4 \overset{\circ}{=} -3Q/4\,, \tag{3.79}$$

$$\alpha_5 \overset{\circ}{=} 0\,,\ \alpha_6 \overset{\circ}{=} \pi + Q/4\,,\ \alpha_7 \overset{\circ}{=} 0\,,\ \alpha_8 \overset{\circ}{=} \pi + Q/4\,. \tag{3.80}$$

Combination of the equations (3.75) and (3.78):

$$\alpha_1 \overset{\circ}{=} 0\,,\quad \alpha_2 \overset{\circ}{=} \pi + Q/4\,,\quad \alpha_3 \overset{\circ}{=} 2Q/4\,,\quad \alpha_4 \overset{\circ}{=} -Q/4\,, \tag{3.81}$$

$$\alpha_5 \overset{\circ}{=} -4Q/4\,,\quad \alpha_6 \overset{\circ}{=} \pi - 3Q/4\,,\quad \alpha_7 \overset{\circ}{=} -2Q/4\,,\quad \alpha_8 \overset{\circ}{=} \pi - Q/4\,. \tag{3.82}$$

The values for α_8 were obtained from the requirement $\alpha_8 - \alpha_7 + \alpha_6 - \alpha_5 + \alpha_4 - \alpha_3 + \alpha_2 - \alpha_1 \overset{\circ}{=} \pi$. The last snake scheme can be simplified by decreasing all snake angles by $2Q/4$, leading to

$$\alpha_1 \overset{\circ}{=} Q/4\,,\quad \alpha_2 \overset{\circ}{=} \pi + 2Q/4\,,\quad \alpha_3 \overset{\circ}{=} 3Q/4\,,\quad \alpha_4 \overset{\circ}{=} 0\,, \tag{3.83}$$

$$\alpha_5 \overset{\circ}{=} -3Q/4\,,\quad \alpha_6 \overset{\circ}{=} \pi - 2Q/4\,,\quad \alpha_7 \overset{\circ}{=} -Q/4\,,\quad \alpha_8 \overset{\circ}{=} \pi\,. \tag{3.84}$$

These snake schemes are shown in Fig. 3.14 where account has been taken of the fact that the actual angle between the snake's rotation axis and the radial direction is $\alpha/2$. Furthermore, advantage has been taken of the fact that the angle $\alpha/2$ only needs to be known modulo π.

Here it is very important to note that the snake angles are independent of $\nu = G\gamma$ and therefore that a snake match has been achieved for all energies. With 4 Siberian Snakes, such an energy independent spin match is not possible.

One could try to repeat the same procedure for a layout with 6 horizontal Siberian Snakes or with combinations of, for example, 6 horizontal Siberian Snakes and two type III snakes. Due to their 3-fold symmetry, this could be of special interest for the RHIC rings. These can be investigated using variations of the methods already presented.

3.3.3 Snake Matching HERA-p

Schemes with 4 snakes: When the spin-orbit-coupling integrals starting at an azimuth θ_0 are minimized, the opening angle of the invariant spin field at θ_0 for the approximation of linear spin-orbit motion is also minimized because

$$P_{lim} = [1+\sum_{k=1}^{3}(|B_{2k-1}|^2+|B_{2k}|^2)J_k]^{-\frac{1}{2}} \ , \ B_k = \frac{I_k}{\mathrm{e}^{\mathrm{i}2\pi(Q_k-\nu_0)}-1} \ . \quad (3.85)$$

according to (3.29).

When snake matching a ring with super-periodicity according to the previously described technique, then all spin-orbit-coupling integrals are zero at one azimuth of the ring, and in linearized spin-orbit motion, the invariant spin field is then parallel to $\boldsymbol{n}_0$ at θ_0 for all particles. It has been seen from the example of a ring with super-periodicity 4 that 8 Siberian Snakes can be used to snake match the spin-orbit-coupling integrals to zero at one azimuth of the ring for all energies. This could be achieved because the snake angles were used to adjust the spin phase advances in such a way that perturbations in one part of the ring were compensated by identical perturbations in one of the identical super-periods of the ring.

Because HERA-p does not posses such a symmetry, it is in general not possible to find snake angles that completely compensate all spin-orbit-coupling integrals. However, in Sect. 3.2.3 it was demonstrated that the 4 identical arc sections of HERA dominate the resonance strength of vertical motion. Thus it would make sense to arrange that the perturbing effect of these arcs cancel each other. A first step in this direction is a symmetrization of the quadrants by an *8fs* snake scheme.

The spin-orbit-coupling integrals from the first regular FODO cell to the last FODO cell of a regular arc in HERA-p will be denoted by $\hat{I}_y^+$ and $\hat{I}_y^-$ and the azimuths of the beginnings of the 4 regular arcs as θ_1, θ_2, θ_3, and θ_4. The central points of the south, west, north, and east straight sections are denoted by S, W, N, and E. The spin phase advances between the arcs are compensated using the snake angles φ_E, φ_N, and φ_W. The spin phase advance between θ_i and θ_j is denoted by Ψ_{ij}. These notations are indicated in Fig. 3.15.

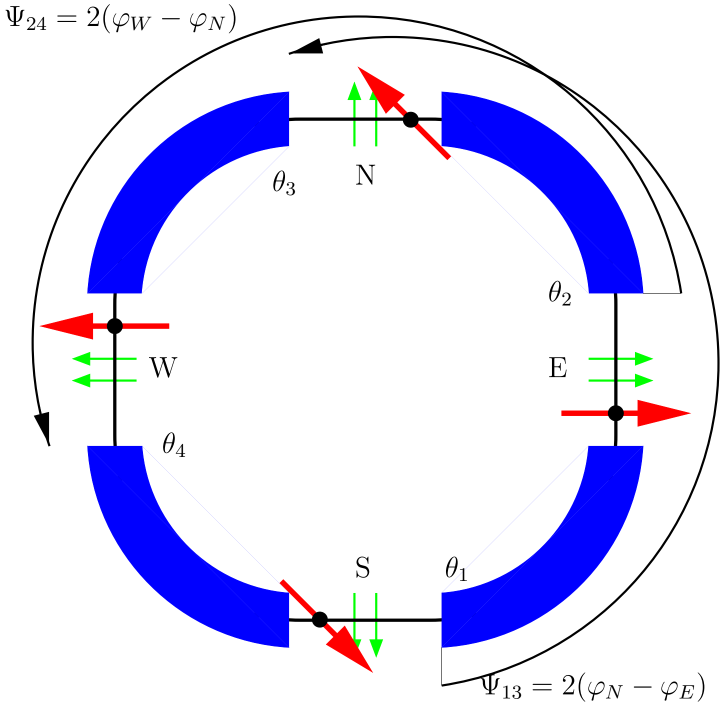

Fig. 3.15. The spin phase advance from the beginning of one regular arc to the beginning of the regular arc on the opposite side of the ring.

With Siberian Snakes in each of the straight sections, the spin phase advance from θ_1 to θ_3 is given by $\Psi_{13} = \Psi_{1E} - 2\varphi_E - \Psi_{EN} + 2\varphi_N + \Psi_{N3}$. In the $8fs$ schemes, the spin phase advance is identical in all quadrants of the ring, and the total spin phase advance is solely determined by the snake angles and is therefore independent of energy: $\Psi_{13} = 2(\varphi_N - \varphi_E)$ and $\Psi_{24} = 2(\varphi_W - \varphi_N)$. The orbital phase advance $\Phi_y(\theta_3) - \Phi_y(\theta_1)$ also does not depend on energy. For simplicity, $\Phi_y(\theta_j) - \Phi_y(\theta_i)$ will now be denoted by Φ_{ij}.

The spin-orbit-coupling integrals at the south interaction point therefore contain the following contributions from the 4 regular arcs:

$$
\begin{aligned}
I^+_{\text{arcs}} &= \hat{I}^+ \mathrm{e}^{\mathrm{i}(-\Psi_{S1}+\Phi_{S1})}(1 + \mathrm{e}^{\mathrm{i}[2(\varphi_E-\varphi_N)+\Phi_{13}]}) \\
&\quad + (\hat{I}^-)^* \mathrm{e}^{\mathrm{i}(2\varphi_E-\Psi_{SE}+\Psi_{E2}+\Phi_{S2})}(1 + \mathrm{e}^{\mathrm{i}[2(\varphi_W-\varphi_N)+\Phi_{24}]})
\end{aligned} \tag{3.86}
$$

$$
\begin{aligned}
I^-_{\text{arcs}} &= \hat{I}^- \mathrm{e}^{\mathrm{i}(-\Psi_{S1}-\Phi_{S1})}(1 + \mathrm{e}^{\mathrm{i}[2(\varphi_E-\varphi_N)-\Phi_{13}]}) \\
&\quad + (\hat{I}^+)^* \mathrm{e}^{\mathrm{i}(2\varphi_E-\Psi_{SE}+\Psi_{E2}-\Phi_{S2})}(1 + \mathrm{e}^{\mathrm{i}[2(\varphi_W-\varphi_N)-\Phi_{24}]})
\end{aligned} \tag{3.87}
$$

This shows that it is always possible to cancel one of the spin-orbit coupling integrals by choosing the snake angles so that the spin perturbation produced in one of the arcs is canceled by the arc on the opposite side of the ring. Because $|\hat{I}^+|$ and $|\hat{I}^-|$ are different, neighboring arcs can in general not compensate each other.

It is however possible to use the eight-snake scheme found for symmetric lattices. The two special 8 Siberian Snake schemes that lead to an energy independent snake match in a ring with super-periodicity 4 will not spin-match HERA-p completely, but the spin perturbation from the arcs, which has been shown to be the dominant perturbation in Sect. 3.2.3, will be compensated exactly. This possibility of having a set of Siberian Snake angles that do not have to be changed with energy and that lead to a tightly bundled invariant spin field is on the one hand very attractive; on the other hand it requires 8 Siberian Snakes of which 4 would have to be installed at the centers of the HERA-p arcs, where technical requirements of moving cryogenic feed-throughs and super-conducting magnets would be very costly. If possible, a four-snake scheme should therefore be found.

Whereas it was shown below (3.67) that a four-snake scheme cannot cancel both spin-orbit-coupling integrals in a ring with super-periodicity, a corresponding cancellation of the spin perturbation due to the arcs in HERA-p can nevertheless be achieved. This is possible because the orbital phase advances between the arcs can be manipulated individually, while these four phase advances are equal for a lattice with super-periodicity 4.

To cancel both spin-orbit integrals in (3.88), 4 phase factors have to be -1. This requires

$$2(\varphi_E - \varphi_N) + \Phi_{13} \overset{\circ}{=} \pi \ , \tag{3.88}$$

$$2(\varphi_E - \varphi_N) - \Phi_{13} \overset{\circ}{=} \pi \ , \tag{3.89}$$

$$2(\varphi_W - \varphi_N) + \Phi_{24} \overset{\circ}{=} \pi \ , \tag{3.90}$$

$$2(\varphi_W - \varphi_N) - \Phi_{24} \overset{\circ}{=} \pi \ . \tag{3.91}$$

For arbitrary betatron phase advances, this equation cannot be solved by a choice of Siberian Snakes, because there are only two free parameters that contain the snake angles. However, the betatron phase advances can be changed appropriately to obtain a complete spin match of the arcs in HERA-p. Subtraction of the first two equations leads to the requirement that the betatron phase advance from θ_1 half-way around the ring to θ_3 is an odd or even multiple of π. The same is true for the phase advance from θ_2 to θ_4. Correspondingly, the spin phase advance over these regions has to be an odd multiple of π when the orbit phase advance is an even multiple and vice versa. With a rather benign change of the vertical optics in HERA-p that does not change the vertical tune, the contribution of the regular arcs to both spin-orbit-coupling integrals can be canceled, even in a four-snake scheme.

The snake scheme $(0\frac{\pi}{2}\frac{\pi}{2}\frac{\pi}{2})8fs$ has $\Psi_{13} = 0$ and $\Psi_{24} = 0$. For this snake scheme, the betatron phase advances from θ_1 to θ_3 and from θ_2 to θ_4 were adjusted to be odd multiples of π. The maximum time-average polarization P_{lim} is plotted (blue) in Fig. 3.16 for the complete range of HERA-p momenta

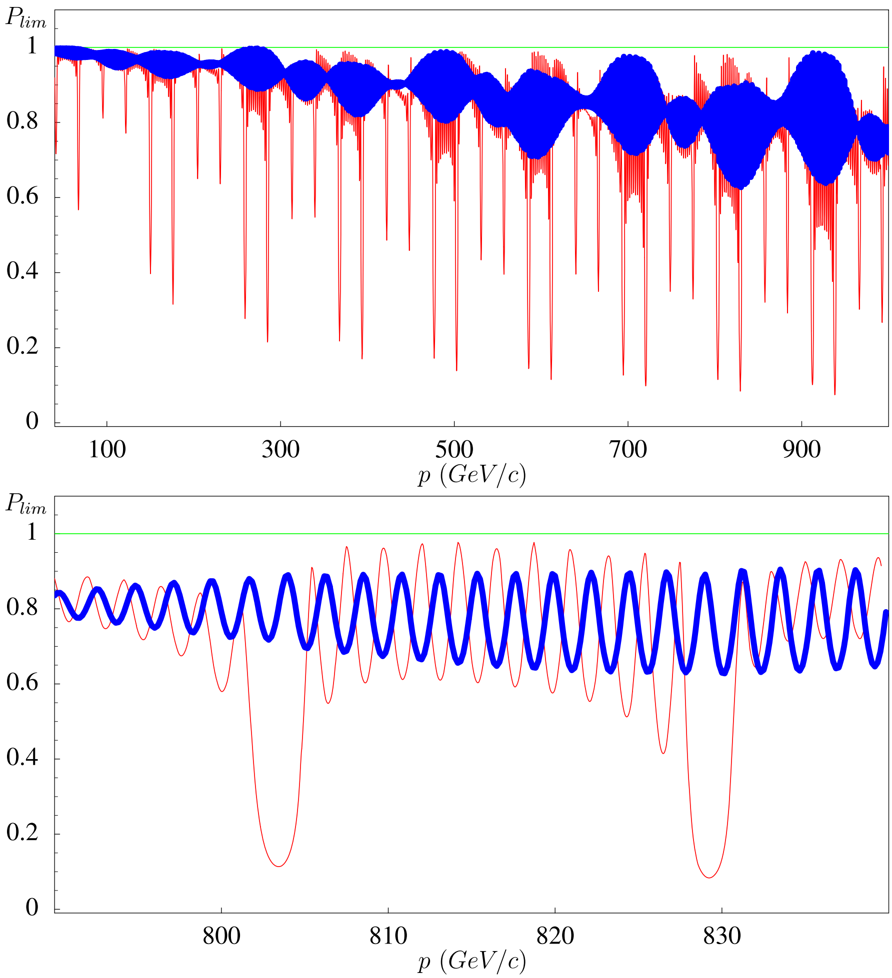

Fig. 3.16. Improvement of P_{lim} by matching 4 snake angles and the orbital phases. The snake arrangement is $(0\frac{\pi}{2}\frac{\pi}{2}\frac{\pi}{2})8fs$ (*blue*). As a comparison, P_{lim} from linearized spin-orbit motion is shown for the same HERA-p optics with a $(\frac{\pi}{4}0\frac{\pi}{4}0)8fs$ snake scheme (*red*).

and for the critical momentum regions above 800 GeV/c. As a comparison, P_{lim} for a standard snake scheme $(\frac{\pi}{4}0\frac{\pi}{4}0)$ (red) is also shown.

The complete snake match of the arcs in HERA-p in deed eliminates all strong reductions of P_{lim} over the complete momentum range. Nonlinear effects will be analyzed later, but as far as the linear effects are concerned, this snake matched lattice of HERA-p would be a rather promising choice for the acceleration of polarized proton beams.

Schemes with 8 Snakes: Although, for the reasons explained, eight snakes are not very practical for HERA-p, significant improvements are in principle possible when 8 snakes are used, as will now be shown. The snake matching schemes of Fig. 3.14 are suitable for rings with super-periodicity 4. They are therefore not directly applicable to HERA-p. However, the cancellation schemes of Fig. 3.13 can still provide a guide to snake matching HERA-p with 8 snakes.

The 8 Siberian Snakes are placed in the straight sections and into the centers of the arcs, so that the horizontal angle between adjacent Siberian Snakes is 45° and therefore $\Psi_j = G\gamma\pi/4$ for all $j \in \{0\dots7\}$. This ensures that the snake match is independent of energy because then the nth octant's contribution $I^{\pm}_{n-1}$ to the spin-orbit coupling integral $I^{\pm}$ can be compensated by the second neighbor's contributions $I^{\pm}_{n+1}$. In particular the Ψ_j cancel in the phase factor in

$$I^{\pm}_{n-1} + \mathrm{e}^{\mathrm{i}[(-1)^n(\Psi_{n-1}-\alpha_n-\Psi_n+\alpha_{n+1})\pm(\Phi_{yn-1}+\Phi_{yn})]} I^{\pm}_{n+1} \ . \tag{3.92}$$

We now seek to construct a snake scheme for HERA-p that is guided by the cancellation scheme of Fig. 3.13 (left). When the first octant's contribution $I^{\pm}_0$ to a spin-orbit coupling integral $I^{\pm}$ is to be compensated by that of its second neighbor $I^{\pm}_2$, the phase factor in

$$I^{\pm}_0 + \mathrm{e}^{\mathrm{i}[-\Psi_0+\alpha_1+\Psi_1-\alpha_2\pm(\Phi_{y0}+\Phi_{y1})]} I^{\pm}_2 \tag{3.93}$$

should be -1. The same should be true for the phase factor in

$$I^{\pm}_4 + \mathrm{e}^{\mathrm{i}[-\Psi_4+\alpha_5+\Psi_5-\alpha_6\pm(\Phi_{y4}+\Phi_{y5})]} I^{\pm}_6 \ . \tag{3.94}$$

These conditions are satisfied for the superscript + as well as − when all the snake angles α_j are zero for $j \in \{1, 2, 5, 6\}$ and the betatron phase advances are chosen appropriately. Similar conditions arise for the phase factors involved in matching I_1 against I_3 and in matching I_5 against I_7. They are also -1 when the betatron phases are chosen appropriately and when α_3 and α_7 are zero. Because α_0 and α_4 do not appear in these matching conditions, they can be chosen freely. But for a closed-orbit spin tune of 0.5, one has to choose $\alpha_0 + \alpha_4 = \pi$. Here $\alpha_4 = 0$ has been chosen, and this snake scheme is then characterized as $(\frac{\pi}{2}0000000)8fs$.

In the case of HERA-p, we cannot cancel the spin-orbit integrals of complete octants, but we can cancel the contribution of the regular arc sections. Therefore, we do not choose the betatron phase advance $\Phi_0 + \Phi_1 \overset{\circ}{=} \pi$ between Siberian Snakes, but rather the betatron phase advances between the beginning of the regular arcs of the first and the second quadrant are chosen in that way, i.e., $\Phi_{12} \overset{\circ}{=} \pi$ with the notation of Fig. 3.15. In this configuration, the regular arc of the first octant cancels that of the third, i.e., the regular arc's contribution to I_2 cancels that to I_0. But also the regular arc of the second octant cancels that of the fourth because the betatron phase advance between the centers of the first and the second arc is then also π mod 2π, i.e., the regular arc part of I_3 cancels that of I_1. Similarly, the octants of the third quadrant cancel those of the fourth quadrant. In the snake scheme $(\frac{\pi}{2}0000000)8fs$, the phase advance over the east straight section was changed by $2\pi \times 0.1028$ to have $\Phi_{12} = 2\pi \times 8.5$. The phase advance over the west was changed by $2\pi \times 0.0208$ to have $\Phi_{34} = 2\pi \times 7.5$. In order to have the same betatron phase advance in the north and the south straight sections and to keep the total tune constant, the linear optics of the north and of the south straight sections were modified.

This cancellation scheme does not agree completely with that of Fig. 3.13 (left) because in $(\frac{\pi}{2}0000000)8fs$ the superscripts + and − have been dealt with simultaneously so that $I_0^{\mp}$ no longer has to compensate $I_4^{\mp}$. Because $\Phi_{12} \overset{\circ}{=} \pi$ and $\Phi_{34} \overset{\circ}{=} \pi$, it is appropriate to take $q = \pi/2$ for the phase advance of one octant of the scheme in Fig. 3.14 (left), for which one then finds a close similarity to the snake scheme $(\frac{\pi}{2}0000000)8fs$. The resemblance would be even closer if the phase advance over the north straight section had been changed so that $\Phi_{23} \overset{\circ}{=} 0$ and if $\alpha_4 = \pi$, $\alpha_0 = 0$ had been chosen. This would require an additional change of Φ_{41} to adjust the orbital tune.

A snake scheme for HERA-p that resembles Fig. 3.13 (right) can also be found. In this cancellation scheme, the phase factors in the following sums have to be −1:

$$I_0^+ + \mathrm{e}^{\mathrm{i}[-\Psi_0+\alpha_1+\Psi_1-\alpha_2+(\Phi_{y0}+\Phi_{y1})]} I_2^{\pm} \tag{3.95}$$

$$I_4^+ + \mathrm{e}^{\mathrm{i}[-\Psi_4+\alpha_5+\Psi_5-\alpha_6+(\Phi_{y4}+\Phi_{y5})]} I_6^{\pm} \tag{3.96}$$

$$I_0^- + \mathrm{e}^{\mathrm{i}[-\Psi_0+\alpha_1+\Psi_1-\alpha_2-\Psi_2+\alpha_3+\Psi_3-\alpha_4-(\Phi_{y0}+\Phi_{y1}+\Phi_{y2}+\Phi_{y3})]} I_4^{\pm} \tag{3.97}$$

$$I_2^- + \mathrm{e}^{\mathrm{i}[-\Psi_2+\alpha_3+\Psi_3-\alpha_4-\Psi_4+\alpha_5+\Psi_5-\alpha_6-(\Phi_{y2}+\Phi_{y3}+\Phi_{y4}+\Phi_{y5})]} I_6^{\pm} \tag{3.98}$$

$$I_1^- + \mathrm{e}^{\mathrm{i}[\Psi_1-\alpha_2-\Psi_2+\alpha_3-(\Phi_{y1}+\Phi_{y2})]} I_3^{\pm} \tag{3.99}$$

$$I_5^- + \mathrm{e}^{\mathrm{i}[\Psi_5-\alpha_6-\Psi_6+\alpha_7-(\Phi_{y5}+\Phi_{y6})]} I_7^{\pm} \tag{3.100}$$

$$I_1^+ + \mathrm{e}^{\mathrm{i}[\Psi_1-\alpha_2-\Psi_2+\alpha_3+\Psi_3-\alpha_4-\Psi_4+\alpha_5+(\Phi_{y1}+\Phi_{y2}+\Phi_{y3}+\Phi_{y4})]} I_5^{\pm} \tag{3.101}$$

$$I_3^+ + \mathrm{e}^{\mathrm{i}[\Psi_3-\alpha_4-\Psi_4+\alpha_5+\Psi_5-\alpha_6-\Psi_6+\alpha_7+(\Phi_{y3}+\Phi_{y4}+\Phi_{y5}+\Phi_{y6})]} I_7^{\pm} \tag{3.102}$$

Again, we cannot cancel complete octants, but to cancel the contributions of regular arc sections, we again choose the beginning of a regular arc as the starting point for the compensation. Now the Φ_{yn} for all even n describe the betatron phase advance from the beginning to the center of the regular arc, and they are therefore equal. For the choice $\alpha_4 = 0$, all phase factors are −1 if and only if $\Phi_{y5} = \Phi_{y1}$ and

$$\alpha_1 \overset{\circ}{=} \Phi_{23}\ , \quad \alpha_2 \overset{\circ}{=} \Phi_{13}\ , \quad \alpha_3 \overset{\circ}{=} \Phi_{14}\ , \tag{3.103}$$

$$\alpha_5 = -\alpha_3\ , \quad \alpha_6 = -\alpha_2\ , \quad \alpha_7 = -\alpha_1\ . \tag{3.104}$$

This snake scheme is referred to as $(\frac{\pi}{2}abc0\text{-}c\text{-}b\text{-}a)8fs$. The condition $\Phi_{y5} = \Phi_{y1}$ was satisfied by changing the betatron phase advance over the east and west straight section without changing the vertical tune.

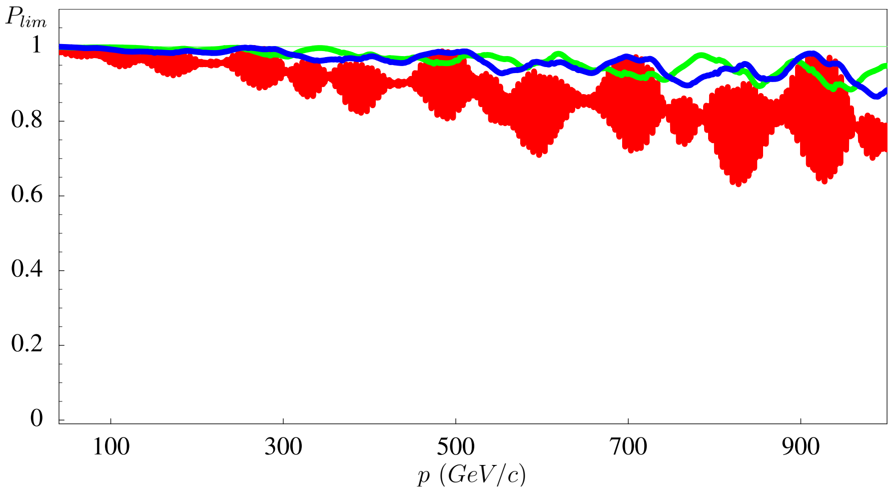

Fig. 3.17. Improvement of P_{lim} by matching 8 snake angles and the orbital phases. The snake arrangement is $(\frac{\pi}{2}0000000)8fs$ (*blue*) and $(\frac{\pi}{2}abc0\text{-}c\text{-}b\text{-}a)8fs$ (*green*). As a comparison, P_{lim} from linearized spin-orbit motion is shown for the snake and phase advance matched four-snake scheme $(0\frac{\pi}{2}\frac{\pi}{2}\frac{\pi}{2})8fs$ (*red*).

Linearized spin-orbit motion leads to a very favorable P_{lim} for both eight-snake schemes as shown in Fig. 3.17, where it is compared with the P_{lim} of the snake and phase advance matched four-snake scheme $(0\frac{\pi}{2}\frac{\pi}{2}\frac{\pi}{2})8fs$.

References

1. A. W. Chao: Polarization of a stored electron beam. In *Conference proceedings 87*. US Particle Accelerator School, Batavia, USA, American Institute of Physics (1981)
2. A. W. Chao: Evaluation of radiative spin polarization in an electron storage ring. *Nucl. Instr. Meth.* 180:29 (1981)
3. D. P. Barber, J. Kewisch, G. Ripken, R. Rossmanith, and R. Schmidt: A solenoid spin rotator for large electron storage rings. *Particle Accelerators*, 17:243–262 (1985)
4. H. Mais and G. Ripken: Theory of spin-orbit motion in electron-positron storage rings. DESY–83–062 (1983)
5. G. H. Hoffstaetter and M. Vogt: SPRINT users guide and reference manual. DESY (2002)
6. K. Heinemann and G. H. Hoffstaetter: A tracking algorithm for the stable spin polarization field in storage rings using stroboscopic averaging. *Phys. Rev.* E 54:4240–4255 (1996)
7. S. R. Mane: Electron-spin polarization in high-energy storage rings. II. Evaluation of the equilibrium polarization. *Phys. Rev.* A(36):120–130 (1987)
8. D. P. Barber and G. Ripken: Radiative polarization in electron storage rings. In A. W. Chao and M. Tigner, editors. *Handbook of accelerator physics and engineering.* World Scientific (1999)
9. A. W. Chao and K. Yokoya: An alternative longitudinal polarization scheme for TRISTAN. KEK–81–7, Tsukuba (1981)
10. K. Yokoya: Improvement of radiative polarization in plane storage rings. In *Polarized Electron Acceleration and Storage.* DESY–M–82–09 and KEK–81–19, Tsukuba (1982)
11. A. W. Chao: In *Polarized Electron Acceleration and Storage*, DESY–M–82–09 (1982)
12. E. D. Courant and H. S. Snyder: Theory of the alternating-gradient synchrotron. *Ann. Phys.* 3:1–48 (1958)
13. K. Steffen: Strong spin matching with and without snakes, a scheme for preserving polarization in large ring accelerators. DESY–88–068 (1988)
14. K. Steffen: Sample lattices for polarized proton acceleration in the SSC. In SSC–SR–1036, SSC Central Design Group (1988)
15. S. R. Mane: Analytical solutions for the invariant spin field for model storage rings. *Nucl. Instr. Meth. A*485:277–297 (2002)
16. S. R. Mane: MILES: a new nonperturbative formalism to calculate the invariant spin field in circular accelerators. *Nucl. Instr. Meth. A*498:1–15 (2003)
17. G. H. Hoffstaetter: Polarized protons in HERA. *Nuclear Physics* A666&667:203–213 (2000)
18. SPIN Collaboration and the DESY Polarization Team: Acceleration of polarized protons to 820 GeV at HERA. UM–HE–96–20, University of Michigan (1996)
19. R. Baiod, C. M. Chu, E. D. Courant, Ya. S. Derbenev, *et al*: A Siberian Snake with overlapping depolarizing resonances. *Phys. Rev. Lett.* 70(17):2557–2560 (1993)
20. S. Y. Lee: *Spin dynamics and Snakes in synchrotrons.* World Scientific (1997)

21. Ya. S. Derbenev and A. M. Kondratenko: Acceleration of polarized particles. *Sov. Phys. Doklady*, 20:562, 1976. also in Russian: *Dokl. Akad. Nauk Ser. Fiz.* 223:830-833 (1975)
22. V. Balandin, N. Golubeva, and D. P. Barber: Studies of the behavior of proton spin motion in HERA-p at high energies. DESY–M–96–04 (1996)
23. D. P. Barber and A. De Roeck, editors: *Proceedings of Polarized Protons at High Energies*, DESY–Proceedings–1999–03 (1999)
24. V. Anferov: 820 GeV/c polarized protons in HERA, SPIN@HERA report update. In [23].
25. A. W. Chao: Workshop summary – accelerator issues. In [23].
26. V. Ptitsin and Yu. M. Shatunov: The investigation of spin resonances in an accelerator with Siberian Snakes. In C. W. de Jager, T. J. Ketel, P. J. Mulders, J. E. J. Oberski, and M. Oskam-Tamoezer, editors, *Proceedings SPIN96*, p. 516–518. World Scientific (1996)
27. E. D. Courant: Hybrid helical snakes and rotators for RHIC. BNL–61920, Brookhaven (1995)
28. Ya. S. Derbenev: Private communication (1998)
29. G. H. Hoffstaetter: Polarized protons in HERA. In DESY–96–05 (1996)
30. H. Rose: Hamiltonian magnetic optics. *Nucl. Instr. Meth.* A258:374–401 (1987)
31. R. Degenhardt: *Korrektur von Aberrationen in der Teilchenoptik mit Hilfe von Symmetrien.* Doctoral thesis, Darmstadt University of Technology (1992)
32. W. Wan: *A Theory of Arbitrary Order Achromats.* PhD thesis, Michigan State University (1995)
33. G. H. Hoffstaetter: Comments on aberration correction in symmetric imaging energy filters. *Nucl. Instr. Meth.* A(427):275–281 (1998)

4 Higher-Order Spin Motion

4.1 Higher-Order Resonances and Snake Schemes

At the critical energies, where the maximum time-average polarization is low during the acceleration process, linearized spin-orbit motion does not describe spin dynamics well. When the spin motion is influenced by several resonance strength in these regions, also the SRM cannot be applied. Thus the simulation results obtained with these computationally quick techniques should always be checked with more time consuming non-perturbative methods if possible. This is also true for the snake-matched lattice of HERA-p with large P_{lim} described in Sect. 3.3.3, even though it avoids large variations of the invariant spin field $\boldsymbol{n}(\boldsymbol{z})$ over the phase space of the beam in linearized spin-orbit motion. When first-order effects are canceled, the higher-order effects become dominant and the quality of the snake-matched lattice of HERA-p can only be evaluated with higher-order theories.

Until 1996, when stroboscopic averaging [1] was introduced, there was no non-perturbative method of computing the $\boldsymbol{n}$-axis at high energy in proton storage rings, where perturbative methods are usually not sufficient [2]. In addition, the method of anti-damping was derived, which also computes $\boldsymbol{n}(\boldsymbol{z})$ non-perturbatively and which can be faster when the $\boldsymbol{n}$-axis is required for a range of phase space amplitudes. Both methods of computing the invariant spin field are implemented in the spin-orbit dynamics code SPRINT, by which also the amplitude-dependent spin tune $\nu(\boldsymbol{J})$ can be computed once $\boldsymbol{n}(\boldsymbol{z})$ is known. Because stroboscopic averaging and anti-damping are based on multi-turn tracking data, they are applicable to all kinds of circular accelerators and they are especially efficient for small rings and for simple model accelerators. Stroboscopic averaging has for example been used to verify solutions for the simple accelerator models with Siberian Snakes in [3, 4].

More recently, a non-perturbative algorithm for computing $\boldsymbol{n}(\boldsymbol{z})$ and $\nu(\boldsymbol{J})$ has been derived [5]. It is called SODOM-2 because it was inspired by the earlier algorithm SODOM [6], which for convergence required the angle between $\boldsymbol{n}$ and $\boldsymbol{n}_0$ to be small. With some routines provided by K. Yokoya, SODOM-2 was incorporated into the program SPRINT [7, 1, 8] and leads to results that agree very well with those of stroboscopic averaging. For motion in one degree of freedom, SODOM-2 is often faster than stroboscopic averaging, especially for large rings like HERA-p where particle tracking is relatively time consuming. But for orbit motion in more than one degree of freedom or in the vicinity of spin-orbit resonances, SODOM-2 becomes exceedingly slow and then stroboscopic averaging and anti-damping are needed. They will be introduced later, but first SODOM-2 will be described.

4.1.1 Computing $\boldsymbol{n}$ and $\nu(\boldsymbol{J})$ by SODOM-2

For phase space motion on an invariant torus, the final angle variables after one turn starting at the angle variables $\boldsymbol{\Phi}_i$ are $\boldsymbol{\Phi}_f = \boldsymbol{\Phi}_i + 2\pi\boldsymbol{Q}$ where the tunes $\boldsymbol{Q}$ can depend on $\boldsymbol{J}$. A spin field $\boldsymbol{f}(\boldsymbol{\Phi},\theta)$ can be described in terms of a spinor $\Psi(\boldsymbol{\Phi},\theta)$ as $\boldsymbol{f}(\boldsymbol{\Phi},\theta) = \Psi^\dagger\boldsymbol{\sigma}\Psi$. Because the action variables $\boldsymbol{J}$ are constants of motion, they are not indicated here. A multiplication of Ψ with an arbitrary phase factor does not change the corresponding spin field. According to (2.47), the spin field after one turn can be described by

$$\Psi(\boldsymbol{\Phi} + 2\pi\boldsymbol{Q}, \theta_0 + 2\pi) = A(\boldsymbol{\Phi})\Psi(\boldsymbol{\Phi}, \theta_0) \; , \tag{4.1}$$

where $A(\boldsymbol{\Phi})$ is the phase space dependent spin transport quaternion for one turn around the ring starting at azimuth θ_0.

Let an invariant spin field on the Poincaré section at θ_0 be described by the spinor $\psi_n(\boldsymbol{\Phi})$. If the initial spin $\boldsymbol{S}_i$ of a particle is parallel to $\boldsymbol{n}(\boldsymbol{\Phi}_i)$, it is described by $\psi_n(\boldsymbol{\Phi}_i)$. After one turn, the final spin $\boldsymbol{S}_f$ is then parallel to $\boldsymbol{n}(\boldsymbol{\Phi}_i + 2\pi\boldsymbol{Q})$ and can be described by $A(\boldsymbol{\Phi}_i)\psi_n(\boldsymbol{\Phi}_i)$ as well as by $\psi_n(\boldsymbol{\Phi}_i + 2\pi\boldsymbol{Q})$. These two spinors therefore have to agree up to an arbitrary phase,

$$A(\boldsymbol{\Phi})\psi_n(\boldsymbol{\Phi}) = \mathrm{e}^{-\mathrm{i}\pi\tilde{\nu}_{\boldsymbol{J}}(\boldsymbol{\Phi})}\psi_n(\boldsymbol{\Phi} + 2\pi\boldsymbol{Q}) \; . \tag{4.2}$$

We now seek a function $\phi_{\boldsymbol{J}}(\boldsymbol{\Phi})$ such that for a new spinor $\Psi_n(\boldsymbol{\Phi}) = \mathrm{e}^{\mathrm{i}\frac{1}{2}\phi_{\boldsymbol{J}}(\boldsymbol{\Phi})}\psi_n(\boldsymbol{\Phi})$ we have the periodicity condition

$$A(\boldsymbol{\Phi})\Psi_n(\boldsymbol{\Phi}) = \mathrm{e}^{-\mathrm{i}\pi\nu(\boldsymbol{J})}\Psi_n(\boldsymbol{\Phi} + 2\pi\boldsymbol{Q}) \; , \tag{4.3}$$

where the phase factor does not depend on the angle variables $\boldsymbol{\Phi}$. The $\nu(\boldsymbol{J}) = 2\pi\tilde{\nu}_{\boldsymbol{J}}(\boldsymbol{\Phi}) - \phi_{\boldsymbol{J}}(\boldsymbol{\Phi}) + \phi_{\boldsymbol{J}}(\boldsymbol{\Phi} + 2\pi\boldsymbol{Q})$ is the amplitude-dependent spin tune introduced in Sect. 2.2.7. Here we see how it appears when spinors are used. A function $\phi_{\boldsymbol{J}}(\boldsymbol{\Phi})$ has already appeared in (2.87). It was then shown that $\nu(\boldsymbol{J})$ is, apart from the addition of an arbitrary linear combination of the orbital tunes Q_i, given by the zeroth Fourier component of $\tilde{\nu}_{\boldsymbol{J}}(\boldsymbol{\Phi})$.

The one turn spin transport quaternion $A(\boldsymbol{\Phi})$ can be determined numerically by transporting particles with spin around a model of the circular accelerator. It is then a 2π-periodic function of $\boldsymbol{\Phi}$ and can be written as a Fourier series. The spinor Ψ_n of the invariant spin field will also be written as a Fourier expansion,

$$A(\boldsymbol{\Phi}) = \sum_{\boldsymbol{j}} A_{\boldsymbol{j}}\mathrm{e}^{\mathrm{i}\boldsymbol{j}\cdot\boldsymbol{\Phi}} \; , \quad \Psi_n(\boldsymbol{\Phi}) = \sum_{\boldsymbol{j}} \Psi_{n,\boldsymbol{j}}\mathrm{e}^{\mathrm{i}\boldsymbol{j}\cdot\boldsymbol{\Phi}} \; . \tag{4.4}$$

The periodicity condition then reads as

$$\mathrm{e}^{-\mathrm{i}2\pi\boldsymbol{j}\cdot\boldsymbol{Q}}\sum_{\boldsymbol{k}}A_{\boldsymbol{j}-\boldsymbol{k}}\Psi_{n,\boldsymbol{k}}=\mathrm{e}^{-\mathrm{i}\pi\nu}\Psi_{n,\boldsymbol{j}}\ . \tag{4.5}$$

This is an eigenvector equation for the infinite-dimensional matrix with components $\mathrm{e}^{-\mathrm{i}2\pi\boldsymbol{j}\cdot\boldsymbol{Q}}A_{\boldsymbol{j}-\boldsymbol{k}}$. When an eigenvector with components $\Psi_{n,\boldsymbol{j}}$ for the eigenvalue $\mathrm{e}^{-\mathrm{i}\pi\nu}$ is found, then the spin tune ν and the spinor $\Psi_n(\boldsymbol{\Phi})=\sum_{\boldsymbol{j}}\Psi_{n,\boldsymbol{j}}\mathrm{e}^{\mathrm{i}\boldsymbol{j}\cdot\boldsymbol{\Phi}}$ can be computed, which in turn leads to the $\boldsymbol{n}$-axis.

For some vector of integers $\boldsymbol{l}$, the vector with components $\Psi'_{n,\boldsymbol{j}}=\Psi_{n,\boldsymbol{j}-\boldsymbol{l}}$ is also an eigenvector corresponding to the eigenvalue $\mathrm{e}^{-\mathrm{i}\pi(\nu-2\boldsymbol{l}\cdot\boldsymbol{Q})}$ because

$$\mathrm{e}^{-\mathrm{i}2\pi\boldsymbol{j}\cdot\boldsymbol{Q}}\sum_{\boldsymbol{k}}A_{\boldsymbol{j}-\boldsymbol{k}}\Psi'_{n,\boldsymbol{k}}=\mathrm{e}^{-\mathrm{i}\pi(\nu+2\boldsymbol{l}\cdot\boldsymbol{Q})}\Psi'_{n,\boldsymbol{j}}\ . \tag{4.6}$$

This leads to the spin tune $\nu+2\boldsymbol{l}\cdot\boldsymbol{Q}$ and to the spinor $\Psi'_n(\boldsymbol{\Phi})=\mathrm{e}^{\mathrm{i}\boldsymbol{l}\cdot\boldsymbol{\Phi}}\Psi_n(\boldsymbol{\Phi})$, which also represents $\boldsymbol{n}(\boldsymbol{z})$.

The spinor $\Psi''_n=i\sigma_2\Psi^*_n$ represents $\boldsymbol{n}''=-\boldsymbol{n}(\boldsymbol{z})$, because

$$\boldsymbol{n}''=\boldsymbol{n}''^*=(\Psi''^{\dagger}_n\boldsymbol{\sigma}\Psi''_n)^*=\Psi^{\dagger}_n\sigma^{\dagger}_2\boldsymbol{\sigma}^*\ \sigma_2\Psi_n=-\Psi^{\dagger}_n\boldsymbol{\sigma}\Psi_n=-\boldsymbol{n}\ , \tag{4.7}$$

where use was made of the relations $\sigma^{\dagger}_2=\sigma_2$ and $\sigma^*_2=-\sigma_2$. This spinor has the Fourier coefficients $\Psi''_{n,\boldsymbol{j}}=i\sigma_2(\Psi_{n,-\boldsymbol{j}})^*$. Similarly, the Fourier coefficients of A^* are $(A^*)_{\boldsymbol{j}}=(A_{-\boldsymbol{j}})^*$. Thus when $\Psi^*_n=-\mathrm{i}\sigma_2\Psi''_n$ is inserted into the complex conjugation of (4.5), one obtains

$$\mathrm{e}^{\mathrm{i}2\pi\boldsymbol{j}\cdot\boldsymbol{Q}}\sum_{\boldsymbol{k}}(A_{\boldsymbol{j}-\boldsymbol{k}})^*\sigma_2\Psi''_{n,-\boldsymbol{k}}=\mathrm{e}^{\mathrm{i}\pi\nu}\sigma_2\Psi''_{n,-\boldsymbol{j}}\ . \tag{4.8}$$

Now, with $\sigma^2_2=1_2$ and $\sigma_2A^*\sigma_2=\sigma_2(a_01_2+\mathrm{i}\boldsymbol{a}\cdot\boldsymbol{\sigma^*})\sigma_2=a_01_2-\mathrm{i}\boldsymbol{a}\cdot\boldsymbol{\sigma}=A$ and after reversing the sign of $\boldsymbol{j}$ and $\boldsymbol{k}$, one finds

$$\mathrm{e}^{-\mathrm{i}2\pi\boldsymbol{j}\cdot\boldsymbol{Q}}\sum_{\boldsymbol{k}}A_{\boldsymbol{j}-\boldsymbol{k}}\Psi''_{n,\boldsymbol{k}}=\mathrm{e}^{\mathrm{i}\pi\nu}\Psi''_{n,\boldsymbol{j}}\ . \tag{4.9}$$

The vector with components $\Psi''_{n,\boldsymbol{k}}$ is therefore an eigenvector to the eigenvalue $\mathrm{e}^{\mathrm{i}\pi\nu}$, which leads to the spin tune $-\nu$. This is consistent with the statement in Sect. 2.2.7 that instead of ν also $\pm\nu+j_0+\boldsymbol{j}\cdot\boldsymbol{Q}$ can be chosen as spin tune.

The eigenvalues described here have only even integers, i.e., $\boldsymbol{j}=2\boldsymbol{l}$. Odd integers appear when $\mathrm{e}^{\mathrm{i}\frac{1}{2}\boldsymbol{l}\cdot\boldsymbol{\Phi}}\Psi(\boldsymbol{\Phi})$ is used to describe an $\boldsymbol{n}$-axis. However, this spinor is not 2π-periodic and can thus not be determined by the Fourier expansion in (4.4). Therefore, the corresponding spin tunes with odd integers in $\boldsymbol{j}$ cannot be found as eigenvalues of (4.5).

When all Fourier harmonics above a given order N are neglected in (4.5), this is an eigenvector problem for a square matrix with 2×2-dimensional matrix components $\mathrm{e}^{-\mathrm{i}2\pi\boldsymbol{j}\cdot\boldsymbol{Q}}A_{\boldsymbol{j}-\boldsymbol{k}}$. Because the square matrix can have several eigenvectors and eigenvalues, the result is not unique.

So far there are no rigorous arguments or proofs about properties of the eigenvalue spectrum of the matrix in (4.5) for a given N. If the number of considered Fourier coefficients is large, one would expect, even though no proof has been given so far, that each eigenvalue of the matrix leads to a good approximation of one possible spin tune. And again for high enough values of N, each eigenvector of the matrix should usually provide a good approximation of one possible spinor Ψ_n and all eigenvectors should then, up to a sign, correspond to the same $\boldsymbol{n}$-axis with high accuracy.

In fact, it has been shown numerically that the various ν computed with SODOM-2 really do differ by multiples of the orbit tune to a high accuracy [5] and that all the resulting $\boldsymbol{n}$-axes are the same to a high degree of accuracy. Moreover, the $\boldsymbol{n}$-axis and ν obtained by SODOM-2 agree well with those obtained by stroboscopic averaging or anti-damping described in Sect. 4.2 and Sect. 4.3.

It has turned out useful to find the eigenvector with the largest zero-Fourier harmonic $|\Psi_{n(0,0,0)}|$ and to determine the spin tune ν from the corresponding eigenvalue. For all results that were obtained with the SODOM-2 method and that will be presented below, only vertical motion was considered and 81 Fourier coefficients were used. And all spin tunes ν that will be given correspond to the spinor with the largest Fourier coefficient $|\Psi_{n(0,0,0)}|$.

4.1.2 Nonlinear Spin Dynamics for Vertical Particle Motion

To check whether the improvements of spin motion obtained in the framework of linearized spin-orbit motion presented in Sect. 3.1 survive when higher-order effects are considered, P_{lim} and ν has been calculated by the SODOM-2 algorithm with the code SPRINT. The result for one of the standard Siberian Snake schemes that used to be considered advantageous by popular opinion is shown for the south interaction point of HERA-p in Fig. 4.1. It has four Siberian Snakes in the $(\frac{\pi}{4}0\frac{\pi}{4}0)6fs$ scheme. Some of the features of P_{lim} were already revealed by linearized spin-orbit motion in Figs. 2.15 and 3.8. Now many higher-order resonances are revealed, causing strong reduction of P_{lim}, and there are corresponding strong variations of the amplitude-dependent spin tune ν [9, 10]. Strong resonances occur especially in the critical energy region where linearized spin-orbit motion in Sect. 3.3 already indicated a very small P_{lim} due to a coherent spin perturbation in all regular FODO cells. Many higher-order resonances overlap in these critical energy regions of Fig. 4.1 (top) where large spin tune jumps can be observed in Fig. 4.1 (bottom). The strongest spin tune jumps occur in the critical energy regions, mostly at the second-order resonance $\nu = 2Q_y$, which is indicated by the top line [12].

Here only 6 flattening snakes were used, and one might think that symmetrizing the ring by 2 additional flattening snakes in the west might reduce the spin tune spread and might lead to an increase of P_{lim}. But because the orbital phase advance between different sections of the ring is not matched by the snake angles in the standard snake schemes like $(\frac{\pi}{4}0\frac{\pi}{4}0)$, the symmetry recovered in the *8fs* scheme does not lead to a significant improvement. Moreover, the special choice of the vertical betatron phase advance described

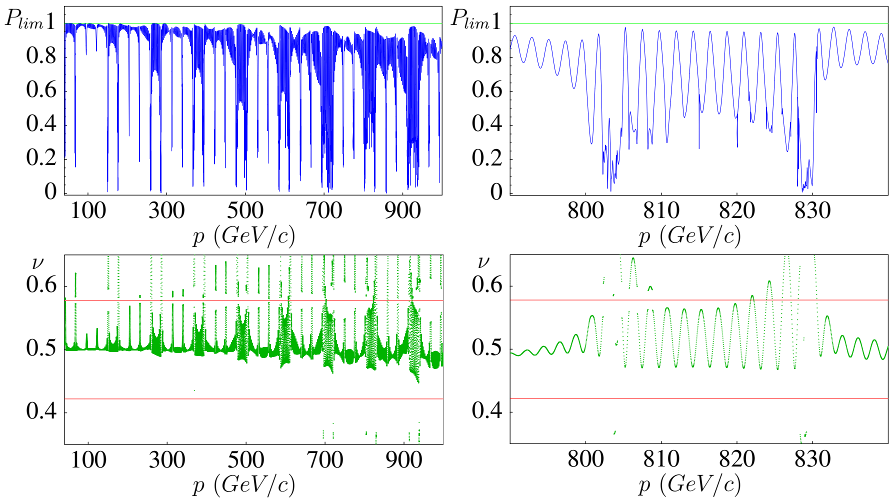

Fig. 4.1. P_{lim} and ν for particles with a vertical amplitude corresponding to the 2.5σ emittance in the HERA-p lattice of the year 2004 with the $(\frac{\pi}{4}0\frac{\pi}{4}0)6fs$ scheme. **Top**: The maximum time-average polarization P_{lim} for the complete acceleration range (*left*) and for the critical energy range above 800 GeV/c which has to be crossed when accelerating to the proposed storage energy of 870 GeV/c. **Bottom**: the corresponding amplitude-dependent spin tune $\nu(J_y)$. The second-order resonances $\nu = 2Q_y$ and $\nu = 1 - 2Q_y$ are indicated by two horizontal lines.

in Sect. 3.3.2 together with the $(\frac{\pi}{4}0\frac{\pi}{4}0)$ snake scheme does not lead to a significant improvement of P_{lim} and ν either as shown in Fig. 4.2. This is not surprising, because this vertical betatron phase advance was custom designed for a snake scheme $(0\frac{\pi}{2}\frac{\pi}{2}\frac{\pi}{2})8fs$.

P_{lim} and ν for higher-order spin dynamics in the snake-matched and phase-advance-matched HERA-p ring are shown in Fig. 4.3. While the overall behavior of P_{lim} over the complete acceleration range of HERA-p looks similar to the result obtained with linearized spin-orbit motion, which was displayed in Fig. 3.16, higher-order effects become very strong at high energies, especially in the vicinity of the critical energies where perturbations of spin motion in each FODO cell accumulate. The spin tune spread at momenta below 400 GeV/c is small, and higher-order effects seem to be benign even at these critical energies. A comparison with Figs. 4.1 and 4.2 shows that the special scheme obtained by matching orbital phases and snake angles would be a very good choice for HERA-p up to 300 or 400 GeV/c. For linearized spin-orbit motion, this snake-matched scheme does not produce a strong reduction of P_{lim} at any critical energy, but the higher-order effects become very pronounced at some top energies of HERA-p. Nevertheless, the advantage over other snake schemes becomes clear in Fig. 4.3 (bottom) where the amplitude-dependent spin tune ν is shown. It comes close to a second-order

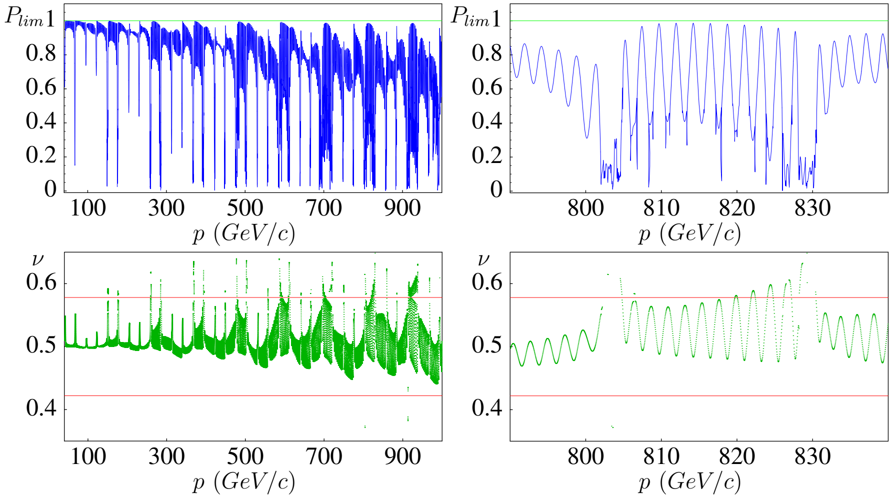

Fig. 4.2. P_{lim} and ν for particles with a 2.5σ vertical amplitude in the HERA-p lattice of the year 2004 after the betatron phase advance between opposite regular arc structures was adjusted to be an odd multiple of π. Together with the snake scheme $(0\frac{\pi}{2}\frac{\pi}{2}\frac{\pi}{2})$, this would lead to a cancellation of the perturbations of linearized spin-orbit motion produced by the arcs. But here results for the standard scheme $(\frac{\pi}{4}0\frac{\pi}{4}0)8fs$ are displayed. **Top**: The maximum time-average polarization P_{lim} for the complete acceleration range (*left*) and for the critical energy range above 800 GeV/c that has to be crossed when accelerating to the proposed storage energy of 870 GeV/c. **Bottom**: The corresponding amplitude-dependent spin tune $\nu(J_y)$. The second-order resonances $\nu = 2Q_y$ and $\nu = 1 - 2Q_y$ are indicated by two horizontal lines.

resonance at fewer places and does not exhibit spin tune jumps that are as strong as those in previous figures of ν.

In this snake-matched scheme, the influence of higher-order effects can be seen very clearly, because the first-order effects have been matched to be very small. The analysis of ν shows that completely snake matching the spin perturbations in the arcs of HERA-p with 4 Siberian Snakes is advantageous, even though dips of P_{lim} due to higher-order resonances can be observed at high energies. Even around 300 GeV/c there are resonant dips of P_{lim} in Fig. 4.3 (middle) but they are less pronounced than those in the previous figures so that the snake-matched scheme should be very advantageous in the complete energy range of HERA-p.

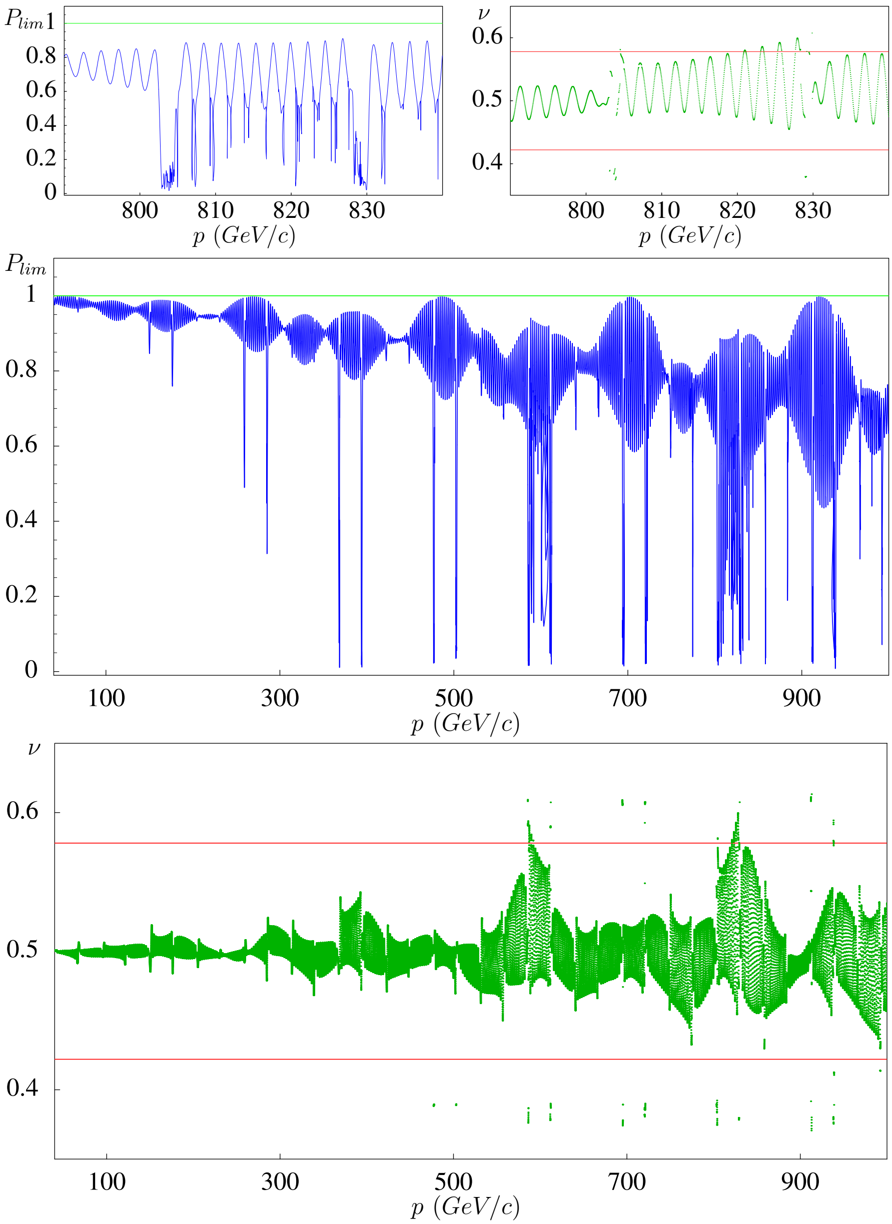

Fig. 4.3. P_{lim} and ν for a 2.5σ vertical amplitude after the betatron phase advance between opposite regular arc structures was adjusted to be an odd multiple of π in the $(0\frac{\pi}{2}\frac{\pi}{2}\frac{\pi}{2})8fs$ scheme. The resonances $\nu = 2Q_y$ and $\nu = 1 - 2Q_y$ are indicated by two horizontal lines.

4.1.3 Filtering of Siberian Snake Schemes

When trying to optimize P_{lim} and the spread of ν, one is therefore faced with two problems: The effect of linearized spin-orbit motion has to be minimized while the higher-order effects are not allowed to build up too strongly.

Because there are no analytical methods for comparing the higher-order effects of different snake schemes, an automated computer algorithm for finding optimal snake schemes called filtering has been employed [1, 13].

The Filtering Algorithm: To find a good directions of the rotation axes of Siberian Snakes:

1. Choose sets of snake angles from which the best snake scheme should be selected. Over 10^6 schemes were investigated.
2. Allow only snake combinations with an even number of horizontal Siberian Snakes and therefore vertical $\boldsymbol{n}_0$. The use of type III snakes was also investigated [14, 15].
3. Select all snake combinations for a flat ring which lead to a spin tune of $\nu_0 = \frac{1}{2}$. The requirement for these schemes is given below (2.78).
4. Compute the maximum time-average polarization $< \boldsymbol{n} >$ over the whole energy range of HERA-p using linearized spin-orbit motion and filter on high average values of $P_{lim}^{(1)}$, the approximation of P_{lim} obtained by linearized spin-orbit motion.
5. For the most promising remaining snake schemes, i.e., those with the highest average $P_{lim}^{(1)}$, compute now P_{lim} and ν non-perturbatively for a vertical oscillation amplitude by the SODOM-2 method. I have usually used a 2.5σ vertical amplitude, which contains 95.6% of the beam if it has a Gaussian distribution in the vertical degree of freedom and all longitudinal and radial amplitudes are allowed. The snake scheme which leads to the smallest spin tune spread is then chosen for further analysis.
6. Use stroboscopic averaging, anti-damping, and spin-orbit tacking as described in the next sections for further analysis of the snake scheme.

The steps 1 to 4 of this filtering algorithm have been very efficiently automated in the code SPRINT [7, 1]. In my investigations, the snake angle of each of the snakes in four-snake schemes were allowed to vary in steps of $22.5°$. In eight-snake schemes, each snake angle was varied in steps of $45°$.

During the filtering analysis in [14], it was found that type III snakes can be helpful but for reasons already described below (3.60), type III snakes will no longer be considered here.

Schemes with 8 Siberian Snakes have been described in [16]. But they are not stressed here because putting Siberian Snakes at the centers of the arcs of HERA-p would be very costly and therefore one should try to avoid schemes with more than 4 Siberian Snakes.

The most destructive energy range that has to be crossed to reach the proposed operation momentum of 870 GeV/c is located between 800 and

835 GeV/c. This is due to the very strong resonances corresponding to $G\gamma\Delta_c = 17 \pm \Delta$ in Fig. 3.7. It should be noted that the result of filtering depends strongly on the energy range over which P_{lim} and the spread of ν are optimized. If one filters snake schemes for an energy range in which there is only one very strong resonance at which the spin phase advance and the orbit phase advance have approximately the relation $-G\gamma\Delta_c \pm \Delta = N_{odd}$ of (3.37), then filtering will mostly compensate the perturbation described by the spin-orbit coupling integral responsible for this resonance enhancement condition, either I_y^+ or I_y^-. This can be seen in Fig. 4.4 (left), for which filtering had been performed in the momentum range from 790 GeV/c to 820 GeV/c. In Fig. 4.4 (bottom), one sees that for linearized spin-orbit motion the destructive influence of all very strong resonances due to the condition $G\gamma\Delta_c + \Delta = N_{odd}$ have been strongly reduced over the whole of the HERA-p momentum range, while for $G\gamma\Delta_c - \Delta = N_{odd}$ these effects are very strong. Correspondingly, filtering over an energy range from 820 GeV/c to 850 GeV/c reduces the effects due to the condition $G\gamma\Delta_c - \Delta = N_{odd}$ in Fig. 4.4 (right) while it does not lead to improvements at energies where $G\gamma\Delta_c + \Delta = N_{odd}$ holds approximately.

Filtering therefore has to be performed over sufficiently large energy ranges. Once a very efficient version of the filtering algorithm had been implemented in the program SPRINT, filtering could be performed for the complete energy range from 40 GeV/c to 900 GeV/c. Figure 4.5 shows P_{lim} and ν for the best snake schemes found for HERA-p with 6 flattening snakes and with 8 flattening snakes. While both snake schemes perform better than the standard schemes of Fig. 4.2, the tune spread is slightly smaller in the $8fs$ scheme where the ring is symmetrized by two flattening snakes in the west.

The best snake scheme found by filtering over the complete momentum range from 40 to 920 GeV after HERA-p has been symmetrized by 8 flattening snakes is the $(\frac{3\pi}{4}\frac{3\pi}{8}\frac{3\pi}{8}\frac{\pi}{4})8fs$ scheme. P_{lim} and ν obtained with the SODOM-2 method for this scheme are shown in Fig. 4.6. Compared with the other snake schemes discussed so far, P_{lim} is high and ν has a remarkably small spread around the closed-orbit spin tune $\nu_0 = \frac{1}{2}$ for most energies. However, at the critical energies the spin tune spread is larger than in the snake-matched scheme. In particular, the small spread of ν in the bottom figure is very favorable for polarized proton acceleration, because fever higher-order resonances will be crossed during acceleration. Because the loss of polarization at higher-order resonances can be described by a Froissart-Stora formula for every isolated higher-order resonance crossing as shown in Sect. 2.2.11, the reduction of the spin tune spread can directly lead to less reduction of polarization during the acceleration cycle.

However, the full energy can only be reached by acceleration through the very strong residual resonance structures at around 804 GeV/c and around 832 GeV/c, and to find out whether the optimized snake schemes can lead to higher polarization at high energy than standard schemes, the process

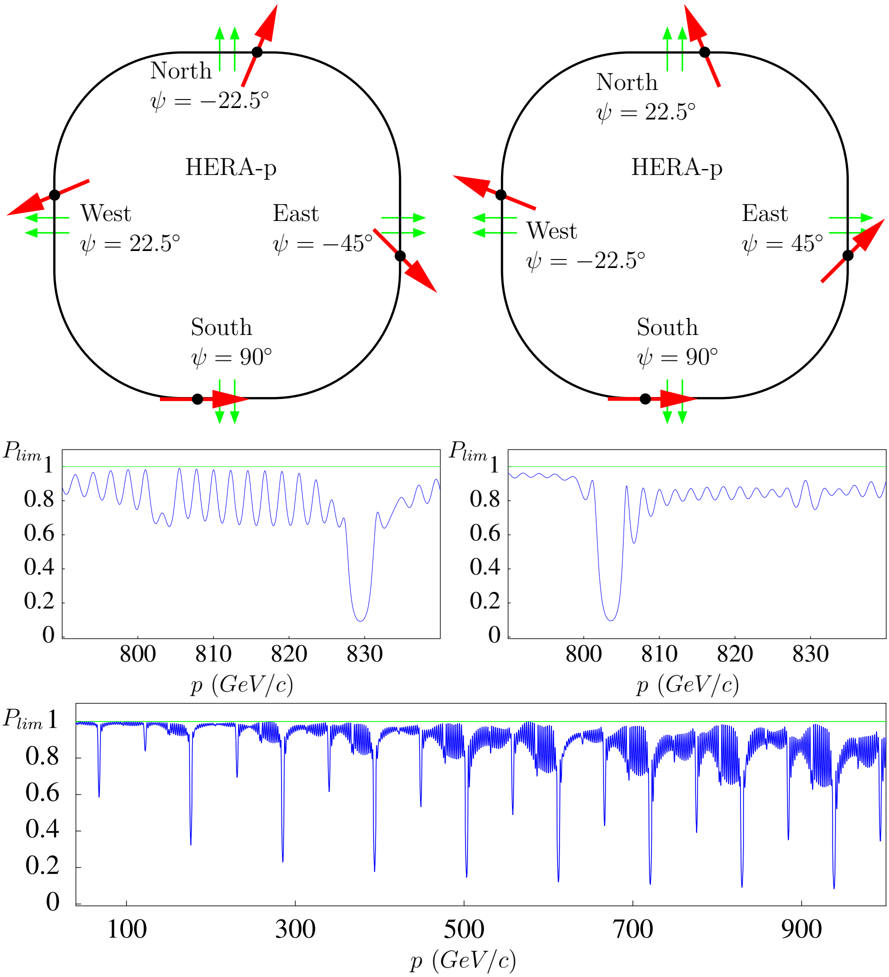

Fig. 4.4. P_{lim} and ν for linearized spin-orbit motion of particles with a 2.5σ vertical amplitude in the HERA-p lattice of the year 2004 after implementing filtered four-snake schemes. **Left**: Snake angles (*top*) and P_{lim} (*middle*) for the snake scheme $(\frac{\pi}{2}\frac{\pi}{4}\frac{\pi}{8}\frac{7\pi}{8})8fs$ found by filtering the $6fs$ scheme in the momentum range from 790 GeV/c to 820 GeV/c. **Right**: The $(\frac{\pi}{2}\frac{3\pi}{4}\frac{7\pi}{8}\frac{\pi}{8})8fs$ scheme found by filtering for the energy range from 820 GeV/c to 850 GeV/c. **Bottom**: P_{lim} for the $(\frac{\pi}{2}\frac{\pi}{4}\frac{\pi}{8}\frac{7\pi}{8})8fs$ scheme for the complete momentum range.

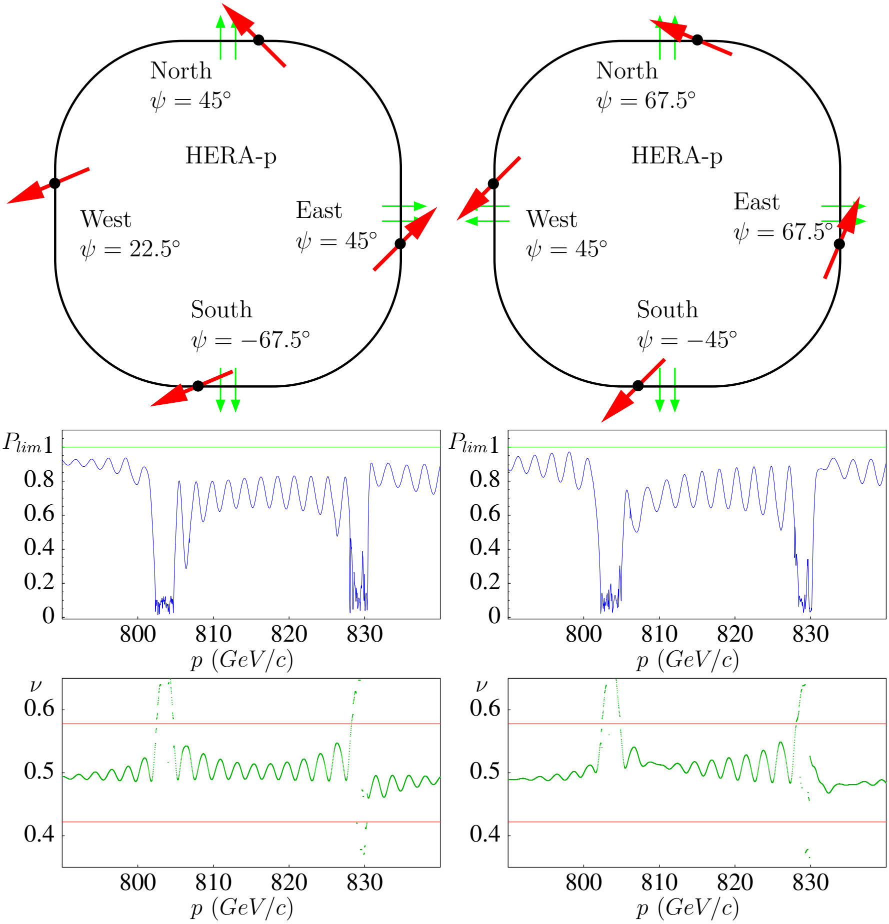

Fig. 4.5. P_{lim} and ν of particles with a 2.5σ vertical amplitude in the HERA-p lattice of the year 2004 after installation of the two best filtered schemes with 4 Siberian Snakes. **Left**: The snake angles (*top*) for the $(\frac{5\pi}{8}\,\frac{\pi}{4}\,\frac{\pi}{4}\,\frac{\pi}{8})6fs$ scheme found by filtering when 6 flattening snakes are used lead to a favorable P_{lim} (*middle*) and ν (*bottom*). **Right**: The best snake scheme found by filtering when HERA-p is symmetrized by 8 flattening snakes (*top*) is $(\frac{3\pi}{4}\,\frac{3\pi}{8}\,\frac{3\pi}{8}\,\frac{\pi}{4})8fs$ and leads on average to an even higher P_{lim} and to an even smaller spread of the amplitude-dependent spin tune ν. The second-order resonances $\nu = 2Q_y$ and $\nu = 1 - 2Q_y$ are indicated by two horizontal lines.

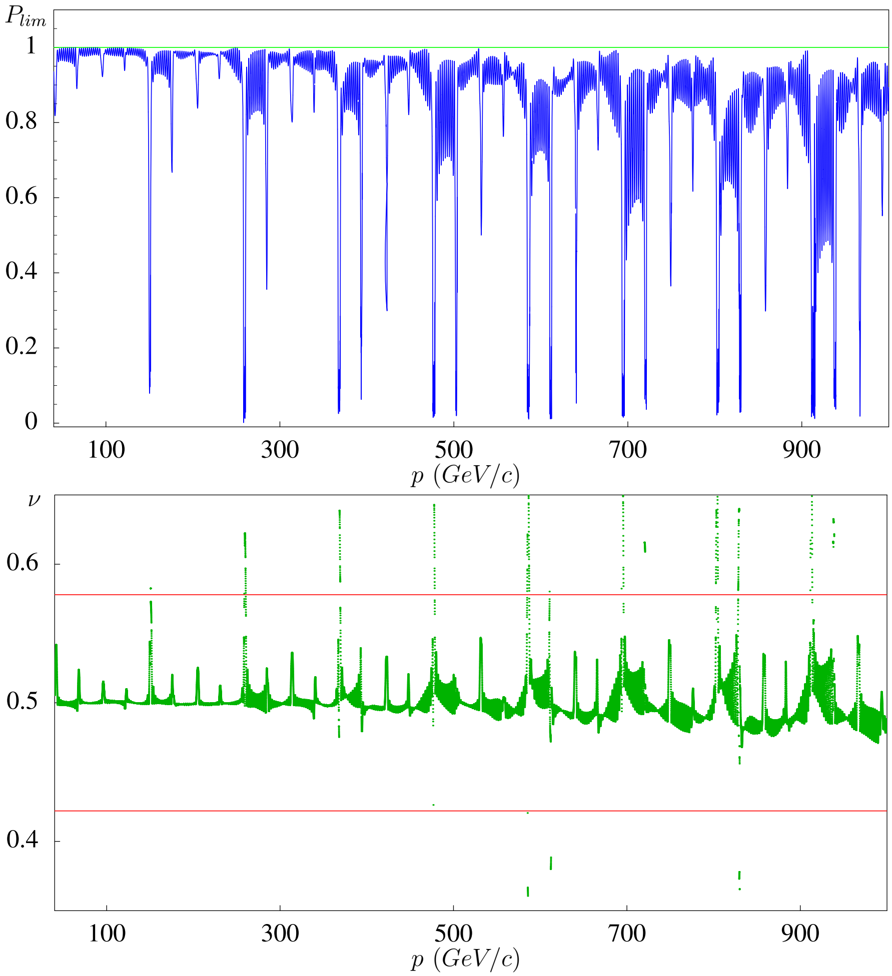

Fig. 4.6. P_{lim} (*top*) and ν (*bottom*) for the $(\frac{3\pi}{4}\,\frac{3\pi}{8}\,\frac{3\pi}{8}\,\frac{\pi}{4})8fs$ Siberian Snake scheme. Together with the snake-matched scheme $(0\,\frac{\pi}{2}\,\frac{\pi}{2}\,\frac{\pi}{2})8fs$, this is the most promising scheme of Siberian Snakes found so far by the filtering algorithm. The second-order resonances $\nu = 2Q_y$ and $\nu = 1 - 2Q_y$ are indicated by two horizontal lines.

of acceleration through the critical energy regions has to be simulated by a tracking program.

4.1.4 A Note on Spin-Orbit Tracking

The comparison in Sect. 4.1.2 of linearized spin-orbit motion and non-perturbative computations of $\boldsymbol{n}(\boldsymbol{z})$ for one degree of phase space motion has shown that accurate simulations of the invariant spin field and the amplitude-dependent spin dynamics in HERA-p are needed. This in turn requires the efficient collection and processing of single particle spin-orbit tracking data, and that is the topic of the following section. Various methods of particle tracking have been developed for analyzing properties of particle optical devices [17, 18, 19, 20, 21, 22]. For proton storage rings, tracking methods for dynamic aperture and lifetime studies have been brought to a high level of sophistication [23, 24, 25, 26, 27, 28]. Because for our purposes Stern-Gerlach forces can be neglected, the orbit motion is not influenced by the spin motion, and these established techniques of symplectic particle tracking can be used. Although these programs are normally used to analyze stored beams, for the analysis of polarized proton motion the acceleration process is of particular importance [29].

Because here the average polarization of the beam is being investigated, and because that gets its main contribution from the core of the beam, spin-orbit motion in the tails of the beam does not have to be simulated very well. In fact, the sophisticated tools that were developed to analyze dynamic aperture and lifetime are custom designed for particle motion in the tails of the beam and are not necessary when the average beam polarization is studied.

In the HERA-p ring, the 1σ normalized emittances corresponding to one standard deviation of the beam size are typically approximately 4π mm mrad in the horizontal and vertical direction and around 17.5π mm rad in the longitudinal direction, which corresponds to 1σ values of $\delta = 1.1 \times 10^{-4}$ and $\tau = 16$cm.

For the linearized spin-orbit motion in Chapter 3 and when analyzing higher-order effects so far in Chapter 4, particles with a 2.5σ phase space amplitude were studied. For one degree of freedom, this amplitude contains 95.6% of the beam if it has a Gaussian distribution and arbitrary phase space amplitudes in the other two degrees of freedom are allowed. One might argue that it would suffice to study smaller phase space amplitudes, because a loss of polarization for 4.4% of the beam can be tolerated. This view has not been adopted here, because (1) computational analysis of an accelerator should leave room for some imperfections in the description of the accelerator and (2) because the polarization can be reduced for particles at large phase space amplitudes in all three degrees of freedom, and only 87% of the particles in a Gaussian beam have phase space amplitudes below 2.5σ in all three degrees of freedom.

As explained in Sect. 2.1, spin is most efficiently propagated along a particle's trajectory using quaternions. This is done by computing the spin transport quaternion of each element. These quaternions then have to be multiplied to obtain the complete transport quaternion.

Without beam-beam interaction, at 2.5σ the particle dynamics is often described well by linear phase space motion. Then nonlinear terms in the transport maps $\boldsymbol{M}_n(\boldsymbol{z})$ of the optical elements are not essential in the core of the beam. Nevertheless, the nonlinear dependence of the spin transport quaternions $B_n(\boldsymbol{z})$ on phase space coordinates can be important and has to be investigated. The spin transport quaternion of the individual elements can be computed in a power expansion with respect to the phase space variables $\boldsymbol{z}$.

The equation of motion for the quaternion (2.38) has the form

$$\frac{\mathrm{d}}{\mathrm{d}\theta}\boldsymbol{A} = \Omega(\boldsymbol{z}(\theta),\theta)\boldsymbol{A}\ , \tag{4.10}$$

where the antisymmetric 4×4 matrix Ω is constructed from the precession vector $\boldsymbol{\Omega}$. The starting conditions are $\boldsymbol{z}(0)=\boldsymbol{z}_0$, $\boldsymbol{A}=(1,\boldsymbol{0})^T$. The quaternion $\boldsymbol{A}(\theta)$ depends on the initial phase space coordinates $\boldsymbol{z}_i$ and can be expanded in a Taylor series with respect to these coordinates. In the following, I devise an iteration method for A_n, which is the Taylor expansion to order n of A [30].

The precession vector $\boldsymbol{\Omega}$ is split into its value on the design curve and its phase space dependent part as $\boldsymbol{\Omega}(\boldsymbol{z},\theta)=\boldsymbol{\Omega}^0(\theta)+\boldsymbol{\Omega}^{\geq 1}(\boldsymbol{z},\theta)$. The spin motion on the design curve is given by the relation $\frac{\mathrm{d}}{\mathrm{d}\theta}\boldsymbol{A}_0(\theta)=\Omega^0\boldsymbol{A}_0(\theta)$. Small phase space coordinates will create a rotation that differs little from $\boldsymbol{A}_0(\theta)$. Thus the phase space dependent rotation is written as a concatenation of $\boldsymbol{A}_0$ and the $\boldsymbol{z}_i$ dependent quaternion $(1+\delta,\boldsymbol{\delta})$, which reduces to the identity for $\boldsymbol{z}_i=0$ because the aberrations δ and $\boldsymbol{\delta}$ vanish on the design curve. With (2.35) one obtains

$$\boldsymbol{A} = \mathsf{A}_0\begin{pmatrix}1+\delta\\ \boldsymbol{\delta}\end{pmatrix}\ . \tag{4.11}$$

The quaternion A is now inserted in the differential equation (4.10) to obtain

$$\frac{\mathrm{d}}{\mathrm{d}\theta}\mathsf{A}_0\begin{pmatrix}1+\delta\\ \boldsymbol{\delta}\end{pmatrix}+\mathsf{A}_0\frac{\mathrm{d}}{\mathrm{d}\theta}\begin{pmatrix}1+\delta\\ \boldsymbol{\delta}\end{pmatrix}=(\Omega^0+\Omega^{\geq 1})\mathsf{A}_0\begin{pmatrix}1+\delta\\ \boldsymbol{\delta}\end{pmatrix}\ . \tag{4.12}$$

Taking into account the equation on the design curve and the fact that A_0^T describes the inverse rotation of A_0, one obtains

$$\frac{\mathrm{d}}{\mathrm{d}\theta}\begin{pmatrix}\delta\\ \boldsymbol{\delta}\end{pmatrix}=\tilde{\Omega}(\boldsymbol{z},\theta)\begin{pmatrix}1+\delta\\ \boldsymbol{\delta}\end{pmatrix}\ , \tag{4.13}$$

with $\tilde{\Omega}=\mathsf{A}_0^T\Omega^{\geq 1}\mathsf{A}_0$. Writing the Taylor expansion of $(\delta,\boldsymbol{\delta})$ to order n in $\boldsymbol{z}_i$ as $(\delta_n,\boldsymbol{\delta}_n)$ and the Taylor expansion of $\boldsymbol{z}$ as $\boldsymbol{z}_n$, one finally obtains the iteration equation

$$\begin{pmatrix}\delta_n\\ \boldsymbol{\delta}_n\end{pmatrix}=_n\int_0^\theta\tilde{\Omega}(\boldsymbol{z}_n(\tilde{\theta}),\tilde{\theta})\begin{pmatrix}1+\delta_{n-1}\\ \boldsymbol{\delta}_{n-1}\end{pmatrix}d\tilde{\theta}\ ,\quad \begin{pmatrix}\delta_0\\ \boldsymbol{\delta}_0\end{pmatrix}=0\ , \tag{4.14}$$

where $=_n$ describes the equivalence up to order n. The first order of this iteration method was used for the spin transport in the program SPRINT [7, 1] and was evaluated up to second order using MATHEMATICA in [31, 32].

These second-order quaternions are ready for use in an analysis of nonlinear spin aberrations of individual optical elements. The Taylor coefficients of δ and $\boldsymbol{\delta}$ are the spin aberration coefficients. The aberrations are not fully independent but they are related by the equation $(1+\delta)^2 + \boldsymbol{\delta}^2 = 1$.

The iteration equation shows that in every iteration order of (4.14), $\tilde{\Omega}$ is multiplied once. This matrix contains terms that are linear in $G\gamma$, due to the transverse field components in the T-BMT equation (2.5). The matrix $\tilde{\Omega}$ can also contain nonlinear parts in $\boldsymbol{z}_i$ due to nonlinear fields, e.g., in sextupoles, which make $\boldsymbol{\Omega}(\boldsymbol{z},\theta)$ a nonlinear function of $\boldsymbol{z}$ and due to the nonlinear phase space motion, which makes $\boldsymbol{z}$ itself a nonlinear function of $\boldsymbol{z}_i$. After separating the first-order part, $\tilde{\Omega} = \tilde{\Omega}^1 + \tilde{\Omega}^{\geq 2}$, one can observe that the first-order part contributes n times to δ_n, leading to terms of $(G\gamma)^n$. The higher-order terms of $\tilde{\Omega}^{\geq 2}$ contribute to aberrations of order n already after fewer iterations and therefore lead to smaller powers in $G\gamma$. For the large value of $G\gamma = 1756$ in the case of HERA-p, this observation explains why nonlinear phase space motion and the contribution of nonlinear fields to $\boldsymbol{\Omega}$ are not very important when computing the spin transport quaternion of individual elements. For all the spin-orbit tracking presented here, only the linear fields of $\tilde{\Omega}^1$ were included for higher-order spin motion.

4.1.5 Polarization Reduction During Acceleration

When simulating HERA-p without non-flat regions, the destructive spin tune jumps at second-order resonances disappear completely. This is due to the fact that a large class of resonances are not excited at all in midplane symmetric rings [33]. But it has been observed in Fig. 3.2 that the non-flat regions lead to significant spin perturbations in HERA-p. To reduce these perturbations, the east region of HERA-p will now be simulated as flat because the HERMES experiment located in this region does not require that the proton beam is on the level of the electron beam.

When a particle is accelerated across the critical momentum region from 800 to 806 GeV/c with a typical acceleration rate of 50 keV per turn, the adiabatic invariance of $J_S = \boldsymbol{n} \cdot \boldsymbol{S}$ can be violated and the level of violation will depend on the orbital amplitude and the snake scheme. This violation is illustrated in the graphs in Fig. 4.7, which, for three different snake schemes, show the average spin action $\bar{J}_S$ at 806 GeV/c, which had initially $J_S = 1$ at 800 GeV/c before they were accelerated.

The change of J_S in the critical energy region depends on the initial phase space angle so that if J_S had been computed only for one particle, it could by chance have had an angle variable for which J_S does not change although it would have changed for other points with the same vertical phase space amplitude. To avoid such a chance effect, which gives the impression that J_S is invariant, three particles were accelerated and the average $\bar{J}_S$ is displayed in Fig. 4.7.

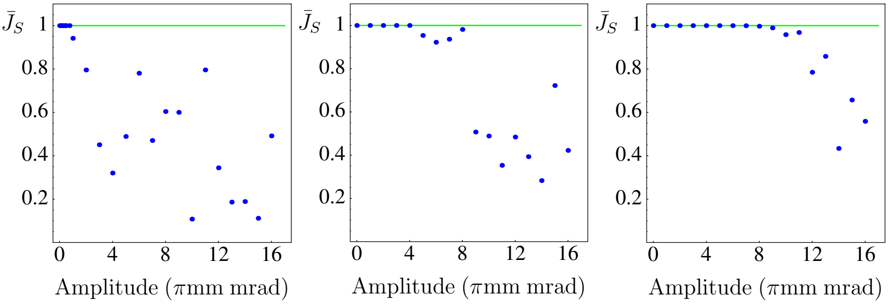

Fig. 4.7. Average spin action $\bar{J}_S$ at 806 GeV for particles starting with $J_S = 1$ at 800 GeV/c for three different snake schemes. **Left**: $(\frac{\pi}{4}0\frac{\pi}{4}0)4fs$, **Middle**: $(\frac{3\pi}{4}\frac{3\pi}{8}\frac{3\pi}{8}\frac{\pi}{4})8fs$, **Right**: $(0\frac{\pi}{2}\frac{\pi}{2}\frac{\pi}{2})8fs$ scheme. Particles with an amplitude above 1 (left), 4 (middle), and 8 (right) lead to a reduction of polarization when the beam is accelerated through this critical energy region.

At small phase space amplitudes, J_S is nearly invariant and therefore $\bar{J}_S = 1$. For each of the three snake schemes, there is a phase space amplitude J_{ymax} above which $\bar{J}_S < 1$ and the regions of the beam with an amplitude above J_{ymax} lead to a reduction of the beam's polarization during the acceleration process.

For the standard snake scheme $(\frac{\pi}{4}0\frac{\pi}{4}0)4fs$, only the part of the beam with less than 1π mm mrad vertical amplitude can remain polarized. For the filtered scheme $(\frac{3\pi}{4}\frac{3\pi}{8}\frac{3\pi}{8}\frac{\pi}{4})8fs$, phase space amplitudes up to 4π mm mrad are allowed. Finally the snake matched scheme $(\frac{\pi}{4}0\frac{\pi}{4}\frac{\pi}{4})8fs$ gives the most stable spin motion and Fig. 4.7 shows that vertical amplitudes of up to 8π mm mrad are allowed. This shows that the snake-matched scheme is superior to the other four-snake schemes studied so far. It stabilizes spin motion for 10 times larger phase space amplitudes than some other snake schemes. Nevertheless, 8π mm mrad is not enough to allow high polarization at top energies in HERA-p.

I have therefore performed two different snake matches for eight-snake schemes. Snake matching eight-snake schemes for rings with super-periodicity 4 has been illustrated in Fig. 3.14. Because HERA-p has no super-periodicity, the snake matching has to be modified in a way similar to that for four-snake schemes in Sect. 3.3.3. This snake match leads to very high P_{lim} and to a very small spin tune spread. But to demonstrate that it is possible to further stabilize spin motion in HERA-p by such schemes, Fig. 4.8 shows the vertical phase space amplitudes for which J_S remains invariant. The more effective of the two snake scheme stabilizes spin motion up to a vertical amplitude of 14π mm mrad.

These results for the various snake schemes are collected in Fig. 4.9, where it becomes clear that snake matching either with 4 or with 8 snakes leads to a significant improvement. But it follows from the discussion in Sect. 4.1.4

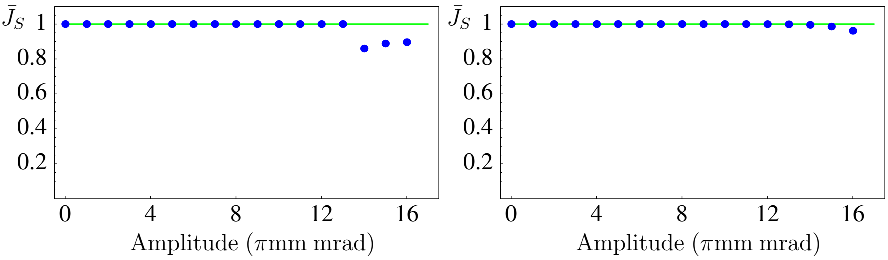

Fig. 4.8. The average spin action $\bar{J}_S$ at 806 GeV for particles that started with $J_S = 1$ at 800 GeV/c for the 2 different snake-matched eight-snake schemes $(\frac{\pi}{2}0000000)8fs$ (*left*) and $(\frac{\pi}{2}abc1\text{-}c\text{-}b\text{-}a)8fs$ (*right*). Particles with an amplitude above 13 (*left*) and 15 (*right*) lead to a reduction of polarization when the beam is accelerated through this critical energy region.

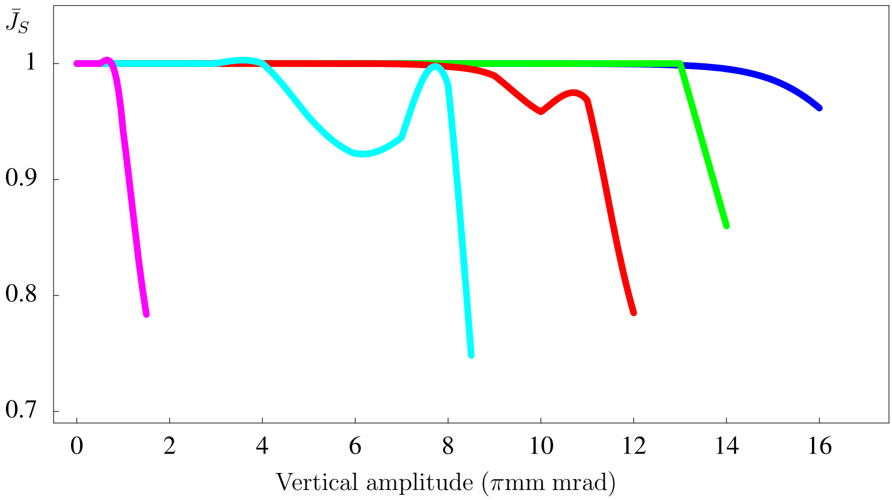

Fig. 4.9. The average spin action $\bar{J}_S$ at 806 GeV for particles that started initially with $J_S = 1$ at 800 GeV/c. Violet: The standard scheme, which stabilizes spin motion for particles within 1π mm mrad. Cyan: The filtered four-snake scheme stabilizes within 4π mm mrad. Red: The snake-matched four-snake scheme stabilizes within 8π mm mrad. Green: The snake-matched eight-snake scheme, which stabilizes within 13π mm mrad. Blue: The snake-matched eight-snake scheme which, stabilizes within 14π mm mrad of vertical phase space amplitude.

that it does not suffice to avoid a reduction of J_S for particles with less than 14π mm mrad amplitude. It would therefore be very helpful to use electron cooling in PETRA [34, 35, 36, 37] so as to reduce the emittance in HERA-p and to allow for an acceleration without loss of polarization for most particles in the beam.

The excellent performance of the two schemes with 8 Siberian Snakes is due to much smaller oscillation of the amplitude-dependent spin tune during the acceleration process, and the destructive second-order spin-orbit resonances indicated in Fig. 4.10 (bottom) are hardly encountered when these snake schemes are chosen. Correspondingly, a strong reduction of the number of higher order resonance conditions can be observed in Fig. 4.10 (top) where P_{lim} is shown.

These results show that it is not possible to give a simple formula for the number of snakes that are required for a given accelerator because different snake schemes with the same number of snakes lead to very different stability of spin motion.

Such a formula has been sought using the following very simple argument: the Siberian Snakes should dominate the spin precession produced by closed-orbit distortions and betatron oscillations. The resonance strength [38] ϵ_κ is a measure for that precession and is shown in Fig. 3.5 for 2.5σ vertical betatron oscillations in HERA-p. Then one obtains the rule of thumb that the number of snakes has to be sufficiently larger than $5\epsilon_\kappa$ [39]. This would lead to more than 4 Siberian Snakes in HERA-p. However, it has become apparent that the efficiency of four-snake schemes depends very much on the snake angles of the individual snakes [14]. Furthermore, it has been shown that 8 snakes are not necessarily better than 4 snakes for the non-flat HERA-p ring [16]. But if eight-snake schemes are snake-matched, they can produce a significantly larger P_{lim}, reduce the fluctuation of P_{lim} and ν with energy, reduce the overlapping of resonances in the critical regions, and ultimately enable the polarization of particles with larger phase space amplitudes to be preserved during the acceleration process. Thus, such a simple rule of thumb should be treated with caution. In the end, detailed evaluation is needed.

4.2 Obtaining $n(z)$ by Stroboscopic Averaging

In the approximation of linearized spin-orbit motion in flat rings without skew quadrupoles and solenoids, radial and longitudinal motion have no effect on spin dynamics. For the actual six-dimensional phase space motion through the spatially varying magnetic fields of an accelerator, the spin motion however certainly depends on all three degrees of freedom. This dependence is recovered when higher-order spin dynamics is taken into account. Especially around critical energies, this dependence can be quite important [2, 40, 16].

In Sect. 4.1.3, the effects of vertical motion in optimized snake schemes were analyzed using the SODOM-2 algorithm. For one degree of freedom, the use of 81 Fourier coefficients has turned out to be sufficient for amplitudes of up to 2.5σ in HERA-p. For more degrees of freedom, this algorithm requires an extremely large number of Fourier coefficients and then needs large amounts of computing power. For such cases, one needs the stroboscopic av-

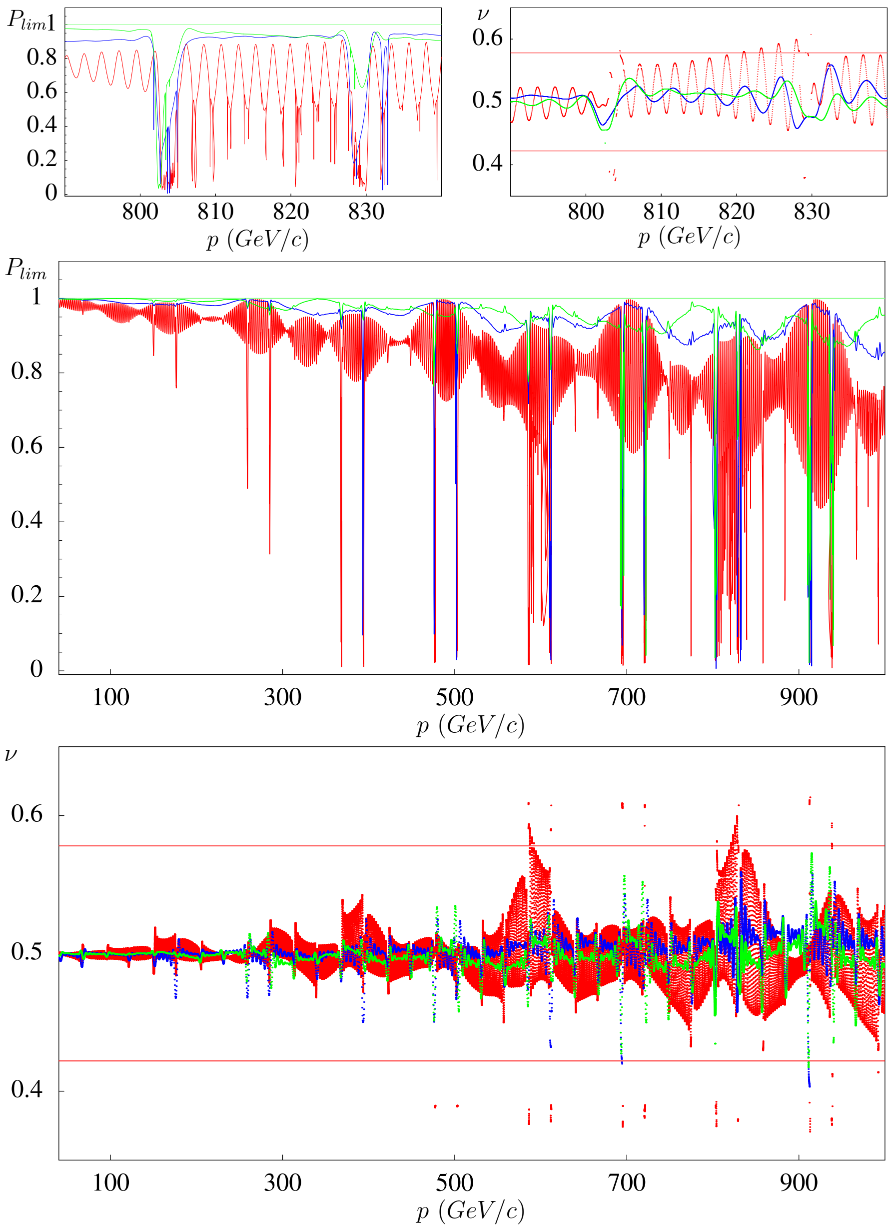

Fig. 4.10. Improvement of the higher-order P_{lim} and $\nu(J_y)$ by matching 8 snake angles and the orbital phases. The snake arrangement is $(\frac{\pi}{2}0000000)8fs$ (*blue*) and $(\frac{\pi}{2}abc0\text{-}c\text{-}b\text{-}a)8fs$ (*green*). As a comparison, P_{lim} from SODOM-2 is shown for the snake and phase advance matched four-snake scheme $0\frac{\pi}{2}\frac{\pi}{2}\frac{\pi}{2})8fs$ (*red*). The resonances $\nu = 2Q_y$ and $\nu = 1 - 2Q_y$ are indicated (also *red*).

eraging algorithm [1]. This provides an efficient way to compute an $\boldsymbol{n}$-axis for all three degrees of freedom.

Consider a particle beam with a spin field $\boldsymbol{f}(\boldsymbol{z},\theta)$. Its initial spin field in the Poincaré section at θ_0 is $\boldsymbol{f}_0(\boldsymbol{z}) = \boldsymbol{f}(\boldsymbol{z},\theta_0)$. In Sect. 2.2.8, it was shown that the time-average polarization at a phase space point $\boldsymbol{z}_0$ in that Poincaré section has no component perpendicular to the invariant spin field if this field exists. The time averaged polarization is therefore either zero or parallel to $\boldsymbol{n}(\boldsymbol{z}_0)$. This knowledge can be used to compute the invariant spin field. The infinite sum involved in the time-average polarization at $\boldsymbol{z}(\theta_0) = \boldsymbol{z}_0$ can be approximated by a sum over N turns,

$$\begin{aligned}\{\boldsymbol{f}\}(\boldsymbol{z}_0,\theta_0) \approx \{\boldsymbol{f}\}_N(\boldsymbol{z}_0,\theta_0) &= \frac{1}{N+1}\sum_{j=0}^{N} \boldsymbol{f}(\boldsymbol{z}_0,\theta_0+2\pi j) \qquad (4.15)\\ &= \frac{1}{N+1}\sum_{j=0}^{N} \mathsf{R}(\boldsymbol{z}(\theta_0-2\pi j),\theta_0-2\pi j;\theta_0)\boldsymbol{f}_0(\boldsymbol{z}(\theta_0-2\pi j)) \; .\end{aligned}$$

If $|\{\boldsymbol{f}\}_N|$ does not vanish, this yields the following approximation to the $\boldsymbol{n}$-axis:

$$\boldsymbol{n}(\boldsymbol{z}_0,\theta_0) \approx \frac{\{\boldsymbol{f}\}_N(\boldsymbol{z}_0,\theta_0)}{|\{\boldsymbol{f}\}_N(\boldsymbol{z}_0,\theta_0)|} \; . \qquad (4.16)$$

This method of computing an $\boldsymbol{n}$-axis is called stroboscopic averaging [1].

For ease of computation, the special choice for the initial spin field $\boldsymbol{f}_0(\boldsymbol{z}) = \boldsymbol{n}_0$ at azimuth θ_0 is usually made and one can simplify $\{\boldsymbol{f}\}_N$ to

$$\{\boldsymbol{f}\}_N(\boldsymbol{z}_0,\theta_0) = \frac{1}{N+1}\sum_{j=0}^{N} \mathsf{R}(\boldsymbol{z}(\theta_0-2\pi j),\theta_0-2\pi j;\theta_0)\boldsymbol{n}_0(\theta_0) \; . \qquad (4.17)$$

Equations (4.15) and (4.16) define an algorithm for obtaining an $\boldsymbol{n}$-axis. The following two kinds of pathologies can occur:

1. The $\boldsymbol{n}$-axis is not unique: if the proposed algorithm converges, then the result could depend on the choice of $\boldsymbol{f}_0(\boldsymbol{z})$.
2. The stroboscopic average $\{\boldsymbol{f}\}_N$ vanishes for $N \to +\infty$ or the sequence in (4.15) does not converge.

Both pathologies can be studied with the algorithm. The first situation occurs when the spin tune is in resonance with the orbit tunes so that the $\boldsymbol{n}$-axis is not unique, as described in Sect. 2.2.7. In almost all examples studied so far, the stroboscopic average seems to converge to a non-zero value, implying the existence of a spin field that satisfies the periodicity (2.82) to high accuracy. The second case is not only problematic computationally but describes a beam with no polarization usable for experiments. In such a beam, the time-average polarization is zero or the polarization is so unstable that the time average does not converge. In either case, there is little average polarization usable for particle physics experiments during most of the approximately 2 billion turns for which protons are typically stored in HERA-p.

In (4.17), one can see that the only information needed from tracking is the set of the $N+1$ phase space points $\boldsymbol{z}(\theta_0), \boldsymbol{z}(\theta_0-2\pi), \ldots, \boldsymbol{z}(\theta_0-2\pi N)$ and the N matrices $\mathsf{R}(\boldsymbol{z}(\theta_0-2\pi), \theta_0-2\pi; \theta_0), \mathsf{R}(\boldsymbol{z}(\theta_0-4\pi), \theta_0-4\pi; \theta_0), \ldots, \mathsf{R}(\boldsymbol{z}(\theta_0-2\pi N), \theta_0-2\pi N; \theta_0)$. Each matrix is a product of one turn spin transport matrices $\mathsf{R}(\boldsymbol{z}, \theta_0; \theta_0+2\pi)$ and describes the spin transport for a particle that finally arrives at $\boldsymbol{z}_0$.

Because only knowledge of spin and phase space coordinates at θ_0 are required, one can reformulate the algorithm in terms of one turn maps $\boldsymbol{M}$ with which $\boldsymbol{z}(\theta_0+2\pi) = \boldsymbol{M}(\boldsymbol{z}(\theta_0))$ and one turn spin transport matrices $\mathsf{R}(\boldsymbol{z})$ with which $\boldsymbol{S}(\theta_0+2\pi) = \mathsf{R}(\boldsymbol{z}(\theta_0))\boldsymbol{S}(\theta_0)$. All other quantities that depend on θ are also taken at the specified azimuth θ_0. For simplification, this azimuth is not indicated in the following. In terms of the one turn map, the periodicity condition for the invariant spin field

$$\mathsf{R}(\boldsymbol{z})\boldsymbol{n}(\boldsymbol{z}) = \boldsymbol{n}(\boldsymbol{M}(\boldsymbol{z})) \tag{4.18}$$

has already been stated in (2.82). Using the one turn map and the one turn spin transport matrix, the stroboscopic average of (4.17) is written as

$$\{\boldsymbol{f}\}_N(\boldsymbol{z}_0, \theta_0) = \frac{1}{N+1} \sum_{j=0}^{N} \prod_{k=1}^{j} \mathsf{R}(\boldsymbol{M}^{-k}(\boldsymbol{z}_0))\boldsymbol{n}_0 \; . \tag{4.19}$$

Here the convention $\prod_{k=1}^{0} \mathsf{R} = 1$ is used and $\prod_{k=1}^{j} \mathsf{R}(\boldsymbol{M}^{-k}(\boldsymbol{z}_0))$ is taken to mean the following order of multiplication: $\mathsf{R}(\boldsymbol{M}^{-1}(\boldsymbol{z}_0)) \ldots \mathsf{R}(\boldsymbol{M}^{-j}(\boldsymbol{z}_0))$.

The following algorithm shows for linear orbit motion how an $\boldsymbol{n}$-axis at $\boldsymbol{z}_0$ and θ_0 can be obtained by evaluating this formula:

1. Compute the linearized one turn phase space transport matrix M with $\boldsymbol{z}(\theta_0+2\pi) = \mathsf{M}\boldsymbol{z}(\theta_0)$.
2. Compute the set of $N+1$ phase space points
$$C = \{\boldsymbol{c}_j = (\mathsf{M}^{-1})^j \boldsymbol{z}_0 | j \in \{0, \ldots, N\}\} \; . \tag{4.20}$$
3. Compute the rotation matrix $\mathsf{R}(\boldsymbol{z}_{c.o.})$ that describes the one turn spin motion starting at θ_0 for particles on the closed orbit $\boldsymbol{z}_{c.o.}(\theta)$ and extract the corresponding rotation vector $\boldsymbol{n}_0$.
4. Starting with a spin parallel to $\boldsymbol{n}_0$ at every phase space point in C, track until the phase space point $\boldsymbol{z}_0$ is reached. For a given j, this requires tracking j turns starting at $\boldsymbol{c}_j$.
5. Compute the set of spin tracking results as
$$\begin{aligned} B = \{&\boldsymbol{b}_0(\boldsymbol{z}_0) = \boldsymbol{n}_0, \boldsymbol{b}_j(\boldsymbol{z}_0) \\ &= \mathsf{R}(\boldsymbol{c}_1) \ldots \mathsf{R}(\boldsymbol{c}_j)\boldsymbol{n}_0 | j \in \{1, \ldots, N\}\} \; . \end{aligned} \tag{4.21}$$
6. Compute the average of the elements in B, $\boldsymbol{S}_N(\boldsymbol{z}_0) = \frac{1}{N+1}\sum_{j=0}^{N} \boldsymbol{b}_j(\boldsymbol{z}_0)$ and for $|\boldsymbol{S}_N| \neq 0$ compute $\boldsymbol{n}_N = \boldsymbol{S}_N/|\boldsymbol{S}_N|$.

If the initial distribution is given by $\boldsymbol{n}_0$ as in the equations (4.17) and (4.19), i.e., $\boldsymbol{f}_0(\boldsymbol{z}) = \boldsymbol{n}_0$, then the average $\{\boldsymbol{f}\}_N(\boldsymbol{z}_0, \theta_0)$ in (4.15) is given by $\boldsymbol{S}_N(\boldsymbol{z}_0)$. Because the invariant spin field does not depend on the initial distribution $\boldsymbol{f}_0(\boldsymbol{z})$, $\boldsymbol{n}_N$ approximates the $\boldsymbol{n}$-axis.

4.2.1 Convergence Properties

The average $\boldsymbol{S}_N$ has been defined by the relation

$$\boldsymbol{S}_N(\boldsymbol{z}_0) = \frac{1}{N+1} \sum_{j=0}^{N} \prod_{k=1}^{j} \mathsf{R}(\boldsymbol{c}_k)\boldsymbol{n}_0 \ . \tag{4.22}$$

To check how well $\boldsymbol{S}_N$ satisfies the same periodicity condition (4.18) as that for the $\boldsymbol{n}$-axis, one can calculate

$$\begin{aligned} \boldsymbol{S}_N(\mathsf{M}\boldsymbol{z}_0) &= \frac{1}{N+1} \sum_{j=0}^{N} \prod_{k=1}^{j} \mathsf{R}(\boldsymbol{c}_{k-1})\boldsymbol{n}_0 \\ &= \frac{1}{N+1}(\boldsymbol{n}_0 + \sum_{j=0}^{N-1} \prod_{k=0}^{j} \mathsf{R}(\boldsymbol{c}_k)\boldsymbol{n}_0) \ , \end{aligned} \tag{4.23}$$

$$\mathsf{R}(\boldsymbol{z}_0)\boldsymbol{S}_N(\boldsymbol{z}_0) = \frac{1}{N+1} \sum_{j=0}^{N} \prod_{k=0}^{j} \mathsf{R}(\boldsymbol{c}_k)\boldsymbol{n}_0 \ , \tag{4.24}$$

$$\begin{aligned} \mathsf{R}(\boldsymbol{z}_0)\boldsymbol{S}_N(\boldsymbol{z}_0) - \boldsymbol{S}_N(\mathsf{M}\boldsymbol{z}_0) &= \frac{1}{N+1}(\mathsf{R}(\boldsymbol{z}_0)\boldsymbol{b}_N(\boldsymbol{z}_0) - \boldsymbol{n}_0) \\ &= \frac{1}{N+1}(\boldsymbol{b}_{N+1}(\mathsf{M}\boldsymbol{z}_0) - \boldsymbol{n}_0). \end{aligned} \tag{4.25}$$

For large N, this difference becomes arbitrarily small. But this does not yet establish the accuracy to which the approximation $\boldsymbol{n}_N$ of the $\boldsymbol{n}$-axis satisfies the periodicity condition because $|\boldsymbol{S}_N|$ might also be very small. To derive this accuracy, it is assumed that the angles between $\boldsymbol{n}_0$ and the vectors $\boldsymbol{b}_j(\mathsf{M}\boldsymbol{z}_0)$ are smaller than some positive number $\xi < \pi/2$ for all $j \in \{1, \dots, N+1\}$. As shown in Fig. 4.11, the length $|\boldsymbol{b}_{N+1}(\mathsf{M}\boldsymbol{z}_0) - \boldsymbol{n}_0|$ is then smaller than $2\sin(\xi/2)$. The length of $\boldsymbol{S}_N$ is at least $\cos(\xi)$, and here it becomes essential that there is a limit of $\pi/2$ on the angle ξ to prevent $|\boldsymbol{S}_N|$ becoming too small. The approximation $\boldsymbol{n}_N$ of the $\boldsymbol{n}$-axis then satisfies the periodicity condition to the following accuracy:

$$\begin{aligned} \Delta_N &= |\mathsf{R}(\boldsymbol{z}_0)\boldsymbol{n}_N(\boldsymbol{z}_0) - \boldsymbol{n}_N(\mathsf{M}\boldsymbol{z}_0)| = \left|\mathsf{R}(\boldsymbol{z}_0)\frac{\boldsymbol{S}_N(\boldsymbol{z}_0)}{|\boldsymbol{S}_N(\boldsymbol{z}_0)|} - \frac{\boldsymbol{S}_N(\mathsf{M}\boldsymbol{z}_0)}{|\boldsymbol{S}_N(\mathsf{M}\boldsymbol{z}_0)|}\right| \\ &= \frac{\left|\mathsf{R}(\boldsymbol{z}_0)\boldsymbol{S}_N(\boldsymbol{z}_0) - \boldsymbol{S}_N(\mathsf{M}\boldsymbol{z}_0) + \frac{|\boldsymbol{S}_N(\mathsf{M}\boldsymbol{z}_0)| - |\boldsymbol{S}_N(\boldsymbol{z}_0)|}{|\boldsymbol{S}_N(\mathsf{M}\boldsymbol{z}_0)|}\boldsymbol{S}_N(\mathsf{M}\boldsymbol{z}_0)\right|}{|\boldsymbol{S}_N(\boldsymbol{z}_0)|} \\ &\le \frac{|\mathsf{R}(\boldsymbol{z}_0)\boldsymbol{S}_N(\boldsymbol{z}_0) - \boldsymbol{S}_N(\mathsf{M}\boldsymbol{z}_0)| + ||\boldsymbol{S}_N(\mathsf{M}\boldsymbol{z}_0)| - |\boldsymbol{S}_N(\boldsymbol{z}_0)||}{|\boldsymbol{S}_N(\boldsymbol{z}_0)|} \end{aligned}$$

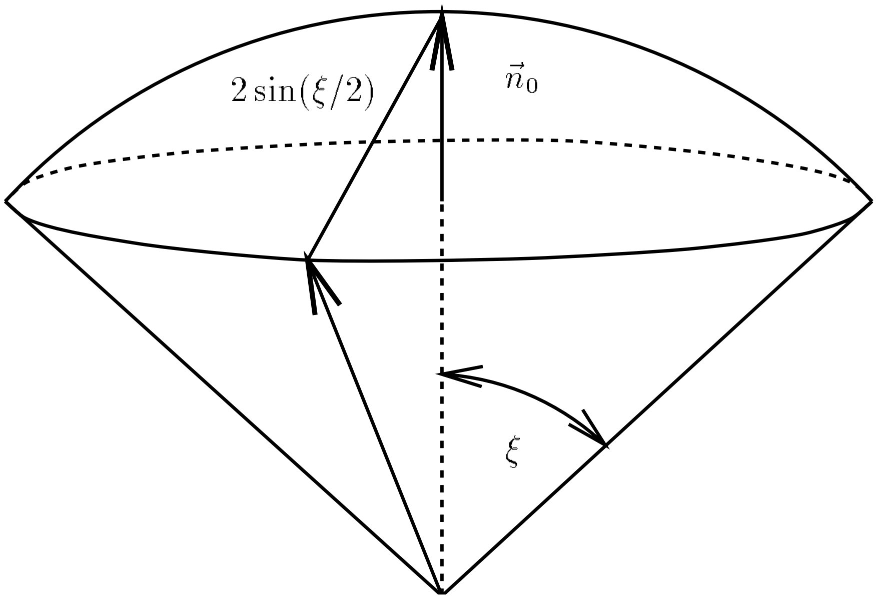

Fig. 4.11. Estimation of convergence rate. To guarantee convergence of the stroboscopic average, the angle ξ between the direction of $\boldsymbol{n}_0$ and the transported spins has to stay below $\pi/2$.

.

$$= \frac{|\mathsf{R}(\boldsymbol{z}_0)\boldsymbol{S}_N(\boldsymbol{z}_0) - \boldsymbol{S}_N(\mathsf{M}\boldsymbol{z}_0)| + ||\mathsf{R}(\boldsymbol{z}_0)\boldsymbol{S}_N(\boldsymbol{z}_0)| - |\boldsymbol{S}_N(\mathsf{M}\boldsymbol{z}_0)||}{|\boldsymbol{S}_N(\boldsymbol{z}_0)|}$$

$$\leq \frac{2}{|\boldsymbol{S}_N(\boldsymbol{z}_0)|}|\mathsf{R}(\boldsymbol{z}_0)\boldsymbol{S}_N(\boldsymbol{z}_0) - \boldsymbol{S}_N(\mathsf{M}\boldsymbol{z}_0)| \leq \frac{4\sin(\xi/2)}{(N+1)\cos(\xi)} \;. \quad (4.26)$$

The error $\varDelta_N$ by which the vector $\boldsymbol{n}_N(\boldsymbol{z}_0)$ violates the periodicity condition (4.18) of the $\boldsymbol{n}$-axis is therefore smaller than $2\sec(\xi/2)\tan(\xi)/(N+1)$ and converges to 0 for large N.

If one can prove the existence of a suitable number $\xi < \pi/2$ for some spin transport system, then $\boldsymbol{n}_N$ satisfies the periodicity condition (4.18) for the $\boldsymbol{n}$-axis up to an error that is smaller than or equal to $2\sec(\xi/2)\tan(\xi)/(N+1)$. Because evaluating B by (4.21) requires tracking $T = (N+1)N/2$ turns, the accuracy is bounded by $\sqrt{2/T}\sec(\xi/2)\tan(\xi)$. This slow convergence with the square root of T is a very serious limitation, and in the next section it will be demonstrated how the rate of convergence can be considerably improved.

Having shown that $\varDelta_n$ converges to 0 linearly with $1/N$, it is interesting to see how $\boldsymbol{n}_N$ converges to the $\boldsymbol{n}$-axis, if an invariant spin field exists. The following derivation is very similar to that in Sect. 2.2.8, which established that the time-average polarization is parallel to $\boldsymbol{n}(\boldsymbol{z})$. It will be assumed that the phase space motion can be described in terms of action-angle variables and that the motion is strongly non-orbit-resonant and non-spin-orbit-resonant according to Sects. 2.2.7 and 2.2.8. The stroboscopic average is now performed in the coordinate system $(\boldsymbol{u}_1, \boldsymbol{u}_2, \boldsymbol{n})$, which has been introduced in Sect. 2.2.7 and in which one writes $\boldsymbol{S}_N = s_{N,1}\boldsymbol{u}_1 + s_{N,2}\boldsymbol{u}_2 + s_{N,3}\boldsymbol{n}$. First the tracking points $\boldsymbol{c}_j$ are established. Note that the amplitude-dependent spin tune $\nu(\boldsymbol{J}) = \nu(\boldsymbol{c}_j)$ is the same for all tracking points because the action variable $\boldsymbol{J}$ is an invariant of motion. In the coordinate system $(\boldsymbol{u}_1, \boldsymbol{u}_2, \boldsymbol{n})$, the vector components of the 2π-periodic spin $\boldsymbol{n}_0$ on the closed orbit are not constant but depend on the phase space position. This vector is transported from the phase space points $\boldsymbol{c}_j$ to $\boldsymbol{z}_0 \hat{=} (\boldsymbol{\Phi}, \boldsymbol{J})$ by the rotation matrix

$$\begin{pmatrix} \cos(j2\pi\nu) & -\sin(j2\pi\nu) & 0 \\ \sin(j2\pi\nu) & \cos(j2\pi\nu) & 0 \\ 0 & 0 & 1 \end{pmatrix} . \tag{4.27}$$

Then the stroboscopic average is

$$\boldsymbol{S}_N = \frac{1}{N+1}\sum_{j=0}^{N} \begin{pmatrix} \cos(j2\pi\nu) & -\sin(j2\pi\nu) & 0 \\ \sin(j2\pi\nu) & \cos(j2\pi\nu) & 0 \\ 0 & 0 & 1 \end{pmatrix} \begin{pmatrix} n_{0,1}(\boldsymbol{\Phi} - j2\pi\boldsymbol{Q}) \\ n_{0,2}(\boldsymbol{\Phi} - j2\pi\boldsymbol{Q}) \\ n_{0,3}(\boldsymbol{\Phi} - j2\pi\boldsymbol{Q}) \end{pmatrix} ,$$

where the dependence of $\boldsymbol{n}_0$ on $\boldsymbol{\Phi}$ in the coordinate system $[\boldsymbol{u}_1, \boldsymbol{u}_2, \boldsymbol{n}]$ is explicitly indicated. The dependence on $\boldsymbol{J}$ is not indicated because the action variables are constant during the particle tracking. The third component of $\boldsymbol{S}_N$ is $\sum_{j=0}^{N} \frac{1}{N+1} n_{0,3}(\boldsymbol{\Phi} - j2\pi\boldsymbol{Q})$. The first and second components in complex notation are

$$\hat{s}_N = s_{N,1} + \mathrm{i}s_{N,2} = \frac{1}{N+1}\sum_{j=0}^{N} \mathrm{e}^{\mathrm{i}(j2\pi\nu)}\hat{n}_0(\boldsymbol{\Phi} - j2\pi\boldsymbol{Q}) , \tag{4.28}$$

where $\hat{n}_0(\boldsymbol{\Phi}) = n_{0,1}(\boldsymbol{\Phi}) + \mathrm{i}n_{0,2}(\boldsymbol{\Phi})$. In terms of the Fourier coefficients $\breve{n}_0(\boldsymbol{k})$ of $\hat{n}_0(\boldsymbol{\Phi})$, one obtains the inequality

$$\begin{aligned} |\hat{s}_N| &= \left| \frac{1}{N+1}\sum_{\boldsymbol{k}}\sum_{j=0}^{N} \mathrm{e}^{\mathrm{i}j2\pi(\nu - \boldsymbol{k}\cdot\boldsymbol{Q})}\breve{n}_0(\boldsymbol{k})\mathrm{e}^{\mathrm{i}\boldsymbol{k}\cdot\boldsymbol{\Phi}} \right| \\ &= \frac{1}{N+1}\left| \sum_{\boldsymbol{k}} \frac{1 - \mathrm{e}^{\mathrm{i}(N+1)2\pi(\nu - \boldsymbol{k}\cdot\boldsymbol{Q})}}{1 - \mathrm{e}^{\mathrm{i}2\pi(\nu - \boldsymbol{k}\cdot\boldsymbol{Q})}}\breve{n}_0(\boldsymbol{k})\mathrm{e}^{\mathrm{i}\boldsymbol{k}\cdot\boldsymbol{\Phi}} \right| \\ &\le \frac{1}{N+1}\sum_{\boldsymbol{k}} \frac{2}{|1 - \mathrm{e}^{\mathrm{i}2\pi(\nu - \boldsymbol{k}\cdot\boldsymbol{Q})}|}|\breve{n}_0(\boldsymbol{k})| . \end{aligned} \tag{4.29}$$

If the components of $\boldsymbol{n}_0$ in the coordinate system $[\boldsymbol{u}_1, \boldsymbol{u}_2, \boldsymbol{n}]$ have an analytic extension in $\boldsymbol{\Phi}$, then the sum over $\boldsymbol{k}$ is finite due to the assumed strong non-spin-orbit-resonance as has been explained after (2.101). Therefore, $\hat{s}_N$ converges to 0 linearly with $1/N$. Similarly one obtains the third component of $\boldsymbol{S}_N$ as

$$s_{N,3} = \breve{n}_{0,3}(0) + \frac{1}{N+1}\sum_{\boldsymbol{k}\neq 0}\frac{1-\mathrm{e}^{-\mathrm{i}(N+1)2\pi\boldsymbol{k}\cdot\boldsymbol{Q}}}{1-\mathrm{e}^{-\mathrm{i}2\pi\boldsymbol{k}\cdot\boldsymbol{Q}}}\breve{n}_{0,3}(\boldsymbol{k})\mathrm{e}^{\mathrm{i}\boldsymbol{k}\cdot\boldsymbol{\Phi}} , \tag{4.30}$$

where the sum over $\boldsymbol{k}$ is finite due to the assumed strong non-orbit-resonance. Therefore, $s_{N,3}$ converges to $\breve{n}_{0,3}(0)$ linearly with $1/N$. Here this equation has been re-derived for clarity, although it can be obtained directly by setting $f_0(\boldsymbol{z}) = \boldsymbol{n}_0$ in (2.102). Because $|\boldsymbol{S}_N| > \cos(\xi)$ and $\xi < \pi/2$, it is guaranteed that $\boldsymbol{S}_N$ does not converge to 0 so that $\breve{n}_{0,3}$ does not vanish. Together with the convergence of $\boldsymbol{S}_N$ the convergence of $\boldsymbol{n}_N$ to either $\boldsymbol{n}$ or $-\boldsymbol{n}$ follows from the relations

$$\begin{aligned}
\mathrm{Min}(|\boldsymbol{n}_N \pm \boldsymbol{n}|^2) &= \mathrm{Min}(\left|\frac{\boldsymbol{S}_N}{|\boldsymbol{S}_N|} \pm \boldsymbol{n}\right|^2) = (1-\frac{|s_{N,3}|}{|\boldsymbol{S}_N|})^2 + (\frac{|\hat{s}_N|}{|\boldsymbol{S}_N|})^2 \\
&= 2\frac{|\boldsymbol{S}_N| - |s_{N,3}|}{|\boldsymbol{S}_N|} < 2\frac{|\boldsymbol{S}_N| - |s_{N,3}|}{|s_{N,3}|} \\
&= 2(\sqrt{1+(\frac{|\hat{s}_N|}{|s_{N,3}|})^2} - 1) < 2(\frac{|\hat{s}_N|}{|s_{N,3}|})^2 .
\end{aligned} \tag{4.31}$$

There is a number N^* such that the absolute value of the N dependent part of $s_{N,3}$ in (4.30) is smaller than $\breve{n}_{0,3}(0)/2$. Taking this number N of turns to be bigger than N^*, one finds

$$|\boldsymbol{n}_N \pm \boldsymbol{n}| < 2\sqrt{2}\frac{|\hat{s}_N|}{|n_{0,3}(0)|} , \tag{4.32}$$

which, together with (4.29), finally establishes that $\boldsymbol{n}_N$ converges to $\boldsymbol{n}$ linearly with $1/N$.

4.2.2 An Algorithm with Faster Convergence

In the previous section, an algorithm was introduced that converged linearly with the inverse square root of the number T of turns tracked. However, it is possible to obtain convergence linear with $1/T$, when one takes advantage of the orthogonality of spin transport matrices. To illustrate this, another algorithm is established.

1. Compute $C = \{\boldsymbol{c}_j = (\mathsf{M}^{-1})^j\boldsymbol{z}_0 | j \in \{0,\ldots,N\}\}$ as before.
2. Define three orthogonal spins $\{\mathbf{e}^{(1)}, \mathbf{e}^{(2)}, \mathbf{e}^{(3)}\}$.
3. Obtain the sets S_j of the three vectors $\boldsymbol{S}_j^{(1)}$, $\boldsymbol{S}_j^{(2)}$, and $\boldsymbol{S}_j^{(3)}$ by tracking the $\mathbf{e}^{(1)}$, $\mathbf{e}^{(2)}$, and $\mathbf{e}^{(3)}$ for $N-j$ turns
$$\boldsymbol{S}_j^{(k)} = \mathsf{R}(\boldsymbol{c}_{j+1})\ldots\mathsf{R}(\boldsymbol{c}_N)\mathbf{e}^{(k)} . \tag{4.33}$$
4. From the set of vectors S_j and the set S_0, one can obtain the spin transport matrix from the phase space point $\boldsymbol{c}_j$ to $\boldsymbol{z}_0$ denoted by $\bar{\mathsf{R}}(\boldsymbol{c}_j)$. The relations $\boldsymbol{S}_0^{(k)} = \bar{\mathsf{R}}(\boldsymbol{c}_j)\boldsymbol{S}_j^{(k)}$ for all k and the matrices $\mathsf{S}_j^{(1,2,3)}$ with the column vectors $\boldsymbol{S}_j^{(k)}$ lead to $\bar{\mathsf{R}}(\boldsymbol{c}_j) = \mathsf{S}_0^{(1,2,3)}\mathsf{S}_j^{(1,2,3)T}$. Obtaining these $N+1$

transport matrices requires the propagation of 3 spins around the circular accelerator for N turns.

5. Now the set $B = \{\bar{\mathsf{R}}(\boldsymbol{c}_j)\boldsymbol{n}_0 | j \in \{0, \ldots, N\}\}$ can be computed, which is identical to the set denoted by B in the previous section.
6. The normalized average of B, denoted by $\boldsymbol{n}_N$, can now again be computed.

In this approach, one only has to track three initial spin directions over N turns, leading to $T = 3N$. The error is therefore bounded by $6\sec(\xi/2)\tan(\xi)/T$. This implies convergence linear with $1/T$. Thus, for example, when the angle ξ happens to be $45°$, and an accuracy at the 10^{-3} level is required, this more efficient approach only requires 6500 tracking turns. When the angle ξ is smaller, even fewer turns are needed.

Backward Tracking: In the two algorithms mentioned above, one needs to find the set C of $N + 1$ backward tracked phase space points, and then to launch spins at these points and track forward so as to compute the set B. In the case of linear motion, it is trivial to obtain these backward tracked phase space points. One simply transforms $\boldsymbol{z}_0$ into the action-angle variables of the linear motion and determines the phase advance per turn of the linear motion. Counting back these phase advances and transforming the action-angle variables back into phase space leads to the points $\boldsymbol{c}_j$. In the case of nonlinear motion, one would have to track for N turns backward around the ring in order to find the starting point in phase space.

For the above-mentioned algorithm with linear convergence, one would now use these starting points to track forward again in order to obtain the spin transport matrices. However, one can obtain these matrices already while tracking backward. For that, one starts with the phase space point $\boldsymbol{z}_0$ and launches three particles with spins pointing along $\mathbf{e}^{(1)}$, $\mathbf{e}^{(2)}$, and $\mathbf{e}^{(3)}$. Tracking backward in azimuth defines the $N + 1$ sets P_j of the spins $\boldsymbol{p}_j^{(1)}$, $\boldsymbol{p}_j^{(2)}$, and $\boldsymbol{p}_j^{(3)}$. The $\boldsymbol{p}_j^{(n)}$ can be written as

$$\boldsymbol{p}_j^{(k)} = \mathsf{R}^T(\boldsymbol{c}_j) \ldots \mathsf{R}^T(\boldsymbol{c}_1)\mathbf{e}^{(k)} \,, \tag{4.34}$$

where advantage is taken of the fact that transposition leads to the inverse of the orthogonal matrices. From the sets P_j and $\{\mathbf{e}^{(1)}, \mathbf{e}^{(2)}, \mathbf{e}^{(3)}\}$, one can then again compute the spin transport matrix $\bar{\mathsf{R}}(\boldsymbol{c}_j)$ and with these matrices one obtains the set B with the elements $\boldsymbol{b}_j = \bar{\mathsf{R}}(\boldsymbol{c}_j)\boldsymbol{n}_0$, which again leads to $\boldsymbol{n}_N$ by averaging.

Forward Tracking: There is a more fundamental problem in the case of nonlinear motion than the computation time involved in first tracking backward and then tracking forward. When the map for the whole lattice or the effects of separate nonlinear elements are computed by nonlinear transport maps, the inverses of these maps might not be known. In this case, the required phase space points $\boldsymbol{c}_j$ cannot be computed at all. Nevertheless, the vector $\boldsymbol{n}_N$ can be obtained as follows. The arguments of the section on backward tracking can simply be repeated for tracking forward. One establishes the phase space points $\boldsymbol{c}_j = \boldsymbol{M}(\boldsymbol{c}_{j-1})$ with $\boldsymbol{c}_0 = \boldsymbol{z}_0$ for $j \in \{1, \ldots, N\}$ and simultaneously the sets S_j by tracking the three unit vectors $\boldsymbol{S}^{(k)}_{j-1}$ for one turn beginning with $\boldsymbol{S}^{(k)}_0 = \mathbf{e}^{(k)}$. As in the fourth step of the previous algorithm, one can then obtain the spin transport matrix $\bar{\mathsf{R}}(\boldsymbol{c}_j)$ from the phase space point $\boldsymbol{z}_0$ to $\boldsymbol{c}_j$. The inverse of this transport matrix is simply obtained by transposition leading to the vectors $\boldsymbol{b}_j = \bar{\mathsf{R}}(\boldsymbol{c}_j)^T \boldsymbol{n}_0$. The normalized average of the vectors $\boldsymbol{b}_j$ is then the stroboscopic average $\boldsymbol{n}_{inv,N}$ of the inverse motion. For this average the error of the periodicity condition for the inverse motion also converges linearly to zero. Fortunately, an $\boldsymbol{n}$-axis of the inverse motion $\boldsymbol{n}_{inv}(\boldsymbol{z})$ is also an $\boldsymbol{n}$-axis of the forward motion, because the periodicity condition of the inverse motion is

$$\mathsf{R}^{-1}(\boldsymbol{M}^{-1}(\boldsymbol{z}))\boldsymbol{n}_{inv}(\boldsymbol{z}) = \boldsymbol{n}_{inv}(\boldsymbol{M}^{-1}(\boldsymbol{z})) \ . \tag{4.35}$$

That this leads to the periodicity condition (4.18) of the forward motion for $\boldsymbol{n}_{inv}$ can be shown by inserting $\boldsymbol{M}(\boldsymbol{z})$ for $\boldsymbol{z}$ and subsequent multiplication with $\mathsf{R}(\boldsymbol{z})$.

4.2.3 Stroboscopic Average of Linearized Spin-Orbit Motion

In this section, linearized spin-orbit motion is used to illustrate and to confirm the chief features of stroboscopic averaging. As in (3.1), a spin's components perpendicular to the rotation axis $\boldsymbol{n}_0$ for the closed orbit is described by the complex coordinate α,

$$\boldsymbol{S} = \Re\{\alpha\}\boldsymbol{m}(\theta) + \Im\{\alpha\}\boldsymbol{l}(\theta) + \sqrt{1 - |\alpha|^2}\boldsymbol{n}_0(\theta) \ . \tag{4.36}$$

The coordinate α is propagated from θ_0 once around the ring by the complex vector $\boldsymbol{G}$, which was introduced in (3.3),

$$\alpha_{j+1} = \boldsymbol{G} \cdot \boldsymbol{z}_j + \mathrm{e}^{\mathrm{i}2\pi\nu_0}\alpha_j \ . \tag{4.37}$$

The complex coordinate of $\boldsymbol{n}_0$ is $\alpha = 0$, so that propagating a spin that is initially parallel to $\boldsymbol{n}_0$ at a phase space point $\boldsymbol{z}_0$ for j times around the ring leads to the final complex spin component

$$\alpha_j = \sum_{k=1}^{j} \mathrm{e}^{\mathrm{i}(k-1)2\pi\nu_0}\boldsymbol{G} \cdot (\mathsf{M}^{-k}\boldsymbol{z}_0) \ . \tag{4.38}$$

With the column matrix A^{-1} of the eigenvectors of the 6×6-dimensional one turn matrix M, this reduces to

$$\alpha_j = \sum_{k=1}^{j} \mathrm{e}^{\mathrm{i}(k-1)2\pi\nu_0}\boldsymbol{G} \cdot [\mathsf{A}^{-1}\mathrm{diag}(\mathrm{e}^{\mp\mathrm{i}k2\pi Q_l})\mathsf{A}\boldsymbol{z}_0]$$

$$= \sum_{k=1}^{j} \mathrm{e}^{-\mathrm{i}2\pi\nu_0} \boldsymbol{G} \cdot [\mathsf{A}^{-1} \mathrm{diag}(\mathrm{e}^{\mathrm{i}k2\pi(\nu_0 \mp Q_l)}) \mathsf{A} \boldsymbol{z}_0]$$

$$= \mathrm{e}^{-\mathrm{i}2\pi\nu_0} \boldsymbol{G} \cdot [\mathsf{A}^{-1} \mathrm{diag}(\frac{\mathrm{e}^{\mathrm{i}2\pi(\nu_0 \mp Q_l)} - \mathrm{e}^{\mathrm{i}(j+1)2\pi(\nu_0 \mp Q_l)}}{1 - \mathrm{e}^{\mathrm{i}2\pi(\nu_0 \mp Q_l)}}) \mathsf{A} \boldsymbol{z}_0] . \quad (4.39)$$

The N-turn stroboscopic average of α for linearized spin-orbit motion is given by

$$\{\alpha\}_N(\boldsymbol{z}_0) = \frac{1}{N} \sum_{j=1}^{N} \alpha_j \quad (4.40)$$

$$= \mathrm{e}^{-\mathrm{i}2\pi\nu_0} \boldsymbol{G}$$

$$\cdot [\mathsf{A}^{-1} \mathrm{diag}(\frac{\mathrm{e}^{\mathrm{i}2\pi(\nu_0 \mp Q_l)}}{1 - \mathrm{e}^{\mathrm{i}2\pi(\nu_0 \mp Q_l)}} (1 - \frac{1}{N} \sum_{j=1}^{N} \mathrm{e}^{\mathrm{i}j2\pi(\nu_0 \mp Q_l)})) \mathsf{A} \boldsymbol{z}_0] .$$

For large $N \to \infty$, the fluctuating term averages to small values, even close to spin-orbit resonances with $\nu_0 = \pm Q_l$. But there the convergence will be very slow. When the distance from the resonance tends to zero, $\lim_{N\to\infty} \{\alpha\}_N(\boldsymbol{z}_0)$ diverges. The equations (4.40) and (3.17) lead to $\lim_{N\to\infty} \{\alpha\}_N(\boldsymbol{z}_0) = \boldsymbol{B} \cdot (\mathsf{A}\boldsymbol{z}_0)$ which agrees with the $\boldsymbol{n}$-axis α_n in (3.11). For large N, the error $|\{\alpha\}_N - \alpha_n|$ converges to zero linearly with $1/N$.

4.2.4 Stroboscopic Averaging for the SRM

In order to illustrate which quantities can be computed and how effective stroboscopic averaging can be in numerical computations, it is now applied to the single resonance model, where the $\boldsymbol{n}$-axis has been derived in (2.127) to be

$$\boldsymbol{n}(\Phi) = \mathrm{sig}(\delta) \frac{1}{\Lambda} \begin{pmatrix} \epsilon_\kappa \cos\Phi \\ \epsilon_\kappa \sin\Phi \\ \delta \end{pmatrix} , \quad \Lambda = \sqrt{\delta^2 + \epsilon_\kappa^2} , \quad \delta = \nu_0 - \kappa . \quad (4.41)$$

If Λ is not an integer, some tedious manipulations lead to [1]

$$|\boldsymbol{n}_N(\Phi, J) - \boldsymbol{n}(\Phi, J)| = \sqrt{2}\sqrt{1 - \tau_N} , \quad (4.42)$$

$$\tau_{N-1} = [1 + (\frac{\epsilon_\kappa}{N\delta})^2 \frac{1 - \cos(N2\pi\Lambda)}{1 - \cos(2\pi\Lambda)}]^{-1/2} . \quad (4.43)$$

One sees that $|\boldsymbol{n}_N - \boldsymbol{n}|$ is an oscillating function of the resonance strength ϵ_κ and therefore of the orbital amplitude J. The local maxima of $|\boldsymbol{n}_N - \boldsymbol{n}|$ increase with J, reflecting the fact that large orbital amplitudes reduce the convergence speed. This behavior is plotted in Fig. 4.12 (top). For all graphs in Fig. 4.12, the parameters $\nu_0 = 0.3$, $\kappa = 0.23$, and $\Phi = 0.32$ were used. For large N, equations (4.42) and (4.43) predict that the convergence is indeed linear with $1/N$, as illustrated by the slope of -1 in Fig. 4.12 (middle). Also one sees that $|\boldsymbol{n}_N - \boldsymbol{n}|$ vanishes for integer values of $N\Lambda$ if Λ is not also an integer. For integer values of Λ, one has

$$\tau_N = \frac{1}{\sqrt{1+(\frac{\epsilon_\kappa}{\delta})^2}} = \frac{|\delta|}{\Lambda} \ . \tag{4.44}$$

Therefore, in this case $\boldsymbol{n}_N$ does not converge to $\boldsymbol{n}$. This is no surprise because an integer Λ amounts to the resonance condition $\nu(\boldsymbol{J}) + j_0 = 0$, which leads to a non-uniqueness of the $\boldsymbol{n}$-axis.

Figure 4.12 (bottom) shows $P_{lim} = \delta/\sqrt{\delta^2 + \epsilon_\kappa^2}$ as a function of the resonance strength (blue curve). Even for N as small as 20, stroboscopic averaging is quite accurate (red points).

4.2.5 Stroboscopic Averaging for HERA-p

Although the existence of the $\boldsymbol{n}$-axis cannot be guaranteed in a realistic accelerator, an approximately invariant spin field can be found if the series $\boldsymbol{n}_N$ converges. To indicate the convergence of this series, $|\boldsymbol{n}_N - \boldsymbol{n}_{20000}|$ is plotted for the phase space point with $y_i = 0.4$ mm and $y'_i = 0$ in the east interaction region for the HERA-p lattice of the year 2000. This corresponds to a vertical amplitude of 69π mm mrad and is therefore a particle at approximately 4σ of the beam distribution. The slope of -1 in the double logarithmic scale of Fig. 4.13 illustrates clearly that the convergence is linear with $1/N$.

For particles that oscillate only in the kth degree of freedom in phase space, one can easily check that the stroboscopic average $\boldsymbol{n}_N$ is a good approximation to an invariant spin field. The phase space points $\boldsymbol{z}_j$ in the Poincaré section at θ_0 obtained by tracking a particle with initial phase space coordinates $\boldsymbol{z}_0$ for many turns are all on the curve with constant J_k, which is referred to as an invariant ellipse. Here this curve is parameterized as $\boldsymbol{z}(\Phi_y)$ with $\Phi_y \in [0, 2\pi)$. The vectors $\boldsymbol{n}(\boldsymbol{z}_j)$ are also all on a closed curve, which is given by $\boldsymbol{n}(\boldsymbol{z}(\boldsymbol{\Phi}_y))$. Such a closed curve on the unit sphere is an invariant curve of spin-orbit motion because it is mapped onto itself under the one turn spin-orbit transport.

If $\boldsymbol{n}_N$ approximates an $\boldsymbol{n}$-axis, the tracked spins $\boldsymbol{S}_j$ for $\boldsymbol{S}_0 = \boldsymbol{n}_N(\boldsymbol{z}_0)$ have to lie approximately on a closed curve on the unit sphere. If the spin of a particle initially has an angle $\vartheta > 0$ with respect to the invariant spin field, the tracked spins would not all be located on a one-parametric closed curve but would wobble around this curve because the angle between the spin and the $\boldsymbol{n}$-axis is a constant of motion.

The pictures in Fig. 4.14 show invariant curves $\boldsymbol{n}(\boldsymbol{z}(\Phi_y))$ on the unit sphere at 820 GeV/c for the east interaction point of the HERA-p lattice of the year 2000. The left curve was obtained before, and the right curve after, the introduction of 4 Siberian Snakes [14] into the accelerator. Here the standard scheme $(0\frac{\pi}{2}00)fs6$ was used. It can clearly be seen that stroboscopic averaging yielded the $\boldsymbol{n}$-axis accurately and that the variation of the $\boldsymbol{n}$-axis

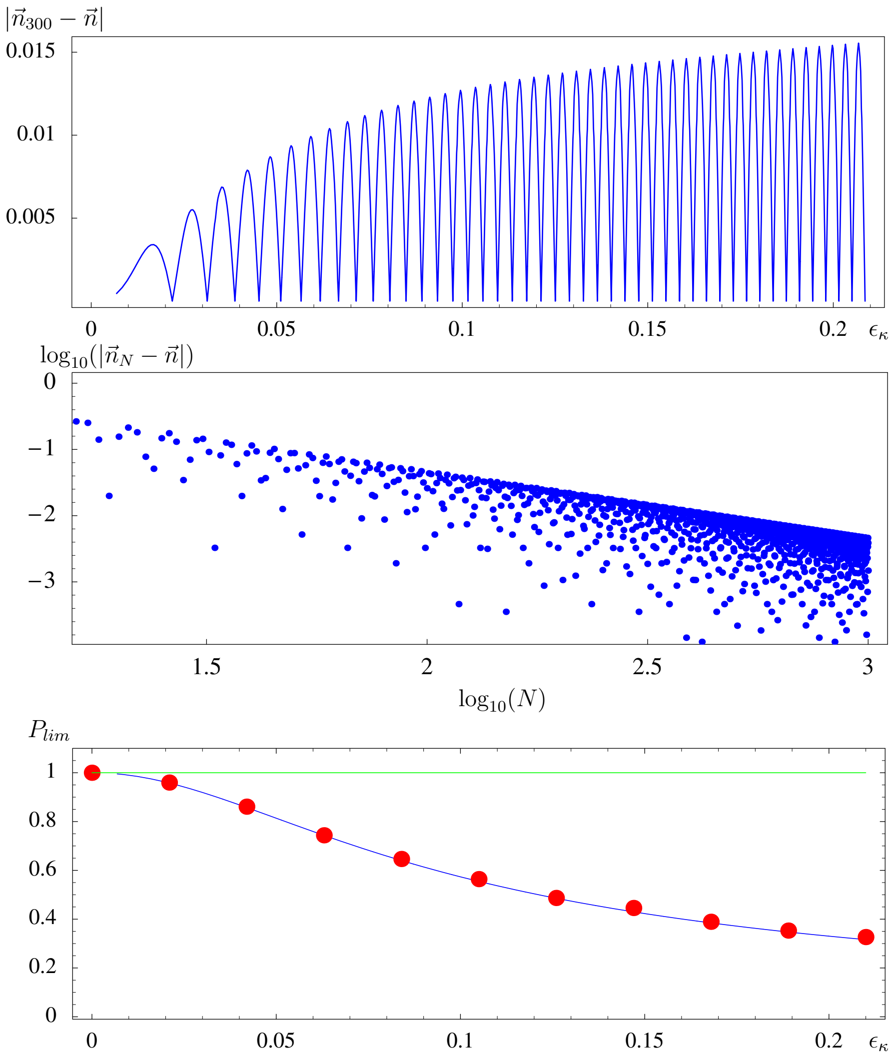

Fig. 4.12. All three graphs refer to the SRM with $\kappa = 0.23$, $\nu_0 = 0.30$. The deviation of the stroboscopic average $\boldsymbol{n}_N$ from the analytically calculated $\boldsymbol{n}$ is shown as a function of ϵ_κ for $N = 300$ (*top*) and as a function of N for $\epsilon_\kappa = 0.2$ (*middle*). P_{lim} (*bottom*) computed by stroboscopic averaging with $N = 20$ (*points*) and the analytically calculated P_{lim} (*curve*).

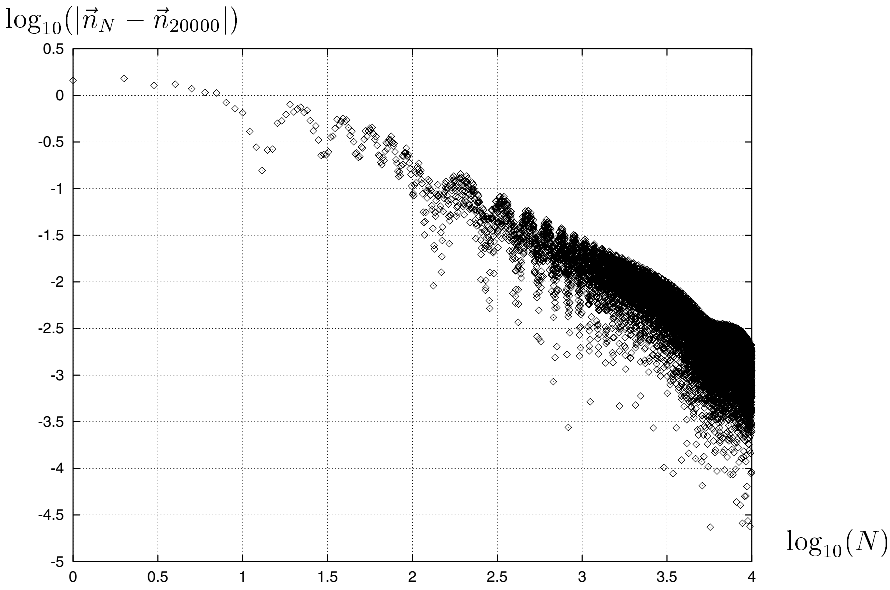

Fig. 4.13. The accuracy $|\boldsymbol{n}_N - \boldsymbol{n}_{20000}|$, where the $\boldsymbol{n}$-axis was computed at the east interaction point of the HERA-p lattice used in 2000. The slope of -1 in the double logarithmic scale illustrates that the convergence of $|\boldsymbol{n}_N - \boldsymbol{n}|$ is linear with $1/N$.

over the invariant torus is strongly reduced when Siberian Snakes are used, leading to a $P_{lim} = \langle\boldsymbol{n}\rangle$, which is close to 1.

Distorted Invariants of Spin Motion: For the single resonance model, the $\boldsymbol{n}$-axis is given by (2.127) as

$$\boldsymbol{n}(\Phi) = \mathrm{sig}(\delta)\frac{1}{\Lambda}\begin{pmatrix}\epsilon_\kappa \cos\Phi \\ \epsilon_\kappa \sin\Phi \\ \delta\end{pmatrix} , \quad \Lambda = \sqrt{\delta^2 + \epsilon_\kappa^2} \; . \tag{4.45}$$

The invariant curves $\boldsymbol{n}(\Phi)$ are therefore circles on the unit sphere. For linearized spin-orbit motion in the kth degree of freedom, the $\boldsymbol{n}$-axis is given by (3.29) as

$$\alpha_n = \sqrt{J_k}(B_k^+ \mathrm{e}^{\mathrm{i}\Phi_k} + B_k^- \mathrm{e}^{-\mathrm{i}\Phi_k}) \; . \tag{4.46}$$

The real and imaginary parts of α_n are therefore each a linear combination of trigonometric functions. This can be described by some 2×2-dimensional matrix B,

$$\begin{pmatrix}\Re\{\alpha_n\} \\ \Im\{\alpha_n\}\end{pmatrix} = \mathsf{B}\begin{pmatrix}\sin\Phi_k \\ \cos\Phi_k\end{pmatrix} , \tag{4.47}$$

which leads to the matrix equation of an ellipse,

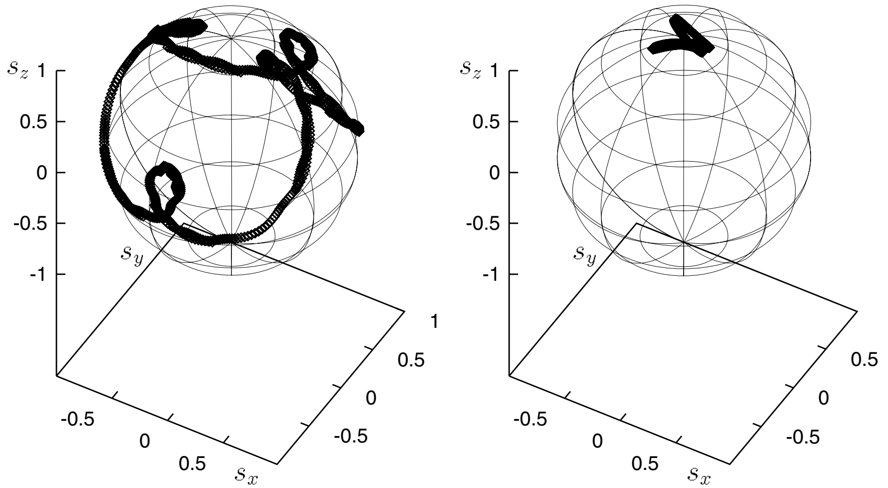

Fig. 4.14. The invariant spin field $\boldsymbol{n}(\boldsymbol{z}(\Phi_y))$ for the 2σ vertical phase space ellipse of 16π mm mrad at 820 GeV in the HERA-p lattice of the year 2000 with 6 flattening snakes. **Left**: Without Siberian Snakes. **Right**: For the $(0\frac{\pi}{2}00)fs6$ snake scheme.

$$(\Re\{\alpha_n\}, \Im\{\alpha_n\})\mathsf{B}^T\mathsf{B}\begin{pmatrix}\Re\{\alpha_n\}\\ \Im\{\alpha_n\}\end{pmatrix} = 1\ . \tag{4.48}$$

The invariant curves for linearized spin-orbit motion are therefore ellipses around $\boldsymbol{n}_0$.

When the invariant spin field is computed non-perturbatively, the invariant curves $\boldsymbol{n}(\boldsymbol{z}(\Phi_y))$ are no longer ellipses and their deviation from an elliptical form can show how inaccurate the approximation of linearized spin-orbit motion is. In Fig. 4.15, such closed curves on the unit sphere are shown for various amplitudes of vertical motion. The initial spin direction $\boldsymbol{n}(\boldsymbol{z}_i)$ has been obtained by stroboscopic averaging, and the curves have been obtained by subsequent multi-turn spin tracking. Even for the very complex invariant curves at high amplitudes, stroboscopic averaging leads to accurate results.

The irregularity of the invariant curves of spin-orbit motion at high energy clearly illustrates the limitations of the first-order treatment [2].

Coupling of the Degrees of Freedom: So far only vertical motion has been considered, and for moderate phase space amplitudes the approximation of linearized spin-orbit motion can work very well for one degree of freedom even at the very high energies. Figure 4.16 was computed for the HERA-p lattice of the year 2000 after the installation of 6 flattening snakes. It shows that for purely vertical motion with a phase space amplitude of 4π mm mrad, the maximum time-average polarization P_{lim} between 818 and 820 GeV/c follows very closely the correct curve computed by stroboscopic averaging using the program SPRINT. The linear approximation fails for 16, 36, and

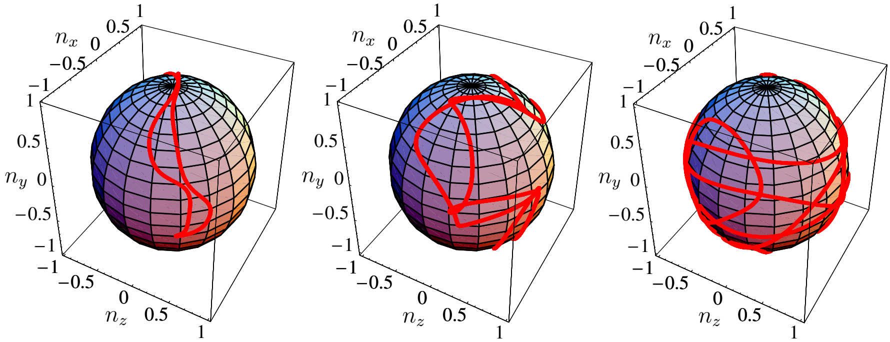

Fig. 4.15. The invariant curves $\boldsymbol{n}(\boldsymbol{z}(\Phi_y))$ on the unit sphere for various phase space amplitudes in the vertical degree of freedom: left: 4, middle: 9, and right: 81π mm mrad at the east interaction point of the HERA-p lattice used in 2000 at 804 GeV/c and with the $(0\frac{\pi}{2}00)6fs$ snake scheme.

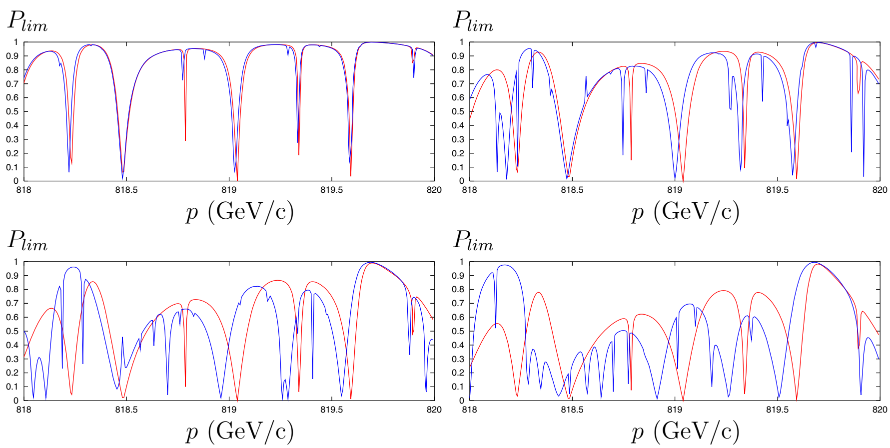

Fig. 4.16. P_{lim} for HERA-p with 6 flattening snakes computed with linearized spin-orbit motion (*light gray*) and with stroboscopic averaging (*dark gray*) for normalized vertical amplitudes of top left: 4, top right: 16, bottom left: 36, and bottom right: 64π mm mrad.

64π mm mrad of vertical amplitude. The location of the resonant reductions of P_{lim} shift with increasing vertical amplitude. This is due to the amplitude dependence of the spin tune $\nu(\boldsymbol{J})$.

A motion without vertical amplitude in a flat ring always leads to an invariant spin field that is parallel to the vertical $\boldsymbol{n}_0$ because the particles travel only through vertical magnetic fields. This property is recovered by linearized spin-orbit motion. When also a vertical amplitude is excited, the fields through which a particle propagates vary with the horizontal and longi-

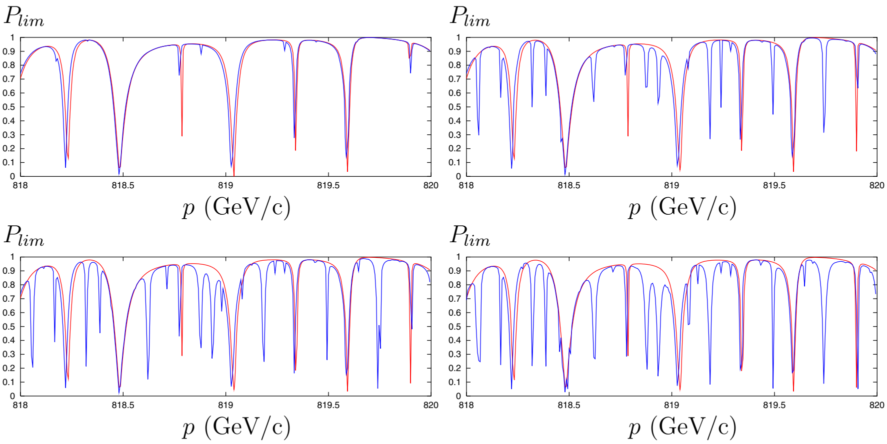

Fig. 4.17. P_{lim} $=\langle \boldsymbol{n} \rangle$ for HERA-p with 6 flattening snakes computed with linearized spin-orbit motion (*light gray*) and with stroboscopic averaging (*dark gray*) for particles with a normalized vertical amplitude of 4π mm mrad and a normalized horizontal amplitude of top left: 0, top right: 4, bottom left: 16, and bottom right: 36π mm mrad.

tudinal amplitude, and therefore P_{lim} changes. Thus there exists a crosstalk between all degrees of freedom and the spin motion, even when the orbital motion is linearly as well as nonlinearly decoupled [2]. The approximation of linearized spin-orbit motion cannot show this property. When a particle in a flat ring has amplitudes in all three degrees of freedom, the P_{lim} of linearized spin-orbit motion only depends on the vertical amplitude and does not change with the horizontal or longitudinal amplitude at all because the linear theory does not include any spin coupling between two different degrees of freedom. However, when the invariant spin field is computed by stroboscopic averaging of element by element tracking data, the crosstalk can be observed clearly as for example in Fig. 4.17 for HERA-p.

The underlying assumption of linearized spin-orbit motion is that the phase-space averaged angle $\langle \angle(\boldsymbol{n}, \boldsymbol{n}_0) \rangle$ is small so that in addition to the orbit motion the spin motion can also be linearized. However, the linearization does not conserve the length of spin and neglects the non-commutation of spin rotations around different axes. In parameter domains for which this underlying assumption is valid, as for example in the case of low-energy electron rings, these weaknesses are not a serious limitation except *very* close to spin-orbit resonances. However, in the proton ring of HERA-p with a $G\gamma$ of about 1756, this approximation can invalidate the calculations. Nevertheless, in Sect. 3.1 linearized spin-orbit motion has turned out to be very helpful for getting a quick estimate on the usefulness of a lattice for polarized proton storage.

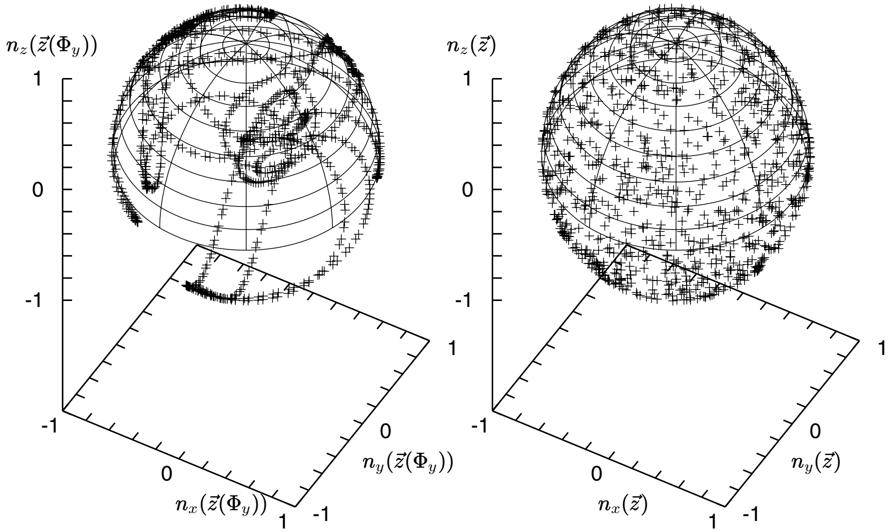

Fig. 4.18. Left: An invariant curve $\boldsymbol{n}(\boldsymbol{z}(\Phi_y))$ of spin-orbit motion on the unit sphere for particles in HERA-p with a normalized vertical amplitude of 64π mm mrad and no horizontal motion. **Right**: With an additional normalized horizontal amplitude of 4π mm mrad, the phase space points depend on two angle variables and $\boldsymbol{n}(\boldsymbol{z}(\Phi_x, \Phi_y))$ is no longer a one-parametric curve, because of crosstalk from horizontal motion to spin motion.

Figure 4.18 shows an invariant spin curve $\boldsymbol{n}(\boldsymbol{z}(\Phi_y))$ on the unit sphere for the amplitude of a relatively large vertical emittance (left). The average polarization is already strongly reduced. When the particle has also a non-zero horizontal amplitude then the invariant curves on the unit sphere get washed out and the average polarization is reduced to zero (right). Because the first-order theories neglect any influence of the horizontal motion on the invariant closed curves, Fig. 4.18 is far out of the range of validity of these theories.

Computing the invariant spin field from straightforward spin and phase space tracking data by stroboscopic averaging has the following features:

- It has been implemented in the code SPRINT but it can be implemented in any existing spin tracking program.
- For an accuracy on the 10^{-3} level, typically less than 3000 turns have to be tracked.
- Because the method is non-perturbative, no resonance denominators appear in the algorithm and it is applicable even close to spin-orbit resonances.

- Because the different degrees of freedom have a coupled influence on the invariant spin field, it is important that stroboscopic averaging can be used for simultaneous motion in all three degrees of freedom.

Since the introduction of stroboscopic averaging in [1], spin tracking in storage rings can now always be initialized with spins parallel to the invariant spin field, and much clearer analysis becomes possible.

4.3 Obtaining $\boldsymbol{n}(\boldsymbol{z})$ by Anti-damping

The $\boldsymbol{n}$-axis can also be calculated using the adiabatic invariance of $J_S = \boldsymbol{S} \cdot \boldsymbol{n}(\boldsymbol{z})$, which has been proven in Sect. 2.2.9. There are three possible procedures:

a) One could start a tracking computation with a spin aligned parallel to $\boldsymbol{n}_0$ at a low energy far away from any resonance where the invariant spin field $\boldsymbol{n}(\boldsymbol{z})$ is essentially parallel to $\boldsymbol{n}_0$ over all of the relevant phase space. Then one would accelerate the particles slowly up to the energy under investigation. As long as J_S remains nearly invariant the spin would end up parallel to $\boldsymbol{n}(\boldsymbol{z})$. The disadvantage of this approach is that at HERA-p one would essentially have to ramp the particle all the way from 40 to 920 GeV/c without violating the adiabatic invariance of J_S. This would not only require a lot of computation time but hundreds of residual resonance structures would have to be crossed, which might lead to a change in J_S. Therefore, a slow acceleration is not a suitable method of computing the invariant spin field. Nevertheless, this method demonstrates well what actually happens to the polarized beam when it is slowly accelerated in HERA-p.

b) One could start a tracking computation with a particle on the closed orbit polarized parallel to $\boldsymbol{n}_0 = \boldsymbol{n}(0)$. When the phase space amplitude is increased slowly, the spin will stay parallel to $\boldsymbol{n}(\boldsymbol{z})$ during the complete tracking run until the phase space amplitude of interest is reached. The energy is not changed during this process. This method has been tested and can be performed with practical speed [41]. It has the advantage over the other methods presented so far that one obtains the field $\boldsymbol{n}(\boldsymbol{z})$ at many phase space amplitudes. One can therefore easily compute the dependence of P_{lim} on $\boldsymbol{J}$. When the amplitude-dependent spin tune comes into resonance with the orbital tunes for some intermediate particle amplitude, J_S can change and the $\boldsymbol{n}$-axis obtained will be inaccurate.

c) A third method that has also been successful starts a tracking run with a particle at the phase space point $\boldsymbol{z}_{-N}$ and a spin parallel to $\boldsymbol{n}_0$. In order to make $\boldsymbol{n}_0$ parallel to the invariant spin field $\boldsymbol{n}(\boldsymbol{z})$, the spin-orbit coupling is switched off, i.e., particles all over phase space have the same spin motion as a particle on the closed orbit. Finally, the spin-orbit coupling is switched on slowly while tracking the particle for N turns until it arrives at the phase

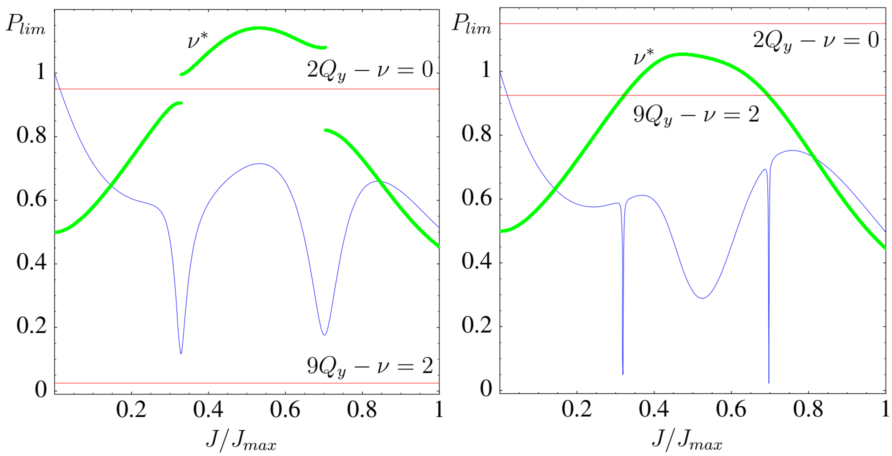

Fig. 4.19. P_{lim} (*blue*) and the magnified spin tune $\nu^* = \frac{1}{2} + 10(\nu - \frac{1}{2})$ (*green*) as functions of the ratio J/J_{max} between the intermediate vertical action J and the final action J_{max}. The final vertical amplitude was 81π mm mrad, which corresponds to 4.5σ of the current proton beam in HERA-p. When the spin tune comes close to one of the resonance lines (*red*), P_{lim} is reduced. **Left**: For $Q_y = 0.2725$. **Right**: For $Q_y = 0.2825$ in the HERA-p lattice of the year 2000 and for the $(0\frac{\pi}{2}00)6fs$ snake scheme.

space point $\boldsymbol{z}$. This procedure is especially helpful when analyzing the influence of resonance strength on the maximum time-average polarization because one obtains P_{lim} for a variation of resonance strength from 0 to a final value, allowing one to compute the maximally allowed resonance strength for a required average polarization. In fact, this technique of finding $\boldsymbol{n}$ by anti-damping the spin-orbit coupling is already contained in the SMILE formalism [42]. There it was not exploited numerically but used for deriving a formalism that leads to the required periodicity in azimuth. Also in this algorithm the accuracy can suffer when spin-orbit resonances occur during the calculation.

In the single resonance approximation of spin motion, the maximum time, average polarization is given by (2.135) as $P_{lim} = |\frac{\delta}{\sqrt{\delta^2+\epsilon_\kappa^2}}|$ where $\kappa = \nu_0 - \delta$ is the frequency of the resonance. The resonance strength ϵ_κ of the resonance (2.74) is the modulus of the Fourier coefficient of a linear function $\boldsymbol{\omega}(\boldsymbol{z}, l)$ of phase space variables and $\kappa = j_0 \pm Q_k$. Therefore, ϵ_κ increases with the square root of the action variable J_k of the kth degree of freedom, $\epsilon_\kappa \propto \sqrt{J_k}$. When one goes beyond this simple model, the polarization depends on the orbital amplitudes in a more complex fashion.

In some cases, as for example in Fig. 4.19 (left), P_{lim} increases with the phase space amplitude after it has decreased at smaller amplitudes [43].

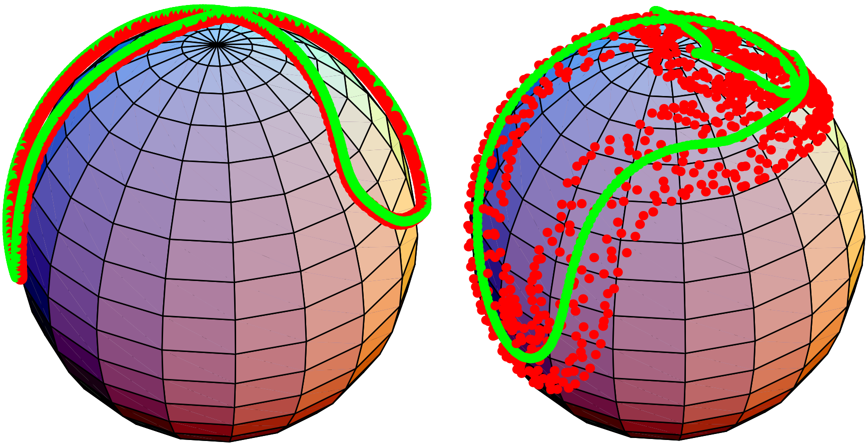

Fig. 4.20. Invariant curves $\boldsymbol{n}(\boldsymbol{z}(\vartheta))$ on the unit sphere computed by anti-damping (*red*) and by stroboscopic averaging (*green*) for a vertical amplitude of 16π mm mrad (*left*) and of 64π mm mrad (*right*) in the HERA-p lattice of the year 2000 with the $(0\frac{\pi}{2}00)6fs$ snake scheme.

This is an indication for amplitude-dependent tunes $\nu(\boldsymbol{J})$ and $\boldsymbol{Q}(\boldsymbol{J})$. While the amplitude changes, the tunes can come close to a resonance condition that causes P_{lim} to drop at some intermediate phase space amplitude. In Fig. 4.19 (left), it is not the vertical orbit tune that changed, because linear orbit motion is simulated so that $\boldsymbol{Q}$ does not depend on the phase space amplitude. The green curves in Fig. 4.19 show $\nu^* = \frac{1}{2} + 10(\nu - \frac{1}{2})$, the magnified distance of the spin tune from $\nu_0 = \frac{1}{2}$. When this tune comes close to the resonance $\nu = 2Q_y$, then $\boldsymbol{n}(\boldsymbol{z})$ varies strongly over phase space and P_{lim} becomes small. At intermediate amplitudes where ν has moved away from this resonance condition, P_{lim} is larger. Figure 4.19 (right) shows the amplitude dependence of the spin tune ν and P_{lim} after the vertical tune has been changed from $Q_y = 0.2725$ to $Q_y = 0.2825$. Therefore, the resonant spin tune values $\nu = 2Q_y$ and $\nu = 9Q_y - 2$ (red lines) also change, which in turn changes the amplitudes where P_{lim} is reduced. Now the spin tune comes close to the ninth order resonance and narrow dips of P_{lim} can be observed at the corresponding amplitudes.

To study such amplitude-dependent depolarizing effects, it is advantageous to have a method that quickly leads to $\boldsymbol{n}(\boldsymbol{z})$ at various amplitudes. The anti-damping method 2 described above has this feature and was implemented into SPRINT for that purpose. However, it is often not as accurate as stroboscopic averaging, because resonances might be crossed during the slow change of the amplitude, and the adiabatic invariance of $J_S = \boldsymbol{S} \cdot \boldsymbol{n}(\boldsymbol{z})$ can be violated. Therefore, Fig. 4.19, where resonances are crossed, has not been computed by anti-damping but by the SODOM-2 method.

Invariant curves on the unit sphere for such a case are shown in Fig. 4.20. They were computed with the $(0\frac{\pi}{2}00)6fs$ scheme for the HERA-p lattice of the year 2000 at 805 GeV/c [41]. While anti-damping (red curves) and stroboscopic averaging (green curves) both allow an accurate computation of the invariant spin field for particles with 16π mm mrad in Fig. 4.20 (left), the accuracy of anti-damping is strongly reduced at 64π mm mrad in Fig. 4.20 (right), because a resonance condition had to be crossed during the anti-damping procedure. The accuracy can be increased by reducing the speed with which the phase space amplitude is increased.

References

1. K. Heinemann and G. H. Hoffstaetter: A tracking algorithm for the stable spin polarization field in storage rings using stroboscopic averaging. *Phys. Rev.* E 54:4240–4255 (1996)
2. G. H. Hoffstaetter, M. Vogt, and D. P. Barber: Higher-order effects in polarized proton dynamics. *Phys. Rev. ST–AB*, 2(11):1–15 (1999)
3. S. R. Mane: Exact solutions for the spin tune for model storate rings. *Nucl. Instr. Meth. A*480:328–338 (2002)
4. S. R. Mane: MILES: a new nonperturbative formalism to calculate the invariant spin field in circular accelerators. *Nucl. Instr. Meth. A*498:1–15 (2003)
5. K. Yokoya: An algorithm for calculating the spin tune in circular accelerators. DESY–99–006 (1999)
6. K. Yokoya: Non-perturbative calculation of equilibrium polarization of stored electron beams. KEK–92–6, Tsukuba (1992)
7. G. H. Hoffstaetter and M. Vogt: SPRINT users guide and reference manual. DESY (2002)
8. D. P. Barber, K. Heinemann, G. H. Hoffstaetter, and M. Vogt: Calculations of the equilibrium spin distribution for protons at high energy in HERA. In *Proceedings of SPIN96*, Amsterdam (1996)
9. D. P. Barber, G. H. Hoffstaetter, and M. Vogt: Using the amplitude dependent spin tune to study high order spin-orbit resonances in storage rings. In *Proceedings SPIN00*, Osaka (2000)
10. D. P. Barber, G. H. Hoffstaetter, and M. Vogt: Proton and electron polarsation in storage rings: some basic concepts. In *Proceedings SPIN00*, Osaka (2000)
11. D. P. Barber and A. De Roeck, editors: *Proceedings of Polarized Protons at High Energies*, DESY–Proceedings–1999–03 (1999)
12. D. P. Barber, G. H. Hoffstaetter, and M. Vogt: Numerical and theoretical spin stability studies for HERA-p. In [11].
13. G. H. Hoffstaetter: Polarized protons in HERA. In *Proceedings of NUCLEON99, Nucl. Phys.* A (1999)
14. G. H. Hoffstaetter: Polarized protons in HERA. In DESY–96–05 (1996)
15. D. P. Barber, K. Heinemann, G. Hoffstaetter, and M. Vogt: The polarization at high energy in HERA. DESY–HERA–96–07 (1996)
16. D. P. Barber, G. H. Hoffstaetter, and M. Vogt: Spin motion at high energy in HERA-p. In UM–HE 99–05, University of Michigan (1999)
17. K. L. Brown: A first- and second-order matrix theory for the design of beam transport systems and charged particle spectrometers. SLAC–75, Menlo Park/CA (1982)
18. E. Forest: Canonical integrators as tracking codes (or how to integrate perturbation theory with tracking). SSC–SR–138, SSC Central Design Group (1987)
19. E. Forest and K. Ohmi: Symplectic integration for complex wigglers. KEK–92–14, Tsukuba (1992)
20. J. S. Berg, R. L. Warnock, R. D. Ruth, and E. Forest: Construction of symplectic maps for nonlinear motion of particles in accelerators. SLAC–PUB–6037, Menlo Park/CA (1993)
21. G. H. Hoffstaetter and M. Berz: Accurate and fast computation of high order fringe-field maps via symplectic scaling. *Nucl. Instr. Meth.* A(363):124–127 (1995)

22. G. H. Hoffstaetter and M. Berz: Symplectic scaling of transfer maps including fringe fields. *Phys. Rev.* E 54(5):5664–5672 (1996)
23. M. Berz: Symplectic tracking through circular accelerators with high order maps. In *Nonlinear Problems in Future Accelerators*, World Scientific, p. 288–296 (1991)
24. E. Forest: Lie algebraic maps and invariants produced by tracking codes. *Particle Accelerators*, 22:15 (1987)
25. Y. Yan: Performance of an implicit algorithm for symplectic one-turn-map tracking. SSCL–Preprint–157, SSC Central Design Group (1993)
26. I. M. Gjaja: A comparison of methods for long-term tracking using symplectic maps. In *Nonlinear problems in accelerator physics*, Institute of Physics. Conf. Ser. No. 131, p. 185–192, London (1993)
27. L. Schachinger and R. Talman: TEAPOT, a thin element program for optics and tracking. *Particle Accelerators*, 22:35 (1987)
28. F. Willeke: Tutorial on modern tools of particle tracking. Lecture held at the CERN school on advanced accelerator physics in Rhodos. DESY–M–94–12 (1994)
29. V. Balandin, N. Golubeva, and D. P. Barber: Studies of the behavior of proton spin motion in HERA-p at high energies. Part II: Acceleration of Polarized Protons in HERA. DESY–M–98–03 (1998)
30. G. H. Hoffstaetter: Successive approximations for charged particle motion. *Ultramicroscopy* 81:111–121 (2000)
31. Ch. Weißbäcker: Nichtlineare Effekte der Spindynamik in Protonenbeschleunigern. *Diploma thesis, Darmstadt University of Technology* (1998)
32. Ch. Weißbäcker and G. H. Hoffstaetter: Nonlinear spin transfer maps. In [11].
33. M. Vogt: Bounds on the maximum attainable equilibrium spin polarization of protons in HERA. *Dissertation, Universität Hamburg*, DESY–THESIS–2000–054 (December 2000)
34. K. Balewski, R. Brinkmann, Ya. Derbenev, K. Flöttmann, *et al*: Studies of electron cooling at DESY. In *Proceedings of ECOOL99*, Uppsala (1999)
35. P. Wesolowski, K. Balewski, R. Brinkmann, Ya. Derbenev, and K. Flöttmann: An injector study for electron cooling at PETRA using a bunched beam. In *Proceedings of ECOOL99*, Uppsala (1999)
36. M. Gentner, D. Husmann, C. Steier, R. Brinkmann, and Ya Derbenev: On the possibilities of electron cooling for HERA. *Nucl. Instr. Meth.* A424:277–295 (1999)
37. R. Brinkmann for the DESY electron cooling study group: Electron cooling studies for PETRA and HERA. In [11].
38. E. D. Courant and R. D. Ruth: The acceleration of polarized protons in circular accelerators. BNL–51270 and UC–28 and ISA–80–5 (1980)
39. S. Y. Lee and E. D. Courant: Tolerance of imperfections in high-energy circular accelerators for polarized protons. *Phys. Rev.* D(41):292–302 (1990)
40. G. H. Hoffstaetter: Polarized protons at HERA: the accelerator issues. In [11].
41. D. P. Barber, M. Vogt, and G. H. Hoffstaetter: The amplitude-dependent spin tune and the invariant spin field in high-energy proton accelerators. In *Proceedings EPAC98*, Stockholm (1998)
42. S. R. Mane: Electron-spin polarization in high-energy storage rings. II. Evaluation of the equilibrium polarization. *Phys. Rev.* A(36):120–130 (1987)

43. D. P. Barber, G. H. Hoffstaetter, and M. Vogt: The amplitude-dependent spin tune and the invariant spin field in high-energy proton accelerators. In *Proceedings SPIN98*, Protvino (1998)

5 Polarized Beams in Other Very-High-Energy Proton Accelerators

By introducing the invariant spin field $\boldsymbol{n}(\boldsymbol{z})$ and the amplitude-dependent spin tune $\nu(\boldsymbol{J})$ and by proving the adiabatic invariance of the spin action $J_S = \boldsymbol{S} \cdot \boldsymbol{n}$, concepts have been provided with which it is possible to systematize many features of the acceleration of polarized beams. Of particular importance among these is the loss of polarization when J_S does not remain invariant. These concepts can also be numerically evaluated with the three non-perturbative algorithms for determining $\boldsymbol{n}(\boldsymbol{z})$ and $\nu(\boldsymbol{J})$ that have been introduced: SODOM-2, stroboscopic averaging, and anti-damping.

These three algorithms have become the basis for an analysis of higher-order effects of spin motion in HERA-p and have also been adopted for the analysis of some aspects of polarized proton motion in RHIC, where already a 205 GeV polarized beam has been stored [1, 2]. Other accelerators where these tools would be essential for the simulation and optimization of polarized proton beams are the TEVATRON and the LHC [3]. For these there are currently no plans to polarize the beams. When polarized beams are desired for any future high-energy ring accelerator for protons, like a possible VLHC [4], the tools presented here will be essential in the design stage. It has been pointed out [6] that dipoles with a strong quadrupole component lead to reduced depolarizing resonance strength at high energies. This effect was observed for a combined function lattice for the VLHC booster [5] and could be used to facilitate polarized beams in future accelerators.

With these advanced computational techniques, it has become possible to determine the strengths of higher-order resonances, and it has been shown that they allow the Froissart-Stora formula to be used to predict the loss of polarization when crossing these resonances.

Furthermore, the construction of the invariant spin field $\boldsymbol{n}$ for the design configuration of an accelerator is a good starting point for the investigation of noise processes that can disturb the invariance of $J_S = \boldsymbol{S} \cdot \boldsymbol{n}$. Examples of such processes are intra-beam scattering (IBS), beam-beam collisions in interaction points, synchrotron radiation in the case of polarized electrons, or time dependent errors in accelerator components, like the RF system. Similarly, computing $\boldsymbol{n}$ is a good starting point for the analysis of coupling due to field errors, of the influence of nonlinear fields on spin motion, and of nonlinear effects of synchrotron motion.

In HERA-p, the maximum time-average polarization is very small at critical energies where the spin perturbations of all FODO cells accumulate. Large first-order resonances and low average polarization due to this accumulation can also be seen for RHIC, the TEVATRON, and the LHC in Figs. 5.2, 5.4 and 5.6. This effect was analyzed in detail for HERA-p with linearized spin-orbit motion and the role of the non-flat regions was stressed. This analysis showed that it is helpful to symmetrize the spin perturbations in HERA-p by the use of 8 flattening snakes. A similar analysis would be required for polarized beams in other high-energy proton or ion accelerators.

It has been found that the various snake schemes have very different abilities to preserve the polarization during the acceleration process in HERA-p, and therefore schemes with optimized snake angles have to be found. For this purpose, a filtering algorithm was devised that tests a huge number of potential snake schemes and selects the scheme with the maximum average P_{lim} and the minimum spread of the spin tune over the phase space amplitudes in a polarized proton beam.

In addition, methods have been found to match the snake angles to a suitably modified vertical betatron phase advance in HERA-p so that P_{lim} for linearized spin-orbit motion does not drop strongly at the critical energies where the spin perturbations in all FODO cells accumulate. When higher-order effects are included, these snake-matched lattices with 4 and 8 snakes were shown to reduce the spin tune spread and to allow the acceleration of polarized beams with significantly larger orbital amplitudes.

Similar optimizations would be required for finding optimal snake schemes for the TEVATRON, LHC, or a possible VLHC. In the following, the resonance strength, the P_{lim} from linearized and from nonlinear spin-orbit motion, as well as the amplitude-dependent spin tune $\nu(\boldsymbol{J})$ are plotted for RHIC, for the TEVATRON, and for the LHC. For the latter two, the snake schemes and the tunes have not been optimized. Thus the strong higher-order resonances that can be observed would have to be reduced by optimizations similar to those made for HERA-p.

In the HERA-p lattice used in 2004, with the optimal scheme of 4 Siberian Snakes, only particles with a vertical phase space amplitude below 11π mm mrad can be accelerated without a reduction of polarization. And even in snake-matched schemes with 8 Siberian Snakes, particles with a vertical phase space amplitude above 16π mm mrad will experience a reduction of polarization. Because these numbers have been computed for the design configuration of HERA-p, an analysis of misalignments, field errors, and realistic closed orbit deviations would lead to somewhat smaller phase space amplitudes for polarized particle transport.

Therefore, it would be very advisable to use electron cooling in HERA-p or in its pre-accelerator so as to reduce the emittance in HERA-p and to allow for an acceleration without loss of polarization for most particles in the beam. Similarly, an emittance reduction by electron cooling would also benefit polarized beam acceleration in all other high-energy polarized proton accelerators.

5.1 The Relativistic Heavy Ion Collider (RHIC)

It has been mentioned several times that RHIC at Brookhaven National Laboratory (BNL) has accelerated polarized proton beams to by far the highest energies. Figure 5.1 shows a layout from [7] of the two rings (blue and yellow) of RHIC that are used for ion-ion collisions as well as for polarized proton-proton collisions. Each of the two rings has two Siberian Snakes and their snake axes are indicated. Furthermore, there are several spin rotators that rotate vertical polarization into longitudinal polarization at collision points and back again after the interaction points. The Siberian Snakes and the spin rotators are both made up of 4 helical dipole magnets and the different types of such magnets are indicated by the labels $R^{\pm}$ and $L^{\pm}$, which indicate the handedness and the direction of current flow. Furthermore, it is shown in which sections of the rings the polarization is up and in which it is down.

Since 2003, a helical partial snake in RHIC's pre-accelerator the AGS has been used to avoid coupling between horizontal and vertical particle oscillations as mentioned in Sec. 2.2.1, and between 40% and 50% of polarization can routinely be injected into RHIC and are then accelerated.

Figure 5.2 shows the first-order resonance strength and P_{lim} of linearized spin-orbit motion for a polarized proton beam for a 2.5σ emittance, assuming the one σ emittance is 4π mm mrad in order to compare with the plots for HERA-p, for which the same emittances were assumed.

Because the resonance strengths are relatively small compared with those in HERA-p, P_{lim} computed non-perturbatively for Fig. 5.3 (up) resembles those of linearized spin-orbit motion quite well. The amplitude-dependent spin tune does not fluctuate strongly away from $\frac{1}{2}$ and more importantly, no large gaps in the spin tune are observed, indicating that there are no strong low order spin-orbit resonances that have to be crossed during the acceleration of polarized protons in RHIC. This is largely due to a good choice of the vertical tune.

However, in Fig. 5.3 (right) where a restricted energy range has been plotted, 11th-order resonances can be clearly seen, and the strength of these resonances can be determined from the spin tune jumps.

5.2 TEVATRON

There are currently no plans to accelerate polarized protons in the TEVATRON. However, a proposal had been prepared in 1994 [8, 9].

Figure 5.4 shows the first-order resonance strength and P_{lim} computed for a 2.5σ emittance. As in the case of HERA-p, the 1σ normalized emittance

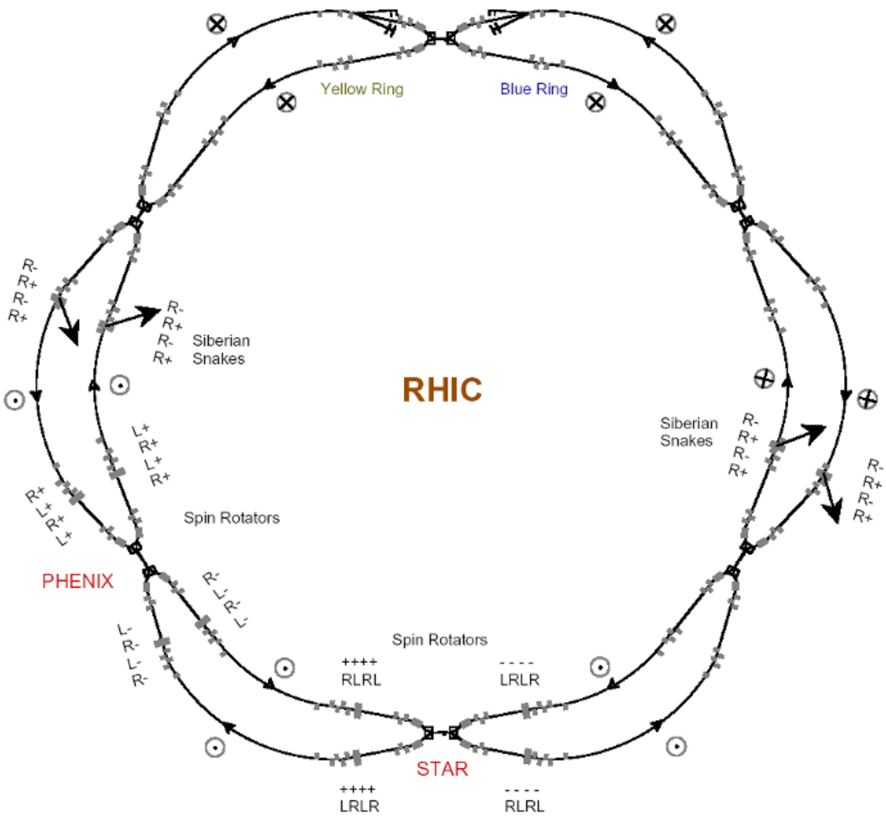

Fig. 5.1. Schematic layout of RHIC at BNL. The two Siberian Snakes per ring and their snake axes are shown.

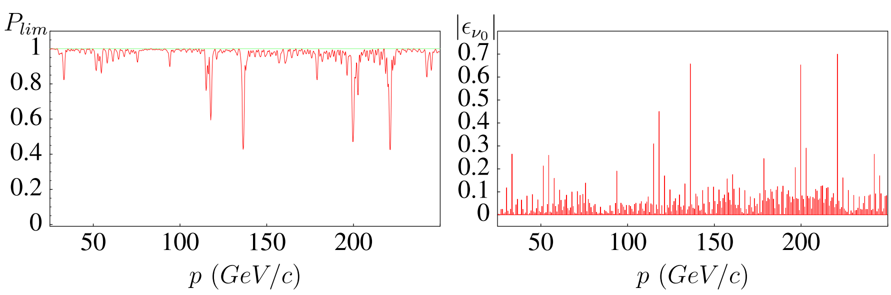

Fig. 5.2. Left: linearized P_{lim} and **Right**: resonance strength for RHIC at BNL.

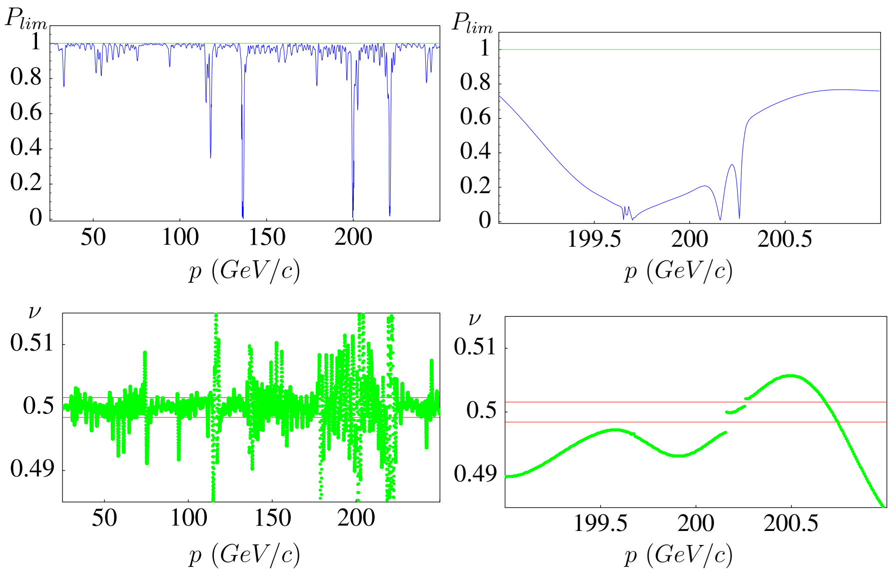

Fig. 5.3. Top: P_{lim} and **Bottom**: ν for RHIC at BNL. The two lines indicate the resonances $\nu = \pm 11 Q_y$ for $Q_y = 29.227$.

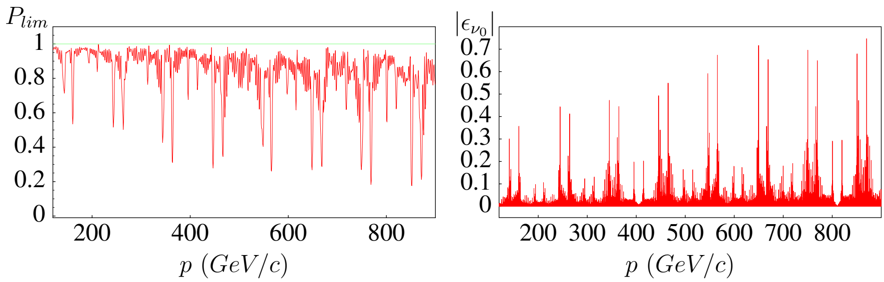

Fig. 5.4. Left: linearized P_{lim} and **Right**: resonance strength for the TEVATRON at Fermilab.

was assumed to be 4π mm mrad. Also for the TEVATRON, the structure of super-strong resonances is again due to a coherent interaction of the spin disturbances in all FODO cells.

Non-perturbative computation of the invariant spin field on the ramp of the TEVATRON leads to the P_{lim} and $\nu(\boldsymbol{J})$ in Fig. 5.5. Spin tune jumps at first- and third-order resonances can clearly be seen. Because the TEVATRON was simulated with exact mid-plane symmetry, second-order resonances as found in HERA-p do not appear.

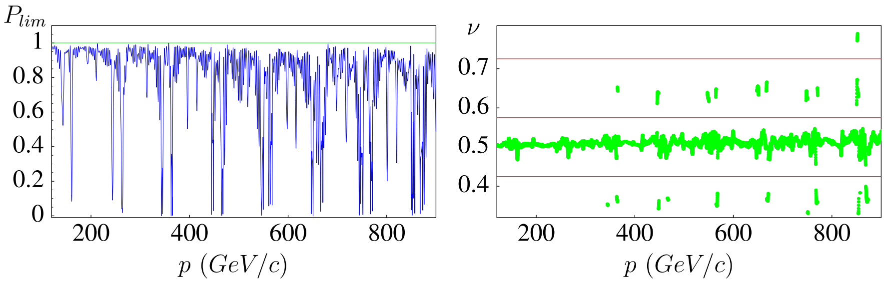

Fig. 5.5. Left: P_{lim} and **Right**: ν for the TEVATRON at Fermilab. The lower two lines on the right indicate the resonances $\nu = \pm Q_y$ Mod 1, and the top line indicates the resonance $\nu = 3Q_y$ Mod 1 for $Q_y = 20.574$.

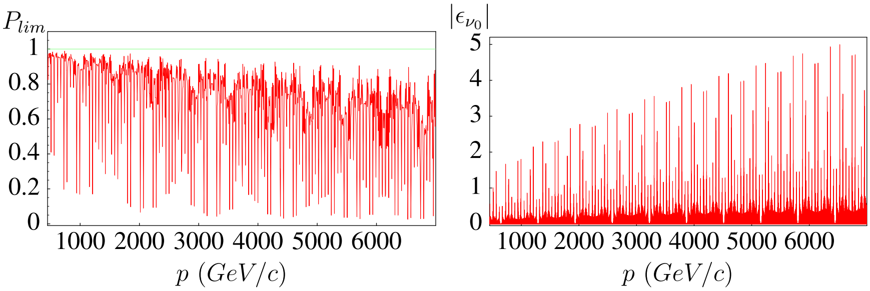

Fig. 5.6. Left: linearized P_{lim} and **Right**: resonance strength for the LHC at CERN.

Here we used a simple non-optimized scheme where the snakes are placed at each of the six symmetry points of the TEVATRON and have snake angles alternating $\pm 45°$. Furthermore, the orbital tunes have not been optimized for polarized beam operation and a rather arbitrary vertical tune of 20.574 has been used that clearly shows resonances in the vicinity of the closed-orbit spin tune of $\nu_s = \frac{1}{2}$.

5.3 LHC

For the LHC, there are currently also no plans to accelerate polarized beams. First-order resonances and P_{lim} of linearized spin-orbit motion are shown in Fig. 5.6. Many very strong resonances where spin rotation in FODO cells add up are clearly visible. P_{lim} and $\nu(\boldsymbol{J})$ for non-perturbative spin-orbit motion are shown in Fig. 5.7. Again normalized 1σ emittances of 4π mm mrad were used, and all simulations were done for 2.5σ emittances.

On the left of Fig. 5.7, many spin-orbit resonances up to order 9 can be seen. On the right, tune jumps at first, fifth, and seventh-order resonances

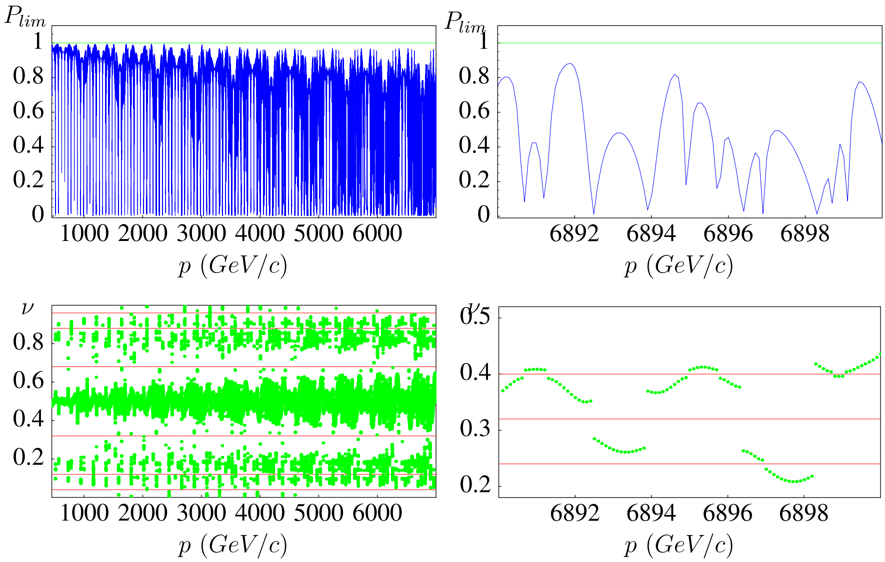

Fig. 5.7. **Top**: P_{lim} and **Bottom**: ν for the LHC at CERN. **Left**: The lines indicate the resonances $\nu = \pm Q_y$ Mod 1, $\nu = \pm 3Q_y$ Mod 1 and $\nu = \pm 9Q_y$ Mod 1 for $Q_y = 59.32$. **Right**: Starting from the bottom, the three lines indicate the resonances $\nu = 7Q_y$ Mod 1, $\nu = Q_y$ Mod 1, and $\nu = -5Q_y$ Mod 1.

can be seen for a restricted energy range. These could be used to determine the strength of these higher-order resonances. However, the orbital tunes were not optimized for polarized beam acceleration and a non-optimized scheme of 8 Siberian Snakes with one snake angle of 90° and 7 snake angles of 0° was used. The higher-order resonance structure could certainly be drastically improved if the optimization techniques described in this tract are employed.

With this I close this modern account high-energy polarized proton beams. The reader will have seen that linearized spin-orbit motion, which is sufficient to design medium-energy accelerators with polarized beams, is no longer sufficient at high energies. One has to watch out for complications due to nonlinear effects that can be evaluated with advanced computational tools.

References

1. W. Fischer: Presentation at the BNL Machine Advisory Committee Meeting (January 2006)
2. T. Roser: RHIC operational status. In *Proceedings PAC05*, Knoxville/TN (2005)
3. The LHC Study Group: The Large Hadron Collider Conceptual Design. Report CERN/AC/95-05, October (2003)

4. M. Blaskiewicz, A. Drees, W. Fischer, R. Gupta, S. Peggs, F. Pilat *et al.*: VLHC accelerator physics. Report FERMILAB-TM-2158, (2001)
5. V. A. Anferov: Weak Depolarizing Resonances in the 3-TeV VLHC Booster, *Phys. Rev. Lett.* 83, 14 p. 2738–2740 (1999)
6. A. W. Chao, Ya. S. Derbenev: Cancellation of the quadrupole effect on spin in high-energy accelerators. *Part. Accel.* 36, 25–32 (1991)
7. I. Alekseev, C. Allgower, M. Bai, Y. Batygin, L. Bozano, K. Brown, *et al*: Design Manual – Polarized Proton Collider at RHIC. Report: Brookhaven National Laboaratory (1998)
8. R. Baiod, P. S. Martin and A. D. Russell for the SPIN Collaboration, Polarized protons in the Tevatron Collider. Proceedings 10th Topical Workshop on Proton-Antiproton Collider Physics, Batavia/IL (1995)
9. L. C. Teng, Accelerating A Polarized Beam In The Tevatron. Proceedings Symposium on Future Polarization Physics, Batavia/IL (1988)

Index

Springer Tracts in Modern Physics

197 **Electroweak Processes in External Electromagnetic Fields**
By A. Kuznetsov and N. Mikheev 2003. 24 figs., XII, 136 pages

198 **Electroweak Symmetry Breaking**
The Bottom-Up Approach
By W. Kilian 2003. 25 figs., X, 128 pages

199 **X-Ray Diffuse Scattering from Self-Organized Mesoscopic Semiconductor Structures**
By M. Schmidbauer 2003. 102 figs., X, 204 pages

200 **Compton Scattering**
Investigating the Structure of the Nucleon with Real Photons
By F. Wissmann 2003. 68 figs., VIII, 142 pages

201 **Heavy Quark Effective Theory**
By A. Grozin 2004. 72 figs., X, 213 pages

202 **Theory of Unconventional Superconductors**
By D. Manske 2004. 84 figs., XII, 228 pages

203 **Effective Field Theories in Flavour Physics**
By T. Mannel 2004. 29 figs., VIII, 175 pages

204 **Stopping of Heavy Ions**
By P. Sigmund 2004. 43 figs., XIV, 157 pages

205 **Three-Dimensional X-Ray Diffraction Microscopy**
Mapping Polycrystals and Their Dynamics
By H. Poulsen 2004. 49 figs., XI, 154 pages

206 **Ultrathin Metal Films**
Magnetic and Structural Properties
By M. Wuttig and X. Liu 2004. 234 figs., XII, 375 pages

207 **Dynamics of Spatio-Temporal Cellular Structures**
Henri Benard Centenary Review
Edited by I. Mutabazi, J.E. Wesfreid, and E. Guyon 2005. approx. 50 figs., 150 pages

208 **Nuclear Condensed Matter Physics with Synchrotron Radiation**
Basic Principles, Methodology and Applications
By R. Röhlsberger 2004. 152 figs., XVI, 318 pages

209 **Infrared Ellipsometry on Semiconductor Layer Structures**
Phonons, Plasmons, and Polaritons
By M. Schubert 2004. 77 figs., XI, 193 pages

210 **Cosmology**
By D.-E. Liebscher 2005. Approx. 100 figs., 300 pages

211 **Evaluating Feynman Integrals**
By V.A. Smirnov 2004. 48 figs., IX, 247 pages

213 **Parametric X-ray Radiation in Crystals**
By V.G. Baryshevsky, I.D. Feranchuk, and A.P. Ulyanenkov 2006. 63 figs., IX, 172 pages

214 **Unconventional Superconductors**
Experimental Investigation of the Order-Parameter Symmetry
By G. Goll 2006. 67 figs., XII, 172 pages

215 **Control Theory in Physics and other Fields of Science**
Concepts, Tools, and Applications
By M. Schulz 2006. 46 figs., X, 294 pages

216 **Theory of the Muon Anomalous Magnetic Moment**
By K. Melnikov, A. Vainshtein 2006. 33 figs., XII, 176 pages

217 **The Flow Equation Approach to Many-Particle Systems**
By S. Kehrein 2006. 24 figs., XII, 170 pages

218 **High-Energy Polarized Proton Beams**
A Modern View
By G.H. Hoffstaetter 2006, 52 figs., 190 pages